THE JOURNAL OF

PHYSICAL

CHEMISTRY

You Are Cordially Invited
To Become
A Charter Subscriber
To The American Chemical Society's
Newest Publication
CHEMICAL TECHNOLOGY

Cutting across all disciplines, the new monthly publication CHEMICAL TECHNOLOGY is written expressly for those charged with industrial innovation. Chemists and chemical engineers in industry will welcome its pragmatic approach.

Designed to be a highly readable, current awareness magazine, CHEMICAL TECHNOLOGY is a valuable addition to existing ACS publications.
Its articles range over areas of immediate interest, while monthly features deal with many facets of industrial life through interviews, articles, stories and anecdotes.

To start CHEMICAL TECHNOLOGY on its way to you, just complete and return the form at the right. You'll get a new outlook on the world of industrial chemistry.

THE JOURNAL OF
PHYSICAL CHEMISTRY

NOTES

COMMUNICATIONS TO THE EDITOR

AUTHOR INDEX

ANNOUNCEMENT

On the last two pages of this issue you will find reproduced the table of contents of the January 1971 issue of the *Journal of Chemical and Engineering Data*.

Kinetics of the Thermally Induced Dehydrofluorination of

1,1,1-Trifluoroethane in Shock Waves[1a]

by E. Tschuikow-Roux* and W. J. Quiring[1b]

Department of Chemistry, University of Calgary, Calgary 44, Alberta, Canada (*Received September 17, 1970*)

Publication costs borne completely by The Journal of Physical Chemistry

The thermal decomposition of 1,1,1-trifluoroethane has been investigated in a single-pulse shock tube between 1080 and 1310°K at total reflected shock pressures from ~2400 to 3400 Torr. Under these conditions, the mode of decomposition consists almost exclusively of the unimolecular elimination of hydrogen fluoride, $CH_3CF_3 \xrightarrow{k_1} CH_2CF_2 + HF$. The first-order rate constant is given by $\log (k_1, \sec^{-1}) = 14.0 \pm 0.4 - (68.7 \pm 2.4 \text{ kcal})/2.303RT$. Relative to ethyl fluoride and 1,1-difluoroethane the activation energy for the dehydrofluorination reaction increases significantly with increased fluorine substitution at the α-carbon position. As a comparative study the dehydrochlorination of ethyl chloride has been carried out in the temperature range 990 to 1200°K. The Arrhenius parameters for this reaction were found to be $\log (A, \sec^{-1}) = 13.6 \pm 0.4$ and $E_{act} = 55.8 \pm 1.9$ kcal mol^{-1} in satisfactory agreement with previous literature values.

Introduction

The thermal gas phase hydrogen halide elimination reactions of alkyl halides are of practical and theoretical interest and have been extensively studied in the case of chlorides, bromides, and iodides.[2,3] In contrast, information on thermal HF elimination from alkyl fluorides has proved more difficult to obtain because of complications resulting from heterogeneous reactions in conventional static systems.[4] Recently, however, Day and Trotman-Dickenson[4] have reported the dehydrofluorination of ethyl fluoride at 410–465° in a Pyrex reaction vessel which was seasoned with C_2H_5F. Measurements in flow systems have been, in general, more promising. Sianesi, *et al.*,[5] have studied the pyrolysis of the fluoroethanes $CH_3CH_{3-n}F_n$ ($n = 1, 2, 3$) in a subsonic flow system at temperatures in the range 600–800° using a platinum-coated reactor. They found that the preexponential factors decrease markedly with additional α-fluoro substitution, while the activation energies show a slight concomitant trend. Most recently, Cadman, *et al.*,[6] have communicated the results of a shock tube study on the same fluoroethanes as well as some propyl and butyl fluorides. In this work a comparative technique was employed with C_2H_5Cl and $n-C_3H_7Cl$ being used as internal standards. Contrary to the results of the Italian investigators, Cadman and coworkers find a significant *increase* in the activation energy with increasing fluorination in the α position, while the preexponential factors remain virtually constant. This trend in the activation energies finds further support by comparison with the critical energies derived from application of the Marcus

(1) (a) Work supported by the National Research Council of Canada. (b) Predoctoral Fellow.

(2) A. Maccoll and P. J. Thomas, *Progr. React. Kinet.*, **4**, 119 (1967).

(3) A. Maccoll, *Chem. Rev.*, **69**, 33 (1969).

(4) M. Day and A. F. Trotman-Dickenson, *J. Chem. Soc. A*, 233 (1969).

(5) D. Sianesi, G. Nelli, and R. Fontanelli, *Chim. Ind.* (*Milan*), **50**, 619 (1968).

(6) P. Cadman, M. Day, A. W. Kirk, and A. F. Trotman-Dickenson, *Chem. Commun.*, 203 (1970).

(RRKM) theory to nonequilibrium chemical activation data.[6]

In order to clarify these apparent discrepancies a systematic study of the thermal decomposition of fluoroethanes has been undertaken in this laboratory using a modified single pulse shock tube (SPST) the reliability of which has been demonstrated.[7,8] The present paper reports the second study in this series, the thermolysis of 1,1,1-trifluoroethane in the temperature range 1080–1310°K. In a previous communication[9] we have reported the consecutive HF elimination from 1,1-difluoroethane and its product CH_2CHF at 1040–1320°K. Parallel, independent studies on CH_2CHF and CH_2CF_2 have also been carried out.[10,11]

As a further test of the SPST technique and our method of data reduction, in particular the determination of the reflected shock temperature, we have determined the rate constant for the decomposition of ethyl chloride to ethylene and HCl which has a well-established temperature coefficient.

Experimental Section

Apparatus. The modified single-pulse shock tube, the recording instrumentation, and operational procedure have been described previously.[7,8] Here it suffices to note only that, for the calculation of reflected shock temperature, both incident and reflected shock velocities were measured using high-frequency pressure transducers in conjunction with two time-interval counters of 0.1-μsec resolution. Further, the wave history near the end plate, including the quenching process by the rarefaction wave was displayed on the face of an oscilloscope and recorded photographically. For the present study the channel section was improved so that the shock tube could be evacuated to 10^{-5} Torr with a leak rate of 10^{-4} Torr min^{-1}. After evacuation the channel was filled with pure argon with the exception of the ball valve. The latter was filled with dilute reactant (CH_3CF_3 in Ar) to the same pressure as the rest of the tube.

Chemicals. 1,1,1-Trifluoroethane of 99% stated purity was obtained commercially (Columbia Organic Chemicals). The impurities which were believed to be of lower molecular weight, were removed by trap-to-trap distillation. The purity of the final reactant was 99.99% as determined by vpc analysis. This material was used to prepare dilute mixtures (~0.5%) of CH_3-CF_3 in argon for charging the ball-valve section. Helium and argon, both of better than 99.99% purity, were obtained from Matheson Co., as were the reference gases: 1,1-difluoroethylene, vinyl fluoride, ethylene, and ethyl chloride. The latter was also used to prepare mixtures of 0.124% C_2H_5Cl in argon for the control experiments.

Analysis. Following the shock the ball valve was closed, and the reactant and products of decomposition were effectively trapped in the end section of the shock tube. A sample of the fully mixed gases was then withdrawn and subjected to gas chromatographic analysis (Varian Aerograph, Model 1740) using flame ionization detection. The sample was introduced by means of a seven-port gas sampling valve and analysis was carried out under isothermal conditions using helium as carrier gas (30 cm^3 min^{-1}). Quantitative identification of the product/reactant ratios was obtained by comparison with standard mixtures prepared for calibration purposes. The CH_2CF_2/CH_3CF_3 mixtures were separated on a 4-m silica gel column at 80°. The per cent conversion of CH_3CF_3 was in the range 0.06% at 1078°K to about 18% at 1280°K. In the control experiments C_2H_4/C_2H_5Cl mixtures were analyzed using a 4-m Porapak Q column at 90° and conversions ranged from ~0.45% (994°K) to ~69% (1196°K).

Computations and Results

CH_3CF_3. The thermal decomposition of 1,1,1-trifluoroethane at reflected shock temperatures between 1080 and 1310°K yields 1,1-difluoroethylene as the only carbon containing product and suggests molecular elimination of hydrogen fluoride

$$CH_3CF_3 \xrightarrow{k_1} CH_2CF_2 + HF \qquad (I)$$
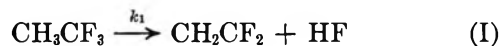
Accordingly, as a first approximation, the rate constants were evaluated from an *assumed* first-order rate law

$$k_{uc} = (1/t_d) \ln (1 + R_t) \qquad (1)$$

where R_t is the product/reactant ratio, $[CH_2CF_2]/[CH_3CF_3]$, and t_d is the calculated reaction time which is related to, and may coincide with, the actual measured "transducer dwell time" through a suitable choice of ball valve and transducer location with respect to the end plate of the shock tube.[12] For reactions with relatively low-activation energies such as in the case of C_2H_5Cl (see below) the rate constant in eq 1 must be corrected for the finite cooling rate which will give rise to additional decomposition in an environment of changing temperature and pressure within the rarefaction wave. The corrected rate constant is conveniently given by[12,13]

$$k_1 = k_{uc}/[1 - (\epsilon/t_d)] \qquad (2)$$

(7) E. Tschuikow-Roux, J. M. Simmie, and W. J. Quiring, *Astronaut. Acta*, **16**, 511 (1970).

(8) J. M. Simmie, W. J. Quiring, and E. Tschuikow-Roux, *J. Phys. Chem.*, **73**, 3830 (1969).

(9) E. Tschuikow-Roux, W. J. Quiring, and J. M. Simmie, *ibid.*, **74**, 2449 (1970).

(10) J. M. Simmie, W. J. Quiring, and E. Tschuikow-Roux, *ibid.*, **74**, 992 (1970).

(11) (a) J. M. Simmie and E. Tschuikow-Roux, *Chem. Commun.*, 773 (1970); (b) *J. Phys. Chem.*, **74**, 4075 (1970).

(12) E. Tschuikow-Roux, *Phys. Fluids*, **8**, 821 (1965).

(13) E. Tschuikow-Roux and J. E. Marte, "Correction for Finite Cooling Rate in Chemical Shock Tube Studies," SPS 37-28, Vol. IV, Jet Propulsion Laboratory, Pasadena, Calif., 1964, p 112.

Table I: Experimental Results (CH_3CF_3)

Mach no.		P_2, Torr	T_2, °K	P_5, Torr	T_5, °K	t_d, μsec	R_t	k_{uo}, sec^{-1}	k_1, sec^{-1}
W_{11}	W_{21}								
2.074	1.242	769	650	2426	1078	252	0.000573	2.27	1.16
2.145	1.235	826	675	2616	1122	365	0.00229	6.27	3.56
2.144	1.254	824	676	2655	1132	223	0.00177	7.95	4.28
2.107	1.261	795	662	2563	1110	486	0.00342	7.03	4.83
2.151	1.244	830	678	2653	1131	366	0.00320	8.74	5.05
2.163	1.238	840	683	2674	1138	340	0.00297	8.70	5.19
2.152	1.268	831	678	2711	1145	484	0.00568	11.7	7.23
2.209	1.269	878	702	2884	1189	459	0.0154	33.4	22.6
2.204	1.260	874	700	2847	1181	619	0.0217	34.7	23.8
2.203	1.272	873	701	2873	1189	565	0.0213	37.3	27.1
2.237	1.241	901	714	2903	1197	725	0.0490	66.0	50.1
2.236	1.268	900	717	2962	1216	675	0.0545	78.5	58.1
2.266	1.281	925	726	3087	1239	728	0.0850	112	83.7
2.296	1.273	952	740	3162	1260	726	0.226	281	163
2.312	1.282	965	749	3235	1281	391	0.151	359	190
2.307	1.293	961	744	3249	1280	730	0.266	280	194
2.317	1.292	969	751	3277	1291	610	0.192	287	214
2.338	1.302	987	760	3370	1313	367	0.204	506	284

where

$$\epsilon = (RT_5^2/Em)\{1 - \exp(-E/[RT_5 - (E/\ln \xi)])\} \quad (3)$$

In eq 3 E is the activation obtained to a first approximation from a plot of log k_{uo} vs. $1/T$; $m = (dT/dt)_i$ is the initial cooling rate which is derived from the oscillographic pressure record ($m \simeq -2.5 \times 10^5$°K sec^{-1}); T_5 is the temperature behind the reflected shock; and ξ ($0 < \xi < 1$) is a cut-off parameter, i.e., an arbitrarily selected rate ratio at which further contribution to the reaction rate can be neglected in comparison with the rate at T_5. In the present calculations $\xi = 10^{-2}$ was selected. All computations were carried out using an IBM 360 computer.

The experimental results are summarized in Table I, where W_{11} and W_{21} denote incident and reflected shock Mach numbers, and subscripts 2 and 5 refer to incident and reflected shock zones, respectively. The temperature dependence of the corrected rate constants, k_1, is shown in Figure 1. A least-squares analysis of the data yields the Arrhenius equation

$$k_1 \text{ (sec}^{-1}) = 10^{14.0 \pm 0.4} \exp[-(68,700 \pm 2400)/RT]$$

where the indicated error limits are standard deviations.

As in our previous studies[8-11] reflected shock temperatures were calculated from *measured* incident *and* reflected shock velocities by a method described earlier[7] which makes no reference to any assumption concerning the particle velocity in the reflected shock zone. This technique has been successfully demonstrated in the case of perfluorocyclobutane,[8] where excellent agreement was found with low temperature data obtained in a static system.[14] Since the Arrhenius parameters in perfluorocyclobutane are fairly high, it was deemed instructive to investigate the dehydrochlorination of
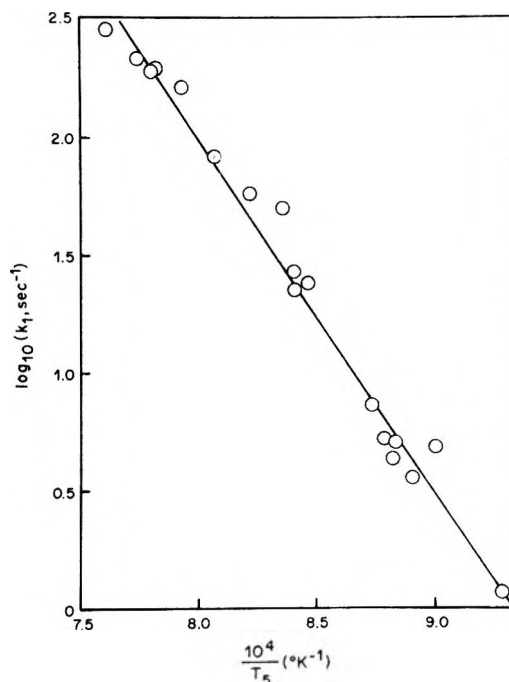
Figure 1. Temperature dependence of the rate constant k_1 for HF elimination from CH_3CF_3.

C_2H_5Cl for which the Arrhenius constants are considerably lower. This would give a range of conditions over which the data reduction method has been tested and would also include the compound of present interest, CH_3CF_3. A high-temperature investigation of C_2H_5Cl is also of interest in view of the fact that this molecule has served as a prototype for four-center elimination reactions.[15]

(14) J. N. Butler, *J. Amer. Chem. Soc.*, **84**, 1393 (1962).

(15) H. E. O'Neal and S. W. Benson, *J. Phys. Chem.*, **71**, 2903 (1967).

Table II: Experimental Results (C_2H_5Cl)

Mach no.		P_2,	T_2,	P_5,	T_5,	t_d,		k_{uc},	k_1,
W_{11}	W_{21}	Torr	°K	Torr	°K	μsec	R_t	sec^{-1}	sec^{-1}
1.975	1.213	694	610	2096	990	53.7	0.00511	94.9	15.8
1.988	1.207	704	616	2120	997	97.2	0.00606	62.2	18.5
1.991	1.207	706	617	2125	999	195	0.00881	45.1	19.7
2.044	1.224	746	638	2303	1047	274	0.0644	227	111
2.074	1.206	769	647	2351	1056	489	0.128	246	160
2.081	1.253	775	652	2470	1087	379	0.190	459	287
2.106	1.231	794	664	2493	1098	564	0.384	576	399
2.107	1.232	795	663	2498	1097	660	0.550	664	483
2.124	1.230	809	666	2544	1103	647	0.530	656	485
2.128	1.255	812	671	2611	1124	437	0.454	856	545
2.143	1.269	824	675	2688	1139	298	0.445	1236	695
2.141	1.242	822	676	2619	1127	535	0.748	1043	725
2.196	1.270	867	697	2847	1180	451	2.12	2518	1635
2.213	1.247	881	704	2842	1181	369	2.36	3285	1743
2.208	1.263	877	701	2865	1184	460	2.43	2675	1831
2.199	1.254	869	697	2817	1173	358	2.11	3176	1839
2.204	1.274	873	698	2880	1185	394	2.21	2956	1914
2.216	1.266	883	707	2897	1196	244	2.55	5196	1966

C_2H_5Cl. The thermal elimination of HCl from ethyl chloride

$$C_2H_5Cl \xrightarrow{k_{1,II}} C_2H_4 + HCl \qquad (II)$$
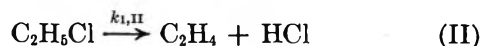
has been reported by several investigators and was included in a recent review.[3] Our results are listed in Table II and cover the temperature range 990 to 1200°K. The temperature dependence of the rate constants is shown in Figure 2 and yields the Arrhenius equation

$$k_{1,II} \ (sec^{-1}) = 10^{13.6 \pm 0.4} \exp[-(55,800 \pm 1980)/RT]$$

which is in satisfactory agreement with the accurate expression of Capon and Ross[16]

$$k_{1,II} \ (sec^{-1}) = 10^{13.46 \pm 0.03} \exp[-(56,620 \pm 90)/RT]$$

obtained in a standard static apparatus over the temperature range 492-772°K. Similar results have also been obtained by Hartmann, et al.[17] (log A = 13.51, E = 56.6 kcal mol^{-1}) in a static apparatus at 662-744°K, and by Tsang[18] (log A = 13.16, E = 56.5 kcal mol^{-1}) using his comparative rate method in a conventional type single-pulse shock tube at 820-1000°K.

Discussion

The absence of hydrocarbon products or their fluoro derivatives other than CH_2CF_2 in the pyrolysis of CH_3CF_3 strongly suggests the molecular elimination of hydrogen fluoride. Thermochemical considerations show that initiation by homolytic bond scission is energetically unfavorable. Thus, the bond strength of the C–H and C–F bonds in CH_3CF_3 is estimated to be similar to the corresponding bonds in ethane,[19] $D(C_2H_5–H) = 98$ kcal mol^{-1}, and ethyl fluoride,[19] $D(C_2H_5–F) = 106$ kcal mol^{-1}, respectively. Evidence has been presented[20] that the carbon–carbon bond in
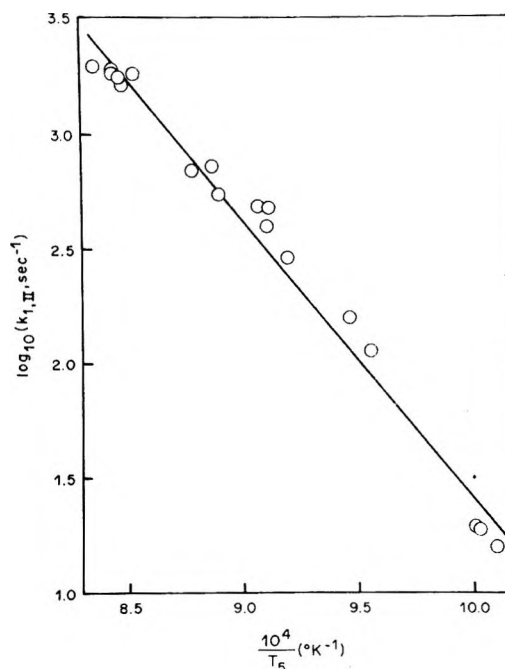
Figure 2. Temperature dependence of the rate constant $k_{1,II}$ for the elimination of HCl from C_2H_5Cl.

CH_3CF_3 may have a value as high as $D(CH_3–CF_3) = 99.7 \pm 2.0$ kcal mol^{-1}. Compared to our experimental activation energy of ~69 kcal mol^{-1} it is clear that free radical reactions are unlikely to occur. Homolytic initiation followed by radical chain reactions could, of course,

(16) N. Capon and R. A. Ross, Trans. Faraday Soc., 62, 1560 (1966).
(17) H. Hartmann, H. G. Bosche, and H. Heydtmann, Z. Phys. Chem. (Frankfurt am Main), 42, 329 (1964).
(18) W. Tsang, J. Chem. Phys., 41, 2487 (1964).
(19) J. A. Kerr, Chem. Rev., 66, 465 (1966).
(20) J. W. Coomber and E. Whittle, Trans. Faraday Soc., 63, 1394 (1967).

lead to a considerably lower overall activation energy. However, our product analysis does not support such a mechanism. Therefore, the *only* alternative is dehydrofluorination, reaction I.

It is also of interest to note the conspicuous absence of any consecutive HF elimination from the product olefin, CH_2CF_2. In contrast, in the pyrolysis of CH_3-CHF_2 under similar reaction conditions the dehydrofluorination of the product vinyl fluoride was observed above $1200°K$.[9] This indicates that the activation energy for HF elimination increases significantly with increasing α-carbon fluorination of the olefin, and corroborates our earlier, independent studies of these fluoroethanes.[10,11]

The rate constants, k_1, reported in Table I are judged to be high-pressure limiting values by comparison with the fall-off data on C_2H_5F reported by Day and Trotman-Dickenson.[4] These authors found that at $452°$ the rate constant becomes pressure independent above 5 Torr. While the higher temperatures in the present study would shift the fall-off region somewhat toward higher pressure, this is more than compensated for by the ~600-fold higher total pressures used in this work and the lower frequency pattern of CH_3CF_3.

The kinetic parameters are summarized in Table III. In agreement with the trend reported by Cadman, *et al.*,[6] our results show that relative to 1,1-difluoroethane the activation energy increases with additional fluorine substitution at the α-carbon position. However, the agreement in the Arrhenius parameters is relatively poor, particularly in the case of the A factors where the difference is outside the experimental error. The reason for this discrepancy is not quite clear because of insufficient information in the preliminary communication by Cadman, *et al.*,[6] but may reside in the temperature determination.[21] The Arrhenius

parameters of Sianesi, *et al.*,[5] are significantly lower; however the absolute values of their rate constants extrapolated to $1100-1300°K$ differ only by factors of ~2.5 to 4 (Table III).

Also listed in Table III is the activation energy derived from ΔH_I, the enthalpy change in reaction I, and E_r, the activation energy for the reverse four-center addition reaction. The latter quantity was evaluated using the electrostatic semiion pair model of Benson and Haugen.[22] According to this model E_r is a function of the longitudinal molar polarizabilities of the species forming the four-center semiion pair, their dipole moments, and some empirically adjusted bond distances. Ground-state dipole moments were taken from the literature:[23] $\mu°_{HF} = 1.91$ D; $\mu°_{CH_2CF_2} = 1.37$ D. Transition state polarizabilities were assumed to be the same as for the ground state.[24] The longitudinal molar polarizability of 1,1-difluoroethylene, $\alpha°_{1,CH_2CF_2} = 5.31$ Å^3, was calculated from longitudinal and transverse bond polarizabilities using the tabulated values of Le Fèvre;[25] and all other parameters (including $\alpha°_{1,HF} = 0.96$ Å^3) were taken from ref 22. The activation energy for the addition reaction was thus found to be $E_r = 49.5$ kcal mol^{-1}. The enthalpy change ΔH_I at $298°K$ is readily obtained from the known standard heats of formation of HF (-64.8 kcal mol^{-1}),[26] CH_2-CF_2, and CH_3CF_3. The standard heat of formation of 1,1-difluoroethylene has been determined by bomb calorimetry by Neugebauer and Margrave (-77.5 kcal mol^{-1})[27] and by Kolesov, *et al.*[28] (-79.6 kcal mol^{-1}). The heat of formation of CH_3CF_3 has similarly been determined by Kolesov, Martynov, and Skuratov[29] (-174.1 kcal mol^{-1}). These values have been reevaluated by Lacher and Skinner[30] using revised

Table III: Thermal Elimination of HF from $CH_3CH_{3-n}F_n$ ($n = 2, 3$)

	log A, sec^{-1}	E, kcal mol^{-1}	Method	Ref
CH_3CHF_2	13.31	61.9 ± 2	Flow system	a
	13.74	66.6 ± 2	Shock tube	b
	13.9 ± 0.3	61.9 ± 1.8	SPST	c
		75	Theoretical	d
CH_3CF_3	12.14	61.4 ± 2	Flow system	a
	13.47	71.1 ± 2	Shock tube	b
	14.8 ± 0.4	68.7 ± 2.4	SPST	e
		80	Theoretical	d

Relative rate constants (CH_3CF_3)

$k_1^a:k_1^b:k_1^e = 0.389:0.098:1$ at $1100°K$
$= 0.235:0.117:1$ at $1300°K$

a See ref 5. b See ref 6. c See ref 9. d Calculated from E_r for reverse reaction using electrostatic semiion pair model of ref 22 and ΔH for forward reaction. e This work.

(21) In ref 6 the competitive shock tube technique of Tsang[18] was indicated. However, the technique was used in a modified form (Dr. P. Cadman, private communication) whereby the need for the determination of the "effective" reaction time rather than the temperature was eliminated between the unknown and the "standard" reaction. Reflected shock temperatures were still based on single shock velocity measurements and therefore are subject to significant error as discussed in ref 7.

(22) S. W. Benson and G. R. Haugen, *J. Amer. Chem. Soc.*, **87**, 4036 (1965).

(23) Handbook of Chemistry and Physics, Chemical Rubber Publishing Co., Cleveland, Ohio, 1966.

(24) In addition to the ground-state polarizabilities, the calculation of E_r requires average values between the ground state and the semiion pair polarizabilities. According to Benson and Haugen[22] the average values, in all cases where they could be determined, were found to be within 10% of the ground-state polarizabilities. For lack of a better guide we have set $\bar{\alpha}_1 = \alpha_1^0$ (ground state).

(25) R. J. W. Le Fèvre, *Advan. Phys. Org. Chem.*, **3**, 1 (1965).

(26) "JANAF Interim Thermochemical Tables," Dow Chemical Co., Midland, Mich., 1965.

(27) C. A. Neugebauer and J. L. Margrave, *J. Phys. Chem.*, **60**, 1318 (1956).

(28) V. P. Kolesov, A. M. Martynov, S. M. Shtekher, and S. M. Skuratov, *Zh. Fiz. Khim.*, **36**, 2078 (1962).

(29) V. P. Kolesov, A. M. Martynov, and S. M. Skuratov, *ibid.*, **39**, 435 (1965).

(30) J. R. Lacher and H. A. Skinner, *J. Chem. Soc. A*, 1034 (1968).

values for ΔH_f(HF, aq) and $\Delta H_f°$(CF$_4$, g) and they recommend $\Delta H_f°$(1,1-C$_2$H$_2$F$_2$, g) $= -82.5 \pm 2.4$ kcal mol^{-1} and $\Delta H_f°$(1,1,1-C$_2$H$_3$F$_3$, g) $= -178.2 \pm 0.4$ kcal mol^{-1}. Using these preferred values for the heats of formation, $\Delta H_I = 30.0 \pm 2.8$ kcal mol^{-1} at 298°K, and hence $E_f = E_r + \Delta H - RT \simeq 80$ kcal mol^{-1}. This value does not agree with our experimental result, $E_{exp} \simeq 69$ kcal mol^{-1}, or any of the other reported data (Table III). A similar disagreement has been found in the case of 1,1-difluoroethane,[9] and it appears that the electrostatic semiion pair model of Benson and Haugen cannot be applied in the case of polysubstituted alkyl fluorides.

It is of interest to compare the experimental A factor with one evaluated in terms of a predicted entropy of activation, $\Delta S^\dagger = S^\dagger - S + R \ln g$, where $S^\dagger$ and S are the entropies of the transition state and ground state, respectively, and g is the reaction path degeneracy. An equivalent procedure is to try and match the $\Delta S^\dagger$ value with that derived from the experimental preexponential factor, $\Delta S_{exp}{}^\dagger = R \ln (hA/ekT)$. It has been shown[15,31] that for reactions of the type RX $\rightarrow$ olefin + HX the principal contribution to $\Delta S^\dagger$ results from symmetry changes and the entropy loss in passing from the hindered internal rotation of the ground state to the torsional mode of the cyclic complex. For CH$_3$-CF$_3$ the barrier to internal rotation is $V = 3.66$ kcal mol^{-1} [32] giving rise to an entropy contribution of 4.75

gibbs mol^{-1} at 1200°K (the mean temperature of this study). The torsional mode can be assigned a value of 500 cm^{-1} [15] and the corresponding entropy contribution at 1200°K is 3.03 gibbs mol^{-1}. The entropy change for this particular mode is therefore $(S_{tors}{}^\dagger - S_{i.h.r.}) = -1.72$ gibbs mol^{-1}. The reaction path degeneracy for CH$_3$CF$_3$ is nine, and, with $A = 10^{14.0}$ sec^{-1}, $\Delta S_{exp}{}^\dagger = 0.772$ gibbs mol^{-1} (1200°K). We then have the entropy balance (neglecting overall rotational contributions)

$$\Delta S_{int}{}'^\dagger = R \ln (hA/ekT) - (S_{tors}{}^\dagger - S_{h.i.r.}) - R \ln g$$
$$= -1.88 \text{ gibbs mol}^{-1}$$

where

$$\Delta S_{int}{}'^\dagger = \sum_i^{3N-8} S_i{}^\dagger - \sum_i^{3N-7} S_i$$

is the residual intrinsic vibrational entropy change due to all the other modes. The negative entropy of activation indicates that the transition state has a less loose structure than the ground state. An attempt to apply the recipe of O'Neal and Benson[15] for the estimation of A factors in the case of CH$_3$CF$_3$ did not prove successful.

(31) S. W. Benson and E. H. O'Neal, NSRDS-NBS 21, 1970.
(32) D. C. Smith, R. A. Saunders, J. R. Nielsen, and E. E. Ferguson, J. Chem. Phys., 20, 847 (1952).

Recoil Tritium Reactions with Trimethylfluorosilane.

A Study on Parameters Affecting Hot-Atom Substitution Reactions[1]

by S. H. Daniel and Yi-Noo Tang*

Department of Chemistry, Texas A & M University, College Station, Texas 77843 (Received September 8, 1970)

Publication costs assisted by the U. S. Atomic Energy Commission

In the recoil tritium reactions with trimethylfluorosilane, abstraction and substitution at the CH bonds are the most predominantly observed processes while reactions at the SiC and SiF bonds are relatively minor. Primary yields of products were evaluated by correcting for the minor amount of decomposition in the gas phase. A comparison of the recoil tritium substitution at various bonds of trimethylfluorosilane and tetramethylsilane have been made after their individual data had been normalized with a specific activity ratio factor obtained from competition experiments. Since the residual part of both molecules is $(CH_3)_3Si$ after the T-for-F and T-for-CH_3 substitution, a comparison can be made of the two reactions to give strong support to a bond-strength effect for hot-atom substitution reactions. Other comparisons in these systems are also consistent with an inductive effect resulting from the presence of a very electronegative atom, F, in trimethylfluorosilane.

The excellent correlation between HT yields from recoil tritium abstraction reactions and bond dissociation energies has been well established by a series of studies by Rowland and coworkers.[2,3] Two models have been proposed for hot-atom substitution reactions. One is based on geometrical and physical properties,[4,5] and the other on bond strength and electron density.[6-8] At the moment, both models are in need of further tests.

Odum and Wolfgang have proposed the rotational inertia hypothesis for the explanation of heavy-group substitution by recoil tritium atoms at the X–Y bonds where the X's are normally alkyl groups or halogen-substituted alkyl groups while the Y's cover a variety of atoms and groups other than hydrogen with different size, mass, electronegativity, and complexity in structure.[4,5] Their theory was based on the decrease in reaction probability for the T-for-F substitution in fluoromethanes as the number of other heavy substituents increased. They commented that heavy substituents tended to hinder rotation and thus decreased the chance for capturing reacting hot tritium atoms. On the other hand, Rowland and coworkers have proposed that chemical effects such as electronegativity and bond dissociation energies are the predominant controlling factors for hot-atom substitution reactions.[6-8] Very recently, they have revealed strong evidence for electron density and electronegativity effects in the substitution of hydrogen atoms by energetic tritium atoms from molecules, RH, by showing the excellent correlation between RT yields and nmr proton chemical shift for a number of alkanes and halomethanes.[7,8] Their work with CH_3X (X = F, Cl, Br, I, or H) molecules also showed a strong variation in tritium for X substitution which was dependent upon the bond

dissociation energy of the C–X bond.[8] The primary purpose of the present work is to give further experimental evidence for the presence of such chemical factors as the controlling parameters in recoil tritium substitution process.

Silicon skeletal groups as X in the molecule X–Y as opposed to carbon skeletal ones normally offers increased differences in electronegativities between X and Y, and increased ranges of X–Y bond dissociation energies.[9] In the present case a detailed study of the recoil tritium reactions with trimethylfluorosilane (TMFS) has been made, and the results are compared with the recently published data on tetramethylsilane (TMS).[10-12] For these two molecules, X is kept con-

(1) Presented in part at the 157th National Meeting of the American Chemical Society, Minneapolis, Minn., April 1969.

(2) W. Breckenridge, J. W. Root, and F. S. Rowland, *J. Chem. Phys.*, **39**, 2373 (1963).

(3) (a) J. W. Root, W. Breckenridge, and F. S. Rowland, *ibid.*, **43**, 3694 (1965); (b) E. Tachikawa and F. S. Rowland, *J. Amer. Chem. Soc.*, **90**, 4767 (1968); **91**, 559 (1969); (c) E. Tachikawa, Y.-N. Tang, and F. S. Rowland, *ibid.*, **90**, 3584 (1968).

(4) R. Wolfgang, *Progr. React. Kinet.*, **3**, 97 (1965); *Ann. Rev. Phys. Chem.*, **16**, 15 (1965).

(5) R. A. Odum and R. Wolfgang, *J. Amer. Chem. Soc.*, **83**, 4668 (1961); **85**, 1050 (1963).

(6) Y.-N. Tang, E. K. C. Lee, and F. S. Rowland, *ibid.*, **86**, 1280 (1964).

(7) F. S. Rowland, E. K. C. Lee, and Y.-N. Tang, *J. Phys. Chem.*, **73**, 4024 (1969).

(8) Y.-N. Tang, E. K. C. Lee, E. Tachikawa, and F. S. Rowland, submitted for publication in *J. Phys. Chem.*

(9) See, for example, (a) E. A. V. Ebsworth, "Volatile Silicon Compounds," Macmillan, New York, N. Y., 1963; (b) "Organometallic Compounds of the Group IV Elements," A. G. MacDiarmid, Ed., Marcel Dekker, New York, N. Y., 1968.

(10) J. Witkin and R. Wolfgang, *J. Phys. Chem.*, **72**, 2631 (1968).

(11) T. Tominaga, A. Hosaka, and F. S. Rowland, *ibid.*, **73**, 465 (1969).

(12) S. H. Daniel and Yi-Noo Tang, *ibid.*, **73**, 4378 (1969).

stant as $(CH_3)_3Si-$ while Y has been changed from CH_3- to F. The mass of CH_3- and F (15 vs. 19 amu) are about the same and therefore "mass" is roughly eliminated as a variable in this comparison. Any possible residue effect due to rotational inertia should be small and certainly not a cause for major differences in these two systems. Since both the electronegativities of Y and the X–Y bond dissociation energies are very different for trimethylfluorosilane and tetramethylsilane, the T*-for-Y substitution in these two molecules should give further evidence as to whether these chemical effects operate during the recoil tritium substitution processes or not.

Another major advantage in employing TMFS instead of its hydrocarbon counterpart for this test is that the unimolecular decomposition of the primary products from this system is less probable. Essentially all the chemical bonds in the expected products from TMFS are fairly strong, and also the elimination of HF from them to give silicon–carbon double-bonded compounds are both unknown and unlikely.[13] On the other hand, the hydrocarbon counterparts, and their recoil tritium reaction products alike, should have a very serious decomposition problem.[6,14–16] The HCl elimination from $(CH_3)_3CCl$ owns an activation energy as low as 41.4 kcal/mol with a frequency factor of log $A = 12.4$ sec^{-1}.[17]

Experimental Section

Chemicals. The recoil tritium atoms for the gas phase samples were obtained by neutron irradiation of appropriate gas mixtures containing ^3He which undergoes the nuclear transmutation $^3He(n,p)^3H$. For liquid phase samples, tritium atoms were produced by neutron irradiation of solid LiF, contained in the liquid samples, which undergoes the nuclear transmutation $^6Li(n, \alpha)^3H$. ^3He was obtained from Mound Laboratory, Monsanto Research Corp., and had a tritium content of less than $2 \times 10^{-11}\%$. Lithium fluoride of natural isotopic abundance was obtained from Riedel-DeHaen A.G., Seelge-Hannover, Germany.

The trimethylfluorosilane and tetramethylsilane were obtained from Peninsular Chemical Co., with a quoted impurity level less than 0.5% and were used without further purification. The purity level was confirmed by gas chromatography.

Oxygen (Airco; Air Reduction Co., Inc.), I_2, and DPPH (both from Baker Chemical Co.) were used without purification.

Sample Preparation. Gas samples containing ^3He, trimethylfluorosilane, and other additives were prepared with a high-vacuum system.[18] For scavenged samples, 5–10 cm of oxygen were added. Gas phase reactions were carried out in Pyrex bulbs with a volume of 12 $\pm$ 2 ml volume. For liquid samples, the components were condensed into Pyrex capillary tubes, containing a small amount of LiF, by means of the high-vacuum

system. I_2, Br_2, or DPPH, mixed with the LiF, was used as the liquid phase scavenger.

Irradiation. The samples were irradiated at the Texas A & M University Nuclear Science Center Research reactor with a neutron flux of 1×10^{13} neutrons/cm^2-sec for 5 min.

Sample Analysis. The analysis of tritium-labeled products after irradiation was preformed by radiogas chromatography using helium as the eluent gas.[18] The gas chromatographic separations were carried out on two or more of the following columns for each sample. The products observed from each are listed in the order of elution. (a) PCA column: 50-ft column of propylene carbonate packed on activated alumina. Temperature of the column was 0°. The products were H_2, CH_4, and C_2H_4. (b) DMS column: 50-ft column of dimethyl sulfolane packed on Chromosorb P, 24°. The products were $(H_2 + CH_4)$, C_2H_4, $(CH_3)_3SiH$, $(CH_3)_2SiHF$, $(CH_3)_2SiF_2$, and $(CH_3)_3SiF$. (c) Safrole column: 50-ft column of safrole packed on Chromosorb P, 0°. The products were $(H_2 + CH_4)$, C_2H_4, $[(CH_3)_3SiH + (CH_3)_2SiHF]$, $(CH_3)_2SiF_2$, and $(CH_3)_3SiF$.

Mass peaks were measured through thermal conductivity response. The radioactivity was assayed by proportional counting of the gas mixture obtained after the addition of propane gas to the helium stream. Measurements were made with a brass counter of 80-ml active volume.

There was no noticeable quenching of the internal counter by the parent compounds in our systems.

Synthesis of Dimethylfluorosilane. Dimethylfluorosilane was synthesized in order to identify its retention time on the gc columns. The synthesis was started by the hydrolysis of dimethylchlorosilane to give 1,1',-2,2'-tetramethyldisiloxane. The procedure used by Emeleus and Onyszchuk was followed.[19]

Results

Primary Products from Recoil Tritium Reactions with Trimethylfluorosilane. There are three types of chemical bonds in the molecule trimethylfluorosilane. For the relatively indiscriminative hot atoms, both abstraction (*of* the lighter group) and substitution (*for* the lighter group) at these three types of bonds are feasible.[4] Therefore, the expected primary products from recoil

(13) Both Si=C and Si=Si are completely unknown and numerous attempts to form them have all failed. See, for example, ref 9.

(14) E. K. C. Lee and F. S. Rowland, *J. Amer. Chem. Soc.*, 85, 897 (1963).

(15) Y.-N. Tang and F. S. Rowland, *ibid.*, 87, 3304 (1965).

(16) Y.-N. Tang and F. S. Rowland, *ibid.*, 90, 574 (1968).

(17) See S. W. Benson, "The Foundation of Chemical Kinetics," McGraw-Hill, New York, N. Y., 1960.

(18) J. K. Lee, E. K. C. Lee, B. Musgrave, Y.-N. Tang, J. W. Root, and F. S. Rowland, *Anal. Chem.*, 34, 741 (1962).

(19) H. J. Emeleus and M. Onyszchuk, *J. Chem. Soc.*, 604 (1958).

Table I: Products from Recoil Tritium Reactions with Trimethylfluorosilane As a Function of Pressure

Gas pressure, cm								
$(CH_3)_3SiF$	4.5	12.9	33.6	55.7	67.3	73.4	79.5	78.7
He	2.3	2.3	2.3	2.4	2.6	2.3	2.4	2.6
O_2	3.3	5.1	6.7		7.6	8.1		0
Br_2				6.5			6.5	
Total pressure	10.1	20.3	42.6	64.6	77.5	83.8	88.4	81.3
Products[a]								
HT	100	100	100	100	100	100	100	100
CH_3T	10.2 ± 0.4	9.9 ± 0.3	10.0 ± 0.3	11.2 ± 0.3	9.9 ± 0.3	10.0 ± 0.3	11.2 ± 0.3	7.9 ± 0.3
$(CH_3)_3SiT$	0.2 ± 0.1	0.4 ± 0.2	0.4 ± 0.2		0.2 ± 0.1	0.2 ± 0.1		0.2 ± 0.1
$(CH_3)_2SiTF$	4.7 ± 0.4	4.8 ± 0.3	5.1 ± 0.3		5.4 ± 0.4	5.0 ± 0.3		3.1 ± 0.3
$(CH_3)_2SiFCH_2T$	101 ± 3	104 ± 3	101 ± 3	102 ± 3	107 ± 3	97 ± 3	99 ± 3	52 ± 3
C_2H_5T	0.8 ± 0.2	0.8 ± 0.2	0.7 ± 0.2		0.3 ± 0.1	0.5 ± 0.1		0.1 ± 0.1
$CH_3SiF_2CH_2T$	1.8 ± 0.3	3.6 ± 0.3	5.8 ± 0.3	0.9 ± 0.2	2.0 ± 0.2	$5.2 = 0.3$	1.2 ± 0.2	0.5 ± 0.2
CH_2TBr				6.5 ± 0.3			6.3 ± 0.5	

[a] Relative to HT yield as 100.

tritium reactions with TMFS are as shown in the following six equations.

$$T^* + (CH_3)_3SiF \longrightarrow HT + (CH_3)_2SiFCH_2 \quad (1)$$

$$T^* + (CH_3)_3SiF \longrightarrow (CH_3)_2SiFCH_2T + H \quad (2)$$

$$T^* + (CH_3)_3SiF \longrightarrow CH_3T + (CH_3)_2SiF \quad (3)$$

$$T^* + (CH_3)_3SiF \longrightarrow (CH_3)_2SiTF + CH_3 \quad (4)$$

$$T^* + (CH_3)_3SiF \longrightarrow TF + (CH_3)_3Si \quad (5)$$

$$T^* + (CH_3)_3SiF \longrightarrow (CH_3)_3SiT + F \quad (6)$$
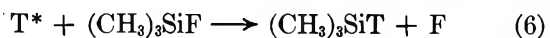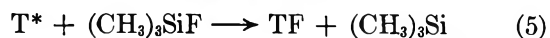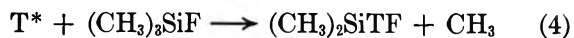
However, TF, the product from (5), is not expected to be measured in these experiments because the labile tritiums are easily exchanged and because TF molecules are very reactive towards our sample transferring and analytical devices. All the other tritium-labeled products are expected to be detected.

Pressure Dependence of Primary Products. The expected primary products from the above equations are essentially the only ones observed when recoil tritium reactions with TMFS were carried out. Besides these, small yields of dimethyldifluorosilane and ethylene were the only other observed peaks. The experimental results are as indicated in Table I. It is obvious that hydrogen atom abstraction and substitution are the two most predominant processes.

Total pressure is the major variable for the series of samples included in Table I. Oxygen and bromine were used as scavengers in all but one case which is an unscavenged sample. Ethylene-scavenged samples (not included in the table) were also studied in order to examine its effect. There was essentially no difference from the O_2-scavenged systems. In this table, HT is chosen as a standard for expressing the relative yields in these pressure studies because its yield is more likely to be pressure independent.[6,14-16]

The relative yields of all the primary products are surprisingly constant over a pressure change of nearly a

factor of 10. This is in contrast to the alkyl halide systems where there is always an unmistakable trend of increasing yields of primary products with higher pressures.[6,15,16] This observation indicates that the unimolecular decomposition of the direct recoil tritium reaction products are probably not serious.

Br_2-scavenged systems were analyzed in order to determine the actual amount of decomposition in some of the primary products. $(CH_3)_2SiFCH_2T$, the tritiated parent, and CH_3T, two of the most predominant products in the TMFS system, are both expected to decompose to give CH_2T whenever they are excited.[20,21] These scavenged methyl radicals were detected as CH_2TBr as indicated in Table I. Using the measured yield of CH_2TBr and assuming that about 15% of the CH_3T formed in the system decomposes,[21] the calculated amount of labeled parent that undergoes secondary decomposition is also approximately 15%.

The minor products, $(CH_3)_3SiT$ and $(CH_3)_2SiTF$, are both similar in structure to the tritiated parent except that they possess Si–T bonds which are also rather strong.[20] Therefore, it should be safe to assume that they decompose roughly to the same extent. The primary yields, corrected for the calculated decomposition, will be used in the discussions.

Recoil Tritium Reactions with Trimethylfluorosilane in the Liquid Phase. Recoil tritium reactions with trimethylfluorosilane have been carried out in the liquid phase, and the results are as shown in Table II. Experiments were performed under different scavenging conditions, and in each case except for Br_2-scavenged

(20) In $(CH_3)_3SiF$, the bond dissociation energy for the SiF bond is listed as 193 kcal/mol. D(Si–C) in $(CH_3)_4Si$ is 85 kcal/mol and D(Si–H) in $(CH_3)_3SiH$ is 88 kcal/mol. See G. G. Hess, F. W. Lampe, and L. H. Sommer, *J. Amer. Chem. Soc.*, 87, 5327 (1965).

(21) Recoil tritium reactions with CH_4 in the presence of a halogen scavenger have shown that approximately 15% of the excited CH_3T being formed underwent decomposition to give CH_2T. See J. W. Root, Ph.D. Thesis, The University of Kansas, 1964.

Table II: Products from Recoil Tritium Reactions with Liquid Trimethylfluorosilane

	Sample Composition				
$(CH_3)_3SiF$	Liquid	Liquid	Liquid	Liquid	Liquid
LiF	Yes	Yes	Yes	Yes	Yes
Scavenger	Br_2	I_2	DPPH	DPPH	None
	Relative Product Yields[a]				
HT	121 ± 3	111 ± 3	118 ± 3	125 ± 4	144 ± 4
CH_3T	53.6 ± 1.2	30.9 ± 0.9	31.8 ± 0.9	31.6 ± 0.9	27.8 ± 0.9
$(CH_3)_3SiT$	NM[b]	NM[b]	0.9 ± 0.1	0.9 ± 0.1	1.0 ± 0.1
$(CH_3)_2SiTF$	NM[b]	NM[b]	8.3 ± 0.4	8.8 ± 0.4	8.8 ± 0.4
$(CH_3)_2SiFCH_2T$	100	100	100	100	100
C_2H_3T	NM[b]	NM[b]	0.8 ± 0.1	0.6 ± 0.1	NM[b]
$CH_3SiF_2CH_2T$	3.9 ± 0.3	3.4 ± 0.3	2.6 ± 0.3	2.5 ± 0.3	2.5 ± 0.3
CH_2TBr	9.8 ± 0.4				

[a] Relative to $(CH_3)_2SiFCH_2T = 100$.   [b] NM = not measured; yield <0.1.

ones the liquid sample was purposely not degassed so that dissolved air could contribute to the scavenging. The results are expressed relative to the tritiated parent as a standard because the HT yield is not a constant under different scavenging conditions due to the ease of hydrogen abstraction by thermal tritium. Products with Si–H (or Si–T) and C=C bonds are not observed in the halogen-scavenged samples because of their chemical exchange or addition reactions with the halogen.

The overall picture of Table II is not consistent with our conclusion derived from data in Table I that unimolecular decomposition of the primary products are not serious in the gas phase. If we convert the values in Table I relative into the tritiated parent instead of HT as 100 and then compare them with those in Table II, it is seen that every product with the exception of the tritiated parent itself increases tremendously in going from gas to liquid phase. This might be due to the stabilization of excited primary products by the larger collision frequency in the liquid phase, but other indications show that this is not the case.

A comparison of the gas and liquid phase yields of CH_3T reveals an increase by a factor of 3–5 in going from the gas to the liquid phase. However, even if it is assumed (this assumption is unrealistic for sure) that all the CH_2TBr produced in the gas phase bromine-scavenged samples was due to decomposition of excited CH_3T, this indicates an upper limit of a factor of 2 for the increase in CH_3T if it is assumed that all the excited CH_3T was stabilized by collisional deactivation. The fact that CH_3T actually increases several times more than the upper limit means that there are complications in the liquid phase. It is likely that the increase in yield for the other products is also complicated by these same causes.

A possible complication that could arise in the liquid phase is the likely reaction between TF, TBr, or TI with

the parent molecule. Also the cage effect and inefficient scavenging in the liquid may contribute to the problem.

Since the gas phase results seem to be free from complications, except for the expected minor secondary decomposition, we are going to obtain the primary yields solely from the corrected gas phase values.

Sources of C_2H_3T and $CH_3SiF_2CH_2T$. C_2H_3T not only appeared here as a minor product, but was also formed in the TMS samples. From both systems, C_2H_3T was expected neither as a primary nor as a direct secondary decomposition product. At the present time, there is no logical mechanism for its formation.

$CH_3SiF_2CH_2T$ was not an expected product from this system either. The high fluctuation of its yield as seen in the tables was traced to be a function of time from irradiation to analysis, and over a period of months its yield gradually leveled off at a value of about 5. There is a mass peak accompanying it with a peak area approximately 1% of that for the parent compound. There is no logical mechanism for the formation of this product at the present time.

Recoil Tritium Competition Reactions with Trimethylfluorosilane and Tetramethylsilane. In order to compare the relative reactivities of various bonds in trimethylfluorosilane and tetramethylsilane, a direct competition between them for recoil tritium atoms is necessary. The experimental data together with calculated results are as shown in Table III. The average specific activity ratio per molecule for the CH bonds in TMFS vs. TMS is 0.88 ± 0.03, while the average specific activity ratio per CH bond is 1.17 ± 0.04. These values can then be used to normalize the two sets of individual data.

Assurance for the Primary Yield of Trimethylsilane-t. Trimethylsilane-t, the T-for-F substitution product from recoil tritium reactions with TMFS, is the most important primary product for the purpose of the pres-

Table III: Calculation of Specific Activity Ratios per Molecule and per Bond for Trimethylfluorosilane and Tetramethylsilane from Recoil Tritium Competitive Reactions

Gas pressure, cm[a]			
$(CH_3)_3SiF$	37.9	38.3	36.3
$(CH_3)_4Si$	36.3	34.4	36.7
Relative yields[b]			
$(CH_3)_2SiFCH_2T$	513 ± 10	522 ± 10	506 ± 10
$(CH_3)_3SiCH_2T$	556 ± 11	547 ± 11	566 ± 11
Specific activity ratio per molecule, $\left(\dfrac{TMFS}{TMS}\right)^c$	0.88 ± 0.03	0.86 ± 0.03	0.90 ± 0.03
Specific activity ratio per bond[d]	1.18 ± 0.04	1.14 ± 0.04	1.20 ± 0.04

[a] Additives including O_2 and ^3He. [b] Relative to the total HT yield as 1000. [c] Specific activity ratio per molecule = $(TMFS\text{-}t/P_{TMFS})/(TMS\text{-}t/P_{TMS})$. [d] Specific activity ratio per bond = $^4/_3 \times$ specific activity ratio per molecule.

ent work. However, its relative yields as shown in Table I are extremely small (only about 0.2 relative to HT as 100 compared with a relative yield of about 7 from the TMS system). This makes one suspect that the majority of the $(CH_3)_3SiT$ produced has been removed by some secondary reaction in the TMFS system. One way to test for this possible problem is to make a detailed product spectrum analysis for the TMFS–TMS competition data, and the result is as shown in Table IV for one of the three competition experiments listed in Table III.

Table IV: Product Spectrum Analysis for the Competition System of Recoil Tritium Reactions with Trimethylfluorosilane and Tetramethylsilane

Tritiated products	Observed parent yields[a]	Expected yields From TMS[b]	Expected yields From TMFS[c]	Total expected yields	Total observed yields
HT		527	503	1030	1000
CH_3T		82	51	133	127
$(CH_3)_3SiT$		38	1	39	34
$(CH_3)_2SiTF$		0	25	25	33
$(CH_3)_3SiCH_2T$	556	(556)	0	(556)	556
$(CH_3)_2SiFCH_2T$	513	0	(513)	(513)	513

[a] Relative to total HT = 1000 in this competition sample. [b] Relative to $(CH_3)_3SiCH_2T$ as 556, relative yields from ref 12. [c] Relative to $(CH_3)_2SiFCH_2T$ as 513.

From the analysis, it is obvious that the observed yields of the primary products are all approximately as expected from the sum of those from the individual systems. In particular, the combined yield of $(CH_3)_3$-SiT expected from both systems is completely preserved in the presence of TMFS. This means its 0.2 value derived from recoil tritium reactions with TMFS alone is real and has not been subjected to any experimental complications.

Discussion

Comparison of Relative Yields of Products from Recoil Tritium Reactions with TMFS and with TMS. The agreement between results from different laboratories on the efficiently scavenged gas phase recoil tritium reactions with TMS are excellent.[10-12] In Table V, we have included these TMS results, corrected by 15% for decomposition except for HT,[22] with the similarly corrected average relative yields of products from TMFS systems derived from the gas phase data of Table I. These TMFS results were normalized to the TMS results by multiplying them by 0.88 which is the normalization factor per molecule derived from the competition experiments as shown in Table III. Then the normalized yield per molecule for each type of primary reaction was divided by the number of bonds in the molecule which is available for this particular kind of reaction. The normalized yields per bond for TMS and TMFS systems can be directly compared as given in Table V.

In normalizing the data, one basic assumption has been made. It is that the energy spectrum of the reacting tritium in these two individual systems are similar. In other words, the moderating properties of the systems are about the same. This assumption should be valid due to the similarities in structure of the two parent molecules. Strong support for this supposition comes from experiments with TMS and TMFS in a tritium energy spectrum normalized by a predominantly perfluorocyclobutene system.[23] A qualitative comparison of the HT and CH_3T yields in these normalized systems is about the same as that obtained in Table V.

Comparison of T-for-X Substitution Reactions; Evidence for Bond Strength Effect in Hot-Atom Substitution

(22) Halogen-scavenged TMS experiments have also indicated a 15% decomposition of the TMS-t being formed.

(23) S. H. Daniel, J. L. Williams, and Y.-N. Tang, unpublished results.

Table V: Normalized Yields of Products per Molecule and per Bond for Recoil Tritium Reactions with Trimethylfluorosilane (TMFS) and Tetramethylsilane (TMS) in the Gas Phase

Primary reactions		TMS yields		TMFS yields		
		Per molecule[a]	Per bond[d]	Relative yields[e]	Normalized per molecule[f]	Normalized per bond[d]
H abstraction		81	6.8	83	76	8.4
H substitution		(100)[b,c]	8.3	100[c]	88	9.8
CH₃ abstraction		15	3.8	10.2	9.0	3.0
T-for-X substitution	T-for-CH₃	6.8	1.7	4.9	4.3	1.4
	T-for-F			0.2	0.2	0.2

[a] From ref 11. [b] Used as an arbitrary standard for normalization. [c] Used as a standard for relative yields. [d] Relative yields per molecule divided by the number of bonds available for each type of reaction. [e] Average of the yields in Table I. [f] The relative yield multiplied by 0.88 which is the normalization factor per molecule derived in Table III.

Processes. The purpose of this work is to study the T*-for-X substitution reactions for different X's in molecules which have the same residue part. In doing this any secondary effect on the substitution process due to the difference in the central atom or other substituents is eliminated.[5] Moreover, since the same product molecule is formed, any *difference* in results due to the decomposition of primary products are also minimized.[6,14-16] As a result, any observed difference in the normalized yields of T-for-X substitution product should reflect only the direct effect of X itself on the substitution process.

There are two major ways an X can be directly involved in effecting its own substitution reactions: one is through its physical geometrical properties of mass and size[5] and the other is through its chemical characteristics such as its electron affinity or electron-sharing abilities which shows up in its bond strength with the central atom.[6-8]

Earlier work on recoil tritium substitution for X in the series of compounds CH₃-F, CH₃-H, CH₃-Cl, CH₃-Br, and CH₃-I had demonstrated that the strength of the CX bonds is probably the most predominant controlling factor.[8,24] In these cases, the residue parts are all CH₃. It is the primary purpose of the present experiment to check whether the bond strength effect is also operating in other systems, especially when all the other three substituents are heavy groups.

In this work, the comparison of T-for-F substitution in TMFS with T-for-CH₃ substitution in TMS essentially deals with one variable, namely, the bond strength. The residue part for the substitution, Si-(CH₃)₃, and the resultant product, Si(CH₃)₃T, are exactly the same for both parent molecules. Any observed difference should therefore be due to the leaving groups, F and CH₃. Among the physical geometrical properties of F and CH₃, the difference between their masses is relatively small (19 *vs.* 15) and is not enough to cause any major discrepancy in reactivity. The radius of a CH₃ group is approximately twice that of F. However, a majority of the collisions are going to

take place at the CH bonds, giving the tritium-labeled parent molecules as the product as witnessed by its extremely high yield. The effective volume available for T-for-CH₃ substitution at the SiC bond is probably the same order of magnitude or at most only slightly larger than that for T-for-F reactions. This means the relative size is not responsible for a significantly higher yield in the T-for-CH₃ substitution over that from the T-for-F process. Consequently, any appreciable difference in Si(CH₃)₃T yield from the TMFS and TMS systems must be due to the difference in the bond strength of the SiF and SiC bonds.

Data in Table V clearly indicate that on the per bound basis T-for-CH₃ substitution in TMS is approximately ten times as likely as T-for-F substitution in TMFS (1.7 *vs.* 0.2). This in turn strongly suggests that bond strength is a major controlling factor in the hot-atom substitution reactions even when all the other three substituents are heavy groups. In TMFS, the SiF bond strength has been assigned a value of 193 kcal/mol, while the SiC bond strength in TMS is only 85 kcal/mol.[20] The lower T-for-F yield is evidently due to the substitution at a much stronger bond.

Inductive Effect for the Recoil Tritium Abstraction and Substitution Reactions. Data in Table V reveal that on the per bond basis both the abstraction and substitution for H at the CH bonds are more reactive while both the abstraction and substitution for CH₃ at the SiC bonds are less reactive in the case of TMFS when compared with those in the TMS system. This can be explained by an inductive effect due to the presence of an extremely electronegative atom, F, in the molecule TMFS.[6-8]

In the TMS molecule, the charge separation according to their respective electron-withdrawing power should be such that the C atom appears to be partially negative and both Si and H appear to be partially positive. As a result, both the SiC and the CH bonds con-

(24) Y.-N. Tang, Ph.D. Thesis, The University of Kansas, 1964.

tain certain ionic contributions in addition to the covalent components of the bond strength.

Replacing a methyl group in TMS by a very electronegative atom, fluorine, will cause the redistribution of electron density in the resulting molecule, TMFS. The inductive effect of the fluorine atom will lead to a more positive character in the neighboring bonded atoms. This effect is steadily diminished by distance down the chain. The *net* inductive effect caused by F on Si, C, and H in TMFS could be viewed as follows.

$$\overset{\delta-}{F} \longleftarrow \overset{\delta+}{Si} \longleftarrow \overset{\delta\delta+}{C} \longleftarrow \overset{\delta\delta\delta+}{H}$$
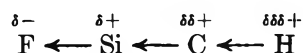
The result is such that in the SiC bond, a *net* partially positive charge is introduced to the Si end. This *extra* charge separation coincides and adds to the original ionic character of the bond, and as a result the bond should be strengthened. The corresponding reactivity of this SiC bond, therefore, should decrease in going from TMS to TMFS.

On the other hand, the inductive effect of F will cause a *net* positive charge to the C end of the CH bond. Since in the original TMS configuration, the C end is the negative end of the CH bond, this additional partially positive charge introduced by the inductive effect will therefore cancel part of the original ionic character of the bond. Since the ionic contribution of the CH bond becomes less, the CH bond in TMFS is therefore more reactive than that in TMS.

A comparison of the above predictions with the data given in Table V clearly demonstrates the presence of an inductive effect in the recoil tritium reactions caused by a fluorine atom. Furthermore, it shows that inductive effects operate not only for controlling reactions at CH bonds but also in controlling the reactivities of other types of linkages such as the SiC bond.

Kinetics of the Attack of Refractory Solids by Atomic

and Molecular Fluorine[1]

by Daniel E. Rosner*[2] and H. Donald Allendorf

Department of Engineering and Applied Science, Yale University, New Haven, Connecticut 06520, and AeroChem Research Laboratories Inc., Division of Sybron Corporation, Princeton, New Jersey 08540
(Received July 24, 1970)

The true high-temperature kinetics of the attack of molybdenum and tungsten surfaces by *atomic* fluorine have now been studied using microwave discharge-fast flow vacuum system techniques coupled with electrical resistance heating of the reacting specimens. Experimental results are reported herein covering the surface temperature range from 700°K to the sublimation thresholds of these metals, at estimated F atom pressures from 6×10^{-4} to 8×10^{-2} Torr. We also have carried out the corresponding experiments using *diatomic* fluorine at comparable fluorine gas pressures, and covering the same filament temperature range. For reasons having to do with the estimation of absolute F-atom concentrations, exploratory kinetic data are also included for the fluorination of titanium, graphite, and boron. It is shown that despite the well-known reactivity of molecular fluorine, prior dissociation produces a marked enhancement in the Mo- or W-atom removal probability at fluorine fluxes and surface temperatures corresponding to appreciable steady-state adatom populations. Interestingly enough, multiple local maxima appear in the Arrhenius diagram for the F-atom attack of Mo(s) and X(s); these maxima are attributed to the formation–desorption of distinct metal fluorides of widely disparate stoichiometry and thermodynamic stability. When one includes the observed high-temperature phenomenon of metal sublimation, it is shown that some metal atom removal rates can be achieved at five distinct surface temperatures. Mechanistic implications of these new results are discussed, together with suggested extensions of this work.

1. Introduction

Despite its toxicity and difficult handling properties, fluorine constitutes an attractive and potent oxidizing agent in many technological applications (*e.g.*, rocket propellants,[3] flash lamps[4,5]) demanding high combustion temperatures. Moreover, fluorine's extreme electronegativity and the volatility of its stable compounds with many metals and semimetals has led to its use in the recovery of valuable elements (*e.g.*, the fluoride volatility process for uranium and plutonium) and as an eligible transporting agent in incandescent filament bulbs.[4-6] Consequently, there have been numerous recent studies of the thermodynamic properties of fluorides,[7] as well as investigations of the rate of chemical attack of many elements and compounds (B, Si, C, Ni, ZrC, HfB, HfC, etc.) by gaseous *diatomic* fluorine.[8-11] Unfortunately, with the exception of the work reported in ref 8, 10, and 11 (performed at F_2 pressures below 10^{-7} atm), the reactivity and experimental techniques have been such that all "chemical kinetic data" above about 1000°K have been falsified by physical phenomena (vapor phase diffusion limitations) and hence cannot be generalized to other configurations, or used as the starting point for reasoning on a molecular level. In addition, despite the low dissociation energy[12] of the F_2 molecule, and the presence of appreciable F-*atom* concentrations in rocket propellant exhaust gases,[13] no studies have yet been reported of the reactivity of this

atom with refractory solid surfaces of current interest. These considerations, coupled with the mechanistic insights made possible by comparing fluorine atom and

(1) This research was supported by the U. S. Army Research Office, Durham, N. C., under Contracts DA31-124-ARO-429 and DAHCO4-70-C-0027. Revision and extension of AeroChem TP-233.

(2) Associate Professor, Chemical Engineering Group; to whom inquires concerning this manuscript should be sent.

(3) M. Farber, *Astronautics*, **34**, 40 (Aug 1960).

(4) L. M. Nijland and J. Schröder, *Philips Res. Rep.*, **21**, 304 (1966).

(5) J. Schröder, *ibid.*, **20**, 111 (1965).

(6) H. Schafer, "Chemical Transport Reactions," Academic Press, New York, N. Y., 1964.

(7) See, for example, R. A. Kent, *et al.*, *J. Inorg. Nucl. Chem.*, **28**, 1419 (1966), and *Proc. Conf. Nucl. Appl. Nonfissionable Ceram.*, 249 (1966); see also M. S. Chandrasekharaiah, Appendix B, in "Characterization of High-Temperature Vapors," J. L. Margrave, Ed., Wiley, New York, N. Y., 1967, p 503 ff.

(8) U. V. Henderson, Jr., H. P. Woods, and G. Poplin, in "Heterogeneous Combustion," Vol. 15, Academic Press, New York, N. Y., 1964, pp 203–226.

(9) A. K. Kuriakose and J. L. Margrave, *J. Phys. Chem.*, **68**, 2671 (1964); *ibid.*, **69**, 2772 (1965); *ibid.*, **68**, 390 (1964); *ibid.*, **68**, 2343 (1964).

(10) J. D. McKinley, *J. Chem. Phys.*, **45**, 1690 (1966).

(11) M. Metlay and G. E. Kimball, *ibid.*, **16**, 779 (1948).

(12) While the bond energy, $D_0°$, of $F_2(g)$ is still the subject of some controversy, with reported values ranging from 30.9 kcal/mol [V. H. Dibeler, J. A. Walker, K. E. McCalloh, *ibid.*, **50**, 4592 (1969)] to 36.7 kcal/mol [see, for example, the review given in JANAF Thermochemical Tables, Dow Chemical Co., Midland, Mich., 1966, Report PB 168 370-1 Clearinghouse for Federal Scientific and Technical Information, Arlington, Va.], it is certainly low compared with, *e.g.*, the well-established values $D_0°(Cl_2) = 57.2$ kcal/mol, $D_0°(O_2) = 118$ kcal/mol.

molecule data with our recently reported chlorine and oxygen attack data[14] on the same solids, motivated the experiments described herein.

2. Experimental Section

Atom Generation. In view of the reported successes of Vanderkooi and MacKenzie[15] and of Radford, *et al.*,[16] in the nonthermal generation of F atoms (for spectroscopic studies) using low-pressure electrodeless electrical discharges, and our previous experience with the microwave discharge production of Cl, O, N, and H atoms, the configuration we used for the generation of F atoms (Figure 1) was a slight modification of that described in ref 14. Gas mixtures of 1% F_2–99% Ar were passed through a 1 cm i.d., 30.5 cm long, dense alumina[17] tube (A, Coors AD-998) at about 1 Torr total pressure, and flow velocities of about 10^4 cm sec^{-1}. Surrounding the alumina tube was an Evenson-type 2450-mHz, microwave discharge cavity[18] (B) supplied by a 125-W Raytheon microwave power source. The electrical discharge products then entered a Pyrex test section (C) where they encountered the filament specimen (G) inserted on a monel probe holder mounted *via* a ground joint (I) in the rear. Downstream of the test section the gas mixture passed through a shallow, loosely packed 8–14 mesh activated alumina bed (to remove fluorine),[19] and then passed through a large (130 CFM) Kinney KDH-130 mechanical vacuum pump. Gaseous fluorine was supplied from a barricaded cylinder in accord with Matheson Co. recommendations.[20] Prior to entering the electrical discharge region, the impurity HF(g) was removed from the fluorine by passing the supply gas through a NaF trap run at 298°K. Aluminum- and Teflon-packed monel or stainless steel valves were used throughout. All stopcock greases and manometer oils were fluorinated hydrocarbons (supplied by Halocarbon Products Corp.). O-Rings were made of Viton A. A large aluminum ventilating hood was installed over the entire apparatus to rapidly remove fluorine in the event of an accidental leak in the gas supply system.

Filament Reaction Rate Measurements, Pyrometry. After using continuous electrical resistance measurements on the central 0.55 cm of some specimens (*cf.* Figure 1) to verify time independence of the reaction rate,[21] direct microscope determinations of mean filament diameter change, Δd, following an exposure of duration Δt (at temperature) were used to compute the corresponding mean substrate element flux. The variation in diameter change along the central portion of the filment was typically less than 8%, which was somewhat smaller than the repeatability of the mean reaction rate measurements as displayed in section 3. The resulting precision was more than sufficient to uncover interesting trends in reactivity, *e.g.*, the existence of multiple local maxima in the reaction rate *vs.* temperature relation for the F-atom attack of molybdenum and
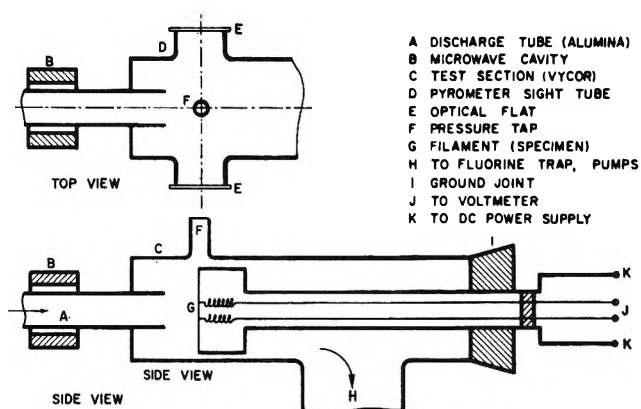
Figure 1. Filament fluorination apparatus (schematic).

tungsten (see Figures 2 and 4; section 3). Filaments used had initial outer diameters between 0.508 (20 mil) and 0.102 mm (4 mil). While the most extensive data pertain to the refractory transition metals molybdenum and tungsten, exploratory work was also done on titanium, an "isotropic" graphite, and an amorphous boron. Supplementary information on these materials is provided in Table I.

(13) Exceeding 10 mol % in the exhaust products of available high energy rocket propellants [see, for example, J. D., Batchelor, J. A. Simmons, and W. E. West, "Chemical Reactions between Plastic Composite Materials and Propellant Exhaust Products," Final Report No. ASD-TDR-63-737, Vol. I, Aeronautical Systems Div. AF Materials Laboratory, Nonmetallic Materials Div., Wright-Patterson AFB, Ohio, AD 422955, 1963]. It should also be remarked that atomic fluorine is thought to be an important decomposition product when Teflon ablates in high enthalpy air.

(14) D. E. Rosner and H. D. Allendorf, *J. Phys. Chem.*, **74**, 1826 (1970); *ibid.*, **72**, 4159 (1968): *ibid.*, **69**, 4290 (1965); *J. Electrochem. Soc.*, **114**, 305 (1967); *J. Chem. Phys.*, **49**, 5553 (1968); *ibid.*, **40**, 3441 (1964); *Carbon*, **3**, 153 (1965); *ibid.*, **7**, 515 (1969); *AIAA J.*, **8**, 166 (1970); *ibid.*, **5**, 1489 (1967); *ibid.*, **6**, 650 (1968); *ibid.*, **3**, 1522 (1965); review papers on this work are contained in "Proceedings, Third International Symposium on High Temperature Technology, "Butterworths, London, 1969, p 707; and "Heterogeneous Kinetics at Elevated Temperatures," Plenum Press, New York, N. Y., 1970, pp 231–251.

(15) N. Vanderkooi and J. S. MacKenzie, *Advan. Chem. Ser.*, **36** (1962).

(16) H. E. Radford, V. W. Hughes, and V. Beltran-Lopez, *Phys. Rev.*, **123**, 153 (1961).

(17) The protective $AlF_3(s)$ film which develops in the interior of the alumina tube has a lower vapor pressure than silicon fluoride [however, the vapor pressure of AlF_3 (10^{-2} Torr at $T \approx 1030°K$) is not so low that the tube could be used as a clean F-atom source at temperatures high enough to *thermally* dissociate $F_2(g)$]. Incidentally, the vapor pressures for $AlF_3(s)$ tabulated in the "Handbook of Chemistry and Physics," 49th ed, Chemical Rubber Publishing Co., Cleveland, Ohio, and in "Chemical Engineers Handbook," J. H. Perry, Ed., McGraw-Hill, New York, N. Y., 1950, are too low, apparently owing to an error in transcribing temperatures (from °C to °K) from the source reference.

(18) F. C. Fehsenfeld, K. M. Evenson, and H. P. Broida, *Rev. Sci. Instrum.*, **36**, 294 (1965); commercially available for Ophthos Instrument Co., Rockville, Md.

(19) We are indebted to Professor J. Margrave and Dr. R. Lagow of Rice University for calling this technique to our attention. Depletion of the alumina was monitored by periodically testing for fluorine (using KI paper) in the gas leaving the bed.

(20) "Matheson Gas Data Book," 4th ed, Matheson Co., Inc., East Rutherford, N. J., 1966, p 237.

(21) Only for reactions forming nonvolatile, semiprotective reaction products (or reactions involving gas dissolution into the specimen) would the reaction rate be time dependent.

Table I: Filament Specimen Data

Material	Supplier	Density[a]	Remarks[b]
Molybdenum	Westinghouse	10	Drawn wire
Tungsten	Westinghouse	19	Drawn wire
Titanium	Materials Research Corp.	4.4	Marz grade wire[c]
Graphite	Speer Carbon Co.	1.7	Electrographitic extruded rod
Boron	Texaco Experiment Inc.	2.3	Pyrolytically deposited on W-substrate

[a] Estimated nominal density, g cm^{-3}, at reaction temperature. [b] Consult ref 14 for further details on material characterization or reactivity in high-temperature oxidizing environments. [c] Present work.

During the course of an experiment the filament power dissipation was adjusted to maintain constant apparent ("brightness") temperature. The latter was obtained using an optical pyrometer (Pyro Instrument Corp., Bergenfield, N. J.) in the nominal temperature range $T \geq 1000°K$, and an infrared detector (API Instruments Co., Chesterland, Ohio) in the nominal temperature range $660 \leq T \leq 1260°K$. Absolute values of the surface temperatures reported were determined by correlating the brightness temperature of the filament with that inferred from its electrical resistance when the filament was exposed to a very dilute F_2–Ar mixture ($p_{F_2}/p_{Ar} \approx 0.6 \times 10^{-3}$) to simulate a possible emittance correction due to adsorbed fluorine.

Measurements at differing total argon–fluorine flow rates were used to rule out the existence of physical limitations[22] on the reported reaction rates. Despite the high filament temperatures attained herein (which, at equilibrium, would be sufficient to completely dissociate fluorine) it is likely that, in the absence of the microwave discharge, F_2 molecules indeed strike the filament owing to inadequate residence time in the filament thermal boundary layer. If the latter is estimated as d^2/D_{F_2-Ar} (where D_{F_2-Ar} is the Fick interdiffusion coefficient and the characteristic time for F_2 dissociation in the gas phase is taken to be $(k_{d,Ar} n_{Ar})^{-1}$ (where $k_{d,Ar}$ is the appropriate homogeneous dissociation rate constant[23] and n_{Ar} is the argon number density), then, at $2000°K$, the F_2-molecule residence time in the thermal layer is too short by over four orders of magnitude.

F-Atom Concentration Determination. Measurement of the atom concentration is important since a microwave discharge is not expected to dissociate every F_2 molecule passing through it. In our previous work on heterogeneous reactions of O, Cl, N, and H atoms, both chemiluminescent "titration" reactions and calorimetric probes have been used to infer relative and absolute atom concentrations. Of course, the convenience of these methods immediately suggested their ex-

tension to fluorine. However, as noted below, our initial attempts to use such methods failed, so that recourse to a less direct estimate of p_F proved necessary.

The simultaneous presence of reactive F_2 molecules seriously complicates conventional titration methods. For example, the sequence

$$F + NOCl \longrightarrow NO + FCl$$

$$F + NO \longrightarrow NOF + h\nu$$
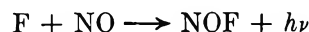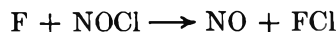
would be complicated by the parallel reaction with F_2

$$F_2 + NO \longrightarrow NOF + F$$
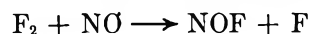
as well as by the reaction of F_2 with NOCl. Preliminary measurements were made of the increased chemiluminescence accompanying microwave dissociation when fluorine and excess NO were mixed. These intensity ratios behaved in a complex manner with increased fluorine flow rate, thereby precluding a simple inference of absolute F-atom concentrations by these means. By analogy with a technique we have already exploited for Cl atoms, *relative* F-atom concentrations could conceivably be determined by following the expected fluorine recombination "afterglow" reaction: $F + F + M \rightarrow F_2 + h\nu$; however, owing to the low F_2 bond energy, this emission would occur in an experimentally inconvenient (ir) region of the spectrum.

Likewise, calorimetric detectors[24] (using Mo, W, Ni, Au, Ag, Pt, Re, or Co) proved unusable or unreliable due to (i) excessive exothermic fluorination of these materials and/or (ii) inadequate F-atom recombination coefficients on the resulting metal fluorides.

Pending the necessary further development of chemiluminescent titration and calorimetric methods, we devised the following indirect procedure for determining absolute F-atom concentrations. Filament reaction rate measurements were made with and without an electrical discharge for a wide class of materials (Mo, W, Ti, C, and B), most showing a local reaction rate maximum at elevated temperatures. Since it is theoretically unlikely that one F atom can, on the average, lead to the removal of more than one substrate atom, this condition and our maximum observed rates (for Ti and B) set a *lower* limit of about 1.6×10^{-2} Torr to the actual atom partial pressure at the specimen location. The atom pressure corresponding to *complete* dissociation (of every molecule entering the discharge region) is only 2×10^{-2} Torr; hence these two conditions alone bracket the F-atom pressure in the range 1.6×10^{-2} Torr $\leq p_F \leq 2 \times 10^{-2}$ Torr. Furthermore, examina-

(22) For a discussion of the possible falsification of heterogeneous reaction kinetics due to external diffusion limitations in flow systems, see, for example, D. E. Rosner, *Symp.* (Int.) *Combust.*, 11th, 181 (1967), and *AIAA J.*, 2, 593 (1964).

(23) See, for example, C. D. Johnson and D. Britton, *J. Phys. Chem.*, 68, 3032 (1964), and R. W. Diesen, *J. Chem. Phys.*, 44, 3663 (1966).

(24) See, for example, E. A. Ogryzlo, *Can. J. Chem.*, 39, 2556 (1961), and D. E. Rosner, *Jet Propul.*, 32, 1065 (1962).

tion of the F-atom and F_2 data for molybdenum revealed that if $p_F \geq 1.7 \times 10^{-2}$ Torr, then the maximum reaction probability for F_2 would *exceed* that for F atoms, an intrinsically unlikely situation for surfaces forming volatile reaction products[14] and unprecedented for the oxidation or chlorination of molybdenum.[14] This additional condition leads us to conclude that p_F is in the acceptably narrow range, 1.6×10^{-2} to 1.7×10^{-2} Torr. In view of our previous experience with the chlorination of boron, for which the maximum inferred Cl-atom reaction probability was ≈ 1, all of our atom reaction rate data were treated assuming $p_F \approx 1.6 \times 10^{-2}$ Torr, corresponding to maximum F-atom reaction probabilities of unity for boron and titanium. Incidentally, an atom pressure of this magnitude corresponds to the dissociation of at least some 78% of the F_2 molecules entering the discharge region.[25] This circumstance, together with our F_2 kinetic data, revealed that the F_2 contribution to the reaction rates observed in the presence of the discharge was never more than 10%. Accordingly, reaction rate data for F atoms reported here have been corrected for the small F_2 contribution on the assumption that the F atom and F_2 contribution are additive. To facilitate an understanding of the atomistic implications of the observed rates (see section 4) all data are reported below in the form of a dimensionless *substrate atom removal probability*, ϵ, calculated as

$$\epsilon \equiv \mathcal{E}_{(S)}/Z_i \tag{1}$$

where $\mathcal{E}_{(S)}$ is the "evaporative" flux of substrate atoms S(S $\equiv$ Mo, W, Ti, C, or B) *regardless of their chemical state of aggregation* and Z_i is the arrival (collision) rate of species i ($i \equiv$ F or F_2) per unit area corresponding to the prevailing reactant pressure, p_i, and surface temperature T. Thus, $\mathcal{E}_{(S)}$ can be inferred from the *measured* rate $\Delta d/\Delta t$ (*via* the specimen density), and

$$Z_i = \frac{1}{4}\frac{p_i}{kT}\left(\frac{8kT}{\pi m_i}\right)^{1/2} \tag{2}$$

where k is the Boltzmann constant and m_i is the mass of oxidizing species i ($i =$ F, F_2). *It is noteworthy that no assumptions regarding product molecule identity enter the calculation of ϵ.*

Below the temperature at which the specimen surface sublimes at a measurable rate, ϵ attains some maximum value, denoted ϵ_{max}. Our measurements and the reasoning on p_F outlined above, lead to the values of ϵ_{max} estimated in Table II. Whereas it might appear from this summary that the F atom has a reactivity comparable to its parent F_2 molecule, this is certainly *not* true at lower temperatures (than those pertaining to ϵ_{max}), as will be demonstrated in section 3. Moreover, on an open, covalently bonded material like graphite,[26] even at their respective peak probabilities, F atoms are more efficient oxidizers than F_2 molecules, presumably be-

Table II: Maximum Inferred Substrate Atom Removal Probabilities[a]

Specimen	F atoms	F_2 molecules[a]
Boron	1 (≥ 1370)[b]	
Graphite	0.3 (1170)	0.1 (1085)
Titanium	1 (1850)	1.5[c](1850)
Molybdenum	0.4 (2090)	0.4 (2090)
Tungsten	0.2 (1980)	0.1 (1980)[d]

[a] At $p_F = 1.6 \times 10^{-2}$ Torr or $p_{F_2} = 1.0 \times 10^{-2}$ Torr, unless otherwise specified. [b] Approximate surface temperature (in °K) at which ϵ_{max} is achieved. At the prevailing fluorine pressures these were local extrema in all cases except Ti. Since our kinetic data on Mo and W are most extensive, only these metals are discussed below (see sections 3 and 4). [c] Owing to the definition of ϵ, values in excess of unity for F_2 attack merely imply the existence of appreciable titanium monofluoride desorption. If every incident F_2 molecule led to the formation-desorption of one TiF molecule, then ϵ would be 2. [d] At $p_{F_2} = 3 \times 10^{-2}$ Torr.

cause of their higher sticking probabilities on such surfaces at low adatom coverages (see section 4).

3. Experimental Results

The Fluorination Kinetics of Molybdenum and Tungsten. Using the F-atom pressure estimates and eq 1 and 2 of section 2, our experimental data on the temperature and reactant pressure dependence of the molybdenum fluorination rate have been cast in terms of Mo-atom removal probabilities, ϵ, with the results shown plotted in Figures 2 and 3. Note that near 1000°K as many as about 100 F_2 molecule strikes are (on the average) required to remove an Mo atom from the filament; however, at this same temperature only some 6 or 7 F *atoms* are required to accomplish this same feat. At present reactant pressures, only near and above 2000°K, does ϵ become nearly the same for F atoms and F_2. Moreover, ϵ_{max} appears at about the same temperature (≈ 2100°K at these fluorine pressures) for F or F_2. A particularly interesting and new feature exhibited by these data is the existence of *two* distinct local maxima in the $\epsilon(T)$ relation prior to the onset of appreciable sublimation.[27] Thus, there is a

(25) For diatomic chlorine passing through the microwave cavity under comparable power conditions, the dissociation "efficiency" was only about 22%.[14]

(26) We anticipate the same conclusion for F and F_2 attack of boron (*cf.* our analogous work on the chlorination kinetics of boron[14]); however, in the only previous kinetic work on the high-temperature B(s)–F_2(g) reaction (ref 8) it is stated that virtually every incident F_2 molecule must have produced a BF(g) molecule above about 1200°K, a quantitative conclusion at variance with our expectations, and apparently unjustified in view of the uncertainties in p_{F_2} and sensitivity in the F_2-jet/target/mass spectrometer configuration employed by Henderson, *et al.*[8]

(27) In Figures 2 and 4 the straight line marked "sublimation" is the locus of apparent values of ϵ corresponding to the setting $\mathcal{E}_{(S)}$ in eq 1 equal to the vacuum sublimation rate of the substrate S at each temperature T. Experimental data (*cf.* points) are seen to follow nicely the trend anticipated based on available vapor pressure
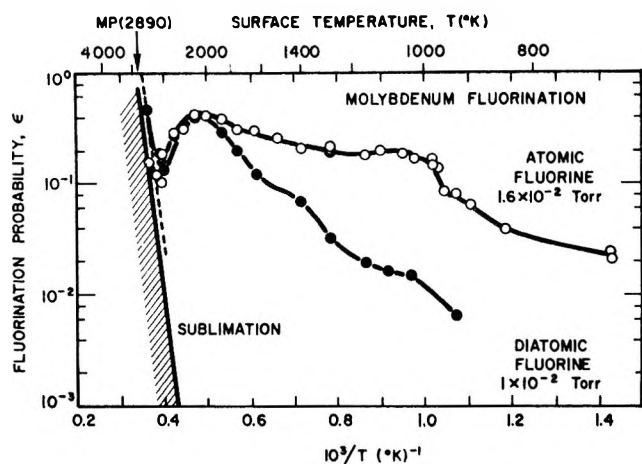
Figure 2. Temperature dependence of reaction probabilities for the attack of molybdenum by fluorine atoms and molecules.
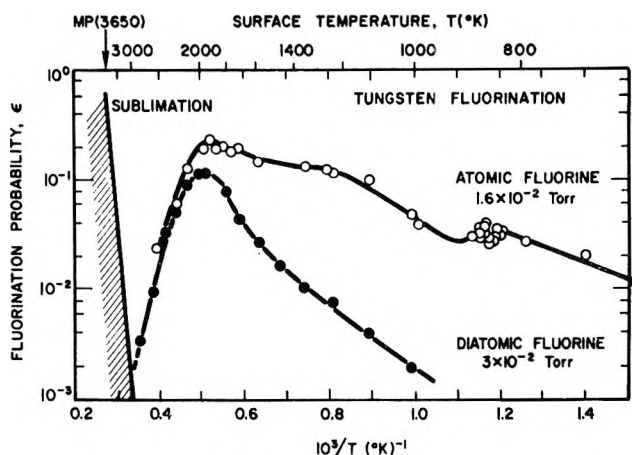
Figure 4. Temperature dependence of reaction probabilities for the attack of tungsten by fluorine atoms and molecules.
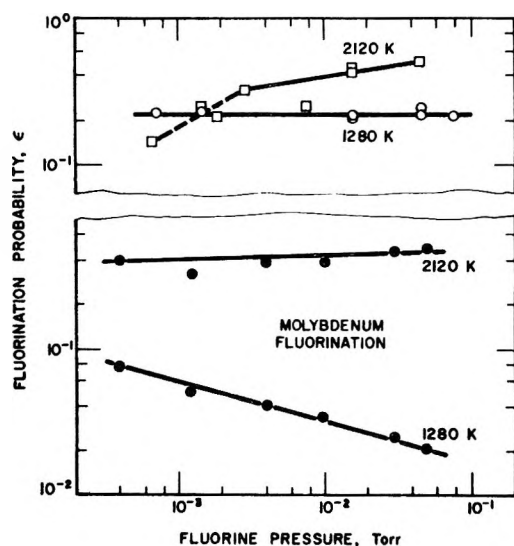
Figure 3. Dependence of molybdenum fluorination probabilities on fluorine pressure: O and □, F atoms; ●, F₂.
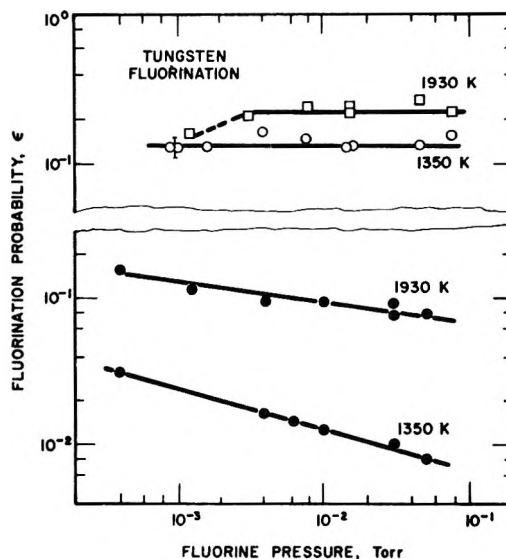
Figure 5. Dependence of tungsten fluorination probabilities on fluorine pressure: O and □, F atoms; ●, F₂.

narrow range of conditions under which *the same Mo-atom removal rate is achieved at five distinct temperatures.*

If it is assumed that the microwave discharge efficiency for atom production is insensitive to the initial F_2 mole fraction in the feed gas, which is reasonable in the present case since the F_2 mole fraction in the gas entering the discharge region never exceeded 5%, then the inferred p_F dependence of the molybdenum fluorination probability is displayed in Figure 3 (together with the corresponding data for F_2, obtained in the absence of the electrical discharge). Near ϵ_{max}, it appears that ϵ is insensitive to fluorine pressure;[28] however, at lower temperatures ϵ remains p_F insensitive but decreases with increasing F_2 pressure.

We have found qualitatively similar trends for the fluorination of tungsten (see Figures 4 and 5); however, in this case, the reaction rate "trough" preceding sublimation is obviously considerably deeper. Thus, after

passing through ϵ_{max} values of the order of 0.1[29]–0.2, higher temperatures cause ϵ to *decrease* by about two orders of magnitude before the anticipated sublimation contribution (see Figure 4). Note that multiple maxima are again observed in the $\epsilon(T)$ relation for F

data for Mo. [See, for example, Ya. I. Gerasimov, *et al.,* "Chemical Thermodynamics in Nonferrous Metallurgy," Vol. III, Israel Program for Scientific Translations (from the Russian), Jerusalem, 1965.] The dashed contour in Figure 2 pertains to $\epsilon_{vap}(T)$ for the F_2-molecule case. Incidentally, the lower temperature rate maximum was much more distinct in our tabular data and large working graphs than would appear from Figure 2.

(28) That is, $\epsilon_{(Mo)}$ is nearly linear in fluorine pressure. Such cases are conventionally termed "first order" in reactant pressure.

(29) In a study oriented toward the electron affinity of F_2 and its dissociation probability on tungsten filaments, Metlay and Kimball[11] (working at $p_{F_2} = 2.4 \times 10^{-3}$ Torr, $1900 \leq T \leq 2250°K$) reported some W-fluorination rate data yielding values of ϵ of the order of only 10^{-2}, with $\epsilon \propto p_{F_2}^{-1}$. Despite differences in experimental technique and conditions, their magnitudes and trends cannot be reconciled with the more extensive W-fluorination data reported here.

atoms, with the low-temperature maximum (now near 850°K) being more prominent[30] than for the corresponding Mo fluorination (cf. Figure 2).

Comparing the fluorination kinetic results on molybdenum and tungsten we see that in both cases the enhancements in ϵ due to fluorine dissociation exceed an order of magnitude below about 1200°K (at these fluorine pressures). Over most of the temperature range investigated, F and F_2 attack molybdenum more "efficiently" than tungsten, but below about 830°K the F-atom reaction rate appears to be be comparable on both metals. The local reaction rate maxima appear at higher temperatures for molybdenum; however, in this case sublimation sets in at a lower temperature. An important practical consequence of the resulting deep ϵ-trough for tungsten is that a W specimen would have a surprisingly long life in a fluorine-containing atmosphere under these particular conditions. For example, instead of being efficiently "gasified" when exposed to a "cold" F_2 beam, such a specimen would be expected to act primarily as a high-temperature F-atom source (see section 4).

4. Discussion

Beyond the immediate relevance of our experimental results to the prediction of corrosion and volatilization rates of these refractory solids in fluorine-containing atmospheres, it is instructive, and not altogether premature, to consider some of the mechanistic implications of these new data within the framework of previous kinetic and thermodynamic studies in chemically analogous systems. Such considerations are partly speculative, being based on only a fraction of the total experimental information one would desire on these systems. However, they can suggest (often by a process of elimination) self-consistent models of events at the gas-solid interface and thereby help, (i) anticipate the results of future experiments or applications, and/or (ii) pinpoint fruitful areas for future experimentation and kinetic analysis.

Undoubtedly, the most interesting new phenomenon encountered in the present F-atom study is the clear existence of multiple local maxima (i.e., "structure") in the resulting metal atom removal rates as a function of temperature (see Figure 2 and, in particular, Figure 4). Despite the fact that at present only the metal hexafluorides, $MeF_6(g)$, are well known and characterized,[31] the most plausible explanation for this behavior is the formation-desorption of at least two distinct metal fluorides, with each becoming dominant at a distinct surface temperature below the metal sublimation threshold.[32] For example, if $\mathcal{E}_n$ represents the evaporation rate of $MeF_n(g)$ (Me = Mo or W; $n = 0, 1, 2, \ldots$, 6) and we neglect the role of polymers of MeF_n, then

$$\mathcal{E}_{(Me)} = \sum_{n=0}^{6} \mathcal{E}_n \tag{3}$$

From its defining equation (eq 1) the metal atom removal probability would, therefore, be the sum of a number of contributions, i.e.

$$\epsilon = \sum_{n=0}^{6} \epsilon_n \tag{4}$$

where

$$\epsilon_n \equiv \mathcal{E}_n/Z_t \tag{5}$$

Product molecules corresponding to most of the eligible valence states of molybdenum and tungsten have in fact been observed in recent low-pressure kinetic studies of the $Me-O_2$ reactions;[33] however, in neither of these cases did the sum $\mathcal{E}_{(Me)}$ reveal more than local maximum. Their appearance here suggests that fewer product species are formed in the present case, with more widely disparate stoichiometries and thermodynamic stabilities (e.g., MeF_6 and MeF (?); see below).

Perhaps equally important are the high absolute probabilities observed for Me-atom removal per F-atom strike over the entire temperature range from about 700 to 2100°K. Indeed, as shown in Appendix A, if the "low"-temperature ϵ maximum is mainly due to the formation-desorption of the metal hexafluoride, $MeF_6(g)$, then our molybdenum data (at $T \approx 1000°K$) reveal that nearly every incident F atom is being utilized for reaction product formation, i.e., a negligible fraction immediately reflect, or initially "stick," but subsequently re-evaporate as F or F_2. Even allowing for present uncertainties in the exact product distribution, and/or absolute F-atom concentration (see section 2), it is quite clear that one cannot neglect product formation-desorption (compared to direct or associative fluorine desorption) in considering the steady-state adatom population balance,[34] an observation which has important implications in considering the reaction order near ϵ_{max} (see below).

The much lower values of ϵ for the $Me(s)-F_2(g)$ reactions observed here below about 2000°K are undoubt-

(30) Indeed, there is even the hint of "structure" within the low-temperature W-removal maximum. This narrow temperature interval will bear further investigation.

(31) See, for example, A. B. Burg in "Fluorine Chemistry," J. H. Simons, Ed., Vol. I, Academic Press, New York, N. Y., 1950, Chapter 2.

(32) A less likely alternative would be the production of a single product molecule by a number of distinct mechanisms, each assuming importance at a different surface temperature. This molecule could not be $MeF_6(g)$, however, since in the case of ϵ_{max} for F-atoms could never exceed $^1/_6$. (See Figures 2 and 4 and the discussion below.)

(33) J. B. Berkowitz-Mattuck A. Buchler, J. L. Engelke, and S. N. Goldstein, J. Chem. Phys., 39 2722 (1963), and P. O. Schissel and O. C. Trulson, ibid., 43, 737 (1965).

(34) While evidently not valid here, the assumption of local adsorption-desorption equilibrium, allowing the use of nonreactive adsorption isotherms in the rationalization of kinetic data, is frequently permissible in the study of surface-catalyzed reactions involving relatively stable reactants. Similar approximations have also been invoked by J. A. Becker, E. J. Becker, and R. G. Brandes [J. Appl. Phys., 32, 411 (1961)] and P. O. Schissel and O. C. Trulson (see ref 33) in analyzing the $W(s)-O_2(g)$ reaction under conditions such that $\epsilon \leq 10^{-2}$. See also, D. F. Ollis, H. G. Lintz, A. Pentenero, and A. Cassuto, Surface Sci., in press.

edly the result of a lower chemisorption probability of $F_2(g)$ on highly populated (fluorine adatom covered) metal surfaces. While never studied directly for Cl_2 or F_2, a sharp decrease in sticking probability, s, is known to occur for O_2 above a threshold coverage on many transition metal surfaces.[35] Thus, only when the metal surface is comparatively bare can one expect s to be high for both atoms and molecules. As discussed below, this would explain the comparable reactivity of F and F_2 observed at and above about 2000°K (see Figures 2 and 4, also the discussion of ϵ_{max} below).

Particularly in a chemical system in which each product molecule desorbed can involve as many as six reactant gas atoms,[36] and perhaps as few as one we should be surprised if the temperature or pressure dependence of the reaction rate were *simple* (e.g., the observed first-order kinetic behavior for the Me–F reactions below 2000°K, see Figures 3 and 5) rather than complex. It is precisely for such systems that one seeks "quasi-equilibrium" postulates in the hope of drastically reducing the number of kinetic "constants" necessary to describe the observed kinetic behavior. The encouraging recent results of Batty and Stickney[37] in applying a one-constant quasi-equilibrium (QE) model to the well-studied $W(s)$–$O_2(g)$ reaction led us to inquire if a similar model could account for the observed multiple maxima and reactivity "trough" described in section 3 for the $W(s)$–$F(g)$ reaction. According to this model, all eligible reaction products are considered to be in thermochemical equilibrium with the substrate and to evaporate (as from a Knudsen cell) at a total reactant element flux fixed (in the steady state) by the rate of reactant element *adsorption*. The latter is written as the product of a sticking (or "equilibration")[37] probability and the element arrival rate. When applied to the $W(s)$–$O_2(g)$ system (for which sufficient thermochemical data are available) a single functional "fit": $s(T;p_{O_2})$ enabled most product molecule desorption trends (and even some absolute values) to be "predicted" remarkably well.[37] Despite the *ad hoc* nature of the $s(T;p_{O_2})$ choice, if the QE model were equally successful in other complex chemical systems, it could prove quite useful. Unfortunately, when applied to available W–F system thermochemical data and the present $\epsilon_{(W)}$ data for the $W(s)$–$F(g)$ reaction (as done in Appendix B), the QE method failed to predict either (i) a transition from $WF_6(g)$ to $WF(g)$ at temperatures approaching 2000°K (considering W-element conservation), or (ii) a transition from $WF_6(g)$ to $F(g)$ desorption at temperatures in excess of 2000°K (considering F-element conservation). We tentatively conclude that either the quasi-equilibrium model fails badly for this atom–solid reaction, or perhaps equally likely, the required thermochemical data are either incomplete (*i.e.*, important tungsten fluorides other than those for $n = 1, 6$ are omitted) or inaccurate (for WF-(g), which appear to be on rather weak grounds).[38]

Inspection of eq A3 and the ancillary estimates below reveal that evaporative loss of adsorbed F atoms[39] can readily explain the *decrease* of ϵ at surface temperatures above that at which ϵ_{max} is attained. Indeed, the fact that this decrease in ϵ does not set in until temperatures in excess of 2000°K at our pressure levels is indicative of the existence of rather tightly bound F atoms on the Me surface. For example, if $\mathcal{E}_F$ is estimated from the absolute rate theory expression

$$\mathcal{E}_F = N_s\theta\left[\frac{kT}{h}\exp\left(-\frac{E_{des}}{RT}\right)\right] \qquad (6)$$

(where N_s is the total number of binding sites per unit surface area, θ is the fraction of sites "covered," h is Planck's constant, E_{des} is the desorption activation energy and R, the universal gas constant), then by making reasonable order of magnitude estimates of $N_s\theta$ and E_{des}, one can compute $\mathcal{E}_F$ and compare it to sZ (the adsorption rate of fluorine) at several temperature levels. Taking E_{des} to be comparable to the single Me–F bond energy (≈ 110–120 kcal/mol)[7] and $N_s\theta \approx 10^{15}$ cm^{-2} one finds[40] that F-atom evaporation would be negligible at 2000°K, but already appreciable at 2500°K, in complete accord with the location of the ϵ trough in Figures 2 and 4.

If the evaporation rate of tightly bound F(ads) is indeed negligible at $T \approx 2000°$K compared with

$$\sum_{n=1}^{6} n\mathcal{E}_n$$

then one can immediately rationalize the fluorine pressure insensitivity of ϵ at $T \approx 2000°$K as follows. Regardless of the reaction mechanism and product stoichiometry (*i.e.*, whatever the dependence of the reaction rate on $N_s\theta$), in the absence of appreciable direct F-atom desorption, the loss of F atoms *via* product desorption must be equal to the *adsorption* rate ($s_F Z_F$ or $2s_{F_2}Z_{F_2}$). Then ϵ_{max} will be proportional to the sticking probability[41] s and will be fluorine pressure indepen-

(35) D. O. Hayward and G. M. W. Trapnell, "Chemisorption," Butterworths, London, 1964.

(36) The WF$_6$ molecule has a bipyramidal structure in which the central W atom is linked to six symmetrically placed F atoms, each located at a W–F bond distance of 1.83 Å. The F–W–F bond angle is 90° (*cf.* JANAF Thermochemical Tables, see ref 12).

(37) J. C. Batty and R. E. Stickney, *J. Chem. Phys.*, **51**, 4475 (1970).

(38) See JANAF Thermochemical Tables in ref 12.

(39) *Associative desorption* (of F_2) can be shown to be thermodynamically unfavorable at all temperatures above about 800°K. Therefore, over most of the temperature range investigated here, $\mathcal{E}_{F_2}$ can be neglected as an F-element loss term (*cf.* eq A3). A high-temperature decrease in ϵ is sometimes alternatively attributed to a decrease in the sticking probability, s, but the experimental evidence for this unlikely assignment is rather meager, especially since the lower steady-state atom coverages associated with higher temperatures, if anything, favor *increased* s.

(40) A typographical error notwithstanding, this same site density was used in our previous adatom desorption estimates for the B(s)/Cl(g) reaction [see footnote 18 in *J. Phys. Chem.*, **72**, 4159 (1968)].

(41) If only a single reaction product, MeF$_n$(g), were produced, the proportionality constants would be, respectively, $1/n$ (for F-atom attack) and $2/n$ (for F_2 attack); *cf.* eq A3.

dent in either case. Of course, the nature of the ϵ decrease at higher temperatures will depend upon the details of the reaction mechanism. For example, if (i) only the metal monofluoride is formed, at a rate proportional to $k_{rxn}(T)\theta$ and (ii) $s \approx$ constant, then, prior to the onset of appreciable sublimation, one would find

$$\frac{s}{1 + (k_{des}/k_{rxn})} = \begin{cases} \epsilon & \text{(F atoms)} \\ \epsilon/2 & \text{(F}_2\text{)} \end{cases} \quad (7)$$

where $k_{des}(T)$ may be identified with the bracketed term in eq 6 and s_F need not equal s_{F_2}. Results of this form reveal that when ϵ drops well below ϵ_{max} the temperature dependence of ϵ will be largely that of k_{rxn}/k_{des}, which is likely to be dominated by that of k_{des}. Thus, the steepness of the ϵ descent is expected to increase with the magnitude of the binding (or desorption) energy E_{bind}. In the present case, there was no observable difference in steepness for all four reactions studied (Mo–F, Mo–F$_2$, W–F, and W–F$_2$; cf. Figures 2 and 4), as might be expected from the chemical similarities involved in the Me–F bonding.

Two important corollaries of the above reasoning are that for comparable sticking probabilities and reactant pressures the temperature at which ϵ_{max} is attained should (i) increase with adatom binding energy and (ii) be similar for both atom and molecule attack of the same solid. Comparing the oxidation, fluorination, and chlorination of the same metal, and assuming that E_{bind} follows the same trends as $D_0°(\text{MeX})$, where $X \equiv O$, F, or Cl; Me $\equiv$ Mo or W, one would expect ϵ_{max} to occur at the lowest temperature for metal chlorinations, at intermediate temperatures for metal fluorinations and at the highest temperatures for metal oxidations. Our experimental data (Figure 2 and ref 14) reveal that this is indeed the case for the attack of polycrystalline molybdenum, which we have studied most extensively.[42]

We conclude this discussion with the caveat that our attributing the enhanced reactivity of microwave-discharged fluorine exclusively to the presence of ground-state F atoms is at this time a highly plausible inference. While direct and indirect measurements using microwave-discharged oxygen, chlorine, hydrogen, or nitrogen have never provided us[14] with evidence of an important reactivity contribution from other species (e.g., electronically excited molecules), direct confirmation of this fact for the Me–F system (Me = Mo or W) must await the further development of reliable absolute F-atom detectors.

5. Conclusions

Based on our experimental data and the foregoing discussion, the following conclusions have been drawn.

1. It has indeed been possible to extend our previously developed microwave discharge, fast flow-vacuum flow system, filament reactor techniques to obtain the first available kinetic information on F atom-

surface reactions at elevated temperatures. F-Atom data on polycrystalline molybdenum and tungsten are reported here in the temperature range from about 700°K to their respective sublimation thresholds and at F-atom pressures in the nominal range 6×10^{-4} to 8×10^{-2} Torr. Preliminary kinetic data are reported for the fluorination of titanium, graphite, and boron by F atoms and F$_2$.

2. Despite the well-known reactivity of molecular fluorine, prior dissociation of fluorine produces a marked enhancement in the W- or Mo-removal probability at temperatures corresponding to appreciable steady-state adatom populations. At the present fluorine pressures these enhancements are over one order of magnitude at temperatures below 1200°K (cf. Figures 2 and 4). A comparison of our results on the two metals also reveals that both F and F$_2$ attack molybdenum more efficiently than tungsten, although the F-atom reaction probability below about 800°K is similar for both materials.

3. Multiple local maxima appear in the Arrhenius diagram for the F-atom attack of Mo and W; these maxima are attributed to the formation–desorption distinct metal fluorides of widely disparate stoichiometry and thermodynamic stability. When one includes the phenomenon of metal sublimation, in some cases the same total metal element removal rate can be achieved at five distinct surface temperatures (see Figures 2 and 4). The local reactivity maxima appear at higher temperatures for molybdenum than for tungsten; however, molybdenum sublimation sets in at a lower temperature. Close to 3000°K (at the present fluorine pressures), ϵ for W-atom removal is considerably below 10^{-2}, suggesting extensive re-evaporation of unreacted F atoms from the tungsten surface at this temperature [i.e., short residence times for F(ads)].

4. Under most conditions investigated, the F-atom reactions on molybdenum and tungsten are approximately first order, resulting in a p_F-insensitive reaction probability. In contrast, the corresponding F$_2$ reactions are first order only near the high-temperature rate maximum, being noticeably fractional order at lower temperatures (see Figures 3 and 5). This latter trend, together with our Arrhenius plots (Figures 2 and 4), imply that an increasing fraction of F$_2$ molecules reflect off the surface as the steady-state coverage of adsorbed fluorine increases. The high reactivity of F atoms under these same coverage conditions reveals the ability of a much larger fraction of incident atoms to successfully form Me–F bonds (Me = Mo or W), ultimately leading to the desorption of metal fluoride vapors.

Further insight into the causes of the large reactivity enhancements which we find attending fluorine disso-

(42) However, on this basis, our tungsten chlorination results[14] indicated an anomalously high temperature at ϵ_{max} (compared to the present results). This suggests the need for a re-examination of thermodynamic and kinetic data in the W–Cl system.

ciation at temperatures below 2000°K must await additional experiments, including the introduction of new measurement techniques. Foremost among these would be mass spectrometric sampling of the reaction products,[10,33] perhaps, ultimately, in combination with reactant beam modulation techniques.[43] However, the present methods have made possible, for the first time, a survey of F-atom reactivity on a variety of refractory solids. While this survey has only just begun, a number of interesting kinetic features are already evident. We hope that these initial measurements and the accompanying discussion will stimulate further activity in this important but hitherto unexamined area of gas–solid reaction kinetics.

Appendix A.

Relationship between ϵ and Adsorption Probability

It is instructive to examine the relationship between species desorption rates, the "sticking" probability,[44] s, and our reported steady-state values of ϵ, since several important conclusions follow which are "model-free." This interrelation follows immediately from the observation that in the steady state the total F-element evaporation rate must be supplied by those incident F atoms which did not immediately reflect. Thus, for F-atom attack we have (in the notation of sections 2 and 4)

$$sZ_F = \mathcal{E}_F + 2\mathcal{E}_{F_2} + \sum_{n=1}^{6} n\mathcal{E}_n \qquad (A1)$$

where, an F-*element* balance in the case of F_2 attack, leads to the analogous relation

$$2sZ_{F_2} = \mathcal{E}_F + 2\mathcal{E}_{F_2} + \sum_{n=1}^{6} n\mathcal{E}_n \qquad (A2)$$

Combining these conservation relations with the defining eq 1 for ϵ and eq 4 yields

$$s \cdot \frac{\sum_{n=0}^{6} \mathcal{E}_n}{\mathcal{E}_F + 2\mathcal{E}_{F_2} + \sum_{n=1}^{6} n\mathcal{E}_n} = \begin{cases} \epsilon & \text{for F atoms} \\ \epsilon/2 & \text{for } F_2 \end{cases} \qquad (A3)$$

which clearly shows that ϵ for F atoms must satisfy the conditions

$$\epsilon \leq s \qquad (A4)$$

and

$$\epsilon \leq \sum_{n=0}^{6} \mathcal{E}_n \bigg/ \sum_{n=0}^{6} n\mathcal{E}_n \qquad (A5)$$

The latter equality holding only in the absence of *both* F-atom reflection $(1 - s = 0)$ *and* unreacted fluorine desorption $(\mathcal{E}_F = 0, \mathcal{E}_{F_2} = 0)$. Again, it should be emphasized that s need not be the same for F and F_2 in eq A1–A3.

Appendix B.

Quasi-equilibrium Model Predictions

W-Element Conservation. While thermochemical data are available for four distinct tungsten *chloride* species, $WCl_n(g)$ ($n = 2, 4, 5,$ and 6), only two tungsten fluorides are listed in the same compendium[12,38] ($n = 1$ and 6), with the data for the monofluoride being rather speculative. Therefore, in making the QE calculations below we (of necessity) assume that our present $\mathcal{E}_{(W)}$ measurements give the sum $\mathcal{E}_0 + \mathcal{E}_1 + \mathcal{E}_6$, and inquire if a combination of (i) available thermochemical data, (ii) our $\mathcal{E}_{(W)}$ measurements, and (iii) the QE model of ref 37, predict a transition from $WF_6(g)$ to $WF(g)$ desorption over the temperature range 800–2000°K, as might be expected from the complexity of Figure 4.

At or below 2000°K, $W(g)$ desorption is negligible (*cf.* ϵ_{vap}, Figure 4); hence, one equation for the two resulting unknowns ($\mathcal{E}_1$ and $\mathcal{E}_6$) is simply

$$\mathcal{E}_{(W)} \approx \mathcal{E}_1 + \mathcal{E}_6 \qquad (B1)$$

According to the QE model[37] WF and WF_6 would be in mutual equilibrium with the tungsten substrate; hence, an additional connection between $\mathcal{E}_1$ and $\mathcal{E}_6$ is established through the gas–solid equilibrium

$$5W(s) + WF_6(g) \rightleftharpoons 6WF(g) \qquad (B2)$$
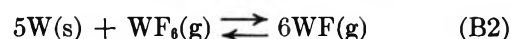
Invoking the Hertz–Knudsen relation (*cf.* eq 2) between molecular flux and equivalent pressure, *viz.*

$$p_n = (4kT)c_n^{-1}\mathcal{E}_n \qquad (B3)$$

[where c_n is the mean thermal speed of $WF_n(g)$] and the law of mass action corresponding to eq B2

$$p_1^6 p_6^{-1} = K_p(T) \qquad (B4)$$

provides the second of the two necessary relations between $\mathcal{E}_1$ and $\mathcal{E}_6$, *viz.*

(43) See, for example, J. N. Smith and W. L. Fite in "Advances in Rarefied Gas Dynamics," J. A. Laurmann, Ed., Vol. 1, Suppl. 2, Academic Press, New York, N. Y., 1963, p 430; D. R. Olander in "The Structure and Chemistry of Solid Surfaces," G. A. Somorjai, Ed., Wiley, New York, N. Y., 1969, paper 45, and J. A. Schwarz and R. J. Madix, *J. Catal.*, 12, 140 (1968).

(44) "Sticking" in the present context merely pertains to a gas–surface interaction during which chemical bond formation occurs, regardless of the residence time of the resulting "product" molecule.

$$\mathcal{E}_1{}^6\mathcal{E}_6{}^{-1} = (4kT)^{-5}c_1{}^6c_3{}^{-1}K_p(T) \qquad \text{(B5)}$$

Introducing the definitions

$$\mu \equiv \mathcal{E}_1/\mathcal{E}_{(W)} \quad \text{(normalized monofluoride flux)} \qquad \text{(B6)}$$

$$\eta \equiv \mathcal{E}_6/\mathcal{E}_{(W)} \quad \text{(normalized hexafluoride flux)} \qquad \text{(B7)}$$

and

$$a \equiv (4kT\mathcal{E}_{(W)})^{-5}c_1{}^6c_6{}^{-1}K_p(T) \qquad \text{(B8)}$$

The system of eq B1 and B5 becomes

$$\mu + \eta = 1 \qquad \text{(B9)}$$

$$\mu^6 = a\eta \qquad \text{(B10)}$$

Inspection of eq B9 and B10 reveals that (i) both products will be of comparable importance ($\mu = {}^1/_2 = \eta$) when $a = ({}^1/_2)^5 \equiv a_{1/2}$, (ii) the hexafluoride will dominate when the temperature level is such that $a \ll a_{1/2}$, (iii) the monofluoride will dominate when the temperature level becomes sufficient to cause $a \gg a_{1/2}$. Upon inserting the above-mentioned kinetic and thermochemical data to evaluate $a(T)$ one finds that, while the hexafluoride is indeed predicted to dominate at 800°K, K_p (eq B2) is never large enough to predict a transition to WF(g) desorption by 2000°K.

F-Element Conservation. In a similar manner one can now inquire whether the QE model would predict a transition from $WF_6(g)$ evaporation to F(g) evaporation for the W(s)–F(g) reaction between, say, 2000 and 2500°K. For this purpose we assume

$$sZ \approx \mathcal{E}_F + 6\mathcal{E}_6 \qquad \text{(B11)}$$

and

$$\mathcal{E}_6\mathcal{E}_F{}^{-6} = (4kT)^5c_6c_F{}^{-6}K_p'(T) \qquad \text{(B12)}$$

the latter corresponding to the assumed equilibrium

$$W(s) + 6F(g) \rightleftarrows WF_6(g) \qquad \text{(B13)}$$

With the introduction of the definitions

$$\phi \equiv \mathcal{E}_F/(sZ) \qquad \text{(B14)}$$

$$\omega \equiv 6\mathcal{E}_6/(sZ) \qquad \text{(B15)}$$

and

$$b \equiv 6(4kTsZ)^{-5}c_6{}^{-1}c_F{}^6[K_p'(T)]^{-1} \qquad \text{(B16)}$$

we again arrive at the system of equations

$$\phi + \omega = 1 \qquad \text{(B17)}$$

$$\phi^6 = b\omega \qquad \text{(B18)}$$

[formally identical with the system B9 and B10]. Inserting experimental values of $Z(T)$, the estimate $s \approx 1$, and calculating $K_p'(T)$ from available thermochemical data,[12,38] one finds that $WF_6(g)$ would never be the favored F-element desorber at such elevated temperatures; *i.e.*, the predicted ω is small even at 2000°K. One must conclude that the quasi-equilibrium model, combined with presently available thermochemical data, does not provide a self-consistent explanation of our observed Arrhenius behavior for the W(s)–F(g) reaction (Figure 4).

Systematics of the Electronic Spectra of the *p*-Oligophenylenes

and Their Substituted Analogs[1]

by I. B. Berlman,* H. O. Wirth, and O. J. Steingraber

Argonne National Laboratory, Argonne, Illinois 60439   (*Received June 3, 1970*)

Publication costs assisted by the Argonne National Laboratory

The fluorescence characteristics (lifetime, quantum yield, Stokes loss, spectral width, etc.) of about 20 variously substituted and bridged *p*-oligophenylenes have been systematically investigated so that the relationship between molecular structure and these characteristics would be better understood. When alkyl chains are employed as substituents to enhance the solubility of a compound, it is important that these substituents be placed in the proper positions, for when in the para or meta positions of terminal rings, their effect on the fluorescence characteristics is minimal, but when placed on the ortho position of the terminal rings or on the meta and ortho positions of the phenylene rings, certain characteristics such as quantum yield are adversely affected by steric crowding. Moreover, an alkyloxy group substituted on the para position will enhance the permanent dipole moment and the molar extinction coefficient. These studies support the contention that the fluorescence transition is allowed and long-axis polarized.

The *p*-oligophenylenes have very desirable fluorescence characteristics, such as high quantum yield and short decay time, that make them very useful as scintillators. In a previous publication[2] it was reported that as the number of phenyl rings in the basic chromophore is increased, the molar extinction coefficent ϵ is increased, the natural fluorescence lifetime is decreased, and both the absorption and fluorescence spectra are shifted toward longer wavelengths. A practical problem that must be overcome is the decrease in solubility as the molecular length is increased. It has been demonstrated by Wirth, *et al.*,[3] that the solubility of *p*-oligophenylenes is dramatically enhanced when alkyl chains are added as substituents. For example, the solubility of *p*-quaterphenyl in toluene at room temperature is about 0.1 g/l., whereas that of tetramethyl-*p*-quaterphenyl (VIII) is over 500 g/l. These substituents may also interfere with the planarity of the chromophore and/or affect its dipole moment in either the ground state and/or first excited state and thus alter the spectroscopic characteristics. A systematic investigation of a large number of variously substituted and bridged *p*-oligophenylenes has been made to gain a better understanding of how the fluorescence characteristics are affected by various types of substituents, their number, and their position. The data are tabulated in Table I and some of the spectra are shown in Figures 1–7.

The procedures employed in measuring the absorption and fluorescence spectra, the fluorescence decay time τ, the natural lifetime τ_0, the quantum yield Q, the Stokes loss, and the full width at reciprocal "*e*" (FWRE) of the maximum value of the spectra have been explained elsewhere.[4,5]

Discussion

A. Davydov's Limit. The *p*-oligophenylenes are composed of rings joined together in the para position by single σ bonds and their general formula is $C_{6n}H_{4n+2}$, where n is the number of rings, ≥ 3. Davydov[6] derived an equation for the determination of the limiting energy of the 0–0 transition as a function of the number of rings, *i.e.*

$$\Delta E = A - 2|M| \cos[\pi(n+1)^{-1}]$$

where ΔE is the transition energy, M is the matrix element of the interaction between neighboring rings, and A is a constant independent of the number of rings n. In the development of this formula it was assumed that these compounds are characterized by *incomplete* delocalization of the π-electron systems (rings), that the interaction between the phenyl rings takes place only between nearest neighbors, and that as the system becomes larger the addition of each successive ring has less of an effect on the fluorescence characteristics. From experimental absorption data, a limiting value of 3280 Å in hexane was predicted.[7] Since the absorption spectra of these compounds are generally very broad, it is very difficult to estimate the value of the

(1) Work performed under the auspices of the U. S. Atomic Energy Commission.

(2) I. B. Berlman, *Mol. Cryst.*, **4**, 157 (1968).

(3) H. O. Wirth, F. U. Hermann, G. Hermann, and W. Kern, *ibid.*, **4**, 321 (1968).

(4) I. B. Berlman, "Handbook of Fluorescence Spectra of Aromatic Molecules," Academic Press, New York, N. Y., 1965, pp 13–26.

(5) I. B. Berlman, *Chem. Phys. Lett.*, **3**, 61 (1969).

(6) A. S. Davydov, *Zh. Eksp. Teor. Fiz.*, **18**, 515 (1948).

(7) H. Suzuki, *Bull. Chem. Soc. Jap.*, **33**, 109 (1960).
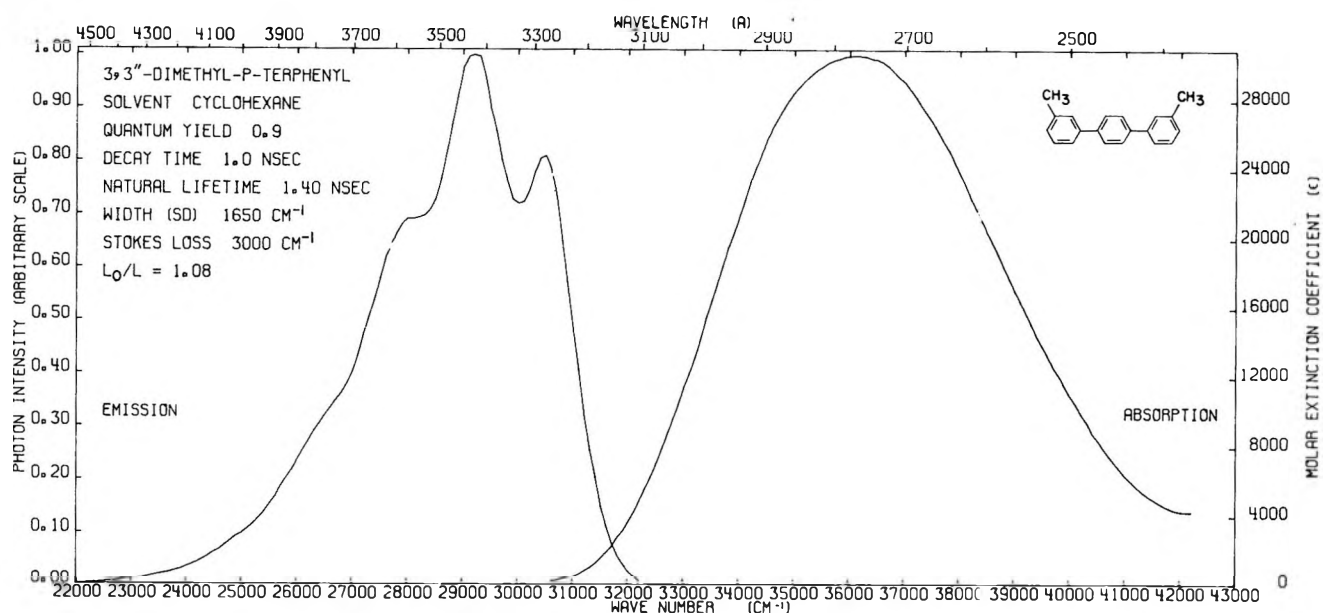
Figure 1. Spectra of 3,3″-dimethyl-p-terphenyl.
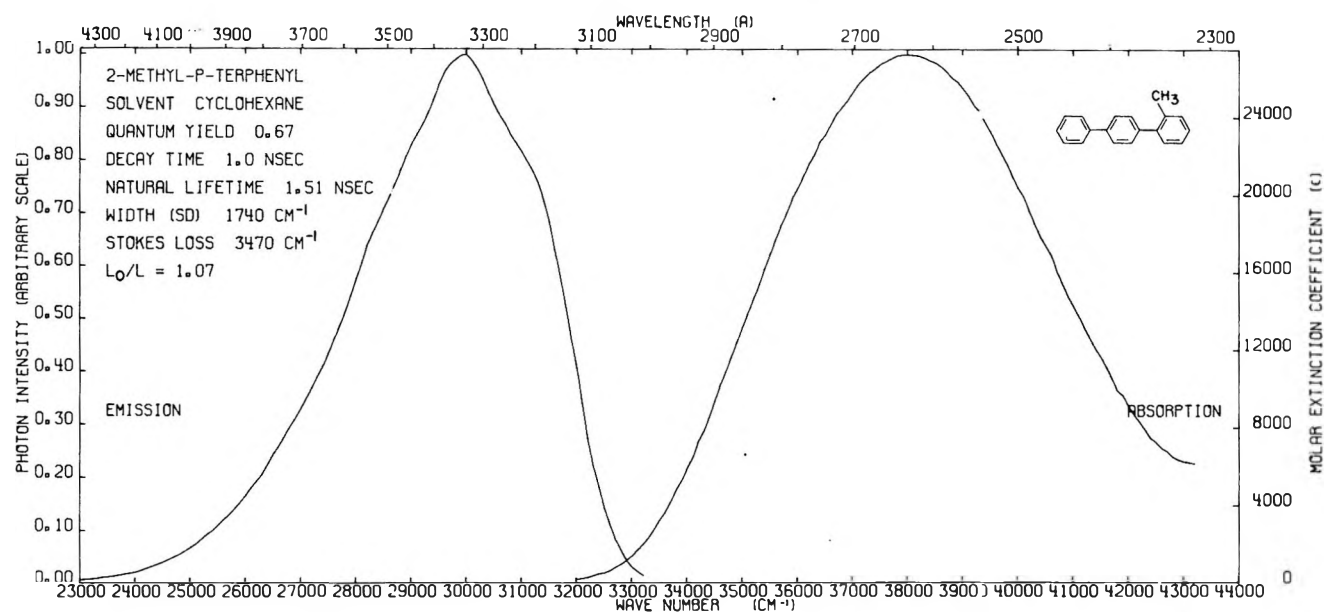
Figure 2. Spectra of 2-methyl-p-terphenyl.

0–0 transition. On the other hand, the fluorescence spectra are structured. If it is assumed that the above limit has the same value in cyclohexane and that the value of Stokes shift for a series of similar p-oligophenylenes is about 340 Å, a limiting center of gravity of the fluorescence spectra λ_{cg} is computed to be about 3620 Å. (The difference in λ_{cg} when one of these spectra is plotted vs. wavelength or wave number is less than 5 Å.) Although a small degree of convergence is observed in our results (Table I and the appropriate figures), a limit is not reached even by compounds with eight rings (XII). The limit is obviously greater than the above value. This discordance between our experimental results and the predicted values leads us to believe that

the interaction and the delocalization is greater than that assumed by Davydov.

B. Natural Fluorescence Lifetime. That the maximum value of the molar extinction coefficient ϵ_{max} of the p-oligophenylenes increases with the number of phenyl rings has been known for some time.[3,8] The relationship between ϵ and the natural fluorescence lifetime can be approximated[2] by the following formula

$$\frac{1}{\tau_0} = A\bar{\nu}_0^2 \int \epsilon d\bar{\nu} \approx A\bar{\nu}_0^2 \epsilon_{max} \Delta\bar{\nu}$$

where $\bar{\nu}_0$ is the wave number of the line of symmetry be-

(8) A. E. Gillam and D. H. Hey, *J. Chem. Soc.*, 1170 (1939).

tween the absorption and fluorescence spectra and $\Delta\bar{\nu}$ is the full width at half-maximum. It is apparent that the larger the values of ϵ_{max}, $\Delta\bar{\nu}$, and $\bar{\nu}_0$, the shorter is the computed lifetime. The p-oligophenylenes have the advantage[2] of having their emission spectra located at relatively shorter wavelengths as compared to other

Table I[a,b]
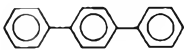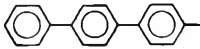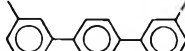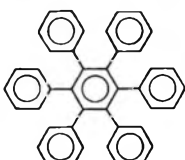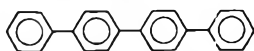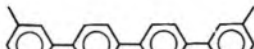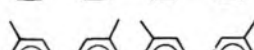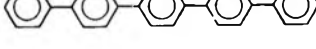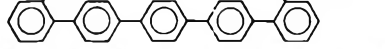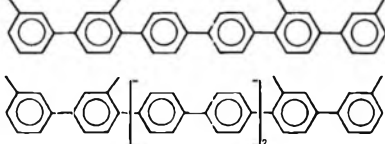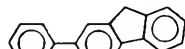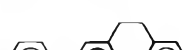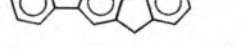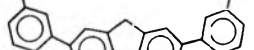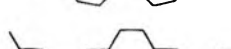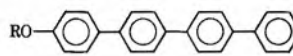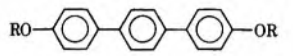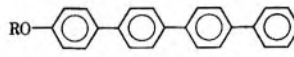
Compound	τ_0, nsec	τ, nsec	Q	Stokes loss, cm^{-1}	FWRE fl, cm^{-1}	abs, cm^{-1}	ϵ_{max}, l. mol^{-1} cm^{-1}	λ_{cg} fl, Å
I	1.25	1.05	0.93	2960	4400	6700	32,000	3445
II	1.31	1.0	0.94	2930	4400	6800	33,400	3485
III	1.39	1.0	0.9	2980	4400	6900	30,600	3480
IV	1.51	1.0	0.67	3470	4500	7200	27,400	3400
V		1.4	0.01	4100	4150			3465
VI	1.25	0.85	0.89	2900	4400	6500	40,750	3685
VII	1.20	0.85	1.0	3000	4350	6650	44,000	3730
VIII	1.20	0.9	0.73	4100	5000	7200	43,300	3570
XI	0.91	0.80	1.0	2900	4150	6350	63,200	3865
X	0.95	0.88	0.92	3200	4500	6700	57,700	3745
XI	0.84	0.76	0.94	3350	4500	7100	62,500	3795
XII	0.75^c	0.65^c		3000^c	4400		76,300^c	3990
XIII	(1.29)	1.5	0.91	2200	3800	7100	30,500	3460
XIV	(1.39)	1.4	0.84	2500	4100	7000	31,700	3540
XV	2.7	2.3	0.9	1480	3100		55,700	3535
XVI	(0.99)	1.05	1.0	2300	4100	6400	47,000	3720
XVII	(1.02)	1.08	0.75	2700	4200	(8200)	44,000	3810
XVIII	1.39	1.05	0.89	2860	4500	6700	34,000	3580

Table I *(Continued)*

Compound	τ_0, nsec	τ, nsec	Q	Stokes loss, cm^{-1}	FWRE fl, cm^{-1}	FWRE abs, cm^{-1}	ϵ_{max}, l. mol^{-1} cm^{-1}	λ_{eg} fl, Å
XIX	1.32	0.85		2900	4200	6500	46,100	3795
XX	1.31	0.95	0.97	2780	4100	6650	41,000	3620
XXI	1.01	0.9	0.93	2800	4200	6600	54,200	3826

a Compounds: I, p-terphenyl; II, 4-methyl-p-terphenyl; III, 3,3''-dimethyl-p-terphenyl; IV, 2-methyl-p-terphenyl; V, sexiphenylbenzene; VI, p-quaterphenyl; VII, dimethyl-p-quaterphenyl; VIII, tetramethyl-p-quaterphenyl; IX, di(3-ethylheptyl)-p-quinquephenyl; X, diethyl-p-quinquephenyl; XI, tetramethyl-p-sexiphenyl; XII, tetramethyl-p-octaphenyl; XIII, 2,2'-methylene-p-terphenyl; XIV, 2,2'-ethylene-p-terphenyl; XV, 2,2'-methylene-5',6''-methylene-p-terphenyl; XVI, 3,3'''-dimethyl-3',2''-methylene-p-quaterphenyl; XVIII, 3,3'''-dimethyl-3',2''-ethylene-p-quaterphenyl; XVIII, 4-(3,3-dimethylbutoxy)-p-terphenyl; XIX, 4-(5-ethylhexoxy)-p-quaterphenyl; XX, 4,4''-dihexahydrofarnesoxy-p-terphenyl; XXI, 4,4''-di(2-butyloctoxy)-p-quaterphenyl. The error in the measurements is estimated to be ±10%. *b* / and R are alkyl groups. *c* Values are for benzene solutions.
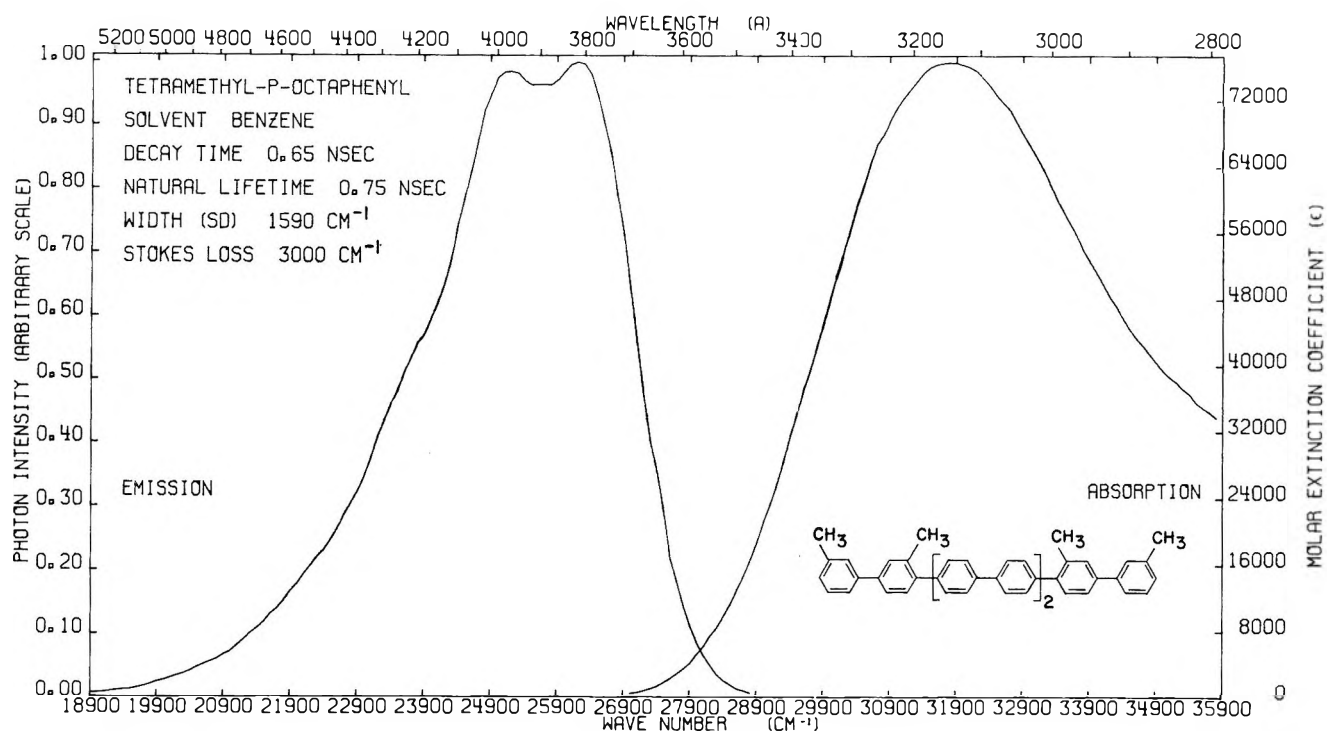
Figure 3. Spectra of tetramethyl-p-octaphenyl.

conjugated systems of equivalent size (larger $\bar{\nu}_0$ values) and of having abnormally wide absorption spectra (large $\Delta\bar{\nu}$).

Since the above equation is approximate, it has not been employed to compute τ_0. Values of τ_0 have been calculated for a series of p-oligophenylenes using a formula derived by Strickler and Berg[9] and these values are tabulated in Table I. The latter formula was derived for an allowed transition, yet from measurements on over a hundred compounds it was found to give an accurate determination even for a symmetry forbidden transition. Compound XII, composed of eight rings, is the longest compound tested, has the largest value of

ϵ_{max}, and has the shortest computed lifetime—about 0.7 nsec—as expected.

C. Molecular Structure vs. Spectral Band Structure. The absorption spectra of unsubstituted p-oligophenylenes such as p-terphenyl[10] and some of the substituted compounds such as 3,3''-dimethyl-p-terphenyl (III), Figure 1, is structureless because in the ground state steric hindrance imposes a nonplanar configuration on the chromophore. Suzuki[7] has computed that the terminal rings of p-terphenyl in solution make an angle

(9) S. J. Strickler and R. A. Berg, *J. Chem. Phys.*, **37**, 814 (1962).
(10) Reference 4, p 138.
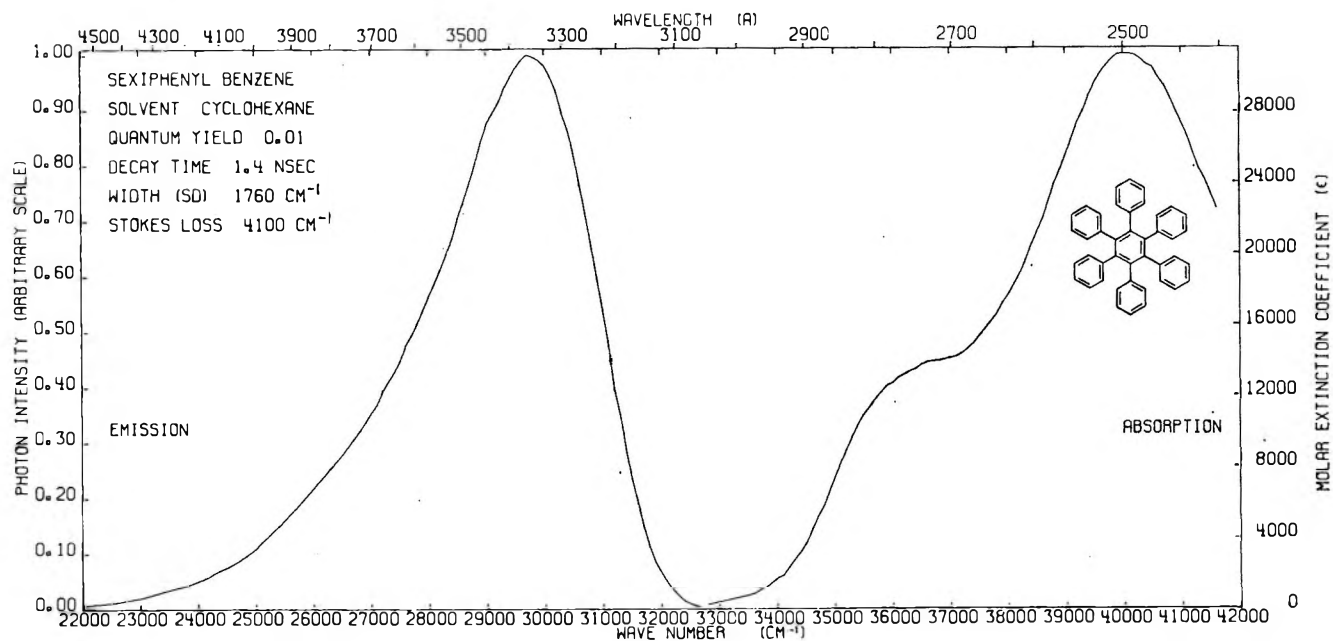
Figure 4. Spectra of sexiphenylbenzene.
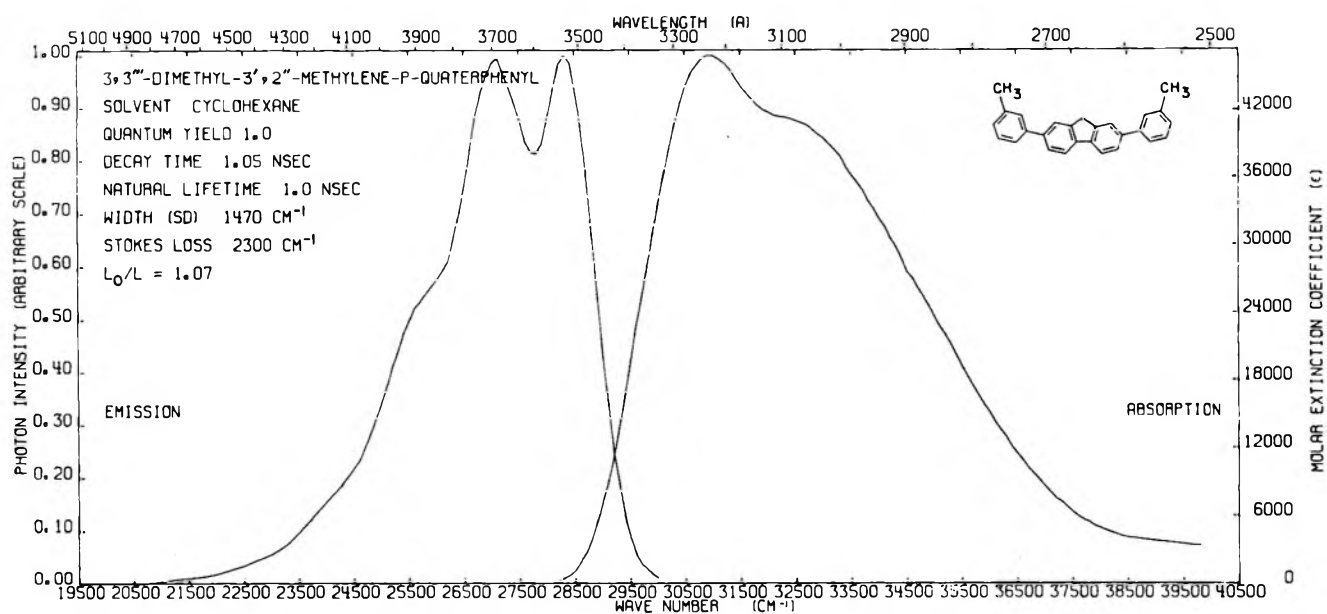
Figure 5. Spectra of 3,3'''-dimethyl-3',2''-methylene-p-quaterphenyl.

of about 10° to the plane containing the central ring. Moreover, the coannular bond is found[11] to be 1.48 Å in biphenyl, p-terphenyl, and p-quaterphenyl. This relatively large value of bond length is interpreted to indicate that the coannular bond has effectively no double bond character when the chromophore is in the ground state. In the excited state, increased resonance interaction between adjacent rings and the addition of some double bond character to each coannular bond coerces the rings into a more planar arrangement.[12] Supporting evidence for this contention is the observation that the fluorescence spectra of compounds with a minimum amount of steric hindrance, i.e., I and III,

have structured spectra and the FWRE values of the fluorescence spectra are much less than those of the absorption spectra. (A comprehensive study of the relationship between conformation and certain spectroscopic characteristics is presented in another publication.[13])

Alkyl chains substituted in the para and meta positions of terminal rings are effective in increasing the sol-

(11) M. D. Burns and J. Iballs, Proc. Roy. Soc., Ser. A, 227, 200 (1955).

(12) H. H. Jaffé and M. Orchin, "Theory and Application of Ultraviolet Spectroscopy," Wiley, New York, N. Y., 1962, p 389.

(13) I. B. Berlman, J. Phys. Chem., 74, 3085 (1970).
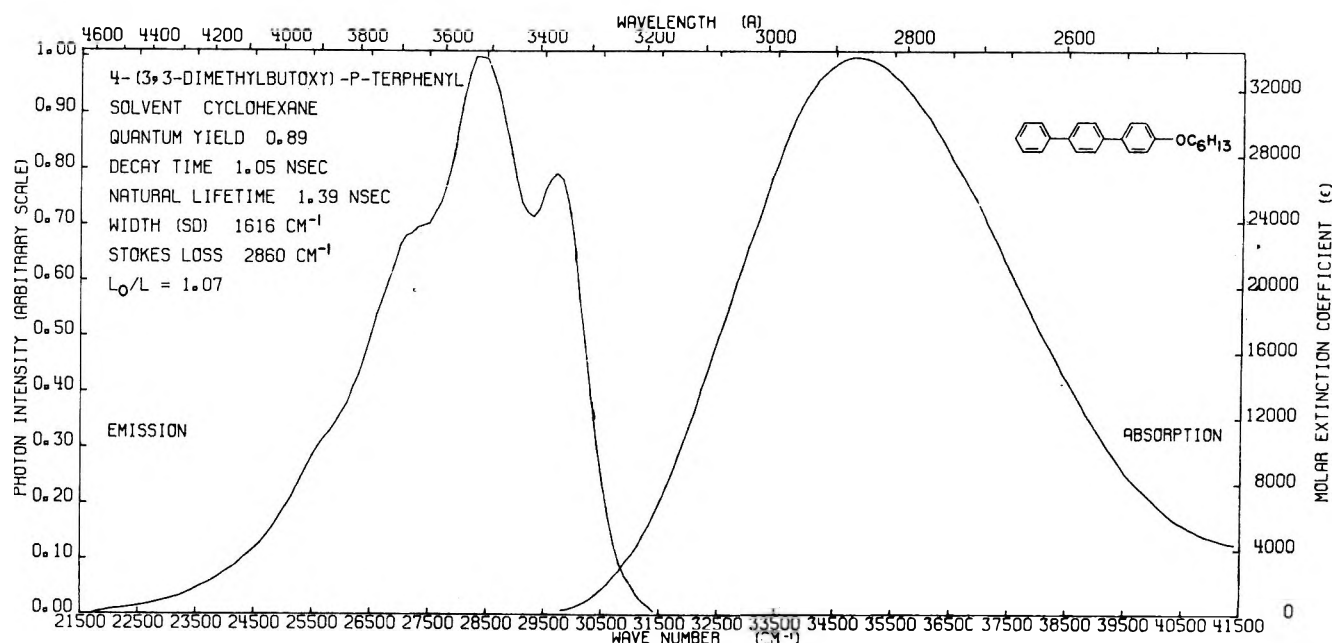
Figure 6. Spectra of 4-(3,3-dimethylbutoxy)-p-terphenyl; solvent is cyclohexane.
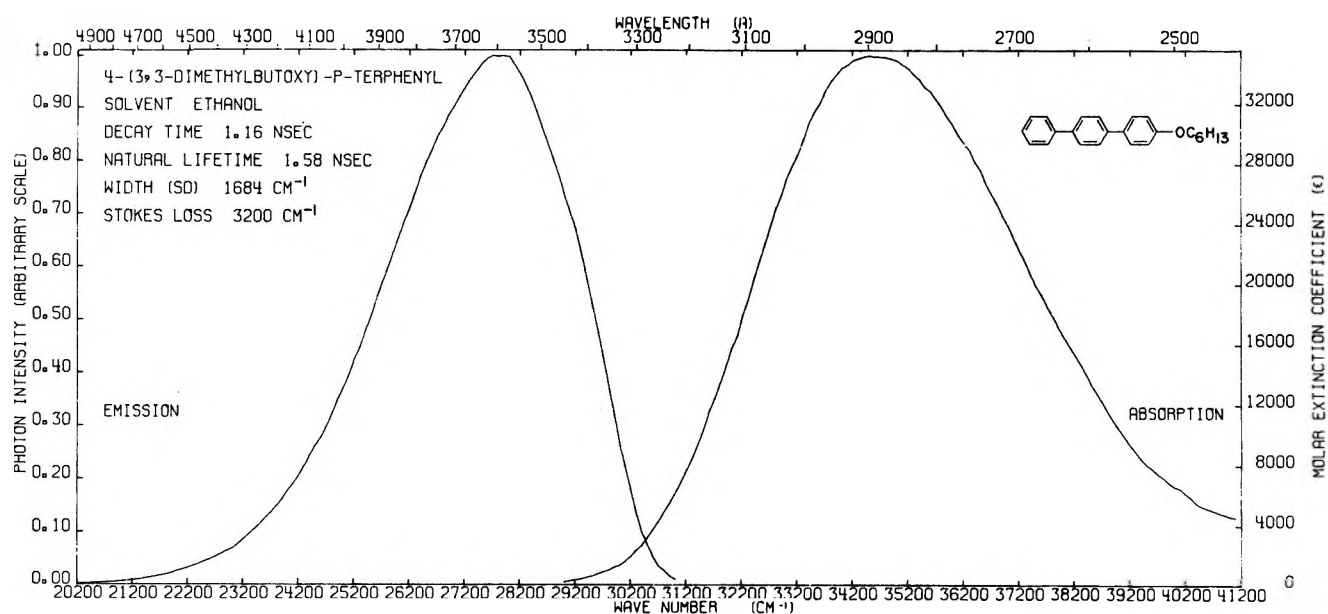
Figure 7. Spectra of 4-(3,3-dimethylbutoxy)-p-terphenyl; solvent is ethanol.

ubility of the compound and yet do not affect the planarity of the chromophore or the strength of the transition. Consequently, compounds so substituted possess characteristics very similar to those of the unsubstituted compounds. On the other hand, if these same substituents are positioned on the ortho position of the end rings or on meta or ortho positions of phenylene rings, the planarity of the basic chromophore is disturbed, and its fluorescence characteristics are affected in the following manner. The long-wavelength absorption band is shifted toward shorter wavelengths; the value of ϵ_{max} is reduced; the value of FWRE of the absorption curve is increased; the fluo-

rescence spectrum becomes less structured; Stokes loss is increased; and the quantum yield is reduced. These effects of steric hindrance are readily noted on comparing the data for III with IV, VII with VIII, and IX with X, in Table I and Figures 1 and 2. If it were not for steric crowding by the substituents and the hydrogen atoms on the basic chromophores of VIII, XI, and XII (Figure 3), their natural fluorescence lifetimes would be even shorter than those tabulated. Compound V (Figure 4) can be considered as tetraphenyl-p-terphenyl and is an illustration of an extreme case of steric hindrance. Its characteristics are typical of a nonplanar molecule. The quantum yield is very

small, the intense transition (the hallmark of the *p*-oligophenylenes) is shifted toward shorter wavelengths, and the Stokes loss is very large. Surprisingly, the absorption spectrum is slightly structured and the FWRE (F1) is abnormally small. These results may be explained by the fact that the six phenyl rings are orthogonal[14] to the central benzene ring so that there is no effective conjugation between the rings, and the fluorescence characteristics correspond to those produced by the $^1L_b \rightarrow {}^1A$ transition of the central benzene ring.

The angle between successive phenyl rings can be held fixed by means of a bridging group as in XIII, XIV, XV, XVI (Figure 5), and XVII. When the planarity is improved by bridging, the absorption and fluorescence spectra become more structured, red shifted, and narrower, the intensity of the transitions is generally increased, *i.e.*, ϵ_{max} and Q/τ are increased, and Stokes loss is decreased. These effects of bridging are readily noted in the data and graphs of bridged and unbridged compounds, *i.e.*, XVI and XVII *vs.* VI. Even the length of a bridge is a factor in influencing the planarity and the characteristics. From an intercomparison of the effects of an ethylene bridge and a methylene bridge, it is noted that in the case of the former the absorption spectrum is less structured, and the values of Stokes loss and FWRE (F1) are larger. Some information on the source of these differences may be obtained from studies on fluorene and 9,10-dihydrophenanthrene, especially since compounds XIII and XIV can be called 2-phenylfluorene and 2-phenyl-9,10-dihydrophenanthrene, respectively. X-Ray data from fluorene and 9,10-dihydrophenanthrene in the crystalline state indicate that the former is planar[11] in the ground state, whereas the latter is nonplanar, the interplanar angle being $20°$.[15] Because the phenyl rings are held in a planar but strained conformation in the ground state by a methylene bridge, the absorption spectrum is structured, whereas 9,10-dihydrophenanthrene is nonplanar and its absorption spectrum is diffuse. The ethylene group is assumed to be more flexible than the methylene group so that a larger change in nuclear conformation takes place on excitation and Stokes loss and FWRE (F1) are larger.[13]

It has been suggested[16] that the broad structureless absorption spectra of biphenyl and the *p*-oligophenylenes are composed of bands from three transitions, two of which are symmetry forbidden, and the third allowed. The following is some of the evidence leading to this interference. Bands from the two more intense transitions are separated and easily observed in the long-wavelength absorption spectrum of the bridged *p*-oligophenylenes, especially in XV. These bands are also resolved in sterically hindered compounds such as *o*-terphenyl and V. W. R. Anderson, at this laboratory, found by means of a polarization experiment, that the transitions producing all of the long-wavelength absorption bands in XV are polarized along the same

(long) axis. Moreover, since certain fluorescence parameters such as decay time τ and quantum yield Q are determined by the characteristics of the lowest excited singlet state, and since the values of these parameters in the *p*-oligophenylenes are $\tau < 3$ nsec and $Q > 0.6$, the fluorescence transition must be allowed, probably a $^1B_b \rightarrow {}^1A$ transition.

Since τ_0 for each of the compounds in Table I is computed by an integration over the whole long-wavelength absorption curve and since a meaningful value of τ_0 is obtained only when the integration is performed over the bands corresponding to the fluorescence transition, the τ_0 values are sometimes in error. Such values are bracketed. In addition, τ_0 may be incorrect for other reasons. It is assumed in all of the formulas for computing τ_0 that the fluorescence transition moment is equal to the absorption transition moment. This assumption is generally true when the nuclear geometry of the excited state is identical with that of the ground state. In the case of many of the *p*-oligophenylenes there is a large change in conformation between the two states; they generally become more planar on excitation. Thus, τ_0 can be incorrect for two reasons. If the integration is performed over interfering bands, τ_0 is too small, and if there is a large change in nuclear topology on excitation, it is too large. In Table I those compounds that are nonplanar in the ground state and planar in the excited state, as I, II, V, VI, and VIII, have computed values of τ_0 that are about 10–20% larger than the values obtained from the ratio of τ/Q. For these *p*-oligophenylenes the change in conformation has a much larger effect on τ_0 than the hidden absorption bands. By contrast, the τ_0 values for III, VII, IX, and X, compounds that are kept nonplanar in both states by steric hindrance, are almost identical with those obtained from the ratio τ/Q.

An alkyloxy substituent in the para position as in XVIII (Figure 6) and XIX is effective in increasing the value of ϵ_{max} and the static dipole moment of the ground and first excited singlet state. This sensitivity of the para position to substitution is in accord with the belief that the fluorescence transition is long-axis polarized.[16] The fluorescence spectra of these compounds in a polar solvent relative to that in a nonpolar solvent are more diffuse and red shifted (Figure 7). These solvent effects, as interpreted by Eisinger and Navon,[17] are produced by an interaction between the dipole moment of the solute and that of the solvent. On the other hand, when two alkyloxy substituents are positioned at opposite para positions of the chromophore, as in XX and XXI, the static dipole moment is no longer large

(14) A. Almenninger, O. Bastiansen, and P. N. Skancke, *Acta Chem. Scand.*, **12**, 1215 (1958).

(15) G. H. Beaven, D. M. Hall, M. S. Leslie, and E. E. Turner, *J. Chem. Soc.*, 854 (1952).

(16) I. B. Berlman, *J. Chem. Phys.*, **52**, 5616 (1970).

(17) J. Eisinger and G. Navon, *ibid.*, **50**, 2069 (1969).

and the solvent effect is reduced. Nevertheless, ϵ_{max} becomes larger, almost as large as that produced by an additional phenyl group.

These compounds have characteristics that make them some of the most efficient and fastest scintillators. Our measured decay time values are presented in column 4 of Table I. (The decay time of some of these compounds has already been published by others.[18])

In conclusion, efficiency and speed are two useful features of a good scintillator, and both of these characteristics depend on large values of the molar extinction coefficient. Not only are a large number of rings desirable, but they should be in a linear and planar conformation. When substituents and bridging groups are employed, they should be so positioned so as to enhance, not interfere, with this arrangement.

(18) E. Michelbacher, *Z. Naturforsch.*, **24A**, 790 (1969).

Vibronic Effects in the Infrared Spectrum of the Anion of Tetracyanoethylene

by J. C. Moore, D. Smith, Y. Youhne, and J. P. Devlin*

Department of Chemistry, Oklahoma State University, Stillwater, Oklahoma 74074 (*Received June 29, 1970*)

A variety of infrared measurements on the alkali metal salts of TCNE$^-$ as well as the weak π complex between TCNE and hexamethylbenzene are shown to be consistent with an unusual assignment of the infrared spectrum of TCNE$^-$ that has been proposed in an earlier publication. This assignment is unique in attributing all bands of appreciable intensity in the 600–4000-cm^{-1} range to normally inactive totally symmetric modes. Supportive evidence includes the movement of the only band in the 600–2000-cm^{-1} range toward the $\nu_{C=C}(a_g)$ value of TCNE as the electron affinity of the associated metal ion is increased through the series cesium to lithium. A time-dependent perturbation calculation for an electron in a box, which gives additional substance to the idea of a vibronic washout of the infrared intensity of the planar b_{1u} and b_{2u} modes in TCNE$^-$, is also presented. A novel explanation for the invariance of the ammonia spectrum with increasing metal concentration in alkali metal–ammonia solutions can also be based on this calculation.

Introduction

In an earlier paper attention was called to the striking difference between the infrared spectra of the anion of tetracyanoethylene (TCNE) and that of the neutral TCNE molecule.[1] One might suppose that, since the TCNE vibrational spectrum has been thoroughly studied,[2-5] it should be a simple matter to interpret the spectrum of the TCNE anion which seemingly has a closely related geometric structure.[6] However, except for a doublet in the cyanide group stretching region (~2200 cm^{-1}), the infrared spectra for the two systems appear unrelated through the 600–4000-cm^{-1} range (Figure 1).

In particular, the anion has only extremely weak features in the 600–1350-cm^{-1} range which encompasses the frequencies where the carbon–carbon single bond stretching modes (b_{1u} and b_{2u}) absorb strongly in neutral TCNE. Equally striking is the very intense absorption at ~1370 cm^{-1} for M$^+$TCNE$^-$ in a region barren of significant absorption by neutral TCNE. The former feature (intensity loss) has been interpreted as resulting from a strong vibronic influence involving the radical electron which results in cancellation of the transition moment for all planar infrared-active modes, while the 1370-cm^{-1} band was explained in terms of an "electron vibration" phenomenon which commonly activates symmetric modes of complexed molecules.[1,7] From this basis the entire anion spectrum was interpreted with the unusual result that the

(1) J. Stanley, D. Smith, B. Latimer, and J. P. Devlin, *J. Phys. Chem.*, **70**, 2011 (1966).

(2) F. A. Miller, O. Sala, P. Devlin, J. Overend, E. Lippert, W. Luder, H. Moser, and J. Varchmin, *Spectrochim. Acta*, **20**, 1233 (1964).

(3) T. Takenaka and S. Hayashi, *Bull. Chem. Soc. Jap.*, **37**, 1216 (1964).

(4) B. Moszynska, *Acta Phys. Polon.*, **33**, 959 (1968).

(5) A. Rosenberg and J. P. Devlin, *Spectrochim. Acta*, **21**, 1613 (1965).

(6) The exchange reaction between TCNE$^-$ and TCNQ which yields TCNE indicates that the anion is formed without severe structural modification [W. D. Phillips, J. C. Rowell, and S. I. Weissman, *J. Chem. Phys.*, **33**, 626 (1960)].

(7) See, for example, E. E. Ferguson, *J. Chim. Phys.*, **61**, 257 (1964).

J. C. Moore, D. Smith, Y. Youhne, and J. P. Devlin
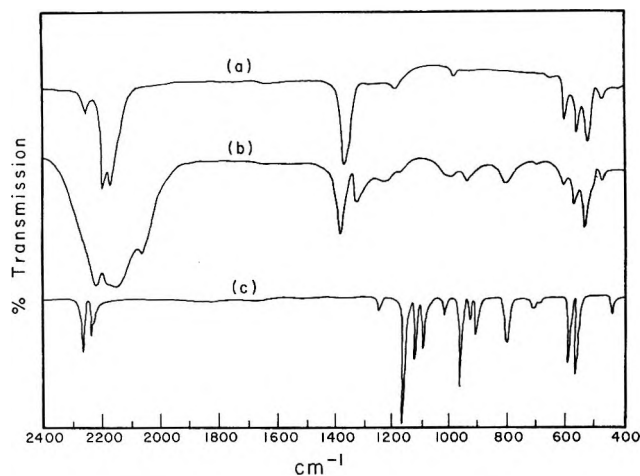
Figure 1. Infrared spectra for (a) CsTCNE and (b) Cd(TCNE)₂ compared with that of (c) TCNE. Spectra are for thin film deposits.

only significant absorptions in the 600–4000-cm⁻¹ range were assigned to symmetric (a_g)[8] vibrational modes which should normally be infrared inactive.

The unusual nature of the proposed TCNE⁻ vibrational assignment suggested that additional support for that assignment should be sought. The main objective of this paper is to present quantitative experimental results and certain theoretical estimates which relate to the concept of "vibronic washout" of the planar infrared-active modes in the TCNE anion. However, the dependence of the peak frequency of the intense absorption at ~1370 cm⁻¹ on the electron affinity of the associated cation will first be examined in an effort to more definitely establish its origin.

Experimental Section

Samples of the salts of the TCNE anion with Li, Cs, and Cd were prepared for infrared sampling by codeposition of molecular beams of TCNE and the metal onto an infrared transparent substrate as previously described for the sodium and potassium salts.[1] Thin films of pure TCNE, the 1:1 complex of TCNE with hexamethylbenzene (HMB), and pure HMB were prepared for absolute intensity measurements by vapor deposition at −180° in a standard infrared cold cell. Sample thicknesses were monitored by the method of Hollenberg and Dows,[9] and intensities were determined assuming randomly oriented polycrystallites. Samples were annealed at −78° prior to the measurement of band areas at that temperature.

Results and Discussion

A. Dependence of $\nu_{C=C}$ on Cation. As mentioned, the C=C stretching mode for KTCNE has previously been assigned as the source of the intense infrared band at 1370 cm⁻¹. Should the D_{2h} symmetry of TCNE be preserved in the anion, this mode should not be active, but its activation can occur by two quite different mech-

anisms. The anion may in fact be of radically different geometric structure, which seems improbable,[6] or it may occupy a site of low symmetry in the crystal. In the latter case, an "electron vibration" between donor and acceptor species accompanying the symmetric TCNE vibrational modes[7] could result in intense absorptions, despite only minor distortion of the D_{2h} molecular symmetry by the crystal field.

Since either explanation of the infrared activity of $\nu_{C=C}$ should be regarded with some skepticism, additional evidence that the C=C stretching mode is responsible for the 1370-cm⁻¹ band was sought. The most direct approach would involve a Raman measurement of $\nu_{C=C}$ for the anion, a feat that may yet prove feasible although attempts to date have been blunted by the intense electronic absorption bands in the visible region. Therefore, the tack used has been based on the idea that the extent of electron back-transfer to the metal cation from the TCNE anion should be a function of the electron affinity of the cation.[10] Since, based on the assignment of $\nu_{C=C}$ = 1370 cm⁻¹, a "complete" electron transfer causes an ~200 cm⁻¹ red shift of $\nu_{C=C}$, a small increase in back-transfer should be reflected by a detectable blue shift. The increase in electron affinity through the cation series cesium (3.89), potassium (4.34), sodium (5.14), and lithium (5.39 eV) should thus cause a sufficient variation in back-transfer to be detectable in the value of $\nu_{C=C}$.

The relevant data from the infrared measurements for this series of compounds are summarized in Table I. Except for an anomaly in the relative positions of the 1370-cm⁻¹ band for the sodium and lithium salts, the results uniformly support the assignment of the 1370-cm⁻¹ band to $\nu_{C=C}$. Thus, the position of the C≡N stretching band (~2200 cm⁻¹) moves noticeably toward the neutral TCNE value in the series CsTCNE to LiTCNE, supporting the concept of increasing back-transfer of charge to the cation with increasing cation electron affinity. Likewise, there is some indication that the extremely weak 1185-cm⁻¹ band attributed to the b_{2u} carbon–carbon single bond mode shifts toward the TCNE value at 1155 cm⁻¹. In this context, the blue shift of the 1370-cm⁻¹ band through this series is strong evidence that the mode involved has a higher frequency in neutral TCNE than for the anion. Since $\nu_{C=C}$ is the only TCNE fundamental between 1280 and 2220 cm⁻¹, the intense 1370-cm⁻¹ band seemingly must be assigned to it.

This assignment, as well as all the data in Table I, is completely consistent with bond order changes predicted from a simple Hückel molecular orbital calcula-

(8) The symmetry notation used herein for the TCNE vibrational modes will be based on the choice of axis used in ref 2.

(9) J. L. Hollenberg and D. A. Dows, *J. Chem. Phys.*, **37**, 1300 (1962).

(10) R. S. Mulliken, *J. Amer. Chem. Soc.*, **74**, 811 (1952).

Table I: Influence of Cation Electron Affinity on Certain Vibrational Frequencies of the Anion of TCNE

	TCNE	HMB·TCNE[a]	LiTCNE	NaTCNE	KTCNE	CsTCNE
$\nu_{C=N}$ (A$_g$)	2236	2230	2198[b]	2197[b]	2190[b]	2187[b]
$\nu_{C=C}$ (A$_g$)	1570	1560	1387	1390	1371	1358
ν_{C-C} (b$_{2u}$)	1155	1155	1184	1187	1187	1190

[a] Crystalline complex. [b] Average value for the infrared doublet.
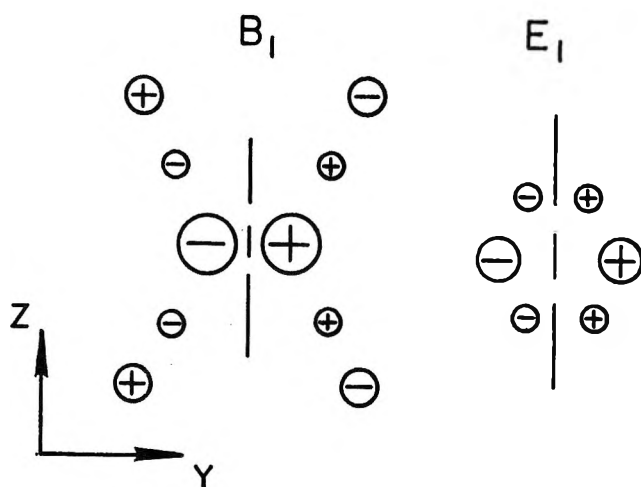
Figure 2. Representations of the lowest empty molecular orbital for TCNE and highest occupied MO of HMB.

tion.[11] Such calculations predict a lowest empty orbital of B$_1$ symmetry for TCNE (Figure 2), such that the bond order changes presented in Table II are expected upon formation of the anion. Qualitatively, the predicted increase in C–C and decrease in C=C and C≡N bond orders are in complete accord with the vibrational frequencies in Table I, and the quantitative comparison is also quite good.

Table II: Influence of Electron Transfer on the π Bond Orders of TCNE as Estimated from a Hückel MO Calculation.[a] Shifts in Band Positions Δ (cm^{-1}) are Compared with Predicted Changes in Bond Order

	C≡N	C=C	C–C
TCNE	0.87	0.76	0.35
TCNE$^-$	0.79	0.58	0.46
Δ (bond order)	−0.08	−0.18	+0.11
Δ,[b] cm^{-1}	−49	−212	+35

[a] From ref 11. [b] Comparison is for CsTCNE with TCNE.

The infrared spectrum for Cd(TCNE)$_2$ has also been recorded with the results presented in Figure 1b. The Cd(TCNE)$_2$ spectrum contrasts with those of the alkali metal salts in at least two respects. The single bands at ~1370, 1185, and 975 cm^{-1} in the alkali metal series are split into two components in Cd(TCNE)$_2$, probably reflecting an increase in dynamical coupling of neigh-

boring anions, and the relationship between the $\nu_{C=C}$ band peak position and electron affinity, established for the alkali metal series, breaks down. Thus Cd^{2+} has a greater electron affinity than any of the alkali metal cations, but $\nu_{C=C}$ has its lowest value (1336 cm^{-1} (av)) in Cd(TCNE)$_2$.

Since back-bonding to Cd^{2+} likely involves d orbitals rather than exclusively s orbitals, as in the case of the alkali metals, it is possible that the symmetry requirements for back-bonding may prohibit the participation of the B$_1$ orbital containing the C=C antibonding radical electron. Rather, back-bonding may primarily involve electrons from C=C bonding MO's such as ψ_5 (B$_3$), the highest occupied MO in neutral TCNE.[11] This could explain the additional reduction in $\nu_{C=C}$ in Cd(TCNE)$_2$.

B. Band Intensities for b$_{1u}$ and b$_{2u}$ Modes. With the original anion assignment substantiated by the band position investigations described in the preceding section, the reason for the lack of intensity in the b$_{1u}$ and b$_{2u}$ (planar) modes of TCNE$^-$ can be considered more seriously. Two somewhat indirect approaches to this problem are described in this section.

1. Free Electron Calculations. It is easy to imagine that the radical electron in TCNE$^-$ is highly delocalized with an unusual mobility and polarizability. The intense absorption in the visible region guarantees that the molecular polarizability in the infrared will be significantly greater than for the colorless TCNE. Electrons in conjugated systems, in general, may play a dominant role in determining infrared band intensities by virtue of their ability to respond to forces which arise during a distortion of the skeletal structure of a molecule (vibronic interaction).[12,13] Such vibronic effects are greatest for systems having low energy electronic transitions of high oscillator strength. The anion of TCNE is clearly in this class.

Brown has presented an elegant formalism for the calculation of vibronic effects in conjugated systems and has given somewhat tentative results for benzene.[12] This would seem to be the best available approach to the theoretical estimation of vibronic effects in the typical conjugated system, but the many necessary as-

(11) B. R. Penfold and W. N. Lipscomb, *Acta Cryst.*, **14**, 589 (1961). Notation for MO symmetries are based on the axis choice in this reference throughout this paper.

(12) T. L. Brown, *J. Chem. Phys.*, **43**, 2780 (1965).

(13) H. B. Friedrich and W. B. Person, *ibid.*, **44**, 2161 (1966).

J. C. MOORE, D. SMITH, Y. YOUHNE, AND J. P. DEVLIN

sumptions and approximations severely limit the quantitative significance of the results. For this reason we have attempted to depict the possible extent of the vibronic response to the skeletal distortions of the TCNE anion by using a simple electron in a box representation of the mobile radical electron. In other words, influenced by the nearly total loss of intensity in the planar modes of TCNE⁻ we have raised the question: if we treat the radical electron as a particle in a box having the dimensions of the anion and use the transition moment of a given TCNE mode as a time varying perturbation on that system, will the response of the electron to that perturbation effectively cancel the transition moment?

Rather than answer this question directly, we have geared our calculation to a system which is more commonly viewed as having particle in the box characteristics: the solvated electron in alkali metal-liquid ammonia systems. Lagowski has searched unsuccessfully for some evidence of the effect of the solvated electron on the cage NH_3 molecule stretching modes over a large range of metal concentrations.[14] He concluded that either the electron does not significantly perturb the cage molecules or the N–H stretching modes are insensitive to the perturbation. We feel that there is a third more probable explanation; namely, the infrared intensity of the perturbed cage molecules is vibronically canceled by the electron in the cage, so that no new infrared features can be expected for the cage molecules regardless of the extent to which the N–H stretching frequencies may be modified.

To test this possibility while simultaneously determining the feasibility of a similar vibronic washout of the b_{1u} and b_{2u} modes of TCNE⁻, we have carried through a time-dependent perturbation calculation on an electron in a box choosing parameters such as box size and perturbation amplitude to correspond to the electron in a cage of ammonia molecules. The model used is epitomized by two coupled NH_3 oscillators sitting one at either end of a one-dimensional box of a length chosen to match the electronic transition at ~6600 cm⁻¹ (Figure 3). The model is realistic in the sense that the vibrational modes of the NH_3 molecules in a given solvent cage will be coupled so that the vibrational transition dipoles are properties of the entire cage. These transition dipoles can then be treated as time varying perturbations on the solvated electron state.

Fortunately, the absolute intensities of the N–H stretching modes of gaseous NH_3 have been determined so there is a basis for estimating the magnitude of the transition moment.[15a] Thus, an oscillating dipole of an amplitude gauged from the known infrared band intensities has been placed at each end of the one-dimensional box with the coupled oscillators imagined to be 180° out-of-phase as required for infrared activity in this centrosymmetric case. The cage vibrational dipole induces a time-varying electron moment
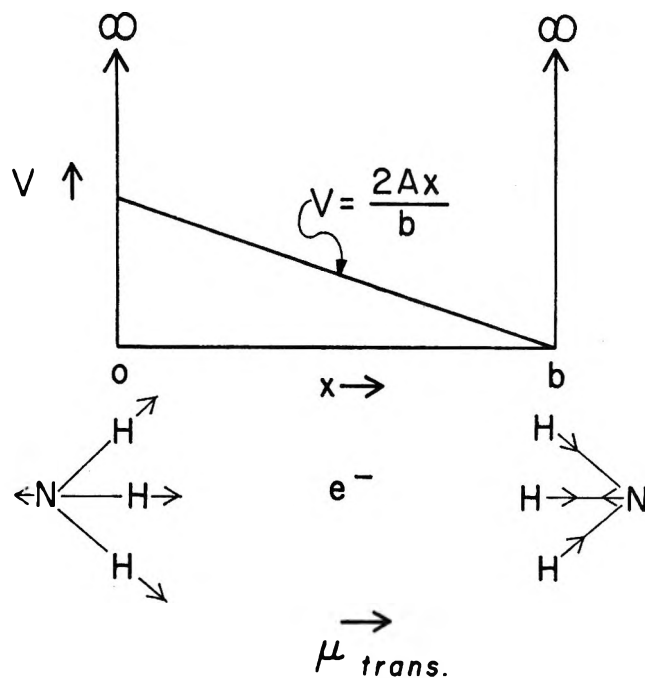
Figure 3. Model for time-dependent perturbation calculation of the response of the solvated electron to the ammonia cage vibrational transition dipole.

described by the expectation value of the electron position. That is

$$e\langle x(t)\rangle = e\langle \Psi^*(x,t)|x|\Psi(x,t)\rangle$$

$$= \text{induced electron moment}$$

From time-dependent perturbation theory

$$\Psi(x,t) = \sum_{n=1}^{\infty} a_n(t)\Psi_n^{\circ}$$

with the $a_n(t)$ determined by solution of the equation

$$H_0\Psi(x,t) + H'\Psi(x,t) = i\hbar\frac{\partial\Psi}{\partial t}(x,t)$$

In the proposed model, $H' = Cx \sin 2\pi\nu t$ where H' represents the time-varying electron potential produced by the cage vibrational moment of frequency ν.

The net dipole transition moment, which is the sum of the induced electron moment together with the perturbing transition moment, has been evaluated as a function of time and is plotted for two periods of the symmetric stretching mode in Figure 4. The plot of the net dipole moment as a function of time shows near cancellation for the first half-period after which the electronic motion and the vibrational dipole tend to move out-of-phase. The latter is a consequence of the nonconservative nature of the time-dependent calcu-

(14) D. F. Burow and J. J. Lagowski, *J. Phys. Chem.*, **72**, 169 (1968).

(15) (a) P. Schatz and D. McKean, *J Chem. Phys.*, **24**, 316 (1956); (b) See, for example, L. Pauling and E. B. Wilson, "Introduction to Quantum Mechanics," McGraw-Hill, New York, N. Y., 1935.
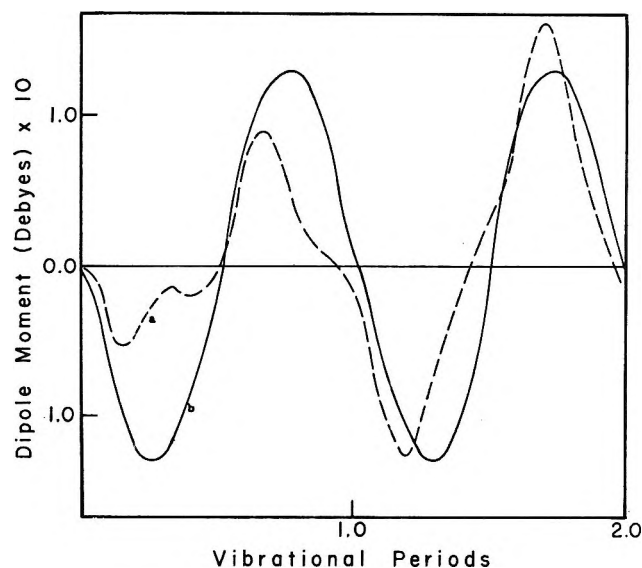
Figure 4. Plot of (a) the "net" transition dipole for the ammonia cage along with its component and (b) the vibrational transition moment.

lation. That is, energy is conserved in the real molecular system, while the perturbation term in the calculation serves to pump energy into the system.[15b] Thus the computed results rapidly lose significance in relation to the system under study.

The key point with respect to Figure 4 is that, for the assumed parameters, one calculates extensive cancellation of the vibrational transition moment as a result of the response of the electron to that moment. This result must seemingly be given considerable credence in the case of the solvated electron for which the electron in a box is generally accepted as being a crude but useful model. More caution may be necessary in viewing the TCNE anion similarly, but the point is made that, insofar as the radical electron in TCNE⁻ can be treated as a particle in a box, it is capable of wiping out the normal infrared activity of the anion. At this stage, the experimental evidence that such a washout actually occurs is much stronger for the TCNE anion than for the ammoniated electron. However, Raman spectra for the alkali metal–liquid ammonia systems should not be seriously influenced by the vibronic effect and might, therefore, clarify whether or not the N–H stretching modes for the cage NH_3 molecules are shifted relative to pure NH_3(liq). If shifted bands are detected in the Raman spectra, then the above explanation for their absence in the infrared will gain significance.

2. TCNE Band Intensities in HMB·TCNE. If, as argued above, the ∼100% electron transfer to TCNE results in an essentially complete washout of the b_{1u} and b_{2u} mode infrared activity, it is reasonable that the ∼5% electron transfer to TCNE in weak complexes, such as HMB·TCNE, should cause a detectable reduction in TCNE band intensities. Results for band in-

tensities for TCNE, HMB, and HMB·TCNE listed in Table III indicate that the b_{2u} band at 1155 cm⁻¹ does experience such a reduction. The 25% decrease in the intensity of this band, the only TCNE band intensity measured during this study, supports the association of this mode with the extremely weak feature in the anion spectrum at ∼1185 cm⁻¹.

Table III: Experimental Absolute Infrared Band Intensities in TCNE, HMB, and the HMB·TCNE Complex. Values are Quoted in Darks = cm/mM

Band	HMB·TCNE	TCNE	HMB
TCNE b_{2u} stretch, 1155 cm⁻¹	856	1140	...
CH_3 deformation, 1380 cm⁻¹	3995	...	1,785
CH_3 wag and rock, 1460 cm⁻¹	7425	...	12,250

The data in Table III also place a quantitative value on the enhancement of the 1390-cm⁻¹ HMB methyl deformation mode that results from the HMB donor action. This enhancement by a factor of 2.2 has also been attributed to a change in vibronic contribution to HMB band intensities.[1] Moszynska has more recently reported data for the C–H stretching region of HMB and its complexes which affirm the importance of changes in vibronic contributions in determining the relative band intensities for various HMB systems.[16] In the present instance, since the 1460-cm⁻¹ band which results from the CH_3 wagging mode experiences a sharp drop in intensity simultaneously with the increase in intensity of the CH_3 deformation mode (Table III), significant changes in vibronic contributions to these band intensities are definitely indicated. This follows, since from a bond moment approach to intensities, the intensities of both the 1460 and 1390-cm⁻¹ bands depend primarily on the magnitude of the same parameter, the C–H bond moment.

Although no quantitative measurements are available, a word regarding the band intensities of several combination tones of TCNE is in order. In neutral TCNE, combination bands at 1114, 1086, 932, 914, and 802 cm⁻¹ rival fundamental bands in intensity. If one accepts published assignments,[2,3] the bands at 1114, 1082, and 914 cm⁻¹ have in-plane transition dipoles while those at 932 and 802 cm⁻¹ have an out-of-plane character. After complexation with HMB only extremely weak features remain corresponding to the in-plane combination tones while the band at 932 cm⁻¹ retains much of its intensity. The 802-cm⁻¹ region is obscured by an HMB absorption. Unaccountably, the above results and discussion are not compatible with one recent report.[4]

(16) B. Moszynska, *Bull. Acad. Pol., Sci. Ser. Math. Phys.*, **17**, 99 (1969).

The foregoing is analogous to the case for the fundamentals in the anion of TCNE wherein the planar modes have lost all intensity while the out-of-plane modes seem relatively unaffected.[1] The implication may be that the combination tones experience a vibronic washout after only ~5% electron transfer, but if so, the reason is obscure. A moderation of the vibrational anharmonicity in the complex is a possible alternate explanation.

C. Miscellaneous Observations. During the course of extended studies on charge-transfer systems involving TCNE a number of isolated, but perhaps noteworthy, observations have been made. These are considered briefly in turn in this section.

1. Anion Stability. It has been stated that the anion of TCNE has a half-life of ~0.5 hr.[17] This does not match our observation that the alkali metal salts of TCNE⁻ can be kept indefinitely under vacuum.[18a] It should be emphasized that such a statement regarding half-life applies only to one particular set of conditions.

2. Tri- and Dianions of TCNE. Strong but sketchy evidence for the presence of $Na_3(TCNE)^{3-}$ as well as the dianion salt was noted in the infrared spectra for certain codeposits of TCNE with the alkali metals. Samples prepared using excess metal routinely absorbed strongly at 1980 and 2090 cm⁻¹. The band at 1980 cm⁻¹ quickly disappears when the thin film deposits are exposed to TCNE vapor while the band at 2090 cm⁻¹, which can be assigned with some confidence to the dianion,[18b] weakens only after a prolonged period of exposure. Since the TCNE MO's available for additional electrons are carbon–nitrogen antibonding, the band at 1980 cm⁻¹ can reasonably be assigned to a C≡N stretching mode in TCNE³⁻.

3. MO Utilized in Weak TCNE Complexes. Although solid state infrared spectra for HMB·TCNE complexes (2:1 and 1:1) indicate that the TCNE molecule occupies a site of relatively low symmetry[19,20] probably not superimposed directly over the HMB ring, a comparison of the frequency shifts for TCNE modes in the HMB complex with those for the anion indicate

that the same TCNE molecular orbital is used in forming both charge-transfer systems. Thus, Table I shows that the magnitude and direction of the shifts for the HMB complex are consistent with a partial transfer of charge into the B_1 MO, the same MO occupied by the radical electron in TCNE⁻. No other available TCNE MO would be expected to give a similar shift pattern.

4. Glassy HMB·TCNE Samples. A glassy deposit of HMB·TCNE formed by sublimation onto a substrate at −180° contains primarily 1:1 units of the HMB·TCNE complex. Two features in the infrared spectrum support this statement. First, $\nu_{C=C}$ appears sharply at 1550 cm⁻¹, at least 10 cm⁻¹ lower than for the crystalline complex so that judging from what has been reported in section A, a more extensive charge transfer is indicated. The greater overlap permitted by direct superposition of molecules in a 1:1 complex unit can account for this extra charge transfer (Figure 2). Second, the glass has an intense infrared band at 1295 cm⁻¹ which is well known to result from an "electron vibration" mechanism[19,20] and which requires that the HMB molecules occupy low symmetry sites such as in the 1:1 unit in solution.[21] The annealing of the glassy complex at −78° results in a slow conversion into the crystalline complex as is evidenced by the disappearance of the 1295-cm⁻¹ band and the shifting of $\nu_{C=C}$ to 1560 cm⁻¹.

(17) (a) D. N. Dhar, *Chem. Rev.*, **67**, 611 (1967); (b) M. G. Ormerod and L. G. Stoodley, *Nature*, **195**, 262 (1962).

(18) (a) Similar stability has been reported by O. W. Webster, W. Mahler, and R. E. Benson, *J. Org. Chem.*, **25**, 1470 (1960); (b) O. W. Webster, W. Mahler, and R. E. Benson, *J. Amer. Chem. Soc.*, **84**, 3678 (1962).

(19) B. Hall and J. P. Devlin, *J. Phys. Chem.*, **71**, 465 (1967).

(20) B. Moszynska and A. Tramer, *J. Chem. Phys.*, **46**, 820 (1967).

(21) E. E. Ferguson and J. Chang, *ibid.*, **34**, 628 (1961).

Carbon-13 Nuclear Magnetic Resonance Spectroscopy. III.

Chloro-Substituted Ethanes and Ethylenes[1]

by Goh Miyajima*

Naka Works, Hitachi, LTD.; Ichige-cho 882, Katsuta, Ibaraki, Japan

and Kensuke Takahashi

*Department of Industrial Chemistry, Nagoya Institute of Technology,
Gokiso-cho, Showa-ku, Nagoya, Japan* (*Received December 30, 1969*)

Publication costs assisted by Sendenbu, Hitachi, Ltd., Tokyo, Japan

Carbon-13 resonances for all the 15 chloro-substituted ethanes and ethylenes have been observed at 15.085 MHz. The observed multiplet structures due to the coupling with indirectly bonded protons indicate that the absolute values of the $^2J_{CH}$ found in these compounds are not larger than 16.5 Hz. Successive substitution of hydrogen, directly bonded to carbon-13 by chlorine, in an ethane series shifted carbon-13 resonances to the lower shielding by about 30 ppm, but substitution in an ethylene series did not give such a large lower shielding shift. The small shift found in ethylene series is attributable to the resonance between the double bond and the chlorine atom.

Carbon-13 nuclear magnetic resonances have been observed earlier by Lauterbur with rapid sweep and dispersion shape.[2] Subsequently, few reports have treated fine multiplet structures of the carbon-13 resonances.[3,4] The resonances of methyl and ethyl halides have been reported by Lauterbur and Spiesecke and Schneider.[5,6] Additive effects of the substituents on carbon-13 chemical shifts have been discussed.[7,8] Such effects are very useful for the structural determination of organic compounds. However, sometimes these additive effects differ with the increase in the number of substituents. Therefore, we present the carbon-13 spectral data for all the 15 chloro-substituted ethanes and ethylenes.

Experimental Section

Carbon-13 spectra were observed with a RF frequency-swept Hitachi R-20 spectrometer operated at 15.085 MHz. The field was locked by the conventional techniques to the proton resonance in an external reference. Spectra were accumulated on Hitachi 400-channel RAH-403 and 1600-channel A-1600A averagers. Most of the samples used in this study are commercially available, and CH_2ClCCl_3 was kindly supplied by Kureha Chem. Ind. Co. LTD. Two carbon-13 enriched samples $^{13}CH_3I$ and $CH_3^{13}COOH$ were used for checking the field homogeneity and field strength. Resonance was observed with pure liquid placed in a spinning 8-mm o.d. 7-mm i.d. tube. Frequencies of both ends of the recorded chart were counted with a frequency counter. Therefore, the chemical shifts and the coupling constants were read on the chart by interpolation. The error of this interpolation technique will not exceed ±0.2% of the total sweep width. The chemical shifts of the samples were

compared with that of 55% carbon-13 enriched methyl iodide diluted with one-third volume of benzene. In this article the values of the chemical shifts were reduced to the second reference of carbon disulfide whose chemical shift was taken as 214.5 ppm from the first reference mentioned above. Although the sample substitution method was employed for referencing, the chemical shifts were not corrected for bulk susceptibility and for glass tube variations.

Results and Discussion

The carbon-13 nmr data obtained are presented in Table I. The observed coupling constants, $^1J_{CH}$ and $^2J_{CH}$, have been discussed before.[4] Consequently, this article is mainly concerned with the chemical shift data of the 15 chloro-substituted ethanes and ethylenes.

A. Carbon-13 Spectra. Some of the typical spectra are shown for ethyl chloride in Figure 1. The methyl carbon resonance peak splits into four parts owing to the $^1J_{CH}$ with three directly bonded protons, but the

(1) This report was presented partly at the 21st Annual Meeting of the Chemical Society of Japan, Osaka, April 1968, Abstract Vol. 1, p 292.

(2) P. C. Lauterbur, *J. Chem. Phys.*, **26**, 217 (1957).

(3) F. J. Weigert and J. D. Roberts, *J. Amer. Chem. Soc.*, **89**, 2967 (1967); **90**, 3543 (1968).

(4) G. Miyajima, Y. Utsumi, and K. Takahashi, *J. Phys. Chem.*, **73**, 1379 (1969).

(5) P. C. Lauterbur, *Ann. N. Y. Acad. Sci.*, **70**, 841 (1958).

(6) H. Spiesecke and W. G. Schneider, *J. Chem. Phys.*, **35**, 722 (1961).

(7) (a) D. M. Grant and E. G. Paul, *J. Amer. Chem. Soc.*, **86**, 2984 (1964); (b) W. M. Litchman and D. M. Grant, *ibid.*, **90**, 1400 (1968).

(8) G. B. Savitsky and K. Namikawa, *J. Phys. Chem.*, **67**, 2430 (1963).
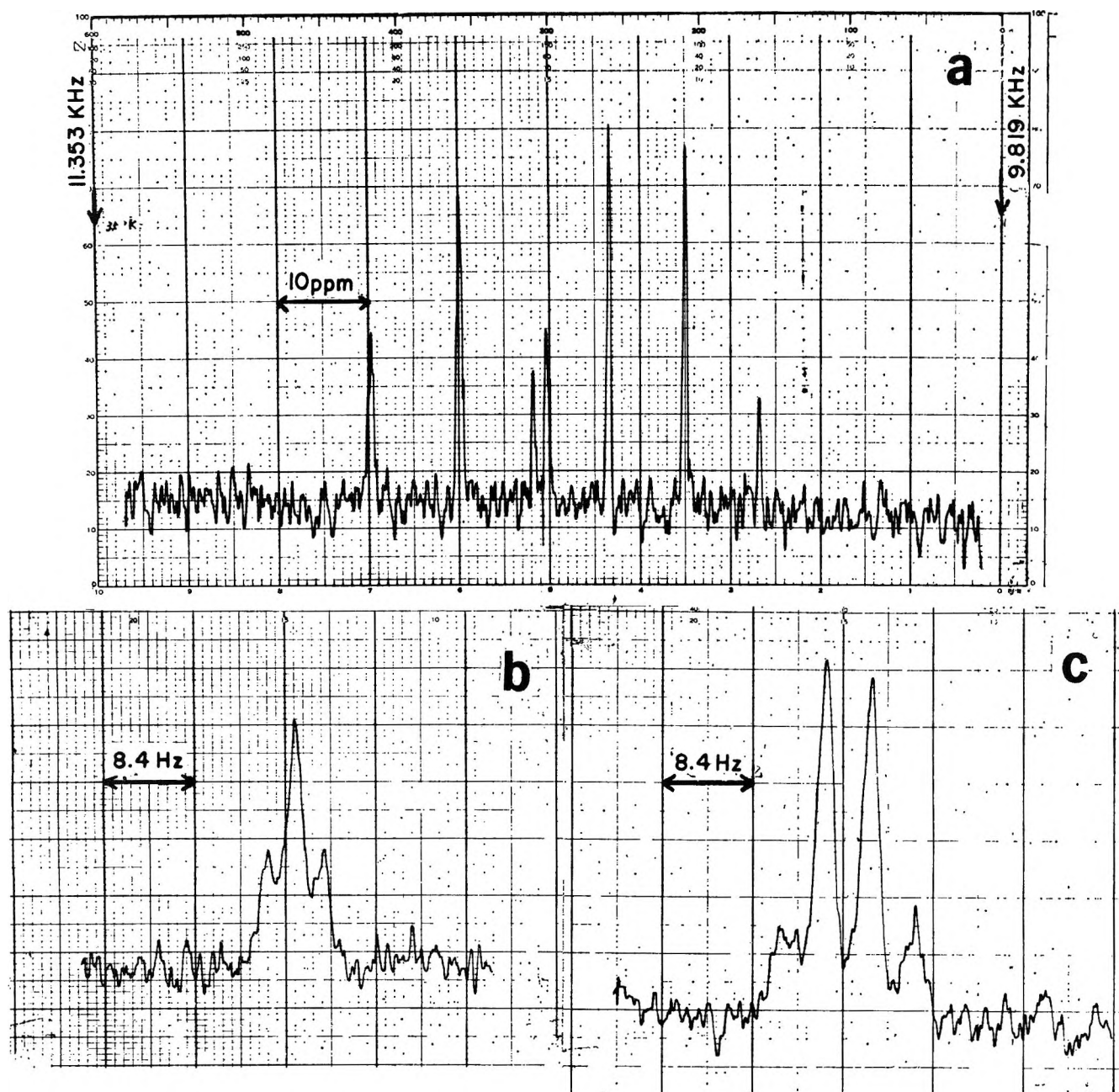
Figure 1.   Carbon-13 nmr spectra of ethyl chloride.   Applied frequency increases from right to left at a constant magnetic
field: a, an entire spectrum with a total sweep width of 100 ppm, signal averaged for 1024 scans; b, an extended spectrum
of the third signal from right in a, signal averaged for 224 scans; c, an extended spectrum of the sixth signal from right
in a, signal averaged for 1024 scans.   The sweep time for one scan was 128 sec in a, b, and c.

methylene carbon resonance peak reveals a further
small splitting owing to $^2J_{CH}$.   This splitting is clearly
noticed in the expanded spectra shown in Figure 1b and
1c.

B. The Chemical Shift.   The chemical shift values
were obtained for the 15 chloro-substituted ethanes and
ethylenes.   The chemical shifts of ethyl chloride were
given previously by Spiesecke and Schneider.[6]   Their
values are consistent with ours except for a small differ-
ence probably attributable to the difference in mea-
suring procedures.   The methyl carbon chemical shifts
of CH_3CH_2Cl, CH_3CHCl_2, and CH_3CCl_3 were previously

given by Lauterbur,[5] and the consistency with ours is
satisfactory.   The chemical shift value of CH_2ClCH_2Cl
reported before[4] was erroneous.   The correct value is
148.6 ppm.   The relation between the number of sub-
stituents and the induced chemical shifts is given for
chloroethanes in Figure 2.   In this figure the com-
pounds are classified as $^{13}CH_{3-m}Cl_mCH_{3-n}Cl_n$ where m is
the number of chlorine atoms directly bonded to the
carbon-13 in problem, and n is the number of chlorine
atoms bonded to the carbon atom adjacent to the car-
bon-13 atom.   Four curves are shown in Figure 2.
The curve at the top is concerned with the chemical

Table I: Carbon-13 Nmr Data of Chloro-Substituted Ethanes and Ethylenes

No.	Compound	Functional group	Shift,[a] ppm	$^1J_{CH}$,[b] Hz	$|^2J_{CH}|$,[c] Hz
1	CH_3CH_3		188.0[d]	124.9[e]	−4.5[e]
2	CH_3CH_2Cl	CH_3	175.0	128	2.6
		CH_2Cl	153.8	150	4.2
3	CH_3CHCl_2	CH_3	161.2	130	<1.2
		$CHCl_2$	124.5	179	5.1
4	CH_3CCl_3	CH_3	147.4	132	
		CCl_3	97.5		5.9
5	CH_2ClCH_2Cl		148.6	155	<2
6	$CH_2ClCHCl_2$	CH_2Cl	142.1	158	<2
		$CHCl_2$	121.4	181	2.5
7	CH_2ClCCl_3	CH_2Cl	133.0	158	
		CCl_3	96.1		3.2
8	$CHCl_2CHCl_2$		118.2	179	<2
9	$CHCl_2CCl_3$	$CHCl_2$	112.5	182	
		CCl_3	92.8		1.5
10	CCl_3CCl_3[f]		87.6		
11	C_2H_4			156.4[e]	−2.4[e]
12	C_2H_3Cl	CH_2	76.5	198	4.3
		$CHCl$	67.6	162	9.3, 6.7
13	trans-$C_2H_2Cl_2$		72.6	199	<1.8
14	cis-$C_2H_2Cl_2$		74.4	198	+16.5[e]
15	gem-$C_2H_2Cl_2$	CH_2	80.4	167	
		CCl_2	66.6		<1.3
16	C_2HCl_3	$CHCl$	76.1	201	
		CCl_2	68.6		8.5
17	C_2Cl_4		72.4		

[a] Referred to the external CS_2. Errors are estimated to be ±0.3 ppm. [b] Errors are estimated to be ±1.4 Hz. [c] Errors are estimated to be ±0.5 Hz. The sign of $^2J_{CH}$ was not determined except the cases specifically given. [d] Reference 6. [e] R. M. Lynden-Bell and N. Sheppard, *Proc. Roy. Soc., Ser. A,* **269,** 385 (1962). [f] Measured for a 31 wt % solution in CCl_4. [g] Reference 4.

Figure 2. Carbon-13 chemical shifts in the series of $^{13}CH_{3-m}Cl_mCH_{3-n}Cl_n$. The number m is the abscissa value.
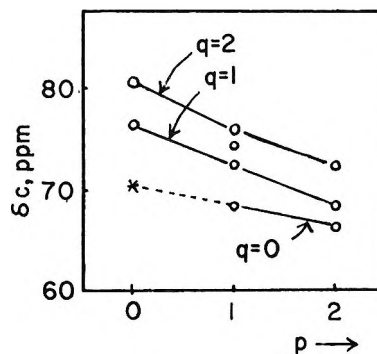
Figure 3. Carbon-13 chemical shifts in the series of $^{13}CH_{2p-}Cl_p=CH_{2-q}Cl_q$. The number p is the abscissa value. *, See ref 11.

shift of carbon-13 bonded to a methyl group (m = 0 ∼ 3, n = 0). As Figure 2 shows, the chemical shift values are arranged in a regular order with the increase of the number of substituents, m and n. Therefore, the additive rule may be applied to these chloro-substituted ethanes, as Litchman and Grant stated it may be applied on various halogen-substituted methanes.[7b] The top curve in Figure 2 is in negative deviation from a straight line, but this situation is different in the lower two curves which are in positive deviation from a straight line, the substitution of one hydrogen atom by a chlorine atom shifts the resonance of carbon-13 by 30 ppm when n = 0, but the shift decreases with the increase of n. This decrease may be interpreted by the mutual interaction between substituents, as Litchman and Grant stated.[7b] The effect of one unit change of n is given by the difference in height of the two neighboring curves in Figure 2 and seems to increase with the increase in n and the decrease in m. The same treatment can be applied to the data of chloro-substituted ethylenes. Although the data of ethylene

series are smaller in number than those of ethane series, the effect of substituents in ethylene series on the chemical shift seems to be meaningful. For convenience, the compounds are classified as $^{13}CH_{2-p}Cl_p=CH_{2-q}Cl_q$, where p is the number of chlorine atoms directly bonded to the carbon-13 in question and q is the number of chlorine atoms bonded to the carbon atom adjacent to the ^{13}C atom. The curve at the top in Figure 3 is associated with the largest value of q, but that in Figure 2 is associated with the smallest value of n. Therefore, the effect of the substituents on the adjacent carbon atom on the carbon-13 chemical shifts in chloroethylenes is the reverse of that in ethane series. We have not yet obtained the experimental chemical shift value of ethylene itself. However, the value for ethylene estimated from

Figure 3 is about 70 ppm. Pople obtained the same value from the data reported by Friedel and Retcofsky.[9,10] Recently Savitsky, et al., have adopted a value of 70.4 ppm (reference CS_2) for ethylene.[11] The observed range of the chemical shifts for the ethylene series is narrower than that of the ethane series although the maximum number of substituents on a carbon atom is smaller by one in the former than in the latter. Three main effects of substituents contributing to the chemical shifts are so-called inductive, magnetic anisotropy, and resonance effects. Inductive effect may be dominant in ethanes, but in ethylenes another effect, which is negligible in ethanes, may contribute to the shift. This effect may be associated with the largest difference between the structures of ethane and ethylene molecules, namely, the presence or absence of the π electron system. The contribution of substituents in ethylenes seems to be reverse in direction with the inductive effect. The following types of resonance forms, I and II, are proposed for interpreting the dipole moment of substituted ethylenes.[12] The effect of such

$$C=C-Cl \qquad -C-C=Cl^+$$
$$\text{I} \qquad\qquad \text{II}$$
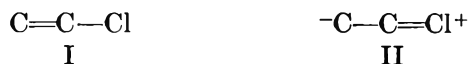
a resonance form on the carbon-13 chemical shift has been discussed before on some vinyl compounds by Maciel.[13] In the series of $CH_2=CCl_2$, $CHCl=CCl_2$, and $CCl_2=CCl_2$ the effect of the directly bonded chlorine atom on the chemical shift is about 4 ppm. This is much smaller than that for the ethane series which amounts to about 30 ppm. Such an effect for ethanes decreases with the increase of n, as described before. We assume that this decrease is attributable to the mutual interaction between substituents. This kind of mutual interaction between substituents seems to increase for the ethylene series because of the absence of free rotation around the carbon–carbon bond, which is found in the ethane series. Thus the effect of the directly bonded chlorine atom on the chemical shift is small for ethylenes. The introduction of a chlorine atom onto the adjacent carbon atom (the increase of q) causes the higher shielding shift on the chemical shift for ethylenes, which is reverse to the effect for ethanes.

This shift is mainly ascribed to the resonance form of II. The polarization of II causes the higher shielding shift for the carbon possessing a negative charge. Two β-positioned chlorine atoms may cause a further effect on the shift in addition to the mutual interaction effect because of the increase of the number of canonical forms, IV and V, as follows. The point referred to as
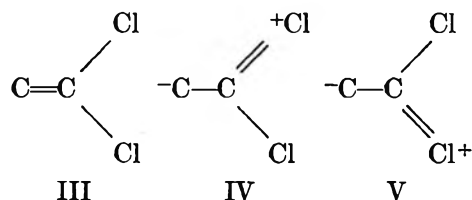
trans-dichloroethylene in Figure 3 is on the straight line of $q = 1$ and that of cis-dichloroethylene is in a small deviation. A cause of the shift in these cis- and trans-chloroethylenes was previously discussed by Savitsky and Namikawa,[14] but their assignment of cis- and trans-dichloroethylenes is the reverse of ours. Their interpretation is based on a steric interaction between substituents. If our assignment is correct, Savitsky and Namikawa's interpretation cannot be applied to dichloroethylenes. We described before the fact that the mutual interaction between substituents may cause the higher shielding shift for ethanes and ethylenes. This interpretation is applicable to these cis- and trans-dichloroethylenes, but such an interpretation cannot be applied to cis- and trans-dibromo- and diiodoethylenes. As pointed out by Spiesecke and Schneider,[6] a magnetic anisotropy effect must be taken into consideration. However, more data must be accumulated for various ethane halides. This study along is now being undertaken.

(9) J. A. Pople, Mol. Phys., 7, 301 (1964).

(10) R. A. Friedel and H. L. Retcofsky, J. Amer. Chem. Soc., 85, 1300 (1963).

(11) G. B. Savitsky, et al., J. Chem. Phys., 49, 2395 (1969).

(12) C. P. Smyth, "Dielectric Constant and Molecular Structure," McGraw-Hill, New York, N. Y., 1955.

(13) G. E. Maciel, J. Phys. Chem., 69, 1947 (1965).

(14) G. B. Savitsky and K. Namikawa, ibid., 67, 2754 (1963).

Conjugated Radicals. IX.[1] Experimental Study and the LCI–SCF Open Shell Calculations on the Electronic Spectra and the Redox Equilibria of the Nitrogen-Containing Violenes

by S. Hünig, D. Scheutzow,

Institute of Organic Chemistry, University of Würzburg, 87 Würzburg, Germany

P. Cársky, and R. Zahradník*[2]

Institute of Physical Chemistry, Czechoslovak Academy of Sciences, Prague, Czechoslovakia (Received May 22, 1970)

Publication costs borne completely by The Journal of Physical Chemistry

Electronic spectra of the eight nitrogen-containing violenes are presented. Calculations undertaken were of the PPP-type combining the open shell SCF procedure of Longuet-Higgins and Pople with configuration interaction. Calculated transition energies and oscillator strengths agree with the absorption curves. Violenes appear to be π-isoelectronic with the corresponding diaza hydrocarbon anion radicals; therefore, the spectra of the latter can be expected to be closely similar to those of violenes. The tendency of bis(1-methylpyridine-4) violene and bis(1-methylpyridine-4)-hexamethine violene to disproportionation is discussed in terms of the coulomb repulsion integrals.

Introduction

In the earlier papers[3–5] of this series we investigated the application of the semiempirical restricted open shell calculations to the electronic spectra of radicals. As rather encouraging results were obtained with the hydrocarbon radicals, an extension of those attempts on the systems containing heteroatoms, therefore, appeared to be straightforward. Violenes I–VIII were
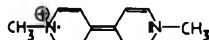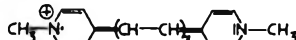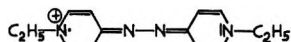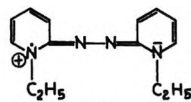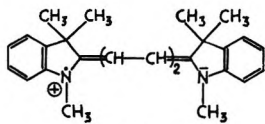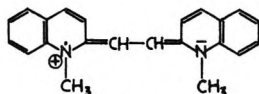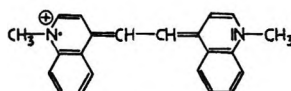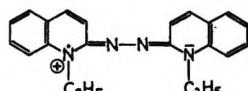
found to represent a suitable series of compounds, since they possess properties which were demanded by the nature of such a study: (1) the series of compounds is sufficiently large, which appears to be a necessary condition for any study exploiting the semiempirical calculations; (2) all members of the series possess only one type of heteroatom, so that with respect to the hydrocarbon systems the number of semiempirical parameters in the calculations increased as little as possible; and (3) all radicals of this series can be handled experimentally without great difficulty, and therefore, the experimental data are reliable.

Experimental Section

Electronic spectra of the system I were reported by Kosower and Cotter.[6] Solutions of the violenes II, VI, and VII in acetonitrile were prepared by the electrolysis of the respective bisquaternary salts (fluoroborates), which were prepared by the methods reported by one of us previously.[7] The electrolysis was carried out in a simple manner similar to that used frequently in esr

(1) Part VIII: P. Cársky and R. Zahradník, *Collect. Czech. Chem. Commun.*, in press.

(2) To whom all correspondence should be addressed at Institute of Physical Chemistry, Czechoslovak Academy of Sciences, Máchova 7, Prague 2, Czechoslovakia.

(3) R. Zahradník and P. Cársky, *J. Phys. Chem.*, **74**, 1240 (1970).

(4) P. Cársky and R. Zahradník, *ibid.*, **74**, 1249 (1970).

(5) P. Cársky and R. Zahradník, *Collect. Czech. Chem. Commun.*, **35**, 892 (1970).

(6) E. M. Kosower and J. L. Cotter, *J. Amer. Chem. Soc.*, **86**, 5524 (1964).

(7) D. Scheutzow, Dissertation, Würzburg, 1966.

spectroscopy: the platinum wire cathode was inserted directly into the quartz cell and the voltage between the two platinum electrodes was gradually increased without a control of the potential until the color of the formed radical appeared. The cathode and anode compartments were separated only by a narrow joint in the quartz cell, but this appeared to be enough to prevent a solution from passing from one compartment into the other. Et_4NBF_4 (0.1 M) served as a supporting electrolyte. This technique enabled us to follow the course of the electrolysis, particularly the two one-electron steps, bisquarternary salt → violene → reduced form (subsequently designated as Ox → Sem → Red), and to estimate roughly the semiquinone formation constants and molar extinction coefficients. The absorption bands appear to be assigned correctly to the radicals II, VI, and VII in the light of the following facts: (1) absorption curves of Sem and Red forms exhibited features which could be expected on the basis of comparison with the absorption curves of the previously prepared[7-9] violenes and their corresponding Red forms, from which some were even isolated as crystalline solids; (2) after exposure the solutions of the electrogenerated Sem and Red forms to air, only the absorption curve of the Ox form was reproduced, which indicates a presence of other species than those of the redox system Ox ⇌ Sem ⇌ Red is unlikely; and (3) esr measurements were done in parallel under the same conditions in a similar apparatus; the increase and decrease of an esr signal corresponded well to the Ox → Sem → Red process. Electrogenerated radicals II, VI, and VII were stable for several hours. The preparation of violenes III-V and VIII was described elsewhere.[7-9]

In the subsequent discussion we compare the electronic spectra of violenes with the available spectral data for corresponding azine and hydrocarbon radical anions. In spite of the fact that the violenes were measured in acetonitrile and azine and hydrocarbon radical anions in dimethoxyethane or hexamethylphosphoramide and even that the counterions were different, we think this comparison is meaningful. A support for this is a finding that solvent effect on the electronic spectra of acenaphthylene, fluoranthene, and aceheptylene radical anions[10] is rather small and that the difference in the respective absorption maxima wavelengths of free and associated polyacene and polyphenyl radical anions with the counterions[11] is usually less than 1000 cm^{-1}.

Calculations

The open shell SCF procedure due to Longuet-Higgins and Pople combined with the limited configuration interaction (LCI) was employed. Details have been given previously.[12] The only new feature appearing in the present calculations was the semiempirical parameters for the nitrogen atoms, viz. the ionization poten-

tial (I_N), one center repulsion integral (γ_{NN}), and the resonance integrals (β_{CN} and β_{NN}). As with the calculations on the hydrocarbon radicals, we tried to use the same parameters which are most frequently employed in the PPP calculations on the respective parent closed shell systems. From inspection of the main resonance structures of violenes, e.g., system I, the nature of the
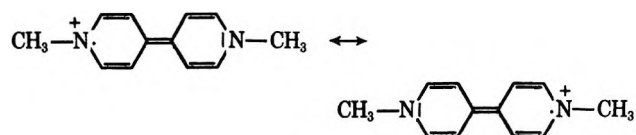
alkylated nitrogen atoms appears to be close to that of the nitrogen atoms in pyrrol- and aniline-like compounds. We performed calculations with the parameters reflecting this behavior, I_N = 30.1 eV, γ_{NN} = 20.4 eV, and β_{CN} = 1.854 eV (β_{CN} = 0.8 β_{CC}), but unsatisfactory results were obtained. The choice of the more suitable parameters was influenced mainly by the two following facts: (1) striking similarity in the electronic spectra of the violene I and bipyridyl anion radical (IX),[13] violene II and 1,6-diphenylhexatriene anion radical,[14] quinoline, acridine, and 9,10-diazaphenanthrene anion radicals[15] and naphthalene, anthracene, and phenanthrene anion radicals, respectively, was found, and (2) if the $\sigma-\pi$ separability was perfect, the
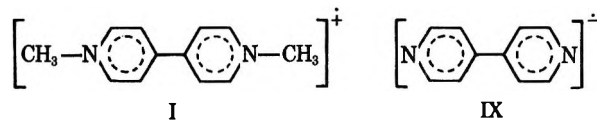
systems I and IX should be π-isoelectronic. From this it follows that the alkylated nitrogen atoms in violenes should be treated as less electronegative. On the basis of our experience with the PPP calculations on the closed shell systems, we selected for all nitrogen atoms the following set of parameters, which appears to be suitable for azacompounds and pyridine-like compounds: I_N = 14.1 eV, γ_{NN} = 12.3 eV, and β_{CN} = β_{CC}.

For all systems an idealized geometry was considered: bond lengths being 1.40 Å, rings were regarded as the regular pentagons and hexagons, and an all-trans configuration was considered whenever a polyene chain

(8) G. Ruider, Dissertation, Würzburg, 1967.

(9) S. Hünig, H. Balli, H. Conrad, and A. Schott, Justus Liebigs Ann. Chem., 676, 36 (1964).

(10) P. Hobza, V. Rejholec, P. Čársky, K. Hafner, and R. Zahradník, Collect. Czech. Chem. Commun., to be published.

(11) K. H. J. Buschow, J. Dieleman, and G. J. Hoijtink, J. Chem. Phys., 42, 1993 (1965).

(12) R. Zahradník and P. Čársky, J. Phys. Chem., 74, 1235 (1970).

(13) C. D. Schmulbach, C. C. Hinckley, and D. Wasmund, J. Amer. Chem. Soc., 90, 6600 (1968).

(14) G. J. Hoijtink and P. H. van der Meij, Z. Phys. Chem. (Frankfurt am Main), 20, 1 (1959).

(15) J. Chaudhuri, S. Kume, J. Jagur-Grodzinski, and M. Szwarc, J. Amer. Chem. Soc., 90, 6421 (1968).
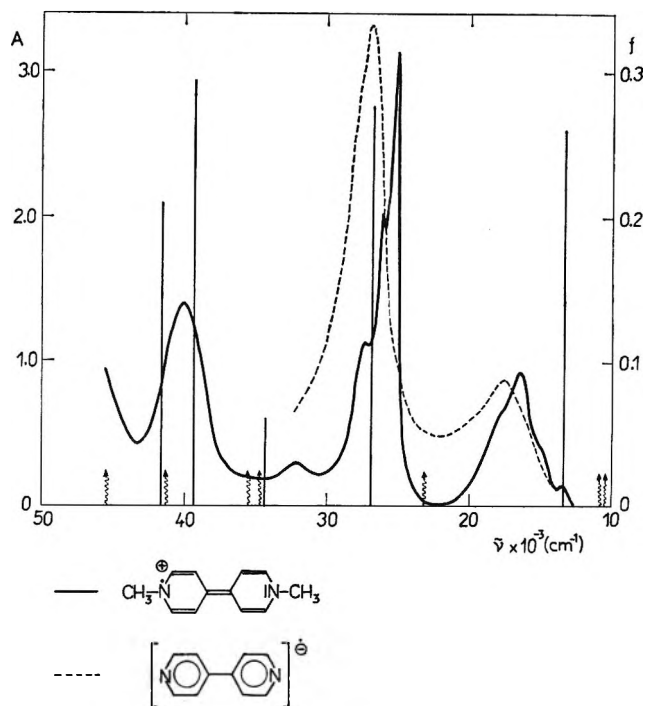
Figure 1. Electronic spectra of the violene I[6] and the
4,4'-bipyridyl radical anion[13] and the results of the semiempirical
calculation. The vertical lines indicate the allowed transitions,
the wavy lines with arrows the forbidden ones. A stands for the
optical density, f denotes the calculated oscillator strengths.
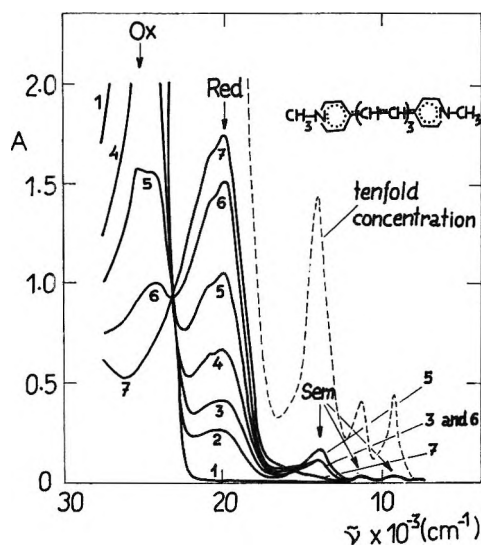
Figure 2. The course of the electrolysis of
1,6-bis(1-methylpyridinium-4)-hexatriene difluoroborate in
acetonitrile as followed by measuring the electronic spectra.
The initial concentrations of the bisquarternary salt (Ox)
were 5×10^{-5} and 5×10^{-4} M, respectively. The absorption
of the bisquarternary salt alone before electrolysis is represented
by curve 1. Curve 5 concerns the moment at which
the concentration of the violene (Sem) during the
electrolysis is the highest and curve 7 represents
the absorption of the reduced form alone.

occurred. The nitrogen atoms bearing a charge were
placed so as to lie as far apart as possible, e.g.
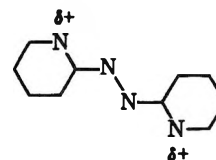
Calculations were carried out on the EL X8 (Elec-
trologica) computer in the Computing Center of the
University of Würzburg.

Results and Discussion

Electronic Spectra. Figure 1 presents the absorption
curves of radicals I and IX, the π systems of which are
isoelectronic. The nature of the spectra is well re-
produced by the calculation, even though the theory
overestimates the intensity of the first band. The
ratio of the observed oscillator strengths of the second
and the first band amounts to 1.9 while the theory pre-
dicts the value 1.1. Violene II exhibits a rather un-
favorable semiquinone formation constant.[16] That
means that in solution considerable disproportionation
of II occurs (2 Sem $\rightleftarrows$ Ox + Red). In order to obtain a
sufficiently high equilibrium concentration of II, a
rather high initial concentration of the bisquaternary
salt had to be used in the electrolysis (Figure 2). Owing
to disproportionation, the absorption of II can be mea-
sured only in the long-wave region where neither the
bisquaternary salt nor the reduced form absorbs. The
recorded absorption curve resembles that of 1,6-diphe-
nylhexatriene anion radical[14] (Figure 3). The calcu-
lations give the same picture, but the theory under-
estimates the red shift when passing from 1,6-diphe-
nylhexatriene anion radical to II. This is probably due
to the parametrization used, which in fact yields the
results for the 1,6-dipyridylhexatriene anion radical.
The observed transition energies of the latter can there-
fore be expected to be in better agreement with the
present calculation. Results of the calculations for
violenes III–V, as seen in Figure 4, agree rather well
with the absorption curves. A somewhat less satisfac-
tory agreement was found with systems VI and VII
(Figure 5), particularly with the latter, where the theory
predicts the location of the first band at too low wave-
lengths. This can be caused by two factors. First,
it is observed in some cases that the larger the conju-
gated system under treatment, the greater the devia-
tions of the calculated transition energies from the
experimental values. A discrepancy of that type was
found, e.g., with the hydrocarbon radical cation, bis-
azulenylethylene, where no problems with the semi-
empirical parameters are encountered. However, rather
unsatisfactory results are obtained even with the com-
mon closed shell PPP calculations on the large benze-
noid hydrocarbons.[17] Secondly, the similarity be-

(16) P. Čársky, S. Hünig, D. Scheutzow, and R. Zahradník, *Tetra-
hedron*, **25**, 4781 (1969).
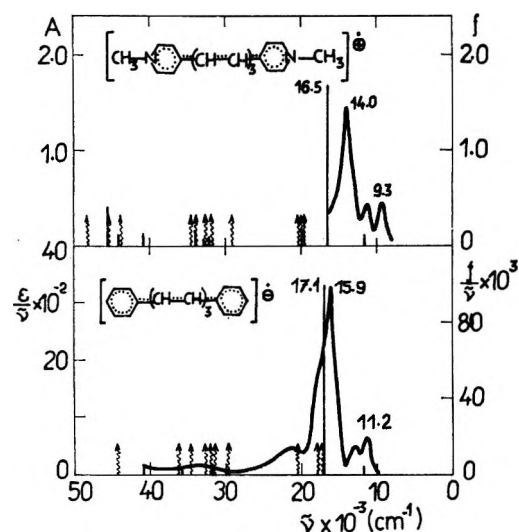
Figure 3. Absorption curves of violene II and the 1,6-diphenylhexatriene anion radical.[14] The results of the semiempirical calculations are indicated by the vertical and wavy lines for allowed and forbidden transition, respectively. The right side scales concern the calculated spectral intensities, where f stands for the oscillator strengths.

Figure 4. Electronic spectra and the results of the semiempirical calculations for violenes III–V. The vertical lines represent the allowed transitions, the wavy lines with arrows the forbidden ones. The right-hand side scales denote the calculated spectral intensities, where f stands for the oscillator strengths.
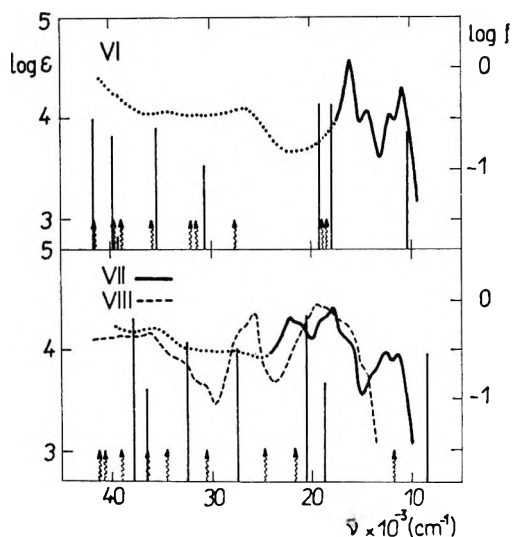
Figure 5. Electronic spectra and the results of the semiempirical calculations for violenes VI and VII. The dotted lines denote the region where the violenes exhibit no strong absorption and where the determined extinction might therefore be influenced by the possible presence of oxidized or reduced form. Calculated allowed transition energies are represented by the vertical lines, the forbidden ones by the wavy lines with arrows. The right-side scales concern the calculated oscillator strengths. For a comparison an absorption curve of the violene VIII (dashed line) is added.

tems I and IX, and therefore, the parametrization can be less realistic in this case. If the nitrogen atoms in VII are treated as amine-like and the semiempirical parameters are changed accordingly, a fit for the first band is obtained. However, it is an easy task in the PPP-type calculation to obtain a fit for one band with the aid of the changed semiempirical parameters. Therefore, we think the utilizability and limitations of the open shell theory can be demonstrated only if the same parameters are used within the whole series of considered systems. The spectrum of VIII is interpreted with the aid of a perturbation treatment.[18] As in the first excited state of VII the prevailing contribution is due to the B(12 → 13) configuration (93%), the effect of the diaza substitution on the location of the first band can be predicted by the equation

$$\delta E(N \longrightarrow V_1) = \sum_\mu (c^2_{13,\mu} - c^2_{12,\mu})\delta\alpha_\mu \qquad (1)$$

where c_{13} and c_{12} are the expansion coefficients of the MO's 12 and 13 in the positions μ where aza substitution takes place and $\delta\alpha_\mu$ means the change in the ionization potential for the mentioned positions. In our case the change in the first transition energy is

$$\delta E = 2[(0.119)^2 - (0.346)^2](-17,500) \approx 3700 \text{ cm}^{-1}$$

tween the violenes VI and VII on the one hand and the respective bisquinolineethylene anion radicals on the other hand does not need to be so large as between sys-

(17) H. Gutfreund and W. A. Little, *J. Chem. Phys.*, **50**, 4468 (1969).

(18) J. N. Murrell, "The Theory of the Electronic Spectra of Organic Molecules," Methuen, London, 1963.

which indicates the presence of hypsochromic shift. As seen in Figure 5, this is in agreement with the experimental finding: the first band of VIII is shifted toward the second band and due to overlap, only one broad band is observed. Hypsochromic shifts upon aza substitution were observed also with the naphthalene (quinoline) and anthracene (acridine) anion radicals,[15] in agreement with the perturbation treatment.

Disproportionation Equilibria. The semiquinone formation constants (K)

$$\text{Ox} + \text{Red} \overset{K}{\rightleftharpoons} 2\text{Sem} \qquad (2)$$

can be predicted with the aid of the coulomb repulsion integrals[16]

$$J_{mm} = \int \varphi_m(1)\varphi_m(2)\frac{e^2}{r_{12}}\varphi_m(1)\varphi_m(2)\,d\tau \qquad (3)$$

where φ_m means the singly occupied MO. We tried to employ this procedure in order to explain the considerable difference shown by violenes I and II in their relative tendencies to disproportionate from the α,ω-diphenylpolyene anion radicals. The latter were found to be stable[14] in dimethoxyethane or tetrahydrofuran in respect of eq 2 in contrast to the series of bis(1-alkylpyridine-4)-violenes[16] in acetonitrile, where the semiquinone formation constant decreases very rapidly as the polyenic chain increases. Thus while the violene I is very stable (log K = 7.0), the violene II disproportionates considerably (log K = −2.6 to −1.5). This trend appears to be general within the series of vinylogs and is confirmed by the calculated J_{mm} values representing the measure of the log K values. As seen in Figure 6, the theory reflects well the behavior of violenes, but overestimates the disproportionation of
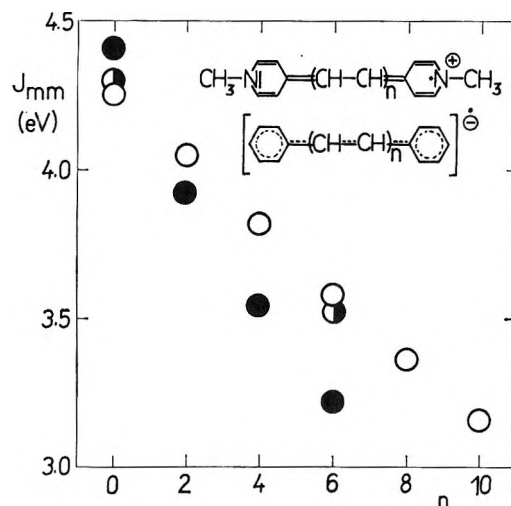
Figure 6. Coulomb repulsion integrals J_{mm} for α,ω-diphenylpolyene anion radicals (O) and violenes calculated with the two sets of semiempirical parameters: ◑ (I_N = 14.1 eV, A_N = 1.8 eV) and ● (I_N = 30.1 eV, A_N = 9.7 eV).

α,ω-diphenylpolyene anion radicals, where the experimentally found log K possesses, surprisingly, the constant value of about 3.5 through 1,12-diphenyldodecahexaene.[14] However, it should be kept in mind that the calculations refer to isolated, unsolvated species. Probably this is just the solvation which makes the comparison of the semiquinone formation constants measured in acetonitrile and dimethoxyethane, respectively, difficult.

New parametrization employed in this paper for nitrogen atoms is believed to change the nature of the previously studied correlations[16] log K *vs.* J_{mm} very little, although it yields somewhat higher J_{mm} values for violenes I and II (Figure 6).

A Potential Surface for a Nonlinear Cheletropic Reaction.

The Decarbonylation of Cyclopropanone

by David M. Hayes, Christopher A. Zeiss, and Roald Hoffmann*

Department of Chemistry, Cornell University, Ithaca, New York 14850   (*Received September 16, 1970*)

Publication costs assisted by the Petroleum Research Fund of the American Chemical Society

The least-motion linear approach of a carbon monoxide molecule to ethylene, or the reverse fragmentation of a cyclopropanone, is a symmetry forbidden reaction. A nonlinear nonleast-motion approach is favored, with unsymmetrical intermediate bonding. The reaction path is shown by the succession of Figures 4, 7, and 5. At large separations there is available to the reacting molecules a large range of geometries at an energy only slightly higher than that of the optimal configuration.

The thermal decarbonylation of the highly reactive cyclopropanones,[1] eq 1, is an exothermic process which has been observed in some instances.[1a] The reaction is

$$ (1) $$
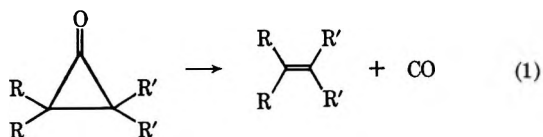
also a prototype nonlinear cheletropic reaction.[2] The significance of the nonlinear designation will become apparent when we draw a level correlation diagram for the least-motion linear decarbonylation or its microscopic reverse, the addition of carbon monoxide to ethylene. Let us locate an ethylene molecule in the xy plane, and consider an approach of carbon monoxide along the z axis, as shown below.
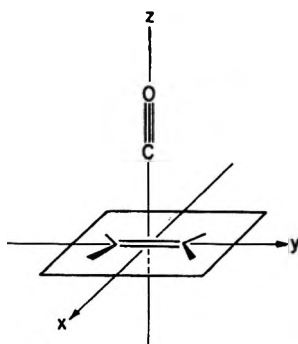
In the correlation diagram (Figure 1) we include the π and π^* levels of the ethylene, the π,π^* and oxygen and carbon lone pairs of carbon monoxide, as well as the corresponding orbitals of cyclopropanone. The approach is of C_{2v} symmetry and the levels are classified accordingly.

It is clear from this correlation diagram that the C_{2v} ground-state reaction is symmetry forbidden.[2] Given the apparent high driving force for fragmentation from the cyclopropanone side it is clear that some way will be

found by the molecule to circumvent the symmetry forbidden least-motion path. Some general arguments for a nonlinear departure have been given;[2] they imply that as the cyclopropanone begins to decompose the CO fragment goes off bending or tilting to one side. To trace the precise nature of this nonlinear departure we have undertaken an exploration of the potential surface by an approximate molecular orbital procedure, the extended Hückel method.[3,4]

Calculations

In our computations we allowed the system six degrees of freedom. Five of these degrees of freedom were varied continuously. These were one distance, D, and four angles θ, ϕ, θ', ϕ' used to describe the location and orientation of a fixed length CO molecule relative to the center of the ethylene (see Figure 2). The sixth degree of freedom was not studied continuously. This was the relaxation of the ethylene moiety from its geometry in free ethylene to its geometry as a fragment of cyclopropanone. We studied in detail only three stages of relaxation. The first geometry, called P, was that of a planar unrelaxed model ethylene with a CC bond length of 1.34 Å. The final relaxed or R geometry was taken from the C_2H_4 fragment of the cyclopropanone structure determined from an analysis of the

(1) (a) N. J. Turro, W. B. Hammond, and P. A. Leermakers, *J. Amer. Chem. Soc.*, **87**, 2774 (1965); N. J. Turro, *Accounts Chem. Res.*, **2**, 25 (1969), and references therein; (b) P. Lipp and R. Köster, *Ber.*, **64**, 2823 (1931); D. A. Semenov, E. F. Cox, and J. D. Roberts, *J. Amer. Chem. Soc.*, **78**, 3221 (1956); W. D. DeMore, H. O. Pritchard, and N. Davidson, *ibid.*, **81**, 5874 (1959); A. Kende, Ph.D. Dissertation, Harvard University, 1956; S. E. Schaafsma, H. Steinberg, and T. J. De Boer, *Recl. Trav. Chim. Pays-Bas*, **85**, 1170 (1966); (c) J. F. Pazos and F. D. Greene, *J. Amer. Chem. Soc.*, **89**, 152 (1967); F. D. Greene and N. M. Weinshenker, *ibid.*, **90**, 506 (1968).

(2) R. B. Woodward and R. Hoffmann, *Angew. Chem.*, **81**, 797 (1969).

(3) R. Hoffmann, *J. Chem. Phys.*, **39**, 1397 (1963), and subsequent papers. We have used here the same parameters as those listed in a previous cyclopropanone calculation in ref 4.

(4) R. Hoffmann, *J. Amer. Chem. Soc.*, **90**, 1475 (1968).
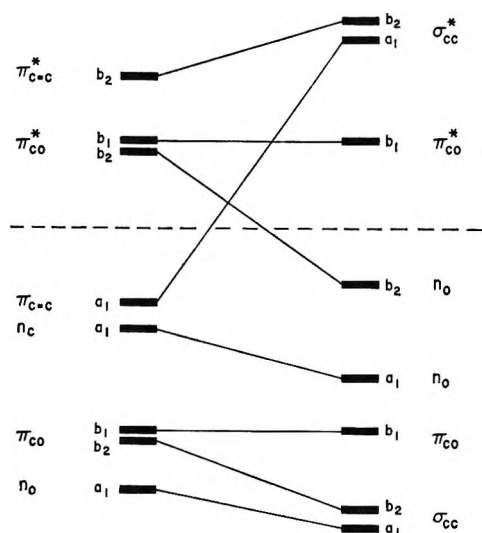
Figure 1. Correlation diagram for the linear addition of CO to ethylene. n_c and n_o at left are carbon monoxide σ levels. The two n_o levels at right are the antisymmetric and symmetric oxygen lone pairs. The exact ordering of bonding and antibonding levels separately is not well defined.
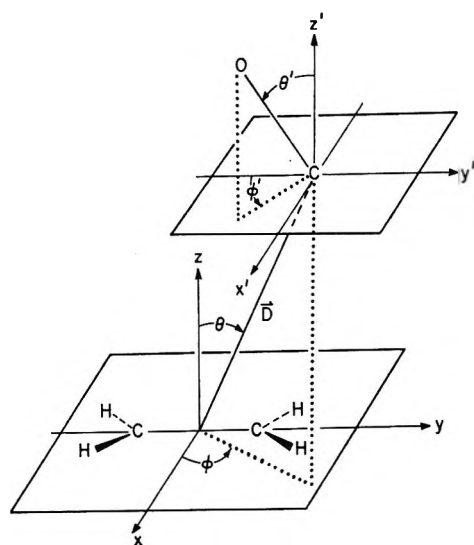
Figure 2. Coordinate system for describing the relative motion of CO and C_2H_4. x',y',z' is a body centered coordinate system with origin at C and axes parallel to x,y,z. Note that the angle ϕ' is measured from the negative y' axis while ϕ is measured from the positive x axis.

microwave spectrum of the molecule.[5] The distinguishing feature of that geometry, aside from its natural puckering of the CH_2 groups from planarity, is the long CC bond of 1.58 Å. The intermediate, or unsymmetrical one carbon planar one carbon relaxed, or PR geometry, was in its bond distances halfway between the planar and relaxed geometries, but had one CH_2 group planar, the other pyramidal as in the totally relaxed structure.

Our computer program was so adapted that for a given D and state of relaxation of the ethylene frag-

ment the values of θ, ϕ, θ', ϕ' were optimized to give the lowest energy. Our only assurance that global minima were located was the achievement of the same set of final angles beginning from very different initial values.

The Reaction Path

Table I lists the global minima found for different values of D. The corresponding energies, relative to separated CO and ethylene, are shown in Figure 3. While the information in Table I is complete, it is not descriptive. We would therefore like to describe in some further detail, with illustrations, the different stages of an approach of carbon monoxide to ethylene.

Table I: Optimum Geometries and Stages of Relaxation as a Function of D

D, Å[a]	Relaxation[b]	θ, deg	ϕ, deg	θ', deg	ϕ', deg
3.00	P	0	0	86	90
2.75	P	0	0	85	90
2.50	P	0	0	84	90
2.25	P	0	0	82	90
2.20	P	0	0	81	90
2.15	PR	27	80	60	49
2.10	PR	27	81	53	41
2.05	PR	27	90	41	0
2.00	R	31	90	24	0
1.80	R	29	90	16	0
1.60	R	21	90	10	0
1.50	R	0	90	0	0

[a] D = distance between CO carbon and center of ethylene. See Figure 2. [b] See text for definition of states of relaxation.

For $D \geq 2.20$ Å we find a not unexpected preference for a planar ethylene fragment. The optimal geometry in this region is quite invariant. Let us call this approach I; three views[6] of a characteristic geometry in this region, that for $D = 2.20$ Å, are shown in Figure 4.

While the preferred orientation is the one illustrated, it should be noted that the energy does not deteriorate significantly if the CO is swung in a circle with the carbon fixed and the oxygen fixed at the same z value (see 1 below). Thus the loss in energy as a result of swinging 90° away from the optimal orientation is 0.12 eV at $D = 2.50$ Å, 0.29 eV at $D = 2.25$ Å. This is to be contrasted with the deterioration on swinging to the least-motion approach, CO along the z axis. This entails an energy loss of 0.99 and 2.22 eV, respectively. Aside from the specific preference for geometry I, this region can thus be characterized by the avoidance of the

(5) J. M. Pochan, J. E. Baldwin, and F. H. Flygare, J. Amer. Chem. Soc., 90, 1072 (1968); 91, 1896 (1969).

(6) These are views, not projections, of the molecule from a vantage point 8 Å removed from the origin, along each of the three coordinate axes. These illustrations were produced by the program OR TEP, C. K. Johnson, ORNL 3794.
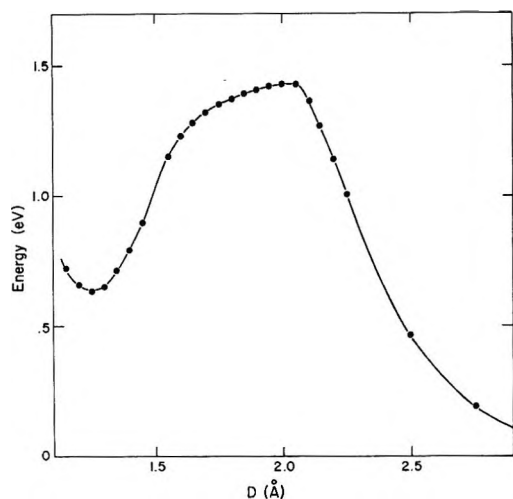
Figure 3. Energy along the reaction coordinate D. The energy zero is for separated CO and C_2H_4.
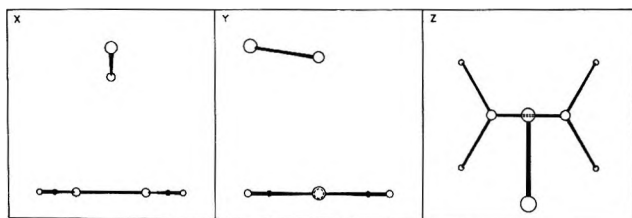
Figure 4. Three views, from vantage points along the positive x, y, and z axes, of an optimal approach geometry at $D = 2.2$ Å. See ref 6.

least-motion approach and a general preference for placing the carbon monoxide molecule in a plane approximately parallel to the plane of the ethylene.

1
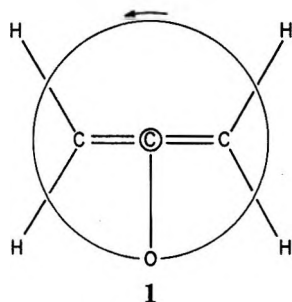
The preference for location of the carbon atom of CO above the ethylene center is probably a consequence of the primary stabilizing interaction in this region, that is between the relatively low-lying π^* orbital of carbon monoxide and the π orbital of the ethylene. The CO π^* is concentrated on the carbon atom. Note the interesting relation between geometry I and the transition state postulated by us for the concerted addition of ketenes to olefins.[2]

It might have been thought that approach I could smoothly move over to cyclopropanone by swinging CO up in the xz plane (i.e., changing θ' gradually from $\sim 80°$ to $0°$). This motion, however, is still a for-

bidden one. Notice that the xz plane remains a symmetry plane throughout such an approach. The resulting correlation diagram remains in its main features identical with that shown in Figure 1. The reduction in symmetry from C_{2v} to C_s correlates a_1 and b_1 to a', and b_2 to a''. There is still a level crossing. The CO molecule must abandon the crucial xz plane if it is to bypass a forbidden reaction.

Our discussion will be made easier if we momentarily skip the transition point around $D = 2.10$ Å and consider the approach region III for $D \leq 2.00$ Å. In this region we essentially are close to cyclopropanone. Full relaxation of the ethylene fragment is accordingly preferred. Three views of a typical optimized geometry, $D = 2.00$ Å, in this region are shown in Figure 5. Geometry III is highly asymmetric, this being also reflected by the charge distribution shown below in 2.

2   3
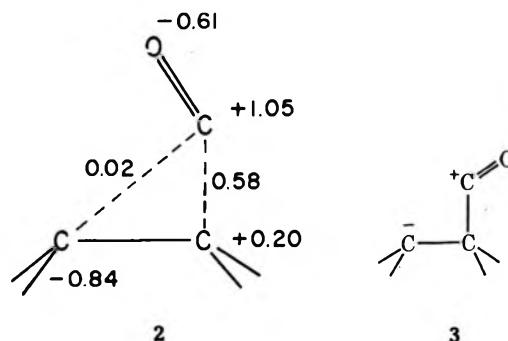
In the case of another nonlinear cheletropic reaction, the addition of singlet methylene to ethylene, we found considerable symmetry in the charge distribution along the reaction path.[4,7] The polarity that is being exhibited in the cyclopropanone case may be an indication that in polar solvents a real zwitterionic intermediate, written as 3, could be stabilized.[8]

The final collapse from III to cyclopropanone is accomplished by a smooth motion of CO to the symmetrical position. This is illustrated by a series of superimposed snapshots in Figure 6.

We now return to region II, the transition region. Our original searches maintained the same intermedi-
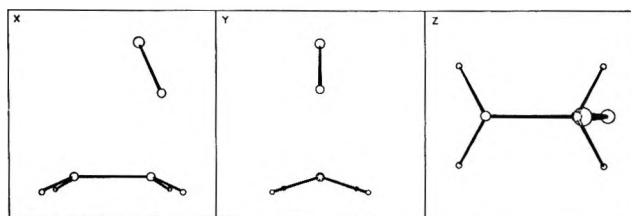
Figure 5. Three views, from vantage points along the positive x, y, and z axes, of an optimal approach geometry at $D = 2.0$ Å. See ref 6.

(7) R. Hoffmann and P. S. Skell, to be published.
(8) See A. S. Kende, Chem. Ind. (London), 1053 (1956); J. E. Baldwin, Can. J. Chem., 44, 2051 (1966).
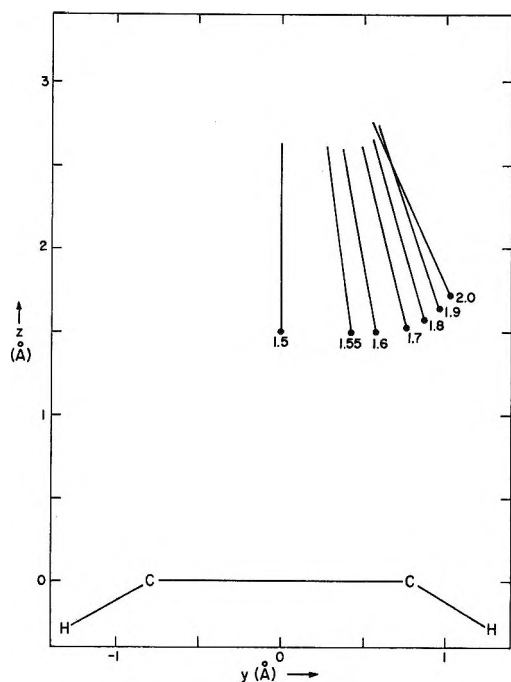
Figure 6. Superimposed snapshots of the terminating approach. A projection on the yz plane is shown. The numbers below the successive CO projections are the values of D.

Figure 7. Three views, from vantage points along the positive x, y, and z axes, of an optimal approach geometry at $D = 2.1$ Å. See ref 6.

Figure 8. Superimposed snapshots of the optimum approach for large D when the CO is constrained to remain in the yz plane. A projection on the yz plane is shown. The ethylene moiety is kept planar.

ate stage of relaxation at both carbon atoms. The very unsymmetrical optimum geometry at the edge of region III, $D = 2.00$ Å, was an indication to us that in region II, the molecule might prefer unsymmetrical relaxation at the two ethylene carbons. This led to the construction of the PR geometry. The PR unsymmetrical geometry is the preferred state of relaxation for $2.00 < D < 2.20$ Å. This appears to be a short interval, but in terms of the other angles very many changes take place in this region. A typical geometry, that at $D = 2.10$ Å is shown in three views in Figure 7. Both from the comparison of Figure 7 with Figures 5 and 4 and from direct examination of the angles in Table I it is clear that geometry II is in every geometrical parameter intermediate between I and III. We have essentially caught a snapshot of a typical molecule as it traverses the region between valleys I and III.

Dynamics

We can now summarize our conclusions on the reaction path for the addition of carbon monoxide to ethylene. For large D, region I, a symmetrical placement of the CO molecule in the xz plane is favored (Figure 4). No relaxation of the ethylene occurs for $D \geq 2.2$ Å. In the region $2.0 < D < 2.2$ Å several changes take place. The carbon monoxide swings to an unsymmetrical position in the yz plane (Figure 7) while the ethylene relaxes the geometry of the nearer carbon. This is region II. Having avoided in this manner the level crossing at the symmetrical position, the carbon monoxide proceeds in region III to fully form the second CC bond.

This is accomplished by a motion toward the symmetrical product structure accompanied by relaxation at the further ethylene carbon.

In the context of modern collision theory the number of molecules traversing precisely this reaction path will be very small. The gross features of the potential surface far in, namely the unsymmetrical approach in region III, will no doubt have consequences on typical molecular trajectories in the cyclopropanone fragmentation. That is, decomposing cyclopropanone molecules will clearly want to avoid the forbidden linear departure and will explore instead unsymmetrical modes in the yz plane. This should have measurable consequences in the isotope effects on the reaction rate entropy of activation for the reaction.

The consequence of the reaction path viewed from the ethylene plus carbon monoxide side is much less certain. It was already pointed out above that in region I the energy does not vary greatly with rotation in a

plane parallel to the xy plane (1). Still another indication of the softness of the potential in this region was obtained from the following numerical experiment. We decided to compute the energy along a trajectory which merged smoothly with a region III geometry. This was accomplished by constraining CO to lie in the yz plane but allowing it the full two degrees of freedom of motion in that plane. The resultant constrained reaction path, Figure 8, indeed merges smoothly with approach III. In the region $2.1 \leq D$ the energy along this path is at most 0.1 eV above the global minimum approach of Figure 4. Clearly, molecules with an approach geometry resembling that of Figure 8 will be nearly as likely to react as those in the optimal geometry of Figure 4. Though we would extrapolate that there is a wide range of reactive impact geometries for this reaction (provided the forbidden approach is avoided), the actual ways in which dynamic effects will manifest themselves must await many-dimensional trajectory calculations.

Given the unsymmetrical reaction path geometries near $D = 2.0$ Å the question arises whether in fact the reaction would be stereospecific. That is, would the stereochemical relationship, cis or trans, of labels in a hypothetical, appropriately labeled cyclopropanone, be retained in the product ethylene. To probe this question we calculated the energy required to twist the far end of the ethylene fragment by 90°. This torsional barrier is understandably large in region I, smaller in region II. It reaches its lowest magnitude near $D = 1.9$ Å, and then rises again as the product cyclopropanone geometry is approached. The lowest value for this torsional barrier is approximately 7 kcal/mol. Though this number is not very reliable we believe the reaction will be stereospecific retaining this particular criterion of a process which though highly unsymmetrical should still be termed concerted.

A Virial Treatment for the Adsorption of Gases on Liquids

by C. M. Greenlief[1]

Department of Chemistry, University of Washington, Seattle, Washington 98105 (*Received November 26, 1969*)

Publication costs borne completely by The Journal of Physical Chemistry

For the adsorption of gases on liquids a virial treatment of the relationship between spreading pressure and gas (bulk) pressure is developed. Analysis of gas–liquid adsorption data in terms of these intensive variables leads to a direct determination of s_0, the distance at which the net interaction between gas and surface is zero, in contrast to the case of gas–solid systems where one obtains the product As_0. Adsorption data for xenon on liquid mercury are analyzed.

I. Introduction

During the past few years a great deal of work has been devoted to the theoretical analysis of high-temperature gas–solid interactions. Due to the paucity of accurate data on gas–liquid interactions, a virial treatment appropriate for the adsorption of gases on liquids has not been formulated. Cassel and Neugebauer made spreading pressure measurements for argon, krypton, and xenon on liquid mercury.[2] The analysis of such data by a virial treatment should provide a valuable supplement and contrast to the gas–solid data.

Theoretical analysis of experimental measurements for the interaction of rare gases with the nearly homogeneous graphitized carbon black P33 is used as a comparative system, since precise measurements were made in the same reduced temperature range. However, this comparison of gas–solid and gas–liquid interaction parameters must be made judiciously since the present analysis assumes the liquid surface is planar, even in the presence of adsorbate molecules. As usual, we assume the adsorbent is unperturbed by the adsorption process.

The study of gas adsorption at the liquid–vapor interface offers certain unique advantages in comparison to the study of the gas–solid interface. Advantages in-

(1) Department of Chemistry, University of Texas, Austin, Texas 78712.

(2) H. M. Cassel and K. Neugebauer, *J. Phys. Chem.*, **40**, 523 (1936).

clude the possibility of reforming a clean, reproducible surface at any time during the adsorption study and the absence of capillaries.

II. Analysis

A gas adsorbed on a surface may be described at low coverages as an imperfect two-dimensional gas. The two-dimensional virial equation of state can be written as

$$\phi/kT = \Gamma + B_{2D}\Gamma^2 + C_{2D}\Gamma^3 + \dots \qquad (1)$$

where ϕ is the spreading pressure (i.e., the decrease in surface tension); k is the Boltzmann constant; T is the absolute temperature; $\Gamma = N_a/A$ is the number of molecules adsorbed per unit area; N_a is the number of molecules adsorbed; A is the surface area; and B_{2D} and C_{2D} are the second and third two-dimensional virial coefficients.

It has been shown that an application of the Gibbs boundary condition to eq 1 yields an equation in terms of gas–surface virial coefficients.[3a,b] In particular

$$P = (kT/B_{AS})[N_a + 2(B_{2D}/A)N_a^2 + \frac{(^3/_2C_{2D} + 2B_{2D}^2)}{A^2}N_a^3 + \dots] \qquad (2)$$

where P is the equilibrium pressure; B_{AS} is the gas–surface second virial coefficient

$$B_{AS} = \int_V \{\exp[-u(\vec{r})/kT] - 1\}d\vec{r} \qquad (3)$$

It must be emphasized that $u(\vec{r})$, the potential energy of interaction of a single molecule with the surface, is a potential of mean force.[4]

B_{2D} and C_{2D} may be expressed in terms of the gas–surface virial coefficients B_{AS}, C_{AAS}, and D_{AAAS}. Clearly, eq 2 is appropriate for the adsorption of gases by solids where one measures P, N_a, and T.

An alternate choice of experimental variables is available when one measures the adsorption of gases on a liquid surface. Namely, one may measure P, ϕ, and T. One may deduce an equation in terms of these variables by inverting eq 1

$$\Gamma = (\phi/kT) - B_{2D}(\phi/kT)^2 + [2B_{2D}^2 - C_{2D}](\phi/kT)^3 + \dots \qquad (4)$$

and substituting eq 4 into eq 2

$$P = (A/B_{AS})\phi + (B_{2D}/kT)(A/B_{AS})\phi^2 + \dots \qquad (5)$$

Data may be analyzed by graphing (P/ϕ) as a function of ϕ. The intercept of this plot is (A/B_{AS}) and the slope is related to B_{2D} as indicated by eq 5.

Cassel and Neugebauer have measured the spreading pressures of argon, krypton, and xenon on liquid mercury. Over the temperature range where mercury remains a liquid, they were unable, within experimental

error, to detect the adsorption of argon. The decrease in surface tension due to adsorbed krypton was measurable at the lower temperatures, but only rather inaccurately. The data for xenon are more extensive and provide a system suitable for analysis. The results of this analysis are summarized in Table I.

Table I: Gas–Surface Virial Coefficients for Xenon Adsorbed on Mercury

T, °K	$(B_{AS}/A) \times 10^6$, cm
293	6.04 ± 0.33
273	8.93 ± 0.12
253	15.1 ± 0.13
237	23.3 ± 1.30

B_{AS} can be expressed in the reduced form

$$B_{AS}(T)/As_0 = B_{AS}^*(kT/\epsilon_{1s}) = B_{AS}^*(T^*)$$

where s_0 is the distance at which the net interaction is zero; ϵ_{1s} is the maximum attractive energy; T^* is the reduced temperature. An assumed form for the potential energy of interaction between a gas molecule and the surface allows us to extract information about ϵ_{1s}/k and As_0 or s_0 from the experimental data. For a solid, one may measure P, N_a, and T, use eq 2, and calculate B_{AS} from experiment. For a liquid adsorbent, when one measures P, ϕ, and T and uses eq 5, one calculates B_{AS}/A, from experiment. The temperature dependence of B_{AS} or B_{AS}/A, with the assumed model potential, allows one to calculate ϵ_{1s}/k. For this choice of experimental variables, the theoretical equations give the product As_0 for a solid and s_0 for a liquid. Consequently, measurements of ϕ as a function of temperature allow s_0 to be determined independently of the area, A. The problem of assigning an area to the surface is eliminated.

We assume that the interaction of an adsorbed molecule with each of the individual atoms of the adsorbent may be adequately described by the Lennard-Jones potential

$$\epsilon = 4\epsilon^0\left[\left(\frac{\sigma}{r}\right)^{12} - \left(\frac{\sigma}{r}\right)^6\right]$$

where $-\epsilon^0$ is the interaction energy at the potential minimum and σ is the distance of zero net interaction. Since the number density in a liquid does not depend strongly upon position, the approximation introduced by an integration process should be small. Thus, in-

(3) (a) J. R. Sams, Jr., G. Constabaris, and G. D. Halsey, J. Phys. Chem., 64, 1689 (1960); (b) W. A. Steele, Advan. Colloid Interface Sci., 1, 3 (1967).

(4) R. A. Pierotti, Chem. Phys. Lett., 2, 385 (1968); T. L. Hill, "Statistical Mechanics," McGraw-Hill, New York, N. Y., 1956.

tegrating this expression over a semiinfinite surface yields the (3–9) potential function

$$u(s) = \frac{3\sqrt{3}}{2}\epsilon_{1s}\left[\left(\frac{s_0}{s}\right)^9 - \left(\frac{s_0}{s}\right)^3\right] \qquad (6)$$

This potential gives $s_m = (3)^{1/6}s_0$ for the equilibrium distance of an adsorbed molecule from the surface and equations which relate the gas–surface interaction parameters to the corresponding gas–gas parameters.

$$s_0 = (2/15)^{1/6}\sigma \qquad (7a)$$

$$\epsilon_{1s} = \frac{10}{9}(3)^{1/2}\pi N_0 s_0^3 \epsilon^0 \qquad (7b)$$

N_0 is the number of atoms per cm^3 in the adsorbent. Computed values of $B_{As}*$ as a function of the reduced temperature are available for this potential.[5,6]

At low reduced temperatures a harmonic approximation to an inverse-power-law energy yields a convergent power series expression for the gas–surface second virial coefficient, B_{As}.[7] In the harmonic approximation the parameter ϵ_{1s}/k depends only on the depth of the potential well and it is independent of the shape of the potential curve and the position of the minimum. The (3–9) potential yields the following form for B_{As}

$$B_{As}/A s_0 = 0.579(T^*)^{1/2}\exp(1/T^*) \times$$
$$[1 + 0.810T^* + 1.501T^{*2}] \qquad (8)$$

The variation of the term in square brackets with respect to temperature is small compared with the variation in $\exp(1/T^*)$. Hence, in this reduced temperature range plots of $\log(B_{As}/A)$ vs. T^{-1} are almost linear.

For purposes of data reduction, eq 8 was rewritten in the linear form

$$\ln[(B_{As}/A)T^{-1/2}] = \ln[0.579(k/\epsilon_{1s})^{1/2}s_0] +$$
$$(\epsilon_{1s}/kT) + [0.810T^* + 1.173T^{*2}] \qquad (9)$$

Experimental isotherms were then plotted as $\ln[T^{-1/2}(B_{As}/A)]$ against $1/T$ and fitted with the best straight line by the method of least squares with one interaction.

The theoretical curve for the temperature dependence of $\log(B_{As}/A)$ for xenon is illustrated in Figure 1, using the parameters of best fit shown in Table II. Also shown in Table II are the parameters for interactions between xenon and the graphitized carbon black P33

Table II: Interaction Parameters of Best Fit for Xenon–Substrate

Molecule	Surface	ϵ_{1s}/k, °K	s_0, Å
Xe	Mercury	1917 ± 17	3.24 ± 0.06
Xe	P33	1919 ± 15	3.00 (KM)
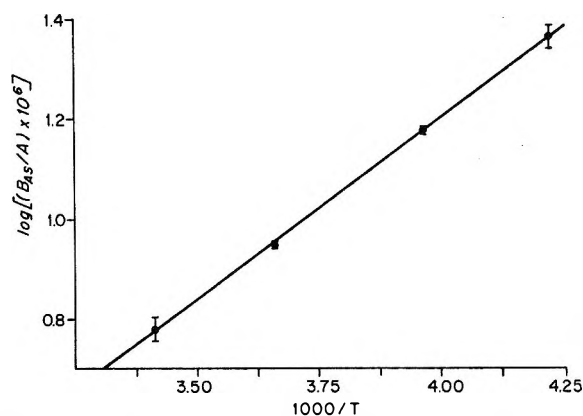
Figure 1. A comparison of the theoretical and experimental temperature dependence of log B_{As}/A is shown for the xenon–liquid mercury system. The continuous curve was calculated for the (3–9) potential.

(2700°).[3a] The errors shown in Table II are the standard deviation of the fit. The value of s_0 shown for the Xe–P33 system was determined by the use of the Kirkwood–Müller equation (eq 13). A comparison between theory and experiment for the spreading pressure isotherms is shown in Figure 2; the continuous lines are computed from theory.

Table II contains parameters of best fit for only the (3–9) potential. In this reduced temperature range the theoretical curves of $\log B_{As}*$ vs. $1/T^*$ for the (3–9), (3–12), and (3–∞) potentials are nearly linear and parallel. From gas phase work, it is well known that equation of state data over much of the reduced temperature range are relatively insensitive to the details of the potential function. Due to these considerations, we did not fit the data to other model potential functions.

An independent estimate of s_0 can be made from the dispersion interaction energy of a rare gas atom with the bulk adsorbent[3a,8]

$$\frac{3\sqrt{3}}{2}\epsilon_{1s} = -\frac{\pi N_0}{6}(K/s_0^3) \qquad (10)$$

where K is the London constant for dispersion forces; several theoretical approximations for this constant exist. The numerical factor $3\sqrt{3}/2$ is necessary to make eq 6 and 10 consistent at large separations.

The nonmetallic interaction equations used to calculate K are offered by London[9] (eq 11), Slater and Kirkwood[9] (eq 12), and Kirkwood and Müller[10,11] (eq 13).

(5) M. P. Freeman, *J. Phys. Chem.*, **62**, 723 (1958).

(6) L. J. Slutsky and G. D. Halsey, Jr., "Physical Chemistry," Vol. II, H. Eyring, D. Henderson, and W. Jost, Ed., Academic Press, New York, N. Y., 1967, Chapter 9.

(7) R. S. Hansen, *J. Phys. Chem.*, **63**, 743 (1959).

(8) F. London, *Z. Phys. Chem. (Frankfurt am Main)*, **B11**, 222 (1930).

(9) H. Margenau, *Rev. Mod. Phys.*, **11**, 1 (1939).

(10) J. G. Kirkwood, *Phys. Z.*, **33**, 57 (1932).

(11) A. Muller, *Proc. Roy. Soc., Ser. A*, **154**, 624 (1936).

$$K_L = (^3/_2) \frac{I_1 I_2}{I_1 + I_2} \alpha_1 \alpha_2 \tag{11}$$

$$K_{SK} = \left(\frac{3}{4\pi}\right) \frac{eh}{m^{1/2}} \frac{\alpha_1 \alpha_2}{(\alpha_1/n_1)^{1/2} + (\alpha_2/n_2)^{1/2}} \tag{12}$$

$$K_{KM} = 6mc^2 \frac{\alpha_1 \alpha_2}{(\alpha_1/\chi_1) + (\alpha_2/\chi_2)} \tag{13}$$

where α is the polarizability of the molecule; I is the ionization potential of the molecule; e is the charge of the electron; h is Planck's constant; m is the mass of the electron; n is the number of electrons in the outer shell of the atom; χ is the diamagnetic susceptibility of the molecule; and c is the velocity of light.

The metallic interaction theories used to determine K are offered by Lennard-Jones (a)[12] (eq 14), Lennard-Jones (b) (eq 15), Bardeen[13] (eq 16), and Margenau and Pollard[14] (eq 17).

$$K_{LJ} = \frac{mc^2 \chi}{2} \left(\frac{6}{N_0 \pi}\right) \tag{14}$$

$$K_{LJ} = \frac{(e^2 h)}{8} \frac{f^0}{4\pi^2 m \nu_0} \left(\frac{6}{N_0 \pi}\right) \tag{15}$$

$$K_B = \frac{(e^2 h)}{8} \frac{f^0}{4\pi^2 m \nu_0} \frac{Ce^2/2r_s h\nu_0}{1 + (Ce^2/2r_s h\nu_0)} \left(\frac{6}{N_0 \pi}\right) \tag{16}$$

$$K_{MP} = \frac{e^2 \alpha}{16} \left[\frac{C}{r_s} - \frac{hn_0}{\pi m \nu_0}\right] \left(\frac{6}{N_0 \pi}\right) \tag{17}$$

where f_0 is the oscillator strength of the resonance transition with frequency ν_0; C is a numerical constant equal to approximately 2.5; n_0 is the number of conduction electrons; r_s is the radius of a sphere containing one metal conduction electron. The factor $(6/N_0\pi)$ appears in the metallic interaction theories due to the way we have chosen to write eq 10.

These interaction formulas have previously been discussed by Pierotti and Halsey,[15] and their discussions need not be repeated here.
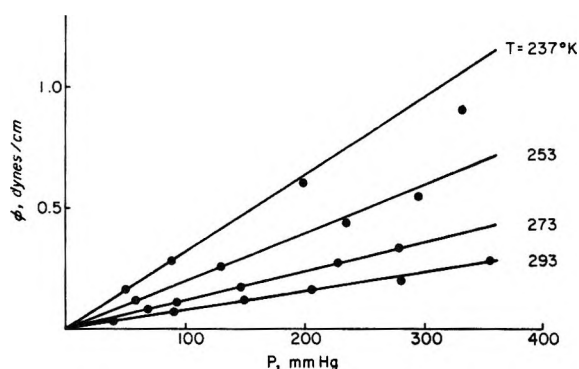
Figure 2. The spreading pressure of xenon adsorbed on mercury is shown as a function of the equilibrium gas pressure. The theoretical lines were calculated from the limiting form of eq 5 for the (3–9) potential.

The result of Prosen and Sachs[16] cannot be put into the form of eq 10 because it has a different dependence on the distance and hence was not considered. A fair comparison of their results with ours would necessitate analysis of the data in terms of a (2–9) potential function.

Values used for the ionization potentials, diamagnetic susceptibilities, polarizabilities, and densities appear in Table III. The values used for the diamagnetic sus-

Table III: Physical Properties of Substances

Molecule	$\alpha \times 10^{24}$, cm^3	$-\chi \times 10^{29}$, cm^3	ρ, g/cm^3	I, eV
Xe	4.021[a]	7.14[b]		12.15[a]
Hg	1.24[b]	9.13[b]	13.615[c]	10.4[c]
C	1.02[b]	13.5[d]	2.25[c]	11.2[c]

[a] B. Linder, *J. Chem. Phys.*, **33**, 668 (1960). [b] J. H. Van Vleck, "The Theory of Electric and Magnetic Susceptibilities," Oxford University Press, London, 1932. [c] "Handbook of Chemistry and Physics," Chemical Rubber Publishing Co., Cleveland, Ohio, 1967. [d] H. T. Pinnick, *Phys. Rev.*, **94**, 319 (1954).

ceptibility and the polarizability of mercury are for the Hg^{2+} ion. The values of s_0 in Å calculated in this manner appear in Table IV.

Table IV: s_0 for Xenon on Liquid Mercury

	(3–9 Model) Experimental 3.24	
KM	London	SK
2.22	1.28	1.34
LJ(a)	LJ(b)	Bardeen	MP
3.48	2.45	1.96	2.10

The results of Table IV show that none of the non-metallic interaction theories give values of s_0 in reasonable agreement with experiment. The Lennard-Jones equation (a) when using the diamagnetic susceptibility in the image force expression is the only expression which gives numerical values close to those deduced from experiment.

A crude estimate for s_0 may be obtained by using the arithmetic-mean rule

$$\sigma_{AB} = (\sigma_A + \sigma_B)/2$$

(12) J. E. Lennard-Jones, *Trans. Faraday Soc.*, **28**, 333 (1932).

(13) J. Bardeen, *Phys. Rev.*, **58**, 727 (1940).

(14) H. Margenau and W. G. Pollard, *ibid.*, **60**, 128 (1941).

(15) R. A. Pierotti and G. D. Halsey, *J. Phys. Chem.*, **63**, 680 (1959).

(16) E. J. R. Prosen and R. G. Sachs, *Phys. Rev.*, **61**, 65 (1942).

Equation 7a shows us that to this degree of approximation, for a (3–9) potential, $s_0 = (2/15)^{1/6}\sigma_{AB}$. For xenon[17] $\sigma = 4.06$ Å and for mercury[18] $\sigma = 3.2$ Å or $\sigma = 2.9$ Å depending on whether one uses the density of the crystal or parameters determined from the viscosity of mercury vapor. This combining rule yields values of s_0 of 2.61 and 2.33 Å. Another estimate of s_0 may be obtained by using eq 7b with the gas–gas[18] (the free space value of ϵ^0 was reduced by 20% to account for the presence of the surface) and the gas–solid interaction energy (Table II); this results in $s_0 = 2.75$ Å. If one uses this same method to determine s_0 for Ar, Kr, Xe, and CH_4 interacting with P33 one obtains 2.53, 2.47, 2.44, and 2.57 Å, respectively.

It is appropriate to point out that Halsey[6] considers s_0 as determined by eq 10 as an adjustable parameter. Namely, the value of $s_m [= (3)^{1/6}s_0]$ that emerges from the treatment of the experimental data is only an approximation to the equilibrium distance that an adsorbed molecule might assume with respect to the surface.

The isoteric heat of adsorption is defined by

$$q_{st} = -\left[\frac{\partial \ln P}{\partial(1/kT)}\right]_\Gamma$$

In the reduced temperature range where eq 8 is a valid approximation to the infinite series result, we can relate the gas–surface energy parameter ϵ_{1s} to the limiting isosteric heat of adsorption.

$$q_{st}(\Gamma = 0) = \frac{d \ln B_{AS}^*}{d(1/kT)} + kT$$

$$= \epsilon_{1s} + \frac{1}{2}kT$$

This same equation has been derived by a model-dependent thermodynamic argument.[19] However, the derivation used here shows this expression is valid only in the harmonic approximation. Also, the temperature must be sufficiently high that the energy due to the single vibrational degree of freedom normal to the surface is given by kT. This assumption of classical behavior is certainly valid for this system. If we assume the vibration of the adsorbed atom normal to the surface is harmonic, then we may simply calculate the vibrational frequency from the assumed potential. The result is

$$4\pi^2\nu^2 = (k_z/m) = m^{-1}\left(\frac{\partial^2 u}{\partial s^2}\right)_{s=s_m} = 27(3)^{-1/3}\left(\frac{\epsilon_{1s}}{s_0^2}\right)$$

Thus, the thermal energy of the oscillator is much greater than the zero-point energy. For this system $kT/h\nu \approx 12$ (i.e., $\nu = 5.1 \times 10^{11}$ sec^{-1}). If the model of a lattice gas is an appropriate description of the system, $q_{st}(\Gamma = 0) = \epsilon_{1s} - (1/2)kT$.[19] Table V shows the experimental isosteric heat of adsorption at zero coverage and the theoretical heats for the limiting models of localized and nonlocalized adsorption. The temperature used is the middle of the range of experimental

Table V: Isosteric Heat of Adsorption at Zero Coverage (kcal/mol)

System	$q_{st}(\Gamma = 0)$	$\epsilon_{1s} + \frac{1}{2}RT$	$\epsilon_{1s} - \frac{1}{2}RT$
Xe–Hg	3.92 ± 0.2^a	4.04	3.56
Xe–P33	4.02 ± 0.03^b	4.11	3.52

a Calculated from data of Cassel and Neugebauer.[1] *b* See ref 3a.

temperatures, 265°K and 297°K for mercury and P33, respectively. The q_{st} ($\Gamma = 0$) data strongly suggest nonlocalized adsorption, which is consistent with the two-dimensional gas model we have applied. Further, Kemball's thermodynamic analysis of a portion of this data,[20] based on consideration of the entropy of adsorption, led him to conclude that on the mercury surface the xenon molecules possessed two translational degrees of freedom and a vibration of low frequency normal to the surface.

III. Discussion

Figure 2 shows that as the coverage increases the spreading pressure curves become concave toward the pressure axis. This curvature is due to the interaction of pairs of molecules with each other and the surface, and B_{2D} or equivalently C_{AAS} is a measure of the importance of these higher order interactions. A consideration of this curvature and eq 5 shows that B_{2D} is positive for the xenon–mercury system. In this same reduced temperature range B_{2D} for the xenon–P33 system is negative. A positive value of B_{2D} means that the net three-body interaction is repulsive.

When one takes into account interactions between molecules both in the adsorbed phase and in the bulk phase

$$B_{2D}/A = -(C_{AAS} - B_{AS}B)/2B_{AS}^2$$

where B is the gas-phase second virial coefficient.

However, the data of Cassel are neither accurate nor extensive enough to allow precise values of B_{2D} to be calculated. Therefore, consistent with the quality of the data we have made an approximate calculation of B_{2D}. We have assumed that the bulk gas imperfections can be neglected and that the very small vapor pressure of mercury need not be corrected for. Using B_{2D}(Hard Disk), hereafter B_{2D}(HD), corrects the theoretical curves in Figure 2 in the proper direction and by the correct order of magnitude. B_{2D}(HD) was calculated from values of σ for the Lennard-Jones

(17) J. O. Hirschfelder, C. F. Curtiss, and R. B. Bird, "Molecular Theory of Gases and Liquids," Wiley, New York, N. Y., 1954.

(18) L. F. Epstein and M. D. Powers, *J. Phys. Chem.*, **57**, 336 (1953).

(19) D. H. Everett, *Trans. Faraday Soc.*, **46**, 453 (1950).

(20) C. Kemball, *Advan. Catal.*, **2**, 233 (1950).
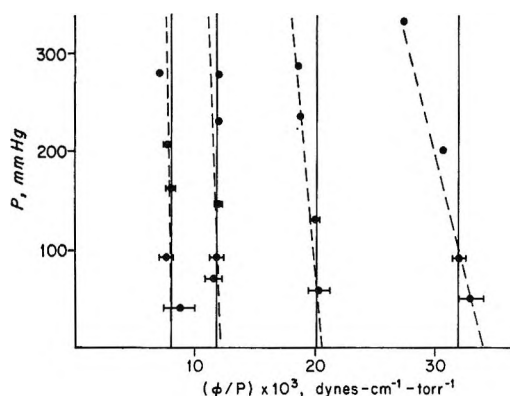
Figure 3. B_{AS}/A for xenon on liquid mercury (solid lines). The temperature of the isotherms increase from left to right. The dashed lines are the isotherms after allowance is made for B_{2D}.

(6–12) potential.[17,18] B_{2D}(experimental) $\approx B_{2D}$(HD)/4. The results of this correction are shown in Figure 3.

All recent work on a mercury substrate examined yields spreading pressure curves which are concave toward the pressure axis. This is true for nonpolar molecules such as rare gases,[2] alkanes,[21-24] and aromatics[24,25] as well as polar molecules, such as alcohols,[26,27] water,[22,26] and carboxylic acids.[26,27]

The above behavior for a mercury substrate is in marked contrast to the results of work carried out on water as a substrate. For a water substrate, spreading pressure curves are convex to the pressure axis. Measurements have been made for alkanes,[28,29] aromatics,[28,30] and polar molecules.[28,30,31] This observation with respect to curvature is not an experimental artifact; it has been observed by a variety of experimental techniques. The techniques employed include the maximum pressure in bubbles, capillary-rise and the vertical film balance for studies with water as the substrate, and in the case of mercury, vertical film balances

and sessile drop measurements have been used to observe the change in surface tension due to adsorption.

Blank and Ottewill[32] measured the spreading pressure and surface potential of benzene adsorbed on 0.1 M sodium chloride solutions. The change in surface potential was attributed to structural rearrangement of the surface due to the presence of adsorbate molecules. The heat of adsorption of n-hexane on water decreases from 13 to 7 kcal/mol (the heat of liquefaction) as θ increases from 0 to 0.3.[33] Thus, the surface of water might be considered as a "soft" surface in which an adsorbed molecule may become imbedded. The water surface is restructured in the presence of adsorbed molecules to provide a cavity which surrounds the adsorbed molecules on all sides except the top. This cavitation process would lead to a smaller value of s_0 and a larger value of ϵ_{1s}, the gas–surface interaction energy, than if the surface had remained planar.

(21) T. Smith, *J. Colloid Interface Sci.*, **28**, 531 (1968).

(22) N. K. Roberts, *J. Chem. Soc. (London)*, 1907 (1964).

(23) J. H. de Boer, *Advan. Catal.*, **8**, 17 (1956).

(24) C. Kemball and E. K. Rideal, *Proc. Roy. Soc., Ser. A*, **187**, 53 (1946).

(25) T. Smith, *J. Colloid Interface Sci.*, **31**, 270 (1969).

(26) C. Kemball, *Proc. Roy. Soc., Ser. A*, **190**, 117 (1947).

(27) T. Smith, *J. Colloid Interface Sci.*, **30**, 183 (1969).

(28) C. L. Cutting and D. C. Jones, *J. Chem. Soc. (London)*, 4067 (1955).

(29) D. C. Jones and R. H. Ottewill, *ibid.*, 4076 (1955).

(30) D. C. Jones, R. H. Ottewill, and A. P. J. Chater, *Proc. Int. Congr. Surface Activ., 2nd*, **1**, 188 (1957).

(31) F. Hauxwell and R. H. Ottewill, *J. Colloid Interface Sci.*, **28**, 514 (1968).

(32) M. Blank and R. H. Ottewill, *J. Phys. Chem.*, **68**, 2206 (1964).

(33) R. H. Ottewill, Ph.D. Thesis, University of London, 1951.

On the Exchange of Chromate Groups in Fresh Lead Chromate[1]

by Luigi G. Conti,* Rodolfo d'Alessandro, and Vito di Napoli

*Laboratorio di Metodologie Avanzate Inorganiche del C.N.R., Istituto di Chimica Generale e Inorganica.
Università di Roma, 00185 Rome, Italy*   (Received March 31, 1970)

The exchange of chromate groups between fresh precipitates of lead chromate and solutions containing radioactive chromate ($^{51}CrO_4{}^{2-}$) has been determined as a function of time, together with the kinetics of monoclinic–orthorhombic phase transition. The results lead to a reexamination of current views on aging of precipitates.

Introduction

Twenty-nine years ago the isotopic exchange at room temperature between solutions containing radioactive lead ($^{212}Pb^{2+}$) and fresh precipitates of lead chromate was studied by Kolthoff and Eggertsen[2] and the results were considered to support strongly a theory of aging,[3] according to which the exchange in fresh precipitates well below their Tammann temperature should be explained as an effect of repeated and rapid recrystallizations (by motion of crystal surfaces in contact with the solution) of the individual microcrystals. In this way the microcrystals would eventually become more perfect.

If these recrystallizations really take place, three main consequences will follow: (1) the exchange and aging rates must depend on the solvation energy of the ions involved, (2) exchange values greater than 100% should be possible, and (3) equal exchange rates for the cation and the anion should be found. The first point has been generally confirmed by the findings of Kolthoff and his coworkers; the second prediction seemed also to be verified by the exchange behavior of lead chromate[2] which showed Pb exchange curves with characteristic peaks much above the asymptotically approached equilibrium value (100% exchange). The third point has been confirmed by Kolthoff and van't Riet[4] in their study of lead sulfate with radioactive sulfate and lead. It should be noted that fresh lead sulfate gives exchange curves[4,5] which asymptotically approach the equilibrium value without showing the characteristic maxima of lead chromate.

Some years ago it was found in this laboratory[6-9] that an orthorhombic–monoclinic phase transition occurs in the fresh precipitates of lead chromate. It appears quite certain that lead chromate always crystallizes in the orthorhombic[6] structure and then, at a rate which depends on the characteristics of the solution, undergoes a phase transition to the stable monoclinic[10,11] structure. Low acidities and concentrations of the reactant solutions prolong the life of the orthorhombic phase. Washing with alcohol and ether helps to preserve this phase. Adsorbed Violetto Brillante Follone S4B (ACNA, S.p.A., Milano, Italy) is particularly effective in stabilization.

The present investigation was undertaken with the aim of examining a chromate exchange curve of fresh orthorhombic lead chromate or determining the effect of the phase transition on the exchange curve itself. To this end, low concentrations and acidities of the starting solutions were used.

Experimental Section

A radioactive Na_2CrO_4 solution[12] furnished the $^{51}CrO_4{}^{2-}$ groups used in the exchange experiments. Its original chromium concentration, activity, and pH were 130 $\mu g/ml$, 30 mCi/ml, and 9.7, respectively. It was diluted 2.2:100 and used as such. The chemicals used for precipitating lead chromate were analytical grade Merck products.

The exchange experiments were done at room temperature of 18°, as follows: 10.00 ml of a 9.79×10^{-4} M $Pb(NO_3)_2$ solution was added in a time of 22 ± 1 sec under good and constant mechanical stirring (using a Pyrex stirrer) to 10.00 ml of a 1.185×10^{-3} M K_2CrO_4

(1) Based on part of the Dr. Chem. Thesis presented by Rodolfo d'Alessandro at the University of Rome, March 1969.

(2) I. M. Kolthoff and F. T. Eggertsen, *J. Amer. Chem. Soc.*, **63**, 1412 (1941).

(3) For the main ideas of the theory and experimental facts see I. M. Kolthoff, *Analyst*, **77**, 1000 (1952); H. A. Laitinen, "Chemical Analysis," McGraw-Hill, New York, N. Y., 1960, p 156.

(4) I. M. Kolthoff and B. van't Riet, *J. Phys. Chem.*, **63**, 817 (1959).

(5) I. M. Kolthoff and C. Rosenblum, *J. Amer. Chem. Soc.*, **56**, 1658 (1934).

(6) G. Collotti, L. G. Conti, and M. Zocchi, *Acta Crystallogr.*, **12**, 416 (1959).

(7) M. Zocchi, Dr. Chem. Thesis, University of Rome, 1956.

(8) L. G. Conti, Report, International School of Nuclear Science and Engineering, Seventh Session, Argonne National Laboratory, 1958.

(9) G. Collotti, L. G. Conti, and N. Zocchi, unpublished results.

(10) S. B. Brody, *J. Chem. Phys.*, **10**, 650 (1942).

(11) S. Quareni and R. De Pieri, *Acta Crystallogr.*, **19**, 287 (1965).

(12) Purchased from the Radiochemical Centre, Inorganic Department, Amersham, Buckinghamshire, England.

solution, which was 2.5×10^{-2} M in KNO_3, in a 100-ml Jena glass centrifuge tube. [The $Pb(NO_3)_2$ solution was slightly acidified with $HClO_4$, the concentration of the acid being that necessary to make the pH of the solution in contact with the precipitate of lead chromate equal to 6.00.[13]] The precipitate was aged for 5 min, including the time spent for the addition of the Pb-$(NO_3)_2$ solution, and then, at time t_0, 1.00 ml of the dilute $Na_2{}^{51}CrO_4$ solution was added to the suspension in a time of 20 sec. After the desired time (the mechanical stirring was never interrupted during the various operations) the suspension was centrifuged for 8 min at 3000 rpm. A 1.00-ml portion of the solution was pipetted in a time of about 20 sec at time t, evaporated under infrared radiation in a thin-walled aluminum dish, and its radioactivity A_t was measured. The radioactivity of the mother solution at time t_0, A_0, was determined repeating the sequence of operations just described, except that the tracer was added to the solution separated from the precipitate by centrifugation after the aging period.

The 0.32-MeV γ rays from ${}^{51}Cr$ were counted by a 3 in. $\times$ 3 in. NaI(Tl) scintillation counter coupled with a 400-channel pulse-height analyzer (Laben, Spectroscope model 400). Such an apparatus permitted integration of the contents of all channels between the two minima around the 0.32-MeV photopeak. After a suitable counting time, the integrated total was printed out. The error was appreciably less than 1% in all measurements. All activity measurements were carried out at fixed geometry (7 mm from the sample to the counter). Owing to the small thickness of the samples, absorption of γ rays was negligible.

The X-ray quantitative analyses of the mixtures of the two polymorphic forms of lead chromate were done as follows. Precipitates were obtained from the same stock solutions used in the exchange experiments. Portions (1.500 l.) of each solution were mixed in a time of about 20 sec in a 4-l. Pyrex beaker under vigorous mechanical stirring at room temperature of 18°. After the desired time stirring was interrupted, the precipitate was separated by filtration in one case (3 hr old precipitate) and by partial decantation and centrifugation in the other two cases. The precipitate was immediately washed, first with alcohol and then with ethyl ether. From 40 to 60 min was necessary for the separation procedures. X-Ray diffraction patterns were recorded after a few minutes by means of a Philips diffractometer unit equipped with a proportional detector, at a scanning speed of $0.5°(2\theta)/min$, and using Cu Kα radiation. Percentages were calculated following the method described by Zocchi[7] which is based on the intensities of the 210 and 102 reflexions of the orthorhombic modification and on the intensity of the 120 reflexion of the monoclinic modification.

Use was made of the following expression

$$\text{per cent monoclinic} = \frac{(I_{(m)120,(r)102} - I_{(r)210}f)100}{I_{(m)120,(r)102} + I_{(r)210}(F - f)}$$

where the intensity $I_{(m)120,(r)102}$, at $2\theta \simeq 27.1°$, is due to the contributions of the two nearly coincident 120 and 102 reflexions of the monoclinic and orthorhombic modifications, respectively. The intensity $I_{(r)210}$, at $2\theta = 26.00°$, is that of the 210 reflexion of the orthorhombic form. Factor f is defined as $I_{(r)102}/I_{(r)210}$ and its value was determined[7] to be 0.70. Factor F is defined as $I_{0(m)120}/I_{0(r)210}$, where the I_0's refer to the pure modifications. Factor F was determined[7] following the phase transition in wet $PbCrO_4$ samples which were placed in the sample holder of the diffractometer. Its value, for typical precipitates, is 2.35.

The percentages found by this method are subjected to an error of about ±3. Considering the various factors of uncertainty in the determination of the "true" kinetics of phase transition (solution volumes and stirring conditions necessarily different from those in the exchange experiments; longer separation procedures), the percentages are probably affected by an error of ±5.

Results and Discussion

Following Kolthoff, the apparent fraction of lead chromate which has participated in the exchange process is given by

$$\text{apparent exchange} = \frac{(A_0 - A_t)M_s}{A_t M_p}$$

where A_0 is the initial radioactivity (at time t_0) of the solution in contact with the precipitate, A_t the radioactivity of the solution at time t, M_s the number of moles of chromate group in solution, and M_p the number of moles of lead chromate. Exchanges calculated by this formula from experimental data, and corresponding times $(t - t_0)$ are given in Figure 1. Figure 1 also shows the kinetics of the phase transition occurring in the precipitate (in this case, times correspond to the addition of alcohol to the wet precipitates).

The quantities M_s and M_p were obtained from the concentrations of the reactant solutions. The experimental values of A_t could be affected by systematic positive errors, and therefore the apparent exchange values by systematic negative errors, if colloidal lead chromate were present in suspension in the mother solution after centrifugation and counted as such together with the solution. A check for this possibility was made examining both the mother solution and the precipitate. Both were obtained following the procedure described in the Experimental Section; the only difference was that 1.00 ml of water was added to the sus-
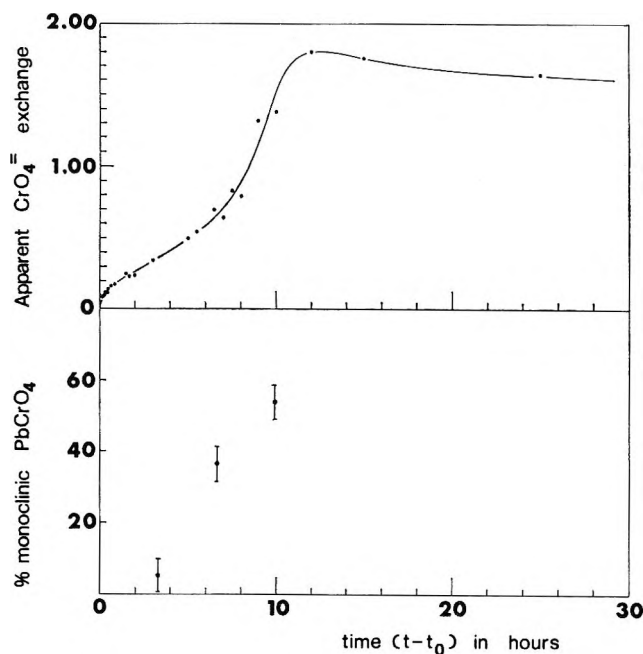
Figure 1. Penetration of $^{51}CrO_4^{2-}$ groups into lead chromate and orthorhombic-monoclinic phase transition.

pension instead of 1.00 ml of the radioactive chromate solution. The solutions obtained from suspensions of various ages (in the case of the 5 min old suspension the separation was carried out by rapid filtration) remained perfectly clear for a period of several days, even though they were made 0.05 and 0.1 M in potassium nitrate and were acidified with perchloric acid. Gravimetric determinations of precipitates of various ages, including the 5 min old precipitate (separated by rapid filtration), in all cases gave for the colloidal solid a value lower than 1% of the total amount of lead chromate. (It should be noted that our search for colloidal lead chromate likewise shows that precipitation is completed within the first 5 min.) Whereas this small value could be ascribed to experimental errors, we have calculated the effect of this 1% of colloidal solid in the apparent exchange curve. Exchange values equal to 0.1, 0.2, and 0.3 should be raised by 1.4, 2, and 2.5%, respectively. The correction to make for the maximum exchange, approximately 1.8, is not easy to calculate. Assuming that the colloidal solid is orthorhombic lead chromate (previous work[9] in this laboratory showed a rather uniform particle size of about 0.1 μ for orthorhombic lead chromate and of 1–10 μ for the needle-shaped monoclinic microcrystals prepared from $10^{-3}\ M$ $Pb(NO_3)_2$ and K_2CrO_4 solutions) we find that the maximum exchange should be raised by appreciably less than 4%.

It can be seen immediately in Figure 1 that exchanges higher than unity are clearly due to the phase transition. This observation and unpublished work in this laboratory by electron microscopy[9] indicate that the phase transition proceeds through the solution, that is, by

solubilization of the orthorhombic microcrystals and crystallization of the monoclinic ones. (Apparent exchanges due *only* to this effect depend on the number of moles of monoclinic $PbCrO_4$ formed after time t_0, M_{mp}, as

$$\frac{M_s}{M_p}(e^{M_{mp}/M_s} - 1)$$

which expression can be much higher than unity.) It can also be seen in Figure 1, perhaps less clearly, that an inflection exists in the exchange curve in correspondence with the inception of the phase transition (for precipitates about 3 hr old). This means that the initial part of the exchange curve of orthorhombic lead chromate has the same shape as the curves of lead sulfate,[4,5] *i.e.*, is concave downward. We do not know if it approaches unity asymptotically as in the case of lead sulfate but, as it will be explained below, there are good reasons for believing so.

The shapes of the exchange curves of lead sulfate strongly suggest a mechanism of diffusion in the microcrystals for the lead and sulfate exchange processes. Such a mechanism can easily explain in a qualitative (but convincing) way also the behavior of lead chromate in the experiments of Kolthoff and Eggertsen[2] (lead exchange) and in ours. The decreasing portions of the exchange curves should be due mainly to the tracers going back to the solution from the enriched monoclinic microcrystals by diffusion. In this way the curves would approach unity asymptotically. This can be seen very clearly from Kolthoff and Eggertsen's work.[2] Curve 1 (15 sec "old" precipitates), Figure 1, in their paper differs little in shape from a diffusion curve and the little maximum should indicate a phase transition starting somewhat before 100% exchange is reached in the orthorhombic microcrystals. Curve 6 in the same figure (1 hr "old" precipitates) should correspond to the end of the transition and indicate diffusional exchange with the monoclinic microcrystals. The time required for the phase transition to be completed, about 1 hr, if our interpretation of Kolthoff and Eggertsen's results is correct, is by no means too short. Transition times as short as few minutes have been observed in this laboratory[7,9] under various experimental conditions. This interpretation accounts in a very natural way for the otherwise strange fact that, plotting the peak values of Kolthoff and Eggertsen's exchange curves against the "age" of the corresponding precipitates, a new curve increasing first from the value 1 and then decreasing to the value 1 is obtained. In another paper[14] Kolthoff and Eggertsen gave (in Table III) apparent Pb-exchange values (up to 100%) for lead chromate aged at room temperature and at 105°, which suggest presence of one modification and diffusional

(14) I. M. Kolthoff and F. T. Eggertsen, *J. Phys. Chem.*, **46**, 458 (1942).

exchange. It is not clear which modification they were concerned with.

Having seen that the exchange in fresh precipitates can be explained by a diffusion process (complicated by eventual phase transition), it remains to present a model which can justify this diffusion in crystals well below their Tammann temperature.

It was suggested[8] some time ago that fresh microcrystals are likely to possess a high density of dislocations, in the core of which the lattice material is more or less hydrated. Thus the activation energy necessary for diffusion to take place along dislocations could be furnished by water present as energy of hydration. (Some experimental evidence for the role of water in dislocations can be found in the work of Tucker and Gibbs,[15] who introduced impurity ions into single crystals of α-Al_2O_3 by exposure to moisture or by boiling such crystals with solutions.) Besides, the presence of water in dislocation cores should facilitate the motion of the dislocations themselves leading to their annihilation[16] or to some stable configuration. In this way a total rearrangement of the lattice of fresh precipitates and the exchange of diffusional type can be accounted for.[17]

Another line of evidence is in favor of our dislocation model. Fresh precipitates obtained from highly supersaturated solutions might present many kinds of imperfections and exchange could be perhaps justified on a different basis. However, fresh monoclinic lead chromate is formed under conditions of very low supersaturation, i.e., that due to the difference in solubility between the two polymorphic forms, and cannot possess other than imperfections introduced in the process of slow crystal growth, namely, mainly dislocations. As we have discussed above also fresh monoclinic lead chromate exchanges at a rate not very dissimilar from that of the orthorhombic salt. (Notice also that the monoclinic microcrystals are larger than the orthorhombic ones.) The conclusion drawn from all this is that high exchange rates (high diffusion coefficients) should be generally observed in experiments with fresh wet crystals, not necessarily only with fresh wet precipitates.

Our dislocation model for exchange allows one to understand the experiments performed by Kolthoff and van't Riet on lead sulfate that show similar exchange rates for the cation and the anion. Evidently dislocations move slowly relatively to the ionic diffusion rates along single dislocations.

Due to the role of water in crystals, our model for exchange (in the absence of phase transitions) could be described also in terms of two-dimensional recrystallizations. With this distinction Kolthoff's theory would retain much of its validity.

(15) R. N. Tucker and P. Gibbs, *J. Appl. Phys.*, **29**, 1375 (1958).

(16) A decrease of lattice defect densities with time has been detected in fresh AgBr by ^{81}Br magnetic resonance absorption, L. G. Conti and R. d'Alessandro, *J. Phys. Chem. Solids*, in press.

(17) A paper by D. Turnbull on alloys, *Defects Cryst. Solids, Rep. Conf.*, 203 (1955), suggested this idea.

The Oxidation of Ethyl Xanthate on Platinum, Gold, Copper, and Galena

Electrodes.   Relation to the Mechanism of Mineral Flotation

by R. Woods

Division of Mineral Chemistry, C.S.I.R.O., Port Melbourne, Victoria 3207, Australia   *(Received June 12, 1970)*

Publication costs assisted by the Division of Mineral Chemistry

Electrochemical investigations of the anodic oxidation of ethyl xanthate to diethyl dixanthogen on platinum, gold, copper, and galena electrodes show that the oxidation proceeds through an adsorbed xanthate radical. The adsorption step can be studied separately from the overall reaction on galena and is found to obey Elovich adsorption kinetics.   The dixanthogen is not chemisorbed but builds up to multilayers on the electrode surface.   The oxidation is accompanied by a change in the surface of the electrodes from a hydrophilic to a hydrophobic condition.   It is concluded that mineral flotation with xanthate collectors proceeds through the electrooxidation of xanthate, oxygen being required to provide a cathodic process.

Introduction

The interaction of mineral sulfides with xanthates, whereby the mineral surface is rendered hydrophobic and gas bubbles can adhere to the surface, has been utilized for many years in practical flotation systems. Much research has been directed towards understanding the mode of interaction, but there is no agreement in the literature on its detailed mechanism.

Simple ion adsorption and precipitation theories[1] have been shown to be inadequate by investigations which proved[2-4] that oxygen is required for the flotation of sulfides with xanthates.   The proposals that account for the role of oxygen, with particular reference to galena (lead sulfide) can be classified into three mechanisms.

(*i*) *Chemical.*   The galena surface is oxidized to a lead–sulfur–oxygen species such as basic thiosulfate and this reacts with xanthate in an ion-exchange process to form lead xanthate

$$2PbS + 2O_2 + H_2O \longrightarrow PbS_2O_3 + Pb(OH)_2 \quad (1)$$

$$PbS_2O_3 + 2ROCS_2^- \longrightarrow Pb(ROCS_2)_2 + S_2O_3^{2-} \quad (2)$$
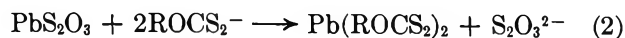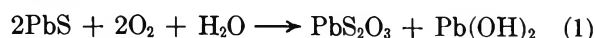
The lead xanthate layer is responsible for rendering the sulfide surface hydrophobic.

(*ii*) *Mixed Potential.*   A hydrophobic layer of dixanthogen is formed on the sulfide surface by two independent simultaneous electrochemical processes, an anodic oxidation of xanthate

$$2ROCS_2^- \longrightarrow (ROCS_2)_2 + 2e \quad (3)$$

and a cathodic reduction of oxygen

$$^1/_2O_2 + H_2O + 2e \longrightarrow 2OH^- \quad (4)$$
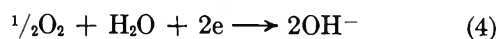
These reactions are related solely through the potential across the mineral–solution interface which assumes a value such that the two processes occur at equal rates.

(*iii*) *Semiconductor.*   The adsorption of oxygen changes the electron energy levels of the semiconducting sulfide to a state where xanthate can be adsorbed and even dixanthogen formed.

Mechanism i is supported by spectroscopic evidence[5-7] for the presence of oxidized lead sulfide and lead xanthate species on the surface of galena and thermochemical measurements[8] of the reaction of lead salts and galena with xanthates.   Mechanism ii was first proposed by Salamy and Nixon[9-11] and is substantiated by their electrochemical investigations with mercury electrodes where a hydrophobic layer of a mercury xanthate was shown to be formed by this type of process.   It is also supported by investigations with metal and sulfide electrodes.[12-14]   Mechanism iii has been developed by Plaskin, *et al.,*[15,16] to account for heterogeneities in surface properties.[15-22]

(1) K. L. Sutherland and I. W. Wark, "Principles of Flotation," Australasian Institute of Mining and Metallurgy, Melbourne, 1955.

(2) I. N. Plaksin and S. V. Bessonov, *Proc. Int. Congr. Surface Activ., 2nd,* **3,** 361 (1957).

(3) I. N. Plaksin, *Trans. AIME,* **214,** 319 (1959).

(4) A. M. Gaudin and N. P. Finkelstein, *Nature,* **207,** 389 (1965).

(5) B. Reuter and R. Stein, *Z. Elektrochem.,* **61,** 440, 450 (1957).

(6) R. G. Greenler, *J. Phys. Chem.,* **66,** 879 (1962).

(7) J. Leja, L. H. Little, and G. W. Poling, *Bull. Inst. Mining Met.,* **72,** 407, 414 (1963).

(8) O. Mellgren, *Trans. AIME,* **235,** 46 (1966).

(9) S. G. Salamy and J. C. Nixon, "Recent Developments in Mineral Dressing," Institute of Mining and Metallurgy, London, 1953, p 503.

(10) S. G. Salamy and J. C. Nixon, *Aust. J. Chem.,* **7,** 146 (1954).

(11) J. Nixon, *Proc. Int. Congr. Surface Activ., 2nd,* **3,** 369 (1957).

(12) R. Tolun and J. A. Kitchener, *Bull. Inst. Mining Metal.,* **73,** 313 (1964).

(13) H. Majima and M. Takeda, *Trans. AIME,* **241,** 431 (1968).

(14) D. Toperi and R. Tolun, *Bull. Inst. Mining Metal.,* **78,** 191 (1969).

(15) I. N. Plaksin and R. Sh. Shafeev, *ibid.,* **72,** 715 (1963).

A comparison of the interaction of xanthate with noble metal surfaces with that with sulfides suggests itself as a way of distinguishing between these mechanisms since in the case of noble metals, only mechanism ii can apply. Tolun and Kitchener[12] compared the electrochemical reactions of ethyl xanthate on galena electrodes with those on platinum and lead. However, they used a technique where the potential was changed stepwise and the current measured after 3 min. Therefore a comparatively large quantity of product is formed at the electrode, much greater than the monolayer level required for flotation.[23] Also the steady-state technique does not give direct evidence of charge-transfer adsorption.

In this communication the electrode reactions of ethyl xanthate on platinum, gold, copper, and galena electrodes are studied by potentiodynamic techniques in which chemisorption processes can be determined.

Experimental Details

Materials. AnalaR sodium tetraborate was recrystallized from doubly distilled water. Its purity was ascertained by an electrochemical method based on the fact that the hydrogen adsorbed on a platinum electrode in aqueous solution can be displaced by surface active impurities. The rate of displacement of hydrogen can be used to indicate impurity level. The borate was recrystallized until a platinum electrode in a 0.1 M solution could be held at +0.08 V $vs.$ a reversible hydrogen electrode for 1 min without measurable displacement of adsorbed hydrogen. "Cyanamid" sodium ethyl xanthate was washed with ether and recrystallized three times from acetone by addition of ether,[1] after which it was stored in a dry nitrogen atmosphere. Solutions in 0.1 M borate were prepared daily and stored under nitrogen. The nitrogen was purified from traces of oxygen by passage over a column of copper deposited on kieselguhr and heated to 200°[24] and then passed through a liquid air trap. All experiments were performed in 0.1 M sodium tetraborate solution of pH 9.1, unless otherwise stated.

Electrochemical Measurements. A conventional H cell with a three-electrode system was used. Potentials were measured against a mercury–mercurous sulfate electrode which had a potential of +0.681 V against a hydrogen electrode in 1 M sulfuric acid. Potentials, except where otherwise stated, are reported against the normal hydrogen electrode, $i.e.$, E_h, assuming this potential is 0.681 V more negative than the mercury–mercurous sulfate electrode. The cell was thermostated in a water bath at 25°.

The electrode potential was controlled by a 68 TS1 Wenking potentiostat programmed with a sweep generator constructed in these laboratories, together with a bias unit of potential dividers and switches to provide potential steps. When current–time curves were recorded, switching was made using a mercury wetted

relay. Current–potential, current–time, and potential–time relationships were recorded with a Hewlett-Packard 7004A X–Y recorder.

Electrodes. The platinum electrode was a length of 28-gauge wire (geometric area 0.08 cm²) sealed into soft glass tubing. The electrode was cleaned with chromic acid and activated by cycling between 0.05 and 1.5 V in 0.1 M borate solution before addition of xanthate to the cell. The electrode tended to lose some activity, due to impurity adsorption, after about 15 min. It could not be reactivated by anodic treatment in the presence of xanthate since dixanthogen, and not a chemisorbed oxygen layer, is formed; therefore, the solution was always replaced with pure borate solution for activation between runs.

The gold electrode was a length of 28-gauge wire sealed into soft glass tubing. It was only partially immersed to avoid possible problems from the gold to glass seal. The geometric area immersed was approximately 0.12 cm². The electrode pretreatment was the same as for platinum.

The copper electrode was a length of 22-gauge wire which passed through a glass tube which was drawn down so that the wire fitted the tube as closely as possible. It was cleaned with sulfuric acid, washed thoroughly, and partly immersed in the cell solution; the surface area immersed was approximately 0.18 cm².

A natural crystal of galena, obtained from the Zinc Corporation mine, Broken Hill, New South Wales, was used an an electrode. Analysis after completion of the electrochemical investigations gave a composition of 86.0% Pb, 13.36% S, 0.22% Sb, 0.06% Ag, 0.06% Cu, and 0.05% Bi, indicating that the crystal contained 99.3% PbS with the trace metals as sulfides. The galena was attached to the end of a glass tube with "araldite" epoxy cement, contact being made with a droplet of mercury inside the glass tube. The geometric area exposed to the solution was 2.2 cm². The electrode was sulfidized in dilute sodium sulfide solution to remove any chemisorbed oxygen or oxidized surface species.[8,12] The electrode was returned to the sulfide solution between runs to desorb xanthate.[25] When the electrode was in the cell its potential was held at

(16) I. N. Plaksin and R. Sh. Shafeev, *Dokl. Akad. Nauk SSSR,* **128,** 777 (1957).

(17) I. N. Plaksin, *Proc. Int. Congr. Surface Activ., 2nd,* **3,** 355 (1957).

(18) I. N. Plaksin and R. Sh. Shafeev, *Dokl. Akad. Nauk SSSR,* **118,** 546 (1958).

(19) I. N. Plaksin, S. P. Zaitseva, and R. Sh. Shafeev, *ibid.,* **119,** 551 (1958).

(20) I. N. Plaksin and V. I. Tiurnikova, *ibid.,* **120,** 155 (1958).

(21) I. N. Plaksin and R. Sh. Shafeev, *ibid.,* **125,** 599 (1959).

(22) I. N. Plaskin and R. Sh. Shafeev, *ibid.,* **135,** 140 (1960).

(23) A. M. Gaudin, "Flotation," McGraw-Hill, New York, N. Y., 2nd ed, 1957.

(24) F. R. Meyer and G. Ronge, *Z. Angew. Chem.,* **52,** 637 (1939).

(25) O. Mellgren and S. L. Lwakarare, *Bull. Inst. Mining Metal.,* **77,** 101 (1968).

−0.46 V, where, at this pH, it is thermodynamically stable.[14]

Results

1. Voltammetry. a. Platinum. The variation of current as a function of potential, obtained by changing the potential linearly with time between −0.46 and 1.07 V, is essentially as expected for platinum at this pH[26] (Figure 1). The current in the region −0.46 to 0 V is due to the adsorption and desorption of hydrogen, and in the region >0 V, to the adsorption and desorption of oxygen; both adsorbed species are obtained by charge-transfer processes from water. The real surface area of the electrode, determined from the saturation hydrogen coverage assuming 210 μC = 1 cm^2,[27] was 0.095 cm^2, giving a roughness factor (real area/geometric area) of 1.2.

In the presence of 5 × 10^{-4} M ethyl xanthate, both hydrogen and oxygen adsorption are inhibited (Figure 1). The inhibition of hydrogen adsorption is due to the adsorption of xanthate ions without charge transfer, analogous to the effect of halide and other ions on platinum.[28-30] This is shown by the fact that when xanthate was added to an electrode held at −0.44 V in a stirred borate solution, the resulting charge passed, obtained by integrating the current–time curve, was only 200 μC/real cm^2. This charge is due solely to the desorption of adsorbed hydrogen to hydrogen ion. Also, when the experiment was repeated at 0 V, where no hydrogen is adsorbed, a negligible charge was passed on addition of xanthate.

There is an anodic current at potentials >0.2 V in the presence of xanthate and when the potential sweep from −0.46 V is taken above 0.2 V, a peak appears on the return cathodic sweep (Figure 1). This peak is due to reduction of the product of the anodic oxidation.

It has been shown[16] that xanthates are oxidized to dixanthogen at a platinum electrode and also[13] that the rest potential at this electrode coincides with the equilibrium potential of xanthate to dixanthogen couples for a number of n-xanthates and isoxanthates over a range of concentration. The redox process responsible for the currents in Figure 1 is, therefore, that of ethyl xanthate to diethyl dixanthogen, the equilibrium potential for 5 × 10^{-4} M xanthate being 0.15.[12,13,31,32]

$$2C_2H_5OCS_2^- \rightleftharpoons (C_2H_5OCS_2)_2 + 2e \qquad (5)$$
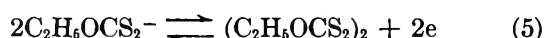
The limiting anodic current is mass transport controlled, as shown by its dependence on stirring (Figure 2). However, the cathodic process is independent of stirring and the greater charge in Figure 2 can be explained by the greater amount of dixanthogen formed on the anodic sweep.

The charge passed on the cathodic sweep was equal to 95, 92, and 84% of the anodic charge due to the formation of dixanthogen for the equivalent of 0.5, 2.0,

Figure 1. Current–potential curves for a platinum electrode in a 0.1 M borate solution at 25°. Triangular potential sweep at 30 mV/sec: Ethyl xanthate concentration, —— 0; —, 5 × 10^{-4} M.

Figure 2. Current–potential curves for a platinum electrode in 0.1 M borate plus 5 × 10^{-4} M ethyl xanthate at 25°. Triangular potential sweep at 40 mV/sec from −0.46 V: quiescent solution, – – – –; stirred solution —.

and 25 monolayers, respectively. Therefore, practically all the dixanthogen remains at the electrode interphase.

Only a single wave appears up to oxygen evolution and, therefore, no further oxidation of dixanthogen takes place at potentials <1.3 V.

"Steady-state" current–potential curves, obtained by changing the potential stepwise and reading the current after an interval of 2 min, have a Tafel slope of >200 mV. These measurements correspond to a situation where there is an increasing quantity of the product dixanthogen present at the electrode. This situation can result in high Tafel slopes as observed for "barrier layer" films[33] and, therefore, "steady-state" curves are uninformative with regard to the reaction mechanism. However, linear sweep voltammograms

(26) W. Bold and M. W. Breiter, *Electrochim. Acta*, 5, 145 (1961).
(27) S. Gilman, "Electroanalygical Chemistry," A. J. Bard, Ed., Arnold Press, London, 1967, Vol. 2, pp 111–192.
(28) A. N. Frumkin, "Advances in Electrochemistry and Electrochemical Engineering," P. Delahay, Ed., Interscience Publishers, New York, N. Y., Vol. 3, 1963, pp 287–391.
(29) M. W. Breiter, *Electrochim. Acta*, 8, 925 (1963).
(30) S. Gilman, *J. Phys. Chem.*, 68, 2098, 2112 (1964).
(31) C. Du Rietz, *Svensk Kem. Tidskr.*, 69, 310 (1957).
(32) N. P. Finkelstein and J. Levin, National Institute of Metallurgy, South Africa, Project C33/62 Report No. 42, 1966.
(33) A. K. Vijh and B. E. Conway, *Chem. Rev.*, 67, 623 (1967).
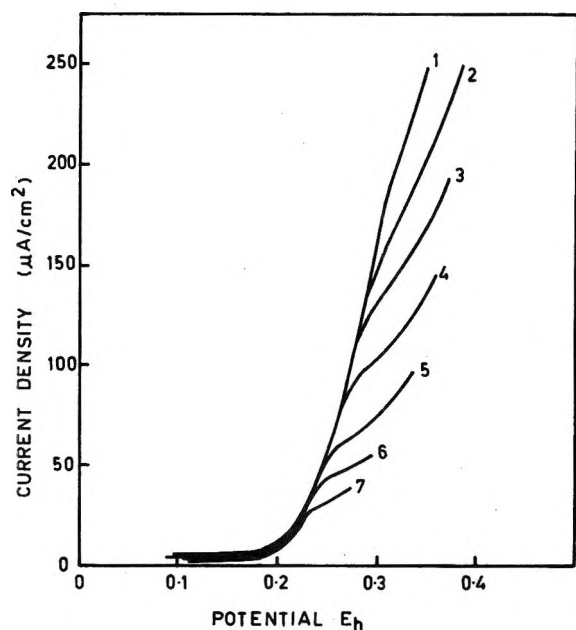
Figure 3. Current–potential curves for a platinum electrode in a stirred solution of 0.1 M borate plus 5.9 $\times$ 10^{-3} M ethyl xanthate at 25°: linear potential sweep at (1) 100, (2) 40, (3) 20, (4) 10, (5) 4, (6) 2, and (7) 1 mV/sec.

can be analyzed for Tafel behavior providing that equilibrium conditions are approached with regard to adsorbed intermediates.

Voltammograms show a significant change in slope at a current value which is dependent on sweep rate (Figure 3). The current value is independent of xanthate concentration or stirring rate provided the current does not become dependent on mass transfer before this value is reached. The change in slope occurs after a constant charge of 250 μC/cm^2 has passed, i.e., the order of a monolayer for a one-electron process. However, the current at a particular potential is independent of sweep rate provided less than 250 μC/cm^2 has passed. This suggests that the current represents an overall process with equilibrium approached with regard to any adsorbed intermediates, since a chemisorption process alone would be expected to give a sweep rate dependent current. The change in slope apparently marks the beginning of inhibition by the product dixanthogen.

The region where the current is independent of sweep rate obeys a Tafel relationship. Voltammograms at 100 mV/sec in stirred solution were recorded at different current sensitivities and the log current was found to vary linearly with potential in the range 20–200 μA/cm^2, with a Tafel slope of 120 mV for all xanthate concentrations investigated, 5 $\times$ 10^{-4} to 1.1 $\times$ 10^{-2} M. The current at constant potential is linearly dependent on xanthate concentration up to 5 $\times$ 10^{-3} M when the current approaches a value which is independent of concentration. Extrapolation of the Tafel lines to the reversible potential gives an exchange current, i_0, of 2.2 μA/cm^2 for 5 $\times$ 10^{-4} M ethyl xanthate.

The reduction of dixanthogen gives a current peak since the quantity decreases during reduction. The initial currents are independent of the amount of product for low quantities but for multilayers, the reduction is considerably retarded.

When the pH of the borate solution was increased from 9.1 to 11.5 by the addition of sodium hydroxide, the voltammogram was unchanged. The rates of the forward and reverse reactions of the redox system are, therefore, independent of pH, as expected for the xanthate–dixanthogen couple.

b. *Gold.* The oxidation of ethyl xanthate on platinum occurs at potentials in the "oxygen adsorption region." Xanthate inhibits this adsorption and there is no evidence to suggest that adsorbed oxygen could play any part in xanthate oxidation. This is confirmed by experiments with a gold electrode which adsorbs oxygen at much higher potentials than platinum.[34] Xanthate oxidation on this electrode takes place in the same potential region as on platinum and much below oxygen adsorption (Figure 4).

The current–potential characteristics are analogous to those on platinum, a change in slope of the current–potential curve occurring after the order of 250 μC/cm^2 of charge has passed. However, the Tafel slope in the region before the change in slope is 60–80 mV in contrast to the 120 mV for platinum. Insufficient curves were plotted to obtain an accurate concentration dependence, but an approximately linear relationship between current at constant potential and xanthate concentration was indicated.

c. *Copper.* A voltammogram in xanthate-free 0.1 M borate (Figure 5) displays anodic and cathodic peaks which occur at the potential expected for the formation and reduction of a passivating oxide or hydroxide layer.[35] This film formation is inhibited in the presence of 5 $\times$ 10^{-4} M xanthate. The limiting current at 0.4 V is equal to the value of the mass transfer controlled
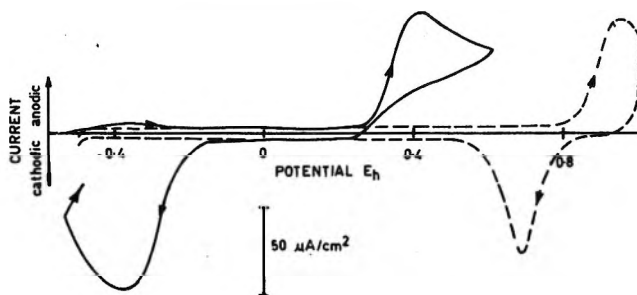
Figure 4. Current–potential curves for a gold electrode in a 0.1 M borate solution at 25°. Triangular potential sweep at 40 mV/sec: ethyl xanthate concentration, —— 0; —, 5 $\times$ 10^{-4} M.

(34) F. G. Will and C. A. Knorr, *Z. Elektrochem.*, **64**, 258, 270 (1960).

(35) M. Pourbaix, "Atlas D'Equilibres Electrochimiques," Gauthier-Villars, Paris, 1963, Chapter IV, Section 14.1.
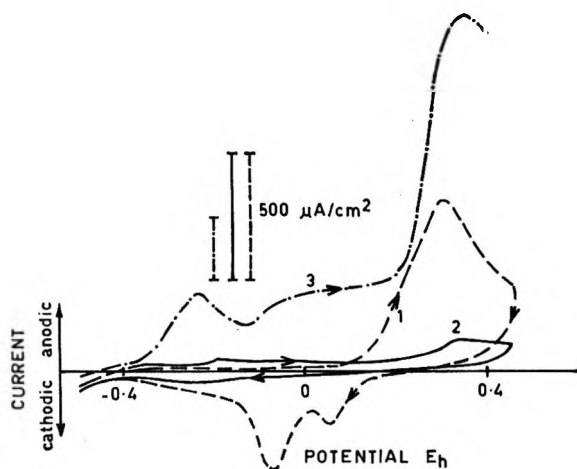
Figure 5. Current–potential curves for a copper electrode in a 0.1 M borate solution at 25°. Curves 1 and 2 are for a triangular potential sweep at 40 mV/sec with ethyl xanthate concentrations of 0 and 5 × 10⁻⁴, respectively; curve (3) is for a linear potential sweep at 100 mV/sec with 1.06 × 10⁻² M ethyl xanthate; curve 1, – – – –; 2, ——; and 3, —·—·.
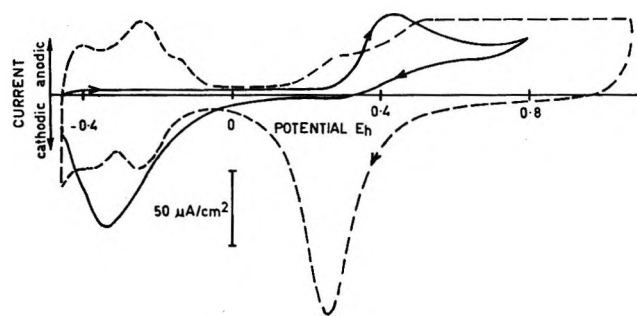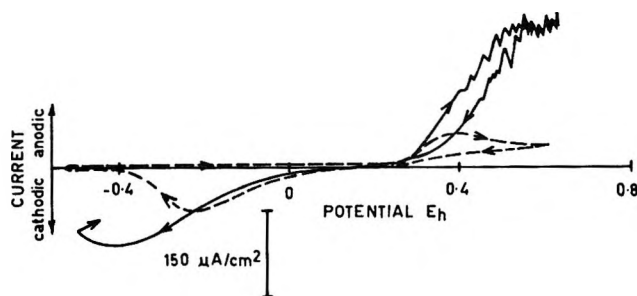

Figure 6. Current–potential curves for a galena electrode in a 0.1 M borate solution at 25°. Triangular potential sweep at 10 mV/sec: ethyl xanthate concentration, – – – –0; —, 9.5 × 10⁻³ M.

xanthate oxidation current on platinum and gold and it is concluded that the currents observed in the presence of xanthate are due to reactions of xanthate alone. In addition to the current at potentials >0.2 V, which corresponds to the oxidation on platinum and gold, there is a current in the region −0.4 to 0.2 V (Figure 5) which increases with increasing sweep rate. The total anodic charge passed in this potential region was determined from the anodic sweep to be the order of 1 mC/cm². A monolayer of a species which is adsorbed as one molecule to each surface copper atom by a one-electron transfer would require 250 μC/cm², assuming equal distribution of 100, 110, and 111 faces exposed. The experimental charge, therefore, would account for the formation of a monolayer of xanthate radicals with a roughness factor of 4.

d. Galena. There is an anodic current on potential sweeps in xanthate-free 0.1 M borate which begins to increase rapidly at 0.25 V; the current is still rising steeply at 0.5 V where it was found to be 1 mA/cm² on a 100 mV/sec sweep. This current is due to oxidation of the galena surface.[12] In the presence of 2 × 10⁻³ M xanthate, the current on an anodic sweep reaches a limiting value which is equal to the mass transfer controlled xanthate oxidation current on platinum and gold. It is concluded that the current observed in the presence of xanthate is due to the reactions of xanthate species alone. Therefore the presence of xanthate inhibits the electrochemical reactions which take place in borate solution alone, on all four electrode materials.

Voltammograms for galena are similar to those found with the metal electrodes in that an anodic current is seen at potentials ≥0.2 V on the anodic sweep and a cathodic peak at −0.3 V on the reverse sweep. However, galena behaves differently from platinum and
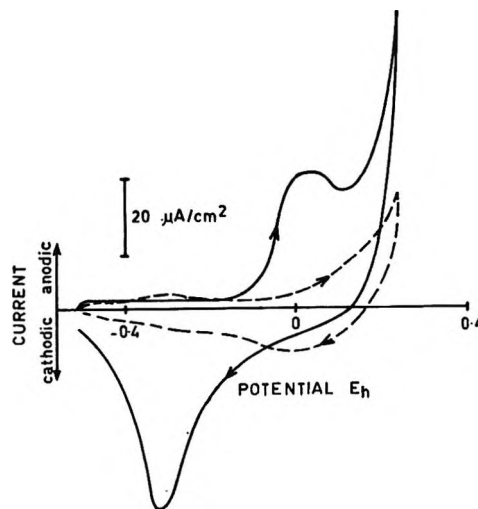
gold, but like copper, in that there is an anodic current at potentials between −0.2 and 0.2 V which increases with increase in sweep rate; the current in the absence of xanthate is small in this potential region (Figure 6). The steady currents at potentials below 0.2 V are small compared with the currents on a potential sweep and this suggests that an adsorption process is taking place. Above 0.2 V, the current increases with potential and the rate of increase is equivalent to a Tafel slope of 150 mV in the current range 50–200 μA/cm². The rate of increase becomes less at higher currents due to the accumulation of dixanthogen; the current is finally limited by the rate of mass transfer.

2. Current–Time Curves. When the potential is stepped from −0.46 to >0.2 V, where dixanthogen is formed, the current decays slowly with time and the charge passed is equivalent to multilayers for all four electrodes.

For galena, a potential step from −0.5 V to between 0 and 0.2 V results in an anodic current which decreases with time. The time dependence of this current is in accordance with the equation

$$i^{-1} = i_{t=0}^{-1} + bt/q_m \qquad (6)$$

where $i_{t=0}$ is the current at zero time, b is a constant and q_m is the charge required for full coverage. This expression is an electrochemical form[36,37] of the Elovich adsorption rate equation[38]

$$dq/dt = a \exp(-bq) \qquad (7)$$

where q is the amount adsorbed and a is a constant.

(36) T. Biegler and D. F. A. Koch, *J. Electrochem. Soc.*, 114, 904 (1967).

(37) T. Biegler and R. Woods, *J. Electroanal. Chem.*, 20, 347 (1969).

(38) D. O. Hayward and B. W. M. Trapnell, "Chemisorption," Butterworths, London, 1964.

The Elovich equation has been found to apply to chemisorption on solids from the gas phase,[38] including oxygen on galena,[39] and also for charge-transfer adsorption of oxygen[27] and organic species[36,40,41] on platinum electrodes.

Typical i^{-1} vs. t plots are shown in Figure 7; they are linear over a wide range of current density. Values of $i_{t=0}$ were obtained by extrapolation and log $i_{t=0}$ found to be a linear function of potential with a slope of 120 mV. At constant potential, $i_{t=0}$ does not vary greatly with xanthate concentration; for example, at 0.1 V $i_{t=0}$ increases by a factor of 1.4 on increasing the xanthate concentration from 2.7×10^{-3} to 1.0×10^{-2} M. At lower xanthate concentrations current–time curves do not obey the Elovich equation.

The charge, q_m, is given by

$$q_m = \int_0^t i dt = (q_m/b) \ln (1 + i_{t=0} tb/q_m) \qquad (8)$$

The integral to infinite time is infinity and consequently the equation cannot be applicable at long times. Therefore, q_m was obtained by integration using (8) over the range in which it is applicable and graphically from the time the Elovich equation breaks down to the time the current approaches its "steady" value. Values of q_m of 320, 450, 470, and 600 $\mu C/cm^2$ were obtained by this method at potentials of 0.03, 0.08, 0.12, and 0.18 V, respectively. The slopes in Figure 7 differ because of the varying value of q_m and yield a constant value of $b = 5 \pm 0.5$.

Galena has a sodium chloride structure with lattice parameter of 5.936 Å[42] and, therefore, a monolayer with one molecule to each surface lead atom would require 92 $\mu C/cm^2$ for a one-electron transfer, assuming equal distribution of the low-index faces exposed. The experimental charge passed on the adsorption of xanthate, 600 $\mu C/cm^2$, would correspond to a monolayer of adsorbed xanthate radicals with a roughness factor of 6.5. However, this charge could correspond to a higher coverage since the surface roughness is not known.

The rate of reduction of adsorbed xanthate was determined by stepping the potential from −0.47 to 0.03, holding at this potential for 30 sec to give a complete layer of adsorbed product, and stepping back to −0.47 V. The reduction was found to obey the Elovich equation, that is i^{-1} varies linearly with t. Equation 6 still applies except that the current is now cathodic; q_m was equal to the value for the adsorption step and b was found to be 4.

When the potential is held in the region where a "steady-state" current is observed, i.e., >0.2 V and then stepped to 0.47 V, the Elovich equation is no longer obeyed, but after an initial current peak, the current is almost time independent before the eventual decrease to zero. This behavior is also observed for platinum and gold electrodes under similar conditions.
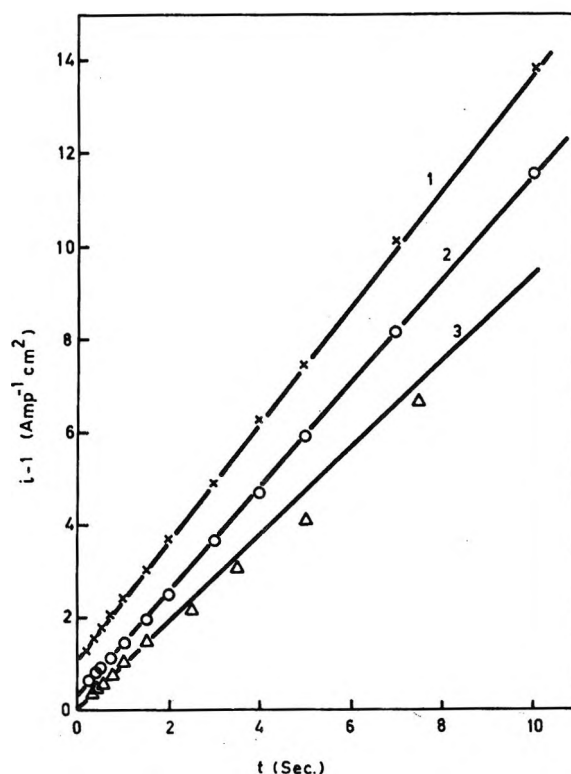
Figure 7. Plots of reciprocal current density against time for a galena electrode in 0.1 M borate plus 7.1×10^{-3} M ethyl xanthate at 25°. Potential stepped from −0.47 V to (1) 0.03, (2) 0.08, and (3) 0.18 V.

3. *Bubble Attachment.* A qualitative determination of whether the surface is hydrophobic or hydrophilic can be made by investigating the ability of small gas bubbles to adhere to the electrode.[12,14] The bubbles were produced throughout the solution by passing nitrogen rapidly through the cell for a short period of time.

When each electrode was held at a potential below that where anodic currents are observed, bubbles did not adhere. At potentials of >0.2 V, i.e., where dixanthogen is formed, bubbles readily adhered to the electrode surface. There is an anodic adsorption current on copper and galena below where dixanthogen is formed. Bubbles do not attach to copper while there is weak attachment to galena in this potential region.

4. *Rest Potentials.* When each electrode was held at −0.46 V in oxygen-free solution and the circuit was broken, the rest potential drifted slowly to higher potentials but did not approach values where dixanthogen is formed or xanthate adsorbed within ∼15 min. Nitrogen bubbles did not attach to the surface.

(39) L. J. Hillenbrand, *J. Phys. Chem.*, **73**, 2902 (1969).

(40) V. S. Bagotskii and Yu. B. Vasiliev, *Electrochim. Acta*, **11**, 1439 (1966).

(41) S. Trasatti and L. Formaro, *J. Electroanal. Chem.*, **17**, 343 (1968).

(42) R. W. G. Wyckoff, "Crystal Structures," Interscience Publishers, New York, N. Y., Vol. 1, 1963, p 89.

When the experiment was performed in oxygenated 10^{-4} M ethyl xanthate solution, the rest potential of the platinum, gold, copper, and galena electrodes increased to 0.26, 0.24, 0.21, and 0.21 V, respectively, that is, values where controlled potential studies have shown dixanthogen to be formed. Bubbles of oxygen adhered to the surface at the final rest potential but not when the electrode was held at -0.46 V. The potential-time curve for galena displays a current arrest at -0.7 V, which corresponds to the adsorption step.

Discussion

A. Mechanism of the Electrooxidation of Ethyl Xanthate. The characteristics of the anodic oxidation of sodium ethyl xanthate and the cathodic reduction of its oxidation product, diethyl dixanthogen, can be explained by a single mechanism for the four electrodes

$$C_2H_5OCS_2^- \rightleftharpoons C_2H_5OCS_{2ads} + e \quad (9)$$

$$C_2H_5OCS_{2ads} + C_2H_5OCS_2^- \rightleftharpoons$$
$$(C_2H_5OCS_2)_2 + e \quad (10)$$

$$2C_2H_5OCS_{2ads} \rightleftharpoons (C_2H_5OCS_2)_2 \quad (11)$$
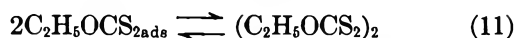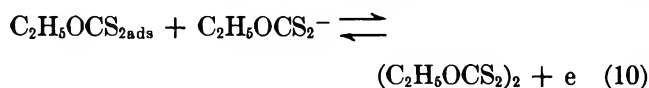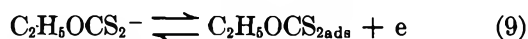
This mechanism is analogous to that which has been proposed for halide–halogen systems.[43]

The rate of the forward reaction 9, assuming adsorption of the intermediate under Temkin conditions,[44] is given by

$$i_1 = Fk_1C(1 - \theta) \exp\left(\frac{\beta FE}{RT}\right) \exp(-\alpha f\theta) \quad (12)$$

where k_1 is a rate constant, C the xanthate concentration at the electrode, β a transfer coefficient, E the electrode potential, α a symmetry factor, f a constant, and θ the coverage of adsorbed intermediate; the other terms have their usual significance.

When the subsequent steps are more rapid, the coverage of intermediate is small and the equation reduces to

$$i_1 = Fk_1C \exp(\beta FE/RT) \quad (13)$$

Therefore, if the overall oxidation reaction rate is determined by (9), the Tafel slope is $RT/\beta F$ (118 mV assuming $\beta = 0.5$) and a linear dependence of current on xanthate concentration. This is the case for platinum.

When either (10) or (11) is rate determining, it can be assumed[44] that (9) is in equilibrium; linear terms in θ are considered[44] to be negligible compared with the exponential term if $0.2 < \theta < 0.8$. Then

$$\exp(f\theta) = (k_1/k_{-1})C \exp(FE/RT) \quad (14)$$

where k_{-1} is the rate constant for the reverse reaction 9. Then the overall current, i, is related to the rates of (10) and (11) by

$$i = 2i_2 = 2Fk_2C\theta \exp\left(\frac{\beta'FE}{RT}\right) \exp(1 - \alpha')f\theta \quad (15)$$

$$i = 2Fk_2(k_1/k_{-1})^{1-\alpha'}C^{2-\alpha'} \times$$
$$\exp(1 - \alpha' + \beta')FE/RT \quad (16)$$

or

$$i = Fv_3 = Fk_3\theta^2 \exp(2\alpha''f\theta) \quad (17)$$

$$= Fk_3(k_1/k_{-1})^{2\alpha''}C^{2\alpha''}\exp(2\alpha''FE/RT) \quad (18)$$

where the terms with suffix 2 and 3 refer to the forward reactions 10 and 11, respectively, and linear terms in θ are neglected in (16) and (18). Therefore, for both desorption reactions, a Tafel slope of F/RT or 59 mV is anticipated (assuming α', α'', and β' to be 0.5). This would explain the Tafel slope for the reaction on gold.

In the case of galena, and possibly copper, reaction 9 occurs at lower potentials than the subsequent steps and can be studied as a separate reaction. The rate of the adsorption reaction is given by (12), which can be rearranged to give[36,37]

$$i_1^{-1} = (Fk_1C \exp(\beta FE/RT))^{-1} + \alpha ft/q_m \quad (19)$$

This is equivalent to (6) and therefore the Tafel slope for $i_{t=0}$ should be 118 mV, which is the experimental value for galena.

Similarly the rate of the desorption step, the reverse of (9), is given by

$$i_{-1}^{-1} = [Fk_{-1} \exp - (1 - \beta)FE/RT]^{-1} +$$
$$(1 - \alpha)ft/q_m \quad (20)$$

which is also equivalent to (6).

Comparison of (6) with (19) and (20), respectively, shows that for the adsorption $b = \alpha f$ and for the desorption $b = (1 - \alpha)f$; this yields values of $f = 9 \pm 1$ and $\alpha \simeq 0.5$, that is, the value expected for a symmetry factor. Although the Elovich equation was originally empirical, it has been derived theoretically and f is considered to be a measure of the heterogeneity of the surface, either an intrinsic property or induced by the adsorption process.[38,44] The "f" value found here is comparable to the values of 9–12 found for the organic adsorption on platinum.[36,40,41]

The concentration dependence of both the overall reaction on platinum at the higher xanthate concentrations investigated, and the adsorption reaction on galena, do not obey the theoretical relationships if the surface concentration of xanthate is considered to be equal to that of the bulk. However, the inhibition of hydrogen adsorption on platinum demonstrates that xanthate ion is adsorbed and therefore the surface and bulk concentrations are not the same; xanthate ion has also been found to adsorb strongly on mercury.[45] The

(43) K. J. Vetter, "Electrochemical Kinetics," Academic Press, New York, N. Y., 1967, Chapter 4.

(44) E. Gileadi and B. E. Conway, "Modern Aspects of Electrochemistry," J. O'M. Bockris and B. E. Conway, Ed., Butterworths, London, 1964, Chapter 5.

(45) S. Salamy, Ph.D. Thesis, Melbourne University, 1952.

anomalous concentration dependence of these reactions can be explained if the surface concentration approaches a limiting value. Low reaction orders due to adsorption of reactant ions have been reported for a number of systems.[43,46-48]

Dixanthogen remains at the electrode interphase and does not diffuse into the bulk solution. Multilayer quantities can be formed and the electrochemical properties are not characteristic of chemisorption. It is concluded that diethyl dixanthogen forms a physically adsorbed layer which, since it is insoluble, is equivalent to a separate dixanthogen phase which adheres to the electrode. Xanthate is chemisorbed while dixanthogen is only physically adsorbed, and it is therefore interesting to note that xanthates readily form compounds with metals, including those of all four electrodes.[23] On the other hand, attempts to isolate adducts of first-row transition metal complexes with diethyl dixanthogen have failed[49] although one would expect dixanthogen to be able, through its sulfur atoms, to act as a ligand in coordination complexes.

Xanthate can be adsorbed and desorbed repeatedly on galena when the potential is cycled between -0.47 and 0.2 V and therefore the adsorption cannot involve a reaction with oxidized galena species which results in the release of sulfur-containing ions into solution.

Mechanisms involving surface processes are often justified by arguments regarding bulk phase thermodynamic properties. It is interesting to note that the adsorption of xanthate on galena occurs at potentials below the reversible potential, E_r, of the equivalent bulk process

$$PbS + C_2H_5OCS_2^- \rightleftharpoons$$

$$Pb(C_2H_5OCS_2)_2 + S + 2e \quad (21)$$
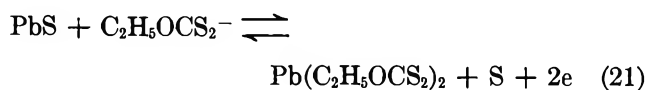
for which[14]

$$E_r = -0.124 - 0.059 \log C \quad (22)$$

where C is the molar concentration of ethyl xanthate. It has been demonstrated[50,51] that the first monolayer of a phase on mercury electrodes can be formed at potentials below that of the bulk phase formation and that such monolayers can be formed at underpotentials.[51] Similarly, the deposition of a monolayer of one metal on another has been found[52,53] to take place at an underpotential. Chemisorption can take place when no equivalent bulk phase exists, for example hydrogen on platinum; where bulk phases have been characterized, chemisorption can occur at potentials below that expected for phase formation, for example oxygen on noble metals.[54] Therefore, bulk phase thermodynamic data must be used with a great deal of caution in elucidating processes involving monolayer formation or chemisorption.

The overall reaction to dixanthogen on galena and copper takes place when the intermediate adsorbed

xanthate radical approaches full coverage, i.e., $\theta \rightarrow 1$. In this case the assumptions made in deriving (16) and (18) do not apply and the overall rate for desorption by (10) is

$$i = 2i_2 = 2Fk_2' \exp(\beta'FE/RT) \quad (23)$$

and for desorption by (11)

$$i = Fv_3 = Fk_3' \quad (24)$$

The overall reaction current on galena and copper is potential dependent and has a Tafel slope of 120-150 mV in agreement with (23). Therefore, (10) is the important desorption step on these electrodes.

The only difference between the xanthate to dixanthogen reaction on the four electrodes is that the adsorption of the radical is rate determining on platinum and $\theta < 0.2$, a desorption step is rate determining on gold and $0.2 < \theta < 0.8$, and the electrochemical desorption step (10) is rate determining on copper and galena and $\theta \rightarrow 1$.

B. Relevance of the Electrooxidation of Xanthate to Flotation. It has been shown that xanthate species can be adsorbed on the electrode in three forms: (a) a specifically adsorbed ion which does not render the surface hydrophobic; (b) a chemisorbed radical which can render it slightly hydrophobic; and (c) physically adsorbed dixanthogen which renders it strongly hydrophobic. On open circuit, in the absence of oxygen, the rest potential of the electrodes remains in the region where only (a) occurs. Oxygen can be electroreduced on all four electrodes at low potentials giving a steady current, and therefore, in the presence of oxygen, the rest potential is increased. It moves into a region where both (b) and (c) occur and the surface becomes hydrophobic. These are the conditions prevailing in practical flotation. The mixed potential mechanism, where the role of oxygen is to provide a cathodic reaction in order that the anodic oxidation of xanthate can take place, fully explains the results with all four electrodes. It therefore explains why a mineral surface becomes hydrophobic and the mineral can be floated. This is supported by nonelectrochemical investigations which show that galena, and other floatable sulfide minerals, are catalysts for the reaction of oxygen with xanthates to form dixanthogens[55] and that the kinetics

(46) S. Schuldiner and C. H. Presbrey, *J. Electrochem. Soc.*, **111**, 457 (1964).

(47) B. J. Bowles, *Electrochim. Acta*, **10**, 717, 731 (1965).

(48) L. Muller, *ibid.*, **13**, 2005 (1968).

(49) G. Winter, private communication.

(50) T. Biegler, *J. Electroanal. Chem.*, **6**, 357 (1963).

(51) R. D. Armstrong and J. D. Milewski, *ibid.*, **21**, 547 (1969).

(52) T. Mills and G. M. Willis, *J. Electrochem. Soc.*, **100**, 452 (1953).

(53) M. W. Breiter, *ibid.*, **114**, 1125 (1967).

(54) J. P. Hoare, "The Electrochemistry of Oxygen," Interscience, New York, N. Y., 1968, Chapter II.

(55) A. A. Golikov and F. I. Nagirnyak, *Sov. J. Non-Ferrous Metals*, **2**, (4), 9 (1961).

of uptake of xanthate on galena from oxygenated solution obey an Elovich rate process followed by an approach to a time-independent rate.[4,56] This kinetic behavior is anticipated by the mixed potential mechanism, the two stages corresponding to the charge-transfer adsorption of xanthate followed by the formation of dixanthogen. Indeed, such a mixed potential mechanism is to be expected for redox processes in solution which take place on conducting surfaces and has been shown to apply to metal corrosion[57] and to catalytic processes.[58,59] The mechanism predicts that the criterion for xanthate to be a collector for the flotation of a mineral is that the mineral must be a catalyst for the reaction of xanthate with oxygen through being an electrocatalyst for both xanthate oxidation and oxygen reduction. It clearly accounts for the ability of xanthates to be efficient collectors for native metals[1,23] such as gold and copper (and metallic copper is also floated in the treatment of oxidized copper ores by the TORCO process[60]) as well as sulfide minerals but not for nonconducting silicates and oxides.

When the concentration of charge carriers in a semiconductor electrode surface is sufficiently large, the whole potential drop occurs in the solution double layer and electrochemical kinetic equations become the same as for metal electrodes.[61] This is the case for galena, probably due to its high intrinsic conductivity. However, semiconductor properties may be important for some minerals and could lead to a decrease in the catalytic activity for either of the electrode processes which make up the mixed potential mechanism.

A chemical mechanism involving an oxidized surface is unrealistic for platinum and gold and has been shown to be unimportant for copper and galena under the experimental conditions of xanthate addition to a surface free of oxidized species. However, there is evidence that, in certain circumstances such as the prolonged exposure to oxygenated solution before xanthate addition, intermediate thiosulfate species are formed on galena,[5-8] although it should be pointed out that the reaction is slow.[62] Infrared spectroscopy[7] and thermochemical measurements[8] show that these species are replaced by xanthates. This reaction, which could be regarded as a desorption of thiosulfate and adsorption of xanthate, is apparently an alternative route for xanthate adsorption. It is essentially the reaction proposed by Toperi and Tolun[14]

$$2PbS + 3H_2O + 4C_2H_5OCS_2^- \longrightarrow$$

$$2Pb(C_2H_5OCS_2)_2 + S_2O_3^{2-} + 6H^+ + 8e \quad (25)$$
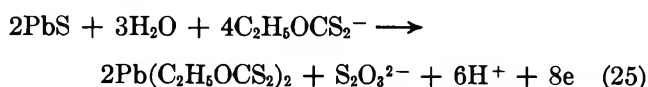
on the ground that it is thermodynamically the more favorable reaction for lead xanthate formation. However, it has been reported[12] that multilayers of lead ethyl xanthate are not hydrophobic. Furthermore, if dixanthogen is required for efficient flotation, a postulate for which there is evidence,[55,63-66] it must be produced by the "mixed potential" mechanism following the ion-exchange process. If either of the two electrode reactions which make up the "mixed potential" mechanism is significantly retarded by multilayers of lead xanthate, then this would explain why excessive exposure of galena to oxygen renders it difficult to float[67] even though ion exchange between xanthate and the oxidized surface took place. This postulate is substantiated by the differences in floatability between galena and anglesite (lead sufate). The latter mineral requires a higher concentration of xanthate and a xanthate with a longer hydrocarbon chain length than ethyl xanthate.[1,23] It is known[1,23] that anglesite can adsorb xanthate, probably by an ion-exchange process, but it is not expected to be a conductor and therefore will not be an effective catalyst for the electrochemical processes required for dixanthogen formation.

It should be noted that the equilibrium potential of the xanthate to dixanthogen reaction is pH independent while that of oxygen to water or hydrogen peroxide decreases by 59 mV per pH unit, predicing a decrease in flotation rate with increase in pH. This must be taken into consideration in the analysis of the upper pH limit of floatability of sulfide minerals.

(56) N. P. Finkelstein, National Institute of Metallurgy (South Africa), Report No. 527, Project C33/62 1969; also Abstracts of the XXII I.U.P.A.C. Congress, Sydney, 1969, p 163.

(57) L. L. Shrier, "Corrosion," L. L. Shrier, Ed., George Newnes, London, 1954, Section 1.

(58) M. Spiro, *J. Chem. Soc.*, 3679 (1960).

(59) R. Woods, *J. Catal.*, 16, 267 (1970).

(60) E. T. Pinkney and N. Plint, *Bull. Inst. Mining Metal.*, 76, 114 (1967).

(61) V. A. Myamlin and Yu. V. Pleskov, "Electrochemistry of Semiconductors," Plenum Publishing Co., New York, N. Y., 1967, Chapter 3.

(62) P. Eadington and A. P. Prosser, *Bull. Inst. Mining Metal.*, 78, 74 (1969).

(63) M. G. Fleming and J. A. Kitchener, *Endeavour*, 23, 101 (1965).

(64) A. A. Golikov, *Sov. J. Non-Ferrous Metals*, 2 (11), 19 (1961).

(65) A. A. Golikov, *ibid.*, 5(5), 15 (1964).

(66) A. A. Abramov, *ibid.*, 39, 11 (1966).

(67) B. L. Cusack, *Australas. Inst. Mining Metal., Proc.*, 224, 1 (1967).

Theory of Hydrophobic Bonding. I. The Solubility of Hydrocarbons in Water, within the Context of the Significant Structure Theory of Liquids

by Robert B. Hermann

Eli Lilly and Company, Indianapolis, Indiana 46206 (Received July 16, 1970)

Publication costs assisted by Eli Lilly and Company, Indianapolis, Indiana

The theory of the thermodynamic behavior of solutions of aliphatic hydrocarbons in water is examined. The water molecules in the layer of water next to the hydrocarbon molecule are assumed to be in an asymmetric electric field, similar to what has been proposed to account for the surface tension of pure water. This asymmetric field acts on the water dipole, restricting the motion of the water molecules. A partition function which accounts for the thermodynamic properties of aqueous solutions of hydrocarbons can then be written in terms of the significant structure theory. The agreement between theory and experiment for the free energy, internal energy, and entropy are good but the calculated heat capacity is too low.

Introduction

It has been recognized for some time that the interaction between a protein and its aqueous environment is a most important factor in determining its conformation. Hydrocarbon side chains are present in all proteins and polypeptides and it is principally these groups that tend to cluster in aqueous solution. The tendency toward the aggregation of such hydrocarbon moieties in aqueous solution is an example of hydrophobic bonding and is related to the insolubility of hydrocarbons in water. In order to understand the origin of hydrophobic bonding, it is necessary to understand the molecular interactions involved in aqueous hydrocarbon solutions which determine the observed thermodynamic properties.

One theory for the thermodynamic properties of hydrocarbon aqueous solutions has been developed by Némethy and Scheraga.[1,2] This theory is based on the Frank and Wen flickering cluster model for water.[3] The distribution of water molecules among species participating in different numbers of hydrogen bonds is formulated in terms of a partition function. The water molecules are distributed over five energy levels, corresponding to four, three, two, one, and no hydrogen bonds per molecule. This model is made to account for iceberg formation around the hydrocarbon, as proposed by Frank and Evans,[4] which in turn accounts for the reduction of unitary entropy[5] and the large heat capacity of hydrocarbon solutions.

In the following treatment some of the thermodynamic properties of hydrocarbon solutions are calculated, within the context of the significant structure theory of liquids.[6] This theory applied to water by Jhon, Grosh, Ree, and Eyring[7] accounts quite well for such properties as the Helmholtz free energy, the entropy of vaporization, and the minimum in the volume at 4°. The minimum in the heat capacity C_p is accounted

for, indicating the quality of the second derivative of the partition function. The theory has been used to account for the surface tension[8] and the dielectric constant[9] of water. While the description of the interactions between hydrocarbon and water proposed here are independent of any particular current theory of liquids, we choose to formulate these interactions in terms of the significant structure theory because of the success and simplicity of this theory and because it has been applied to water.

Partition Function for Hydrocarbon Solutions

It is assumed that the mole fraction of hydrocarbon in water solution is so low that there are always at least two layers of water molecules between hydrocarbon molecules. The partition function for the solution of a hydrocarbon in water may be written as a function of partition functions for the hydrocarbon f_R, for the adjacent water layer f_L, and for the bulk water f_w

$$f_{sol} = M f_R{}^{N_2} f_w{}^{N_1 - LN_2} f_L{}^{LN_2} \tag{1}$$

$$N_1 + N_2 = N \tag{2}$$

(1) G. Némethy and H. A. Scheraga, *J. Chem. Phys.*, **36**, 3382 (1962).

(2) G. Némethy and H. A. Scheraga, *ibid.*, **36**, 3401 (1962).

(3) H. S. Frank and W. Y. Wen, *Discuss. Faraday Soc.*, **24**, 133 (1957).

(4) H. S. Frank and M. W. Evans, *J. Chem. Phys.*, **13**, 507 (1945).

(5) W. Kauzmann, *Advan. Protein Chem.*, **14**, 1 (1959).

(6) H. Eyring and T. Ree, *Proc. Nat. Acad. Sci. U. S.*, **47**, 526 (1961); H. Eyring and R. P. Marchi, *J. Chem. Educ.*, **40**, 562 (1963). See also subsequent papers. For a complete summary of contributions to the theory, see H. Eyring and M. S. Jhon, "Significant Liquid Structures," Wiley, New York, N. Y., 1969.

(7) M. S. Jhon, J. Grosh, T. Ree, and H. Eyring, *J. Chem. Phys.*, **44**, 1465 (1966).

(8) M. S. Jhon, E. R. Van Artsdalen, J. Grosh, and H. Eyring, *ibid.*, **47**, 2231 (1967).

(9) M. E. Hobbs, M. S. Jhon, and H. Eyring, *Proc. Nat. Acad. Sci. U. S.*, **56**, 31 (1966).

where M is a random mixing factor, N is Avogadro's number, N_1 and N_2 are the respective numbers of total water and hydrocarbon molecules. L is the number of molecules of water in the surface layer of water surrounding each hydrocarbon molecule.

This model assumes that the hydrocarbon adjacent water layer and remaining bulk water are all statistically independent. They will, however, influence each other through time average forces and this will manifest itself in the parameters which enter into each species.

The partition function from which will be calculated the free energy and entropy change associated with dissolving a hydrocarbon in water is defined as

$$f_D = M^{-1} f_{sol}/g_R{}^{N_2} \cdot f_W{}^{N_1} \qquad (3)$$

where g_R is the partition function for pure hydrocarbon and f_W is the partition function for pure water. The random mixing factor is omitted to simplify comparison with earlier work,[2] so it is the unitary free energy and unitary entropy which is calculated.

Incorporation of the Hydrocarbon Partition Function. According to significant structure theory the partition function for the hydrocarbon is written

$$g_R = \left\{ f_{s_2} e^{E_{s_2}/RT} \left(1 + n_2 \frac{V_2 - V_{s_2}}{V_{s_2}} \times \right. \right.$$
$$\left. \left. e^{-a_2 E_{s_2} V_{s_2}/(V_2 - V_{s_2})RT} \right) \right\}^{V_{s_2}/V_2} f_g{}^{(V_2 - V_{s_2})/V_2} \qquad (4)$$

where E_{s_2}, V_{s_2}, n_2, and a_2 are parameters characteristic of the hydrocarbon.[6,10] The function f_{s_2} represents the solid-like degrees of freedom and is assumed to be

$$f_{s_2} = \frac{1}{[1 - e^{-\theta_2/T}]^3} f_{rot_2} f_{vib_2} \qquad (5)$$

while for the gas-like degrees of freedom

$$f_{g_2} = f_{trans_2} f_{rot_2} f_{vib_2} \qquad (6)$$

where f_{trans_2}, f_{vib_2}, f_{rot_2} are the translational, vibrational, and rotational (or librational) partition functions, respectively, and θ_2 is the Einstein characteristic temperature. For $V_2 = V_{s_2}$, the partition function reduces to that of the corresponding solid, while for appropriately larger values of V_2, it represents a liquid or a gas. The function f_R in eq 1 will have the same form as g_R in eq 4, but the parameters E_{s_2}', θ_2', n_2', a_2' in f_R will not necessarily be the same as the corresponding parameter in g_R.

In the theory of significant structures, for simple liquids, n_2 and a_2 are functions of V_2 and V_{s_2} only.[6] If it is assumed that the available hydrocarbon volume V_2 remains approximately unchanged upon dissolving the hydrocarbon in water, the effects of differences between n_2 and n_2' and between a_2 and a_2' may be neglected.

In the case of E_{s_2}', the value of this parameter is determined in the following way. The hydrocarbon in solution is now bound to L water molecules so

$$E_{s_2}' = L \cdot {}^1\!/_2 E_{RW} \qquad (7)$$

where E_{RW} is the average interaction energy between the hydrocarbon molecule and a bordering water molecule. This replaces the E_{s_2} for the pure hydrocarbon which is one-half the average interaction energy between the hydrocarbon and its hydrocarbon neighbors. The actual value of this parameter is determined by fitting the data.

The parameter θ_2 is assumed to remain unchanged. Changes in θ have previously been taken to be proportional to the square root of changes in the sublimation energy[11]

$$\theta \sim k E_s{}^{1/2} \qquad (8)$$

The change in characteristic temperature for the hydrocarbon–water structure may be considered to be a function of the average increase in energy of the overall hydrocarbon–water layer structure and may be incorporated if necessary *via* a change in the corresponding characteristic temperature for the water layer only.

The above approximations to the parameters allow f_D to be written

$$f_D = f_L{}^{LN_2} (e^{+E_{s_2}'/RT})^{V_{s_2}N_2/V_2} f_W{}^{(N_1 - LN_2)} /$$
$$[e^{E_{s_2}/RT}]^{V_{s_2}N_2/V_2} \cdot f_W{}^{N_1} \qquad (9)$$

The value for V_2 to be used is partially dependent on the nature of the experimental data. The experimental data given in Table II were compiled by Nemethy and Scheraga[2] and refer to the process[12] of dissolving a pure liquid hydrocarbon RH_1 in water.

$$RH_1 \ (X = 1, T, p = 1 \text{ atm}) \longrightarrow$$
$$RH_{aq} \ (X_{std}, T, p = 1 \text{ atm}) \qquad (10)$$
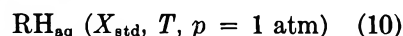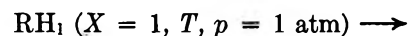
Propane and butane are gasses at the pressures and temperatures of interest, so it is assumed that the following process may be substituted for (10)

$$RH_1 \ (X = 1, T, p = P_{eq}) \longrightarrow$$
$$RH_{aq} \ (X_{std}, T, p = 1 \text{ atm}) \qquad (11)$$
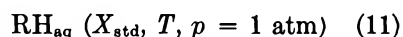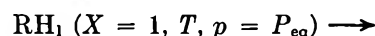
because of the small vapor pressure and compressibility of the liquid.

In the case of methane and ethane the critical temperatures are below the temperatures of interest. It was assumed that data for the following process may be used to estimate parameters for the process (10)

(10) The formula $E_s = 0.7 + 1.82n$ kcal was used for the sublimation energy of aliphatic hydrocarbons. This was given in ref 14, p 579.

(11) W. C. Lu, M. S. Jhon, T. Ree, and H. Eyring, *J. Chem. Phys.*, **46**, 1075 (1967).

(12) X_{std} refers to the standard state mole fraction which is unity here.

$\mathrm{RH_{sol}}\ (X\ =\ 1,\ T,\ p\ =\ 1\ \mathrm{atm})\ \longrightarrow$

$$\mathrm{RH_{aq}}\ (X_{std},\ T,\ p\ =\ 1\ \mathrm{atm})\quad (12)$$
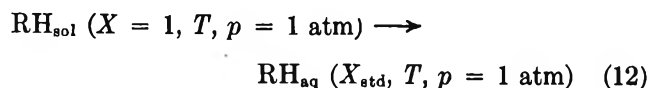
where $\mathrm{RH_{sol}}$ represents a nonpolar solution of the hydrocarbon.

The appropriate volume, V_2, to be used in eq 9 is the one corresponding to the state represented by the left-hand side of (10). In the case of methane and ethane the appropriate volume would be the partial molal volume for the left-hand side of (12). This volume is arbitrarily taken to be the volume of the pure liquid hydrocarbon at the melting point. For simple liquids the volume increase on melting is about 12%. This fact is used in significant structure theory to arrive at appropriate values for n and a. Due to the difficulties with methane and ethane noted above, it is assumed for simplicity that for all hydrocarbons treated here, that $V_{s2}/V_2 = 1/1.12$.

Incorporation of the Partition Function for Water and Preliminary Calculation of f_D. In this section the partition function f_D is calculated for hydrocarbon solutions, incorporating the partition function for water as given by Jhon, Grosh, Ree, and Eyring.[7] Parameters defining the first water layer around the hydrocarbon are, in general, different from the bulk liquid. It is shown in this section that the only way to get a reasonable entropy is to adjust θ for the first water layer. Due to the meaning of this parameter, any physical interpretation is difficult, especially when an attempt is made to apply it to a single layer of molecules.

The partition function for water, according to Jhon, Grosh, Ree, and Eyring is[7]

$$f_w = f_g^{(V_1 - V_{s1})/V_1} \left\{ f_s e^{(+E_{s1}/RT)}(1 + n_h e^{-\epsilon/RT}) \right\}^{(V_{s1}/V_1)}$$

$$(13)$$

where

$$f_g = f_{tr_1} f_{rot_1} f_{vib_1} \qquad (14)$$

$$f_s = f_E f_{lib_1} f_{vib_1} \cdot K^{K/(1+K)q} \qquad (15)$$

$$n_h = n_1 (V_1 - V_{s1})/V_{s1} \qquad (16)$$

$$\epsilon = a_1 E_{s1} \left(\frac{V_{s1}}{V_1 - V_{s1}} \right) \qquad (17)$$

The functions f_{tr_1}, f_{rot_1}, f_{vib_1}, f_E, and f_{lib} refer to the translational, rotational, vibrational, Einstein, and librational partition functions, respectively, K is the equilibrium constant between ice I and ice III, and q is 46, the number of water molecules per cluster. For f_{lib} those authors choose

$$f_{lib} = f_E \qquad (18)$$

so that the three Einstein degrees of freedom for the crystal vibration and the three degrees of libration are given the same functional form and the same characteristic temperature of 216.1°. Further details may be found in ref 7.

For the first layer of water, the partition function f_L will have the same form as f_W, but the parameters E_{sL}, θ_L, n_{h_L}, and ϵ_L are not necessarily the same as E_{s1}, θ_1, n_{h_1}, and ϵ_1. The parameter E_{sL} will be different from E_{s1} in the following manner. Assuming a single monolayer of ice which contains a maximum number of water molecules, three of the four bonds from a given water molecule will be bound to other water molecules in that layer. Half of the water molecules must be bound to the layer of water above and half to the layer below. Then in a planar surface layer only an average of $1/8$ of the water-water bonds are broken. Assuming that each water molecule is in some fashion bound to the hydrocarbon molecule

$$E_{sL} = (7/8)E_{s1} + (1/2)E_{RW} \qquad (19)$$

represents the sublimation energy associated with a molecule in the first layer of water.

The value of n_{hL} should remain unchanged from n_h according to the following argument. In the case of simple liquids a molecule in the bulk is surrounded by six positions in its own layer, three in the layer above and three in the layer below. A molecule at a wall or other boundary is surrounded by six positions in its own layer and three in the second layer. Any hole traveling through the second layer to the boundary layer must be reflected at the boundary, otherwise holes would pile up at the boundary layer. When the hole is reflected it goes through the second layer once again. Thus during the same time interval the probability of finding a hole next to a molecule is the same whether the molecule is at the boundary layer or not. Since the parameter n for water is similar to that for simple liquids, and water could be similarly divided into layers, the above argument, with some modification as to the number of neighbors, should apply to water. The "boundary" here is represented by a large hydrocarbon molecule. If the hydrocarbon molecule is about as small as a water molecule, then the problem of the boundary would not arise. Holes would then move

---

Table I: Butane Solution Quantities at 298.15°K Using Partition Function from Eq 18

	I	II	III	IV
		—Calculation no.—		
θ_L, °K	216.1	219.4	255	216.1
E_{RW}, cal	1883	1883	1883	2879
V_L,[a] cc	17.91	17.91	17.95	17.71
ΔA, kcal	0.479	0.84	5.27	−17.19
ΔE, kcal	−0.634	−0.78	−0.85	−20.74
ΔS, eu	−3.73	−5.44	−20.6	−11.91
c_v, cal mol⁻¹	1.3	0.6	4.0	8.2

[a] The calculated V_s at 298.15°K is 17.6564 cc and V_1, the calculated bulk molar volume of water, is 18.009 cc. V_L then indicates the degree of increased cluster formation.

Table II: Aliphatic Hydrocarbon Solution Quantities at 298.15°K Using Partition Function Containing Restricted Rotation Terms[a]

Hydrocarbon	L^b	$V_L{}^c$	ΔA	ΔE	ΔS	c_v	ΔG^b	ΔH^b	ΔS^b	$c_p{}^b$
Methane	13	18.164	1.48	−2.848	−14.53	7.1	2.51 to 3.15	−2.86 to −2.25	−18.4 to −16.8	25
Ethane	16	18.164	2.93	−2.400	−17.88	8.3	3.32 to 3.86	−2.37 to −1.27	−19.5 to −16.8	60
Propane	18	18.164	4.44	−1.559	−20.12	9.8	4.90 to 4.91	−2.09 to −1.45	−23.5 to −21.3	69
Butane	20	18.164	5.59	−0.7183	−22.36	11.0	5.82 to 6.0	−0.96 to −0.72	−22.7 to −21.9	80

[a] Equation 23. [b] From ref 6. [c] V_s at 298.15 is 17.6564 cc/mol and V, the bulk volume of water, is 18.009 cc/mol. V_L then indicates degree of decreased cluster formation.

freely through the liquid and n_{hL} would again be equal to n_L.

The value of ϵ remains unchanged since the energy required to push aside another water molecule would not be expected to change for any reason other than a change in sublimation energy. The value of ϵ does not affect the results greatly, because of the small value of the parameter a.

With the above parameter changes, f_D was evaluated for butane ($L = 20$) at 298.15°K. The results for several values of θ_L and E_{RW} are given in Table I. In each case the Helmholtz free energy was minimized with respect to volume. Column 1 uses $\theta_L = \theta_1$ and E_{RW} was adjusted so as to obtain the experimental ΔE. In column 2, θ_L is adjusted in accord with eq 8. E_{RW} is again adjusted slightly to get the experimental ΔE (Table II). Neither treatment gives an acceptable entropy.

If degree of iceberg formation is defined as the per cent decrease in volume V_L of the water layer next to the hydrocarbon from the calculated volume of bulk water at 298.15°K ($V_w = 18.009$) to the calculated cluster volume at the same temperature ($V_s = 17.6564$), then there is about 17% iceberg formation, since V_L was found to be 17.950 cc.

In column 3, the value of θ_L is adjusted to give a reasonable entropy. Because of the oversimplified model of molecular motions represented by a characteristic temperature, the physical interpretation of the increased value of θ_L is not apparent.

In column 4 a value of E_{RW} is assumed, which gives about 87% iceberg formation. The value of E_{RW} needed is much too high so that the ΔA is of the wrong sign. The entropy is still too low, although a contribution could come from an adjustment of θ_L.

Introduction of an Asymmetric Electric Field in the First Water Layer. In order to more easily account for the negative entropy change for the solution of hydrocarbons, it is assumed that the same sort of increased order is present in the first layer of water molecules that has been proposed[8] to be present in the surface layer of pure water. This increased ordering of water molecules at the surface of pure water is responsible for the large surface tension of this liquid. The idea of relating surface tension itself to hydrophobic bonding

directly has been considered by Sinanoglu, who previously correlated solvent effects on molecular association with surface tension.[13]

According to Jhon, *et al.*,[8] the surface tension of water is due in part to the asymmetric electric field in which the surface layer exists. This asymmetry does not exist in the interior and the bulk water molecules are randomly oriented, but at the surface, these water molecules have their dipoles oriented with respect to the layer below.

In the case of hydrocarbon solutions the first layer water molecules are also in an asymmetric electric field, since they are flanked by randomly oriented water dipoles below and a hydrocarbon molecule above. The potential energy μX responsible for the orientation is due to the dipole μ of the water molecule interacting with the effective electric field X at the water dipole.

In order to properly modify the water layer by the potential μX it is necessary to modify the partition function for water so that the librational degrees of freedom are represented by a function representing restricted rotation[14] and incorporating a restricting potential B. Then it is only necessary to modify such a function by increasing the restricting potential B by μX. The function f_{lib} in eq 15 is changed to

$$f_{lib} = f_{1RR} \cdot f_{2RR} \qquad (20)$$

where

$$f_{1RR} = \frac{(2\pi I_B kT)^{1/2}}{h} \int_0^{2\pi} e^{-B \cos \phi / kT} d\phi \cong$$

$$\frac{(2\pi I_B kT)^{1/2}}{h} \left[\frac{2\pi kT}{B} \right]^{1/2} e^{B/RT} \qquad (21)$$

$$f_{2RR} = \frac{8\pi^2 (I_A I_C)^{1/2} kT}{2h^2} \left[\frac{kT}{B} \sinh \frac{B}{kT} \right] \qquad (22)$$

where I_A, I_B, and I_C are the three moments of inertia of water.

Since θ now represents the Einstein degrees of freedom

(13) O. Sinanoglu, "Molecular Associations in Biology," B. Pullman, Ed., Academic Press, 1968, p 427.

(14) E. A. Moelwyn-Hughes, "Physical Chemistry," 2nd ed, revised, Pergamon Press, New York, N. Y., 1961.

only, the parameter B was chosen to give the same entropy at the melting point that is given by eq 18. The parameter E_{s_1} then has a new value of 8924.19 cal and a_1 is then 0.00001993, found in accord with the technique of ref 7.

The function f_{1RR} represents one degree of freedom of restricted rotation. This gives kT for the internal energy in the above approximation, the same as that of a harmonic oscillator. The function f_{2RR} represents two degrees of rotational freedom whose total internal energy goes from kT to $2kT$ as the applied field goes from zero to infinity. The internal energy is then represented correctly at the limits as the motion goes from free rotation to that of a harmonic oscillator. The function (20) reduces to the partition function for three degrees of free rotation for $B = 0$. The partition function (13), using this function (20) with $B = 8.215 \times 10^{-14}$ erg reproduces, with considerable accuracy, the results from using the function (18). The quantities A, E, S, and V at 293.15° are obtained to an accuracy of five significant figures. At 100°, the results are the same to an accuracy of at least four significant figures.

The partition function for the first layer of water is then

$$f_L = \left(f_{tr_1} f_{rot_1} \left[\frac{kT}{\mu x} \sinh \frac{\mu X}{kT} \right] f_{vib_1} \right)^{(V_L - V_{s1})/V_L} \times$$

$$[f_E f_{vib_1} f_{1RR} f_{2RR}' e^{E_{sL}/RT} (1 + n_h e^{-\epsilon/RT})]^{V_{s1}/V_L} \quad (23)$$

where

$$f_{2RR}' = \frac{8\pi^2 (I_A I_C)^{1/2} kT}{2h^2} \frac{kT}{B + \mu X} \sinh \frac{B + \mu X}{kT} \quad (24)$$

Making use of eq 23 and the modification given by eq 20 for f_w, eq 9 is evaluated, adjusting the two parameters μX and E_{RW} and minimizing the free energy with respect to the volume V_L.

Results from the Modified Function

The calculated values of the thermodynamic properties from eq 23 are compared with the experimental quantities in Table II. It was impossible to find acceptable values for the parameters μX and E_{RW} at $V_L < V_1$. For a slight increase in volume the parameters are $\mu X = 1.0 \times 10^{-13}$ erg and $E_{RW} = 1.8196$ kcal. The pV term is neglected because of its smallness and ΔG may be compared directly with ΔA.[2]

In the case of butane, Figure 1 shows the behavior of the solution Helmholtz free energy with temperature and a comparison with experiment. Figure 2 shows the behavior of the entropy with temperature. It is seen that the calculated entropy increases with temperature, but not fast enough. The negative entropy contribution is due to the restricted rotation of the water molecules, and the intensity of the potential was adjusted to give roughly the correct value at 298.15°. However, the change with temperature may depend on
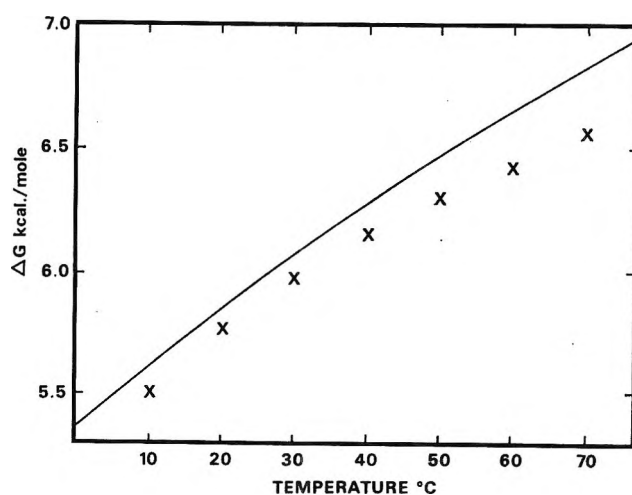
Figure 1. Unitary free energy of solution of butane in water: $\times$, experimental taken from ref 2, Figure 9; solid line is calculated using eq 23. It is assumed here for the calculated values that $\Delta A = \Delta G$.
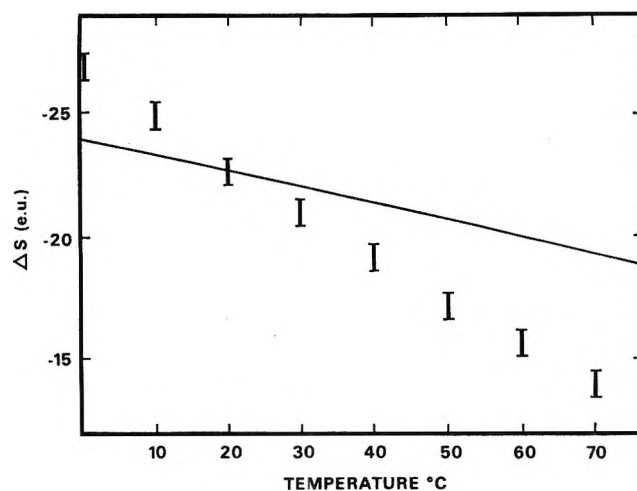
Figure 2. Unitary entropy of solution for butane in water. Vertical bars indicate experimental quantities taken from ref 2, Figure 11; solid line is calculated using eq 23.

the shape of the potential itself. The idealized potential chosen, the rotation of a dipole in an electric field, is probably not an accurate enough function. Account should be taken of the different energy requirements of two possible orientations of a water molecule with respect to the hydrocarbon, one orientation having a hydrogen directed toward the hydrocarbon, the other having the oxygen as a nearest neighbor to the hydrocarbon.

Table II gives the partial molal heat capacities of the hydrocarbon solutions at 298.15°. It is seen that these again are too small, although a strict comparison of c_p and c_v is difficult. The heat capacity is given by

$$C_v = T \left(\frac{\partial S}{\partial T} \right)_v \quad (25)$$

Again, a preferred orientation of the water molecule

with respect to the hydrocarbon should be taken into account.

The calculated increase in volume in the water layer next to the hydrocarbon molecule appears not to be in accord with the observed decrease of partial molal volume as measured experimentally.[15] Actually the theory does not treat all aspects of the volume change. From the volumes V_1, V_2, and V_L only quantities referring to the fraction of molecules having gas-like or solid-like degrees of freedom can be obtained. Thus in the layer f_L, $(V_L - V_s)/V_s$ indicates the relative number of holes $vs.$ molecules. The theory assumes that the molecular volume remains constant for a given structure. It does not account for the fact that a water molecule may have a different volume next to hydrocarbon molecule from that when it is surrounded by other water molecules.

Discussion of Parameters

The parameter B in the water partition function was taken to be the same for all three degrees of restricted rotation for simplicity. The value found was 8.215×10^{-14} erg. The values of the partition functional degrees of freedom are different for the three directions because of the different moments of inertia.

For lack of any good way of determining θ_L it is taken as equal to θ. Since θ_L would be expected to vary as $(E_s)^{1/2}$, then a decrease in internal energy of about -1 to -3 kcal is distributed over 13–20 water molecules and a hydrocarbon molecule. This leads to a 2% change in the sublimation energy per molecule and a 1% change in θ_L. This could possibly account for a decrease in entropy of only 1–2 eu, as in the analogous case in Table II, columns 1 and 2.

The value 1.8196 kcal found here for E_{RW} is between that for two methane molecules ($^1/_2E_s/12 = 0.1$ kcal/mol)[14] and two water molecules (5–6 kcal/mol).[16]

E_{RW} enters into the partition function through eq 7 and 19. If the water surface around the molecule is assumed to be concave rather than planar, fewer water–water bonds would be calculated to be broken. Then the coefficient of E_{s_1} in eq 19 would be larger, and as a result, the absolute magnitude of E_{RW} necessary to fit the data would be correspondingly smaller. Since the average curvature of the surface was not considered, the value of E_{RW} found here may be somewhat too high.

The value 1.0×10^{-13} found for μX leads to a slightly high value of the entropy for several members of the series. The value found is reasonable in the light of the value $\mu X = 1.416 \times 10^{-13}$ erg found necessary to account for the surface tension of water,[8] although the comparison is not straightforward. The parameter μX of that paper compares with $B + \mu X$ of this paper and in that paper only one degree of freedom is represented by a restricted rotation potential. This may also be compared with the energy of interaction of two side by side parallel dipoles of the magnitudes of water dipoles and separated by the distance 2.73 Å, which is 1.6×10^{-13} erg.

The parameters μX and E_{RW} are connected to the thermodynamic functions ΔE and ΔS in a complicated way. For $T = 298.15°$K, if μX is set equal to zero and E_{RW} is varied, then the volume V_L can be adjusted so as to minimize the energy. An energy ΔE in the range 0 to -1 kcal/mol is found and the volume $V_L < V_1$. In order to decrease the entropy, μX is then increased. Increased internal energy accompanies the increased restricted rotation. By increasing μX and changing E_{RW} to compensate for the increased internal energy and then minimizing the free energy with respect to volume, the appropriate values of μX and E_{RW} can be found. With a wide range of variation of μX (from 7×10^{-14} to 12×10^{-14} erg) and the corresponding acceptable values of E_{RW} (to give $\Delta E \sim -1.0$ kcal) only a narrow range of molar volumes is found (18.10–18.25 cc).

The parameter L, the number of water molecules which can be packed around a given hydrocarbon molecule, was taken directly from ref 2. The structure of this surface layer is unknown but would hopefully form a network of five- and six-membered rings as in ice I and III. The usefulness of the theory in computing ΔE and ΔS for hydrophobic bonding for larger, more interesting systems from the point of view of biochemistry is based on estimating L in terms of molecular models.[17]

(15) W. L. Masterton, *J. Chem. Phys.*, **22**, 1830 (1954).

(16) G. C. Pimentel and A. L. McClellan, "The Hydrogen Bond," W. H. Freeman, San Francisco and London, 1960, and references therein.

(17) G. Némethy and H. A. Scheraga, *J. Phys. Chem.*, **66**, 1773 (1962).

Dependence of Micelle Aggregation Number on Polar Head Structure.

I. Light Scattering by Aqueous Solutions of Decylammonium

Salts and Related Surfactants[1]

by Richard D. Geer, Edwin H. Eylar, and E. W. Anacker*

Department of Chemistry, Montana State University, Bozeman, Montana 59715 (*Received August 19, 1970*)

Publication costs assisted by the National Science Foundation

Aggregation numbers of decyl-, decylmethyl-, decylethyl-, and decylpropylammonium chloride in 0.1 m NaCl, of decyl-, decylmethyl-, decyldimethyl-, decyltrimethyl-, decyldiethyl-, and decyltriethylammonium bromide in 0.5 m NaBr, and of decylquinuclidinium bromide and decyldiazabicyclo[2.2.2]octanium bromide in 0.5 m NaBr were determined by light scattering. The smallest micelles were formed by decyltriethylammonium bromide (aggregation number = 37) and the largest by decylammonium bromide (aggregation number > 1000). The mean distance of closest approach of a counterion to the charge center of the surfactant ion, hydrophobic bonding between alkyl groups on adjacent polar heads, and polar head–water interaction appear to be factors which must be given serious consideration in any evaluation of the polar head's role in the micellization process.

Although the aggregation of surfactant ions in aqueous solution has been under investigation for well over half a century, relatively few studies of the role of the polar head's structure in the micellization process have been made. McDowell and Kraus[2] measured conductances of the bromates of octadecyltriethyl-, tri-*n*-propyl-, tri-*n*-butyl-, and tri-*n*-amylammonium ions in water and found that as the size of the substituent groups increased, the critical micelle concentration (cmc) shifted toward lower concentrations. They concluded that "the larger the number of carbon atoms (in the substituent groups), the lower the concentration at which micelles appear" and "the larger the heads of the micellar ions...the smaller the number of counterions bound by the micelle." Whether these statements apply to surfactants having, in addition to the long hydrocarbon chain, but one or two short alkyl chains on the nitrogen, or having different small alkyl groups on the nitrogen, was not determined.

An attempt[3] was made in our laboratory a number of years ago to study the effect of polar head size and constitution on surfactant aggregation number. Aqueous solutions of some dodecylalkyl-, dodecyldialkyl-, and dodecyltrialkylammonium chlorides were examined by light scattering. Since solubility considerations forced the use of a rather broad temperature range and because no supporting electrolyte was employed, it was impossible to make meaningful comparisons of the calculated micellar weights. The work clearly showed, however, that micelle size is strongly dependent on polar head structure. In agreement with this finding are the results of Venable and Nauman,[4] who later determined the aggregation numbers of three surfactants with a common hydrocarbon tail and counterion, but with different polar heads. In 0.05 M NaBr, they obtained aggregation numbers of 274, 150, and 120 for micelles of tetradecylpyridinium, tetradecyltrimethylammonium, and tetradecyltripropylammonium bromide, respectively.

In the present investigation, we have tried to elucidate the polar head's role in micelle formation by determining in aqueous solution the aggregation numbers of a group of related surfactants, *viz.*, some decyl-, decylalkyl-, decyldialkyl-, and decyltrialkylammonium bromides and chlorides. Systematic structural alterations of the polar head were achieved by replacing protons on the nitrogen with methyl, ethyl, and propyl groups.

Experimental Section

Materials. In general, a substituted decylamine salt was prepared by mixing *n*-decyl bromide with an excess of the appropriate amine, adding ethyl ether when a solvent was desired, and allowing the mixture to stand at room temperature for 2 or 3 weeks.

When the amine was tertiary, a quaternary salt eventually separated from the mixture, either as a solid or as an oil. In general, the surfactant could be crys-

(1) Presented in part at the 157th National Meeting of the American Chemical Society, Minneapolis, Minn., April 1969.

(2) M. J. McDowell and C. A. Kraus, *J. Amer. Chem. Soc.*, **73**, 2173 (1951).

(3) E. H. Eylar, M.S. Thesis, Montana State College, Bozeman, Mont., 1955.

(4) R. L. Venable and R. V. Nauman, *J. Phys. Chem.*, **68**, 3498 (1964).

Table I: Per Cent of Halide in Prepared Surfactants

Surfactant	Symbol	Calcd	Found
Decylammonium chloride	DAC	18.30	18.36
Decylmethylammonium chloride	DMAC	17.06	17.14
Decylethylammonium chloride	DEAC	15.98	15.96
Decylpropylammonium chloride	DPAC	15.03	15.12, 15.06[a]
Decylammonium bromide	DAB	33.54	33.51
Decylmethylammonium bromide	DMAB	31.68	31.62
Decyldimethylammonium bromide	DDMAB	30.01	30.06
Decyltrimethylammonium bromide	DTMAB	28.51	28.47
Decyldiethylammonium bromide	DDEAB	27.15	27.16
Decyltriethylammonium bromide	DTEAB	24.79	24.68
Decylquinuclidinium bromide	DQB	24.04	24.04
Decyldiazabicyclo[2.2.2]octanium bromide	DDBOB	23.97	23.88

[a] Two samples were prepared and used.

tallized from the latter by titurating with ether and cooling for several days.

When the amine was primary or secondary, a minimum of 2 moles was required for each mole of decyl bromide. Since the primary and secondary amines used are stronger bases than the substituted decylamines formed, the main reactions were

$$2R_2'NH + RBr \longrightarrow R_2'NH_2Br + RR_2'N$$

$$2R'NH_2 + RBr \longrightarrow R'NH_3Br + RR'NH$$
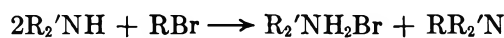
The salts, $R_2'NH_2Br$ and $R'NH_3Br$, separated from the reaction mixtures as solids and oils.

Each substituted decylamine salt ($RR_2'NHBr$, $RR'NH_2Br$, or one of the corresponding chlorides) was obtained in the following manner. The corresponding reaction mixture was first extracted with water to remove simple amine salts, and then with ether. After the ether had been removed from the latter extract, the remaining residue was mixed with an excess of ammonium bromide or chloride, depending upon which salt was being prepared. Sufficient methanol to put most of the ammonium salt into solution at the boiling point was added. The mixture was heated and then evaporated to dryness, ammonia being released in the process. The residue was washed with ether to remove unreacted decyl bromide and other soluble impurities and then treated with hot acetone. The substituted decylamine salt dissolved, leaving behind most of the excess ammonium halide and simple amine salts not removed earlier.

Decylammonium chloride and decylammonium bromide were prepared in a manner similar to that just described for the substituted decylamine salts. Starting materials were decylamine and either ammonium chloride or ammonium bromide.

All surfactants were purified by three to six crystallizations from various mixtures of acetone, methanol or ethanol, and ether. Traces of solvent and H_2O were removed by drying under vacuum and storage over

P_4O_{10}. Surfactants were analyzed for halide content with the results given in Table I.

The sodium bromide and sodium chloride used in preparing solutions were of reagent grade and oven dried. Water used in solution preparation was doubly distilled, the second distillation being from alkaline permanganate.

Apparatus and Procedure. Scattering and refractive index measurements were made at 4358 Å in Brice-Phoenix instruments. Viscosity measurements were made with a modified Ostwald viscometer similar to that employed by Bueche.[5] Its construction features a long coiled capillary, which increases the flow time significantly over that of the unmodified viscometer without making the instrument's size unmanageable. Water flow time at 27° was about 280 sec; reproducibility was about 0.2 sec.

All solutions were prepared by weight. Those used for scattering measurements were filtered under nitrogen pressure through an ultrafine, fritted Pyrex glass funnel directly into a cylindrical cell (catalog C105). When solubility permitted, measurements were made at 25°, otherwise at 30°.

Micellar aggregation numbers were calculated from an equation developed earlier[6,7]

$$Km_2'/R_{90} = A + Bm_2' + \ldots \tag{1}$$

where

$$K = 2\pi^2 n^2 (dn/dm_2')_{m_3}^2 V^0/L\lambda^4 \tag{2}$$

$$A = 4N[(2N - fp)^2 + pf^2]^{-1} \tag{3}$$

$$B = pA[(1 + p)N^{-1} - A](2m_3)^{-1} \tag{4}$$

The symbols have the following meanings: m_2' is the

(5) P. Debye and A. M. Bueche, Technical Report RRC 1755, Office of Rubber Reserve, Reconstruction Finance Corporation.

(6) E. W. Anacker and A. E. Westwell, *J. Phys. Chem.*, **68**, 3490 (1964).

(7) E. W. Anacker and H. M. Ghose, *J. Amer. Chem. Soc.*, **90**, 3161 (1968).

molality of the micellar salt (primes refer to quantities in terms of monomer units), *i.e.*, total molality of surfactant minus the cmc; R_{90} is Rayleigh's ratio for a 90° scattering angle; n is the solution refractive index; m_s is the molality of supporting electrolyte; $V°$ is the volume of solution containing 1 kg of water; L is Avogadro's number; λ is the wavelength under vacuum of the light used; N is the micellar aggregation number, *i.e.*, the number of surfactant ions per micelle; p is the effective micellar charge; and $f = (dn/dm_3)_{m_2'}/(dn/dm_2')_{m_3}$.

A and B are the intercept and limiting slope, respectively, of the Km_2'/R_{90} vs. m_2' plot. The effective micellar charge p and the micellar aggregation number N are calculated from

$$p = [2fm_3B + (8m_3B)^{1/2}]A^{-1}(2 - fA)^{-1} \quad (5)$$

$$N = p(p + 1)A(2m_3B + pA^2)^{-1} \quad (6)$$

Assumptions inherent in eq 1 are: there is no depolarization of the scattered light at 90°; the micelles are small compared to λ (*i.e.*, there is no dissymmetry); R_{90} represents the scattering of a solution in excess of that at the cmc; and unmicellized surfactant, concentration assumed equal to that of the cmc, can be lumped in with the supporting electrolyte.

We have written and used a FORTRAN program to work up the experimental scattering data provided by the Brice-Phoenix photometer. It yields the cmc, A^{-1}, N, and p corresponding to the best (least-squares) linear plot of Km_2'/R_{90} vs. m_2'. The value of K used is that appropriate at the cmc. A listing of the program is available upon request.

Results and Discussion

It was our original intention to examine only bromides in 0.5 *m* NaBr at 25°. However, decylethylammonium bromide and decylpropylammonium bromide proved to be insufficiently soluble under these conditions to permit meaningful measurements. By changing the counterion to chloride, the solvent to 0.1 *m* NaCl, and the temperature to 30°, we were able to work with the decylalkylammonium salts.

Within experimental error, refractive index *vs.* surfactant molality plots were linear over concentration ranges of interest. The least-squares slopes of these plots appear in Table II under the $(dn/dm_2')_{m_{NaX}}$ heading. Values of 0.0104 and 0.0147 kg/mol[8] were used for dn/dm_{NaCl} and dn/dm_{NaBr}, respectively.

The light scattering data collected at 90° are plotted in Figures 1–4. Only the results from the second sample of DPAC are shown. Solvent scattering, *i.e.*, scattering from either 0.1 *m* NaCl or 0.5 *m* NaBr, has been subtracted from the total scattering of each solution. To get R_{90} values appropriate for the calculation of an aggregation number (see eq 1–6) from a plot, one must subtract the ordinate at the cmc from the plotted

Table II: Concentration Gradients of the Refractive Index, Critical Micelle Concentrations, Aggregation Numbers, and Effective Micellar Degrees of Ionization

Surfactant[a]	$(dn/dm_2')_{m_{NaX}}$, kg/mol	10^3 cmc, mol/kg	N	$p' = p/N$
1. DAC	0.0289	34	78	0.16
2. DMAC	0.0304	36	53	0.16
3. DEAC	0.0322	34	61	0.17
4. DPAC[b]	0.0351	29.3	58.7	0.18
5. DPAC[c]	0.0356	28.6	56.5	0.17
6. DAB	0.0322	16	1100	0.07
7. DMAB	0.0334	20[d]	670[d]	0.07
8. DDMAB	0.0358	12	69	0.08
9. DTMAB	0.0380	18	48	0.13
10. DDEAB	0.0409	9.3	65	0.13
11. DTEAB	0.0463	17	37	0.23
12. DQB	0.0507	12	58	0.12
13. DDBOB	0.0510	20	51	0.20

[a] For the first four surfactants, the solvent was 0.1 *m* NaCl and the temperature 30°. For the last eight surfactants, the solvent was 0.5 *m* NaBr and the temperature 25°. [b] First preparation. [c] Second preparation. [d] Based on surfactant concentrations above 0.03 *m*. A cmc of 0.011 and an aggregation number of 271 result from the use of just the third and fourth points from the left in the DMAB plot of Figure 2.
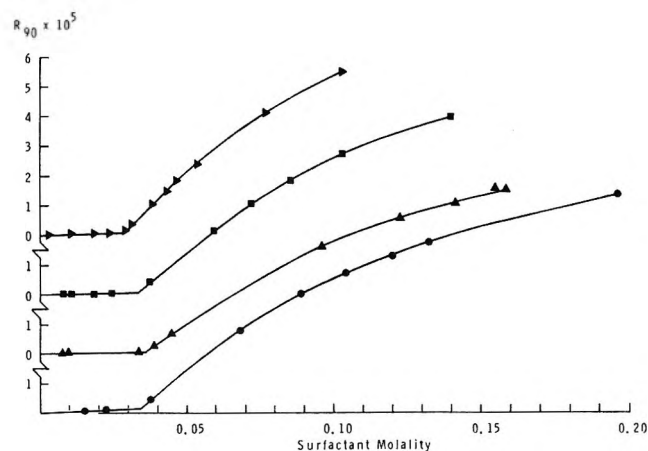
Figure 1. Scattering at 90° by solutions of DAC (●), DMAC (▲), DEAC (■), and DPAC (▶) in 0.100 *m* NaCl.

ordinates. Scattering at 45 and 135° was measured for each solution; within experimental error, no dissymmetry was detected in any solution examined. The concave upward curvature present in the decylmethylammonium bromide plot at low surfactant concentrations presumably reflects a strong dependence of micelle size distribution on surfactant concentration. Similar behavior has been observed before.[7-9]

Computed cmc values, aggregation numbers, and

(8) E. W. Anacker and H. M. Ghose, *J. Phys. Chem.*, **67**, 1713 (1963).

(9) P. Debye and E. W. Anacker, *J. Phys. Colloid Chem.*, **55**, 644 (1951).
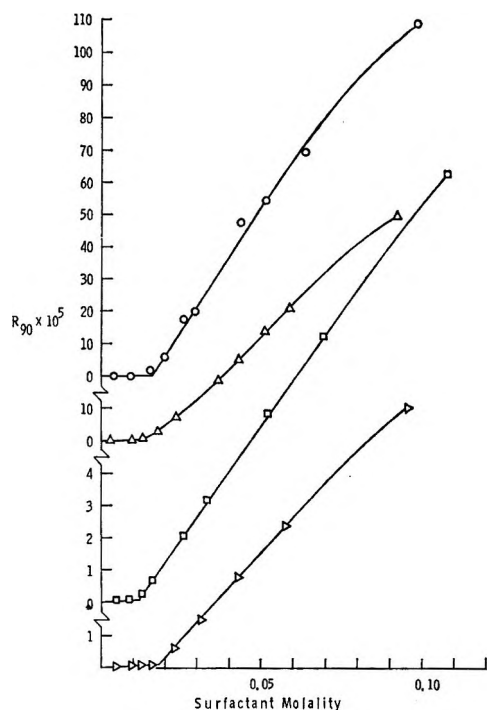
Figure 2. Scattering at 90° by solutions of DAB (O), DMAB (△), DDMAB (□), and DTMAB (▷) in 0.500 m NaBr.
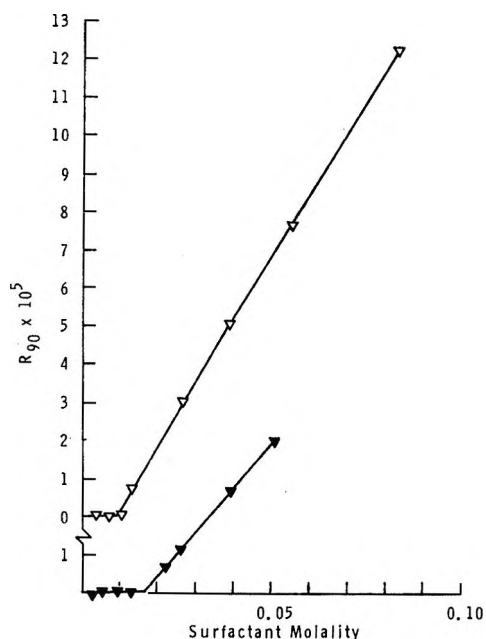
Figure 3. Scattering at 90° by solutions of DDEAB (▽) and DTEAB (▼) in 0.500 m NaBr.

Figure 4. Scattering at 90° by solutions of DQB (◇) and DDBOB (◆) in 0.500 m NaBr.

effective charges (effective degrees of ionization) are shown in Table II.

Although temperature and supporting electrolyte concentration changes are responsible in part, the major factor behind the difference in aggregation numbers of decylammonium micelles for entries one and six of Table II is most likely counterion specificity. Previous work[7,8] has shown that the bromide ion has a greater aggregating power than the chloride. Whether this should be attributed to the bromide ion's greater polarizability, greater water-structure breaking ability, or to some combination of properties is not clear.

We note that the largest and smallest micelles are composed of decylammonium and decyltriethylammonium ions, respectively. If hydrophobic bonding between ethyl groups on adjacent polar heads and/or between ethyl groups and those portions of the decyl chains making up the exterior layer of the micelle's hydrocarbon core[10] were the only factor to be considered, one would expect the decyltriethylammonium ions to form the larger micelles. Since the opposite is true, there must be at least one opposing factor. A possibility is the mean distance of closest approach of the counterion to the nitrogen of the surfactant's polar head. All other factors being equal, the smaller this distance, the more effective a given counterion should be in screening out repulsive electrical forces between surfactant ions and, consequently, the larger the micelle. The relative values of the aggregation numbers of entries six through eleven of Table II are consistent with this interpretation. Although a p' value is only a

(10) D. Stigter, *J. Phys. Chem.*, **68**, 3603 (1964).

rough approximation to a degree of ionization, the trends exhibited by this quantity are what one would predict according to the above view, i.e., the smaller the polar head the more tightly bound the counterion.

In the sequence decyl-, decylmethyl-, decylethyl-, and decylpropylammonium chloride, the aggregation number exhibits a definite minimum at the second member. In a sense, the minimum is also present in the decyl-, decylmethyl-, and decylethylammonium bromide sequence since there is a decrease in aggregation number from the first to the second member and an increase to "infinity" for the essentially insoluble third member. Apparently, the lengthening of a single substituent chain beyond the first carbon has little effect on the mean distance of closest approach of the counterion but it does result in increased hydrophobic bonding. This cannot be the whole story, if indeed it is part of it, since the apparent leveling off, or possible decrease, of the aggregation number after the ethyl group is not explained. Taken at face value, the data suggest that the aggregation number rises with the addition or subtraction of a $-CH_2-$ to a single substituent chain having an odd number of carbon atoms and falls when the addition or subtraction leads to a chain with an odd number. It is interesting to note that Lange and Schwuger[11] observed an odd–even alternation in the Krafft temperatures and Mukerjee[12] found an odd–even alternation in the free energies of micelle formation in a homologous series of sodium alkylsulfates. Mukerjee suggests that such alternations are evidence for the presence of solid-like (ordered) structures in micelles. Until more information is available, the value of any suggestion that an odd–even alternation in aggregation numbers exists in a homologous series of decylalkylammonium chlorides must remain in limbo.

The cmc trends shown by entries six through eleven of Table II are not all in accord with McDowell and Kraus's observation[2] that the larger the number of carbon atoms in the substituent groups, the lower the cmc. Thus, decyltrimethylammonium bromide has a higher cmc than decyldimethylammonium bromide and decyltriethylammonium bromide a higher cmc than decyldiethylammonium bromide.

Usually, an increase in the concentration of added supporting electrolyte to solutions of a given ionic surfactant is accompanied by a decrease in the cmc and an increase in the aggregation number. It is obvious from Table II, however, that the attainment of a lowered cmc through a structural change in the surfactant ion's polar head does not guarantee a concomitant increase in the aggregation number. Thus, there can be no simple relationship between cmc and aggregation number, even though the length of the surfactant ion's hydrocarbon tail, the supporting electrolyte concentration, and the counterion are held constant. The structure of the polar head is an important factor.
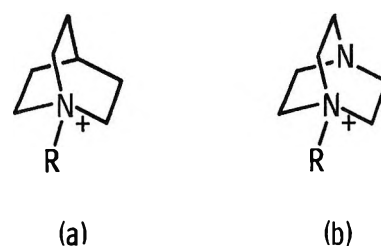
Figure 5. Polar head structures of the decylquinuclidinium (a) and decyldiazabicyclo[2.2.2]octanium (b) ions. The decyl chain is denoted by R.
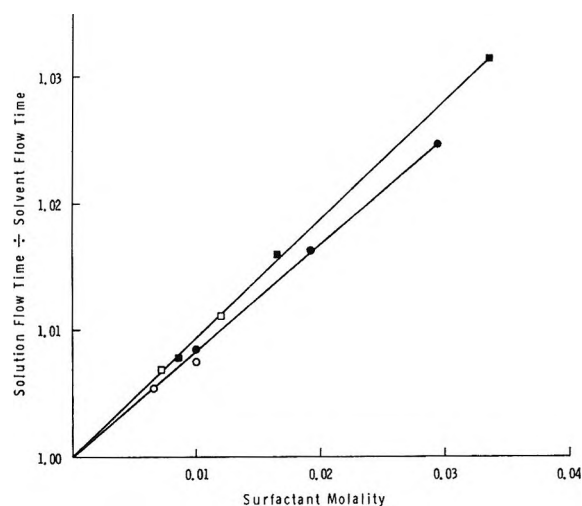
Figure 6. Relative viscosity vs. surfactant concentration for DDBOB in water (■), DDBOB in 0.500 m NaBr (□), DQB in water (●), and DQB in 0.500 m NaBr (○).

The possibility was raised earlier that the relative smallness of the decyltriethylammonium bromide micelle is due primarily to the comparatively large mean distance of closest approach of the bromide ion to the charged nitrogen of the surfactant ion's polar head. If this suggestion has merit, tying the three ethyl groups together should enable a counterion to approach a nitrogen more closely in a lateral direction and thus promote the formation of larger micelles. The tying together of the ethyl groups is accomplished in decylquinuclidinium bromide and in decyldiazabicyclo[2.2.2]octanium bromide and does, as seen in Table II, result in larger micelles.

Decylquinuclidinium bromide and decyldiazabicyclo[2.2.2]octanium bromide possess polar heads of similar size, structure, and shape (Figure 5). It is somewhat remarkable, therefore, that appreciable differences exist in their aggregation numbers and in their cmc's. These differences most likely stem from a dissimilarity in their interactions with the solvent. The lone pair electrons on the terminal nitrogen of the polar head of

(11) H. Lange and M. J. Schwuger, Kolloid-Z. Z. Poly., 223, 145 (1968).

(12) P. Mukerjee, ibid., 236, 76 (1970).

the decyldiazabicyclo[2.2.2]octanium bromide would facilitate hydrogen bonding with solvent. This, in turn, would enhance the solubility of unaggregated surfactant, i.e., increase the cmc. If the hydrogen bonding persisted in the micellized state, the polar heads would have less freedom of movement in the Stern layer[10] than otherwise would be the case. Consequently, the entropy of micellization would be less positive when hydrogen bonding between solvent and aggregated polar heads existed than in its absence. All other considerations being equal, a smaller entropy of micellization would be consistent with a smaller aggregation number. In this way, perhaps, the differences in properties of the two micelles can be rationalized.

The limiting slopes of the Km_2'/R_{90} vs. m_2' plots for decyldiazabicyclo[2.2.2]octanium bromide and decyl-

quinuclidinium bromide are 0.039 and 0.014 kg mol^{-1}, respectively. To the extent that these values are measures of solute–solvent interaction, they indicate that the former surfactant interacts more strongly with water than the latter. To test our conjecture that the interaction is influenced significantly by the nature of the surfactant ion's polar head, we measured the relative viscosities of dilute solutions of the two surfactants. For a concentration below the cmc, monomer–solvent interactions should predominate over micelle–solvent interactions. The results are shown in Figure 6 and suggest a stronger polar head–solvent interaction for the decyldiazabicyclo[2.2.2]octanium ion than for the decylquinuclidinium ion.

Effect of Urea and Other Organic Substances on the Ultrasonic

Absorption of Protein Solutions

by J. Lang, C. Tondre, and R. Zana*

C.N.R.S., Centre de Recherches sur les Macromolécules, Strasbourg, France   (*Received August 31, 1970*)

The ultrasonic absorption titration curves have been determined in the acid pH range for bovine serum albumine, β-lactoglobuline, and lysozyme solutions in H$_2$O–urea (8 M) and in the alkaline pH range for lysozyme dissolved in H$_2$O–urea (8 M). Similar measurements have been performed on diglycine and acetylglycine solutions in H$_2$O–urea (8 M). The results cannot be interpreted in terms of conformal changes. Proton-transfer reactions, however, provide a satisfactory explanation for all the experimental results. These results as well as those obtained in this work in studying the effect of various organic additives on the absorption of protein solutions seem to indicate that the ultrasonic absorption is sensitive to the overall conformation of the protein but not to the equilibrium between conformations.

I. Introduction

Various chemical processes have been proposed to explain the ultrasonic absorption properties of aqueous protein solutions, owing to the complexity of protein molecules. For instance, the acoustical properties of protein solutions at a pH close to the isoelectric point have been explained in terms of keto–enol equilibrium on the peptide link[1] and water–protein interactions.[2] Recently, the effect of pH on the ultrasonic absorption of aqueous protein solutions has been investigated and absorption maxima observed both in the acid[3,4] and alkaline[4] pH regions. Kessler and Dunn[3] interpreted these maxima in terms of conformal changes of the

bovine serum albumine (BSA) molecule which they used in their work. On the other hand, the study of dilute solutions of BSA, β-lactoglobulin (βL), and lysozyme (L) led Zana and Lang[4] to propose a different explanation for the absorption maxima. As the nature of the protein was found to have only little influence on the magnitude of the maximum and on the pH at which

(1) A. Meyer and H. Vogel, *Z. Naturforsch. B*, **20**, 85 (1965).

(2) J. Burke, G. Hammes, and T. Lewis, *J. Chem. Phys.*, **42**, 3520 (1965).

(3) L. Kessler and F. Dunn, *J. Phys. Chem.*, **73**, 4256 (1969); **74**, 2736 (1970).

(4) R. Zana and J. Lang, *ibid.*, **74**, 2734 (1970).

it occurs, these maxima were interpreted in terms of proton-transfer reactions on the protein side chain CO_2H and NH_2 for the acid and alkaline ranges, respectively. However, the possibility that the observed changes of absorption with pH would be partly due to conformal equilibria was not ruled out.

The purpose of this paper is twofold: (1) to bring additional evidences that the absorption maxima are due to the following proton-transfer reactions

$$-CO_2H \underset{k_{-1}}{\overset{k_1}{\rightleftharpoons}} -CO_2^- + H^+ \quad (1)$$
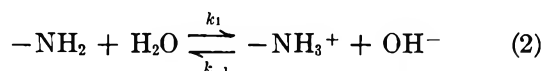
$$-NH_2 + H_2O \underset{k_{-1}}{\overset{k_1}{\rightleftharpoons}} -NH_3^+ + OH^- \quad (2)$$
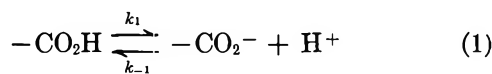
and (2) to show that the ultrasonic absorption is sensitive to the overall conformation of the protein molecule but that it does not appear to be sensitive to equilibria between different conformations.

Two series of absorption measurements were performed.

1. The ultrasonic absorption titration curves were determined for solutions of BSA, βL, and L in H_2O–NaCl (0.2 M)–urea (8 M) (in the following this solvent will be referred to as H_2O–8U). It is known[5-8] that in concentrated urea solution protein molecules are unfolded and behave like coils at pH higher than in aqueous solutions in the acid region and at pH lower than in aqueous solutions in the alkaline range. Therefore, it may be thought that conformal changes induced through pH variations in aqueous protein solutions will be strongly modified and/or will not occur in H_2O–8U while proton-transfer reactions persist. However, from other works[9,10] one must expect the pK's for the protein side chain NH_2 and CO_2H to be shifted in presence of urea, thereby modifying the position of the absorption maxima.[4] Measurements were also carried out on model compounds, acetylglycine (AcGly) and diglycine (DiGly).

2. The absorption of βL solutions was measured at constant pH in the presence of increasing amounts of urea, formamide, dimethylformamide (DMF), dioxane, and ethylene glycol (EG). From the work of Tanford, et al.,[6,11-13] the effect of these various substances on the conformation of the βL molecule is known. We had hoped to correlate the variation of absorption with the per cent of additive to the conformal changes as detected by optical rotatory dispersion[6,11-13] (ORD). As it will be seen later no correlation could be found.

II. Experimental Section

The absorption coefficient α was measured at 25° and 2.82 and 5.04 MHz using a two-crystal interferometer, which was already described.[14] All proteins and solvents used in this work were highly purified products (recrystallized several times or distilled twice).

The nitrogen contents of the various protein samples

were determined and compared with the literature values[15] in order to obtain the water content of the samples. The weigh-in concentrations corrected for this water agreed within 2% of the concentrations determined directly through dry content of the protein solutions. Protein concentrations were usually kept between 0.008 and 0.012 g/cm^3.

The protein solutions in H_2O–NaCl (0.2 M) and in H_2O–8U were prepared by directly dissolving the protein just before use. The pH changes were obtained through additions of small amounts of concentrated HCl or NaOH in order to avoid changes of concentration. For the solutions containing dioxane, EG, and DMF the following procedure, similar to that of Tanford, et al.,[11-13] was adopted. The protein and NaCl were first dissolved in water and the pH was adjusted to the desired value. The adequate amount of organic solvent was slowly added. The amounts of protein and NaCl were calculated in order to obtain the right concentrations in the final solution.

In several instances it was checked that the observed changes of ultrasonic absorption with pH were reversible. The effect of ionic strength was found to be small and almost within the experimental accuracy.

III. Results

Figure 1 shows the ultrasonic absorption titration curves for BSA, βL, and L in the acid range. The quantity $10^{15}\Delta\alpha/N^2C$ (N = ultrasonic frequency, $\Delta\alpha = \alpha - \alpha_0$ is the difference between the absorption coefficients of the solution and of the solvent, respectively, and C = concentration in g/cm^3) is plotted as a function of pH. With respect to the titration curves obtained in H_2O–NaCl (0.2 M), the presence of urea brings about (1) a shift of pH_M, pH value at which $\Delta\alpha/N^2C$ goes through a maximum, toward higher values by about 1 ± 0.2 pH unit, and (2) an increase of the magnitude of the absorption maximum defined as $A = \{\Delta\alpha_{pH_M} - \Delta\alpha_{pH\,1}\}/N^2C$. This increase is the largest for βL, while A is left unchanged for BSA. In defining A the value of $\Delta\alpha/N^2C$ at pH 1 rather than at

(5) H. McKenzie, M. Smith, and R. Wake, *Biochem. Biophys. Acta*, **69**, 222, 240 (1963).

(6) N. Pace and C. Tanford, *Biochemistry*, **7**, 198 (1968).

(7) J. Leonis, *Arch. Biochem. Biophys.*, **65**, 182 (1956).

(8) E. Edelhoch and R. Steiner, *Biochem. Biophys. Acta*, **60**, 365 (1962).

(9) H. Bull, K. Breese, G. Ferguson, and C. Swenson, *Arch. Biochem. Biophys.*, **104**, 297 (1964).

(10) J. Donavan, M. Laskowski, and H. Scheraga, *J. Mol. Biol.*, **1**, 295 (1959).

(11) C. Tanford and P. De, *J. Biol. Chem.*, **236**, 1711 (1966).

(12) C. Tanford, P. De, and V. Taggart, *J. Amer. Chem. Soc.*, **82**, 6028 (1960).

(13) C. Tanford, C. Buckley, and P. De, *J. Biol. Chem.*, **237**, 1168 (1962).

(14) S. Candau, *Ann. Phys.*, **9**, 271 (1964); R. Zana, D.Sc. Thesis, University of Strasbourg, 1964; R. Cerf, *Acustica*, **13**, 417 (1963).

(15) G. Tristram, "The Proteins," Vol. I, Part A, Academic Press, New York, N. Y., 1953, p 210.
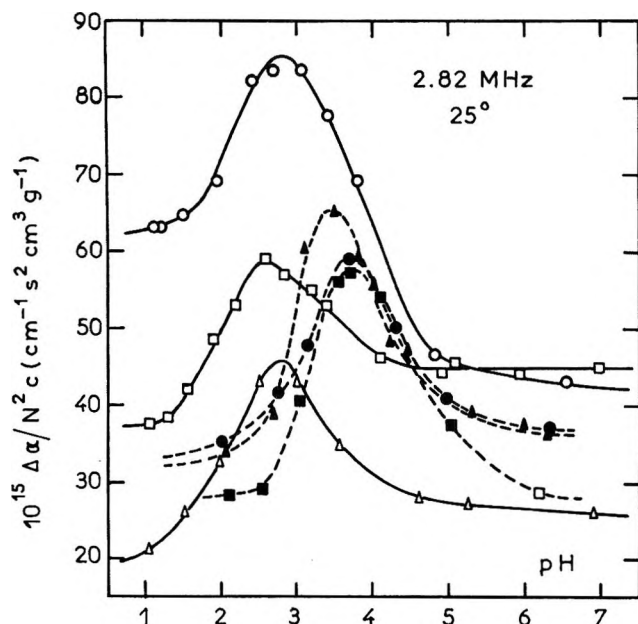
Figure 1.   Ultrasonic absorption titration curves in the acid range for BSA in water (O), in H_2O–8U (●), β-lactoglobuline in water (□), in H_2O–8U (■), lysozyme in water (△), and in H_2O–8U (▲).

Figure 3.   Ultrasonic absorption titration curves in the alkaline range for lysozyme (2.82 MHz) in water (O), in H_2O–8U (●), for diglycine (5.04 MHz) in water (▽), and in H_2O–8U (▼).   The left ordinate scale is relative to diglycine.

Figure 2.   Ultrasonic absorption titration curves in the acid range for acetylglycine in water (△), in H_2O–8U (▲), diglycine in water (O), and in H_2O–8U (●).
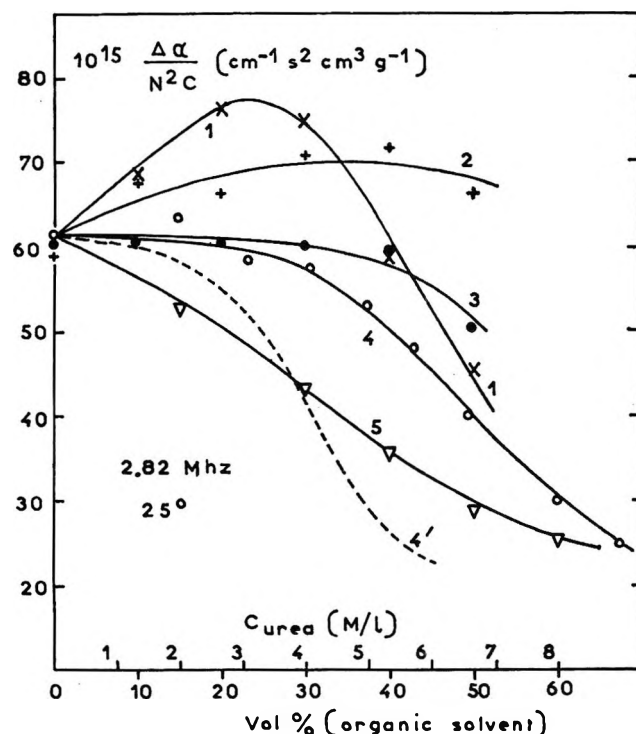
Figure 4.   Variation of $\Delta\alpha/N^2C$ for β-lactoglobuline solutions: upon addition of dioxane (×); DMF (+); EG (●); urea (O and curve 4'); and formamide (▼);   pH is 2.8–2.9, and ionic strength is 0.04 M KCl.   For curve 4', the concentration of urea has been expressed on an apparent volume basis by dividing the experimental weight concentration by the density of urea.

pH 7 has been introduced because it is known that in the native state proteins have different structures, while at pH 1 they are unfolded and may be thought to be not too different.

Figure 2 shows that in the acid range the effect of urea on the curves $\Delta\alpha/N^2C$ = f(pH) relative to AcGly and DiGly is quite similar to that for proteins, pH_M is shifted by about +1 pH unit and A is increased, though more than for protein solutions.   It must be pointed out that these results were obtained at 5.04 MHz while those on Figure 1 are relative to N = 2.82 MHz. However, we found that pH_M is independent of frequency while A varies only slowly with N.[4]   This makes possible a qualitative comparison of the results on Figures 1 and 2.

In Figure 3 are plotted the results obtained for the effect of urea on the ultrasonic absorption titration curves for L at 2.82 MHz and DiGly at 5.04 MHz in the alkaline range.   In the presence of urea, the pH_M value for L is shifted by only 0.35 pH unit as compared with +0.75 pH unit in the acid range.   No shift is observed

for DiGly. Moreover, in H_2O-8U A is much smaller than in H_2O for both L and DiGly while the opposite was observed in the acid range (Figure 1).

In Figure 4 is represented the variation of $\Delta\alpha/N^2C$ for a βL solution as a function of the concentration of various additives, at constant pH and ionic strength. When dioxane is added to the βL solution $\Delta\alpha/N^2C$ goes through a well defined maximum at about 25% dioxane. With additions of DMF there is only a rather flat maximum. Additions of EG up to 40% produce no change, of $\Delta\alpha/N^2C$ while additions of urea and formamide bring about a decrease of $\Delta\alpha/N^2C$ in the whole concentration range.

IV. Discussion

1. Implications of the Existence of Absorption Maxima in Presence of Urea. First it must be pointed out that these maxima are not due to some reaction involving urea alone since, in this work, it was found that the absorption coefficient of H_2O-8U is not very different from that of water and that it is pH independent.

Uv absorption, sedimentation, diffusion, and ORD measurements[6] have shown that the BSA molecule is unfolded in H_2O-8U even at pH as high as 7.8. On the other hand, ORD measurements indicate that the unfolding of the βL molecule occurs at pH > 4 in H_2O-8U.[6] As for lysozyme, the available literature data[7,8] do not give any precise indication concerning the stability of this protein in H_2O-8U. However, these data[7,8] show that in urea solutions, lysozyme is the most stable of the three proteins studied in this work. The solvent perturbation technique[16] has led others[17,18] to the same conclusion. Therefore from the above, and if the absorption maxima do result from conformal changes, one should expect the pH_M values to be shifted by different amounts according to the nature of the protein when the titration is conducted in H_2O-8U. For BSA in this solvent the absorption maximum should even disappear. Our experimental results contradict these predictions. In urea solutions, for the three proteins, the maxima occur at about the same pH (3.6 ± 0.1) and the A values are almost equal. Moreover, Figures 1 and 2 show great similarities between the effect of urea on the absorption titration curves for the three proteins and for AcGly and DiGly. However, no conformal change analogous to those for proteins can occur for AcGly and DiGly.

From the above and from the facts reported in ref 4 one can conclude that the absorption maxima are not due to conformal changes. On the contrary, all the results in Figures 1–3 can be explained in terms of proton–transfer equilibria such as (1) and (2) modified by the presence of urea.

One may expect such reactions to occur whatever the conformation of the protein molecule and the nature of the solvent. However, the dielectric constant of the solvent must be large enough to allow a sufficient ioniza-

tion of the CO_2H and NH_2 groups; otherwise the absorption term due to reaction 1 or 2 becomes 0. As H_2O-urea mixtures have dielectric constants larger than that of water[19] the ionization in such mixtures should, therefore, be sufficient.

2. Explanation for the Increase of pH_M in Urea Solutions. pH_M is given by[20]

$$pH_{M,a} = {}^1/_2(pK_a - \log C_a) \qquad (1')$$

for reaction 1 (acid range) or

$$pH_{M,b} = {}^1/_2(14 + pK_a + \log C_b) \qquad (2')$$

for reaction 2 (alkaline range) C_a and C_b are, respectively, the concentrations of acid (CO_2H) and basic (NH_2) groups involved in equilibria 1 and 2; they can be calculated[4] from the known protein molecular weight M_w, concentration C, and number $n_{a,b}$ of titrable CO_2H and NH_2 groups[21] according to

$$C_{a,b} = 10^3 n_{a,b} C/M_w \qquad (3)$$

It is known that n_a and n_b are increased in the presence of urea since buried groups become accessible upon unfolding.[10,21] On the other hand, a study on small molecules has shown[9,10] that upon addition of urea there is an increase of pK_a, this increase being larger for carboxylic acids than for amines.[10] In the following it will be assumed that the pK_a's of the protein residues bearing CO_2H or NH_2 on their side chain are modified in the same manner as those of small model molecules.

Alkaline Range. Donavan, et al.,[10] found an increase of +0.3 unit for the pK_a of *n*-butylamine when going from water to H_2O-8U. For proteins this would yield a $pH_{M,b}$ increase of +0.15 to which must be added the increase due to the effect of urea on n_b. If we assume that n_b is increased by a factor 2 (this represents approximately the ratio of the number of titrable groups to the total number of groups[21]) the total increase of $pH_{M,b}$ may reach 0.3, *i.e.*, about what can be observed on the curves relative to lysozyme of Figure 3.

Acid Range. The pK_a of acetic acid is increased by +0.7 unit when going from water to H_2O-8U.[10] For $pH_{M,a}$ this would result in a +0.35 unit increase from which must be substracted the effect of urea on n_a. The resulting increase is 3–4 times smaller than what appears in Figures 1 and 2. A possible explanation for these differences may be found in the well established reaction of urea with H^+ [22,23] which results in a decrease of the

(16) T. Herskovits, *J. Biol. Chem.*, **240**, 628 (1965).

(17) C. Bigelow and T. Krenitsky, *Biochem. Biophys. Acta*, **88**, 130 (1964).

(18) T. Herskovits and L. Mescanti, *J. Biol. Chem.*, **240**, 639 (1965).

(19) "Landolt–Bornstein Tables," Vol. 6, Part II, Springer Verlag, Berlin, Göttingen, Heidelberg, 1959, p 777.

(20) K. Applegate, L. Slutsky, and R. Parker, *J. Amer. Chem. Soc.*, **90**, 6909 (1968).

(21) C. Tanford, *Advan. Protein Chem.*, **17**, 69 (1962).

(22) R. Paul and S. Chadha, *Spectrochim. Acta*, **23**, 1243 (1967).

proton activity. For instance the pH of HCl solutions is increased by $+1.6$ units in $H_2O-9.5U$ with respect to water.[10] Also, we found that the $pH_{M,a}$ values of 0.1 M solutions of acetic and propionic acids are increased by $+1.1$ units when going from water to H_2O-8U. These two acids are good model compounds for the side chain of aspartic and glutamic acids which constitute most of the carboxylic acid residues in proteins. Therefore, it may be assumed that similar increases of $pH_{M,a}$ are likely to occur in protein solutions.

3. Changes of A Upon Addition of Urea. It is known[20,24] that for weak acids and bases A is proportional to $\Delta V_0^2/k_{-1}$, where ΔV_0 is the volume change associated with equilibrium 1 or 2 and k_{-1} is the rate constant for the association reaction.

It has been shown[25] that the electrostriction of ions is smaller in urea solutions than in water. Therefore, one can expect ΔV_0 to be smaller in H_2O-8U than in water.

On the other hand, k_{-1} may be written[26]

$$k_{-1} = K(D_1 + D_2)/\epsilon f(\epsilon) \qquad (4)$$

where K is a constant, $D_{1,2}$ are the diffusion constants, and $f(\epsilon)$ a function of the dielectric constant ϵ. We shall assume that eq 4 applies to protein solutions with the index 1 relative to H^+ or OH^- according to the reaction under consideration, and the index 2 relative to the protein residue involved in the reaction. Since this residue is part of the protein molecule it is likely that $D_2 \ll D_1$. When one goes from water to H_2O-8U, k_{-1} decreases because: (1) of the increase of ϵ;[19] this is a small effect, however, since H_2O-8U has a dielectric constant only 20% larger than for water and, (2) of the effect of urea on D_1. Diffusion coefficients and equivalent conductivities Λ° of ions are roughly proportional. On the other hand it has been shown that Λ° values are decreased in presence of urea,[9,27] particularly $\Lambda^\circ_{H^+}$. For instance, from Bull's data[9] one can estimate a 7.5-fold decrease for $\Lambda^\circ_{H^+}$ and a 2-fold decrease for $\Lambda^\circ_{OH^-}$ when going from water to H_2O-8U. For reaction 1 the addition of urea may then result in a small increase of A if the large decrease of k_{-1} overcompensates that of ΔV_0^2. In the alkaline range, the decrease of k_{-1} may not be sufficient to compensate that of ΔV_0^2, therefore yielding a decrease of A for reaction 2 (Figure 3).

4. Sensitivity of the Ultrasonic Absorption to the Overall Protein Conformation. On Figure 1 the results relative to aqueous protein solutions show that the values of $\Delta\alpha/N^2C$ are different for the protein in the native state, at pH close to the isoelectric point (pH $\sim6-7$), and in the unfolded state (pH ~1). This indicates that the ultrasonic absorption is sensitive to the conformation of the protein. Another indication of this sensitivity can be found in the titration curve of BSA in $H_2O-NaCl$ (0.2 M). The increase of $\Delta\alpha/N^2C$ for BSA starts at pH 5 while for L and βL this occurs at

pH 4.3. This particular behavior justifies the definition of A adopted above and may be related to the conformal change of BSA discussed by others.[3] This sensitivity of the absorption to the protein conformation may result either from absorption processes which differ according to the conformation or, more likely, from identical processes the contribution of which depend on the conformation. Protein-solvent interaction[2] may be one of these processes. At this point it is noteworthy that at pH ~1.5, in $H_2O-NaCl$ (0.2 M) the $\Delta\alpha/N^2C$ values for the three proteins are quite different in contrast with solutions in H_2O-8U in which the three proteins are characterized by the same $\Delta\alpha/N^2C$.

Our results, however, seem to indicate that the absorption is not sensitive to the equilibrium between the different conformations since such a sensitivity would imply the absorption titration curves in H_2O-8U to be dependent on the protein nature (see part IV. 1). As seen earlier, this is not so: the A values are almost equal for the three proteins and the three ultrasonic absorption titration curves are practically coincident.

Also, as it will be seen now, the effect of organic additives on the absorption of βL solutions (Figure 4) does not indicate a sensitivity of the ultrasonic absorption to conformal equilibria. Tanford, et al.,[6,11-13] have shown that at pH 2.8 the action of DMF and dioxane on the conformation of βL occurs in two stages. At concentrations above 25% there is first an unfolding and then a refolding of the βL molecule.[12] The final conformation has a higher helical content than the native one. With urea and formamide the refolding does not occur since these compounds are able to H-bond with the peptide links, therefore preventing the formation of intraprotein H bonds.[11] At pH 2.8, 6 M urea or 45% formamide causes a complete unfolding.[11] Additions of EG up to 60% do not produce any change of conformation. In Figure 4, one sees that, except for EG, $\Delta\alpha/N^2C$ starts varying at concentration of organic additives much lower than those which modify the ORD.[6,11-13] For dioxane, $\Delta\alpha/N^2C$ is constant precisely in the concentration range (20-50%) in which the change of conformation occurs, i.e., in which the various conformations are at equilibrium.[12]

The data in Figure 4 have been obtained at a pH (2.8-2.9) for which the absorption term due to reaction 1 is not negligible (see Figure 1). Therefore, the changes of $\Delta\alpha/N^2C$ at those additive concentrations

(23) J. Radell, B. Brodman, and J. Domanski, *J. Phys. Chem.*, **71**, 1596 (1967).

(24) B. Michels and R. Zana, *J. Chim. Phys.*, **66**, 240 (1969).

(25) W. Hargraves and G. Kresheck, *J. Phys. Chem.*, **73**, 3249 (1969).

(26) M. Eigen and L. De Maeyer, "Techniques of Organic Chemistry," Vol. 8, Part II, Interscience, New York, N. Y., 1963, Chapter 18, p 1032.

(27) W. Ebeling, H. Falkenhagen, and W. Kraeft, *Ann. Phys.*, **18**, 15 (1966).

for which the ORD is not modified may result from changes of the contribution of reaction 1 and/or a modification in protein–solvent interactions if such equilibria do contribute to the absorption of protein solutions.

V. Conclusions

This study shows that the absorption maxima present on the curves absorption = f(pH) relative to protein solutions are due to proton transfer reactions. The ultrasonic absorption appears to be sensitive to the overall protein conformation maybe through different protein–solvent interactions according to the protein conformation. However, the absorption does not seem to be sensitive to conformal equilibria perhaps because the associated volume changes are too small

to give rise to a measurable absorption or because such equilibria are too slow to be detected by the ultrasonic techniques used in this work. At this point it is worth noting that Owen, et al.,[28] and French and Hammes[29] interpreted recent results of T-jump measurements on lysozyme and ribonuclease, respectively, at pH close to the isoelectric point in terms of conformal changes. The measured relaxation times are in the millisecond range, i.e., much larger than what can be detected with ultrasonic absorption in the megahertz range.

(28) J. Owen, E. Eyring, and D. Cole, J. Phys. Chem., 73, 3918 (1969).

(29) T. French and G. Hammes, J. Amer. Chem. Soc., 87, 4669 (1965).

Tracer and Mutual Diffusion Coefficients of Proteins[1]

by Kenneth H. Keller,* Edgardo R. Canales, and Su Il Yum

Department of Chemical Engineering, University of Minnesota, Minneapolis, Minnesota 55455   (Received July 29, 1970)

Publication costs borne completely by The Journal of Physical Chemistry

The diffusion coefficients of hemoglobin and serum albumin were measured over a broad range of concentrations by both tracer and mutual diffusion techniques. It was found that, within the accuracy of experimental measurements, there was no detectable difference between tracer and mutual diffusion coefficients of these globular protein molecules. In examining the variation of diffusion coefficient with solute concentration, it was found for both molecules that the decrease in diffusion coefficient with increasing concentration was initially nonlinear, but rapidly achieved an asymptotic linear form that extended to volume fractions as high as 0.25. From measurements at 25 and 37°, the rate of change of hemoglobin diffusion coefficient with temperature was estimated as 3.3 ± 0.1%/°C over the entire range of solute concentrations studied.

Introduction

Protein diffusion appears to play a significant role in a variety of the biological transport phenomena that have been the subject of investigations in recent years. As examples, one may cite the oxygen carrier role of hemoglobin and myoglobin postulated by several workers,[2-4] the importance of protein diffusion in the extracorporeal ultrafiltration of blood associated with artificial kidneys,[5] its importance in the postulated intracorporeal ultrafiltration associated with atherosclerotic plaque formation,[6] or its role in such ubiquitous processes as thrombosis and antigen–antibody reactions.

In analyzing and interpreting these phenomena, it is often necessary to know the diffusion coefficient of the protein involved. In general, the protein of interest is globular and present in a system containing a relatively high volume fraction of identical or similar protein

molecules. For example, in normal human blood, proteins constitute approximately 6% of the plasma volume[7] and reach substantially higher concentrations near the region of interest in ultrafiltration problems.[5] Intracellularly, proteins may constitute as much as 25% of the cell volume.[8] Thus, values of the diffusion coefficient at high concentrations are needed.

(1) This work was supported in part by NSF Grant GK-1196.

(2) P. F. Scholander, Science, 131, 585 (1960).

(3) J. B. Wittenberg, J. Biol. Chem., 241, 104 (1966).

(4) J. Wyman, ibid., 241, 115 (1966).

(5) A. A. Kozinski and E. N. Lightfoot, to be published.

(6) K. H. Keller in "Biomaterials," L. Stark and G. Agarwal, Ed., Plenum Press, New York, N. Y., 1969, p 103.

(7) H. A. Harper, "Review of Physiological Chemistry," 6th ed, Lange Medical Publications, Los Altos, Calif., 1957, p 128.

(8) A. White, P. Handler, E. L. Smith, and D. Stetten, "Principles of Biochemistry," 2nd ed, McGraw-Hill, New York, N. Y., 1959, p 10.

Unfortunately, experimental measurements of protein diffusion coefficients are limited in number. Of those that exist, several have been conducted only in very dilute solutions[9,10] and no adequate theoretical basis is presently available for extrapolating these results to higher concentrations. The few studies that have been conducted in concentrated solutions have measured diffusion under various circumstances: some were mutual diffusion measurements,[11] some were tracer measurements,[12,13] and one[14] was a hemoglobin–albumin or quasitracer study. There is no *a priori* reason for expecting these different diffusion coefficients to have the same value and there are not sufficient data over similar ranges of concentration to assess the differences among them.

In view of this situation, we undertook an experimental study of globular protein diffusion coefficients over a wide range of concentrations. Our purpose was to obtain data on specific proteins of interest useful in itself and sufficient to allow a comparison of different kinds of diffusion coefficients—in particular, those associated with tracer and mutual diffusion experiments. We also hoped to establish trends in the variation of diffusion coefficient with concentration which might have general applicability.

The proteins selected for the study were hemoglobin (mol wt = 67,000) and serum albumin (mol wt = 69,000). These molecules can be approximated as prolate spheroids with diameter ratios of 1.05 and 1.25, respectively,[15] and approximately equal densities of 1.34 g/ml. Since they are blood proteins, they are readily available, easily purifiable, and important in a number of the phenomena cited in the first paragraph.

Experimental Apparatus and Procedures

The Diaphragm Diffusion Cell. Measurements were made in the diaphragm diffusion cell shown in Figure 1. The principles of the diaphragm cell method are discussed at length by Gordon.[16] Fundamentally, the apparatus consists of two well stirred reservoirs separated by a porous diaphragm. The concentration of the diffusing species differs in the two reservoirs. After calibrating the diaphragm, the diffusion coefficient is determined by measuring concentration change with time in the reservoirs.

The device shown in Figure 1 was constructed of Lucite. The lower reservoir had a net capacity of 2.97 ml and was completely filled during operation. The upper reservoir had a capacity of about 27 ml, but actually contained only 2.97 ml of solution during operation. The two reservoirs were separated with a Type WS Millipore filter which replaced the glass fritted disk normally used in such cells. These filters are 150 ± 10 μ thick, have a porosity of 45% and a pore diameter of 3.0 ± 0.9 μ. Two models of this device were used in one of which the diameter of the exposed portion of the filter was 2.0 cm, and in the
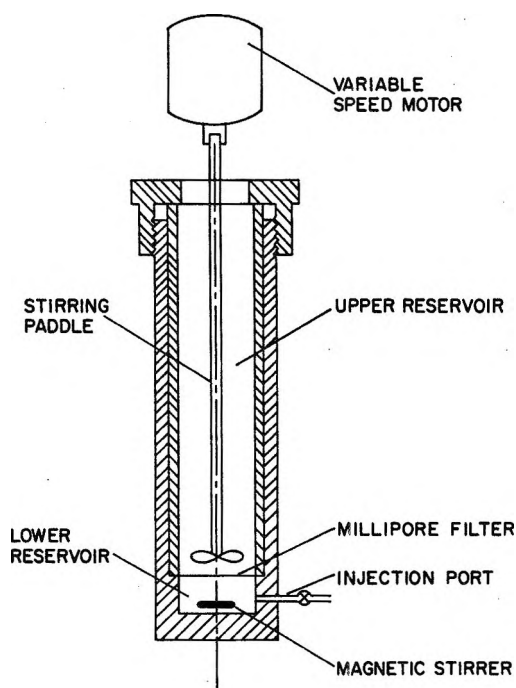
Figure 1. Diagrammatic representation of the diaphragm diffusion cell used in the present study.

other of which it was 1.55 cm. By using such filters the time required to reach steady state was decreased about a 100-fold below that required with a fritted disk and the diffusion flux was increased tenfold. This shortened the time required for an experimental run, a distinct advantage when dealing with relatively labile proteins with low diffusion coefficients.

In operation the cell was oriented vertically and placed in a constant-temperature bath. In those experiments in which a difference in density existed between the two reservoirs, the more dense solution was placed in the lower reservoir to prevent convective flows through the filter pores. Leakage around the edges of the Millipore filter was prevented by placing Teflon gaskets above and below the filter. The contents of the bottom reservoir were stirred with a magnetic stirring bar at approximately 100 rpm, a rate found to be sufficiently high that diffusion fluxes were independent of stirring speed. The contents of the upper chamber were stirred at a slightly higher rate by a paddle. After each run, the filter was changed.

(9) L. J. Gosting, *Advan. Protein Chem.*, 11, 430 (1956).

(10) O. Lamm and A. Polson, *Biochem. J.*, 30, 528 (1936).

(11) K. H. Keller and S. K. Friedlander, *J. Gen. Physiol.*, 49, 663 (1965).

(12) W. Moll, *Resp. Physiol.*, 1, 357 (1966).

(13) J. H. Wang, C. B. Anfinsen, and F. M. Polestra, *J. Amer. Chem. Soc.*, 76, 4763 (1954).

(14) L. R. Adams and I. Fatt, *Resp. Physiol.*, 2, 293 (1967).

(15) C. Tanford, "Physical Chemistry of Macromolecules," Wiley, New York, N. Y., 1960.

(16) A. R. Gordon, *Ann. N. Y. Acad. Sci.*, 46, 285 (1945).

Sample Preparation. Hemoglobin was obtained from outdated human blood supplied by the blood bank of the University of Minnesota Hospitals. The plasma was removed by centrifugation at 3000 rpm for 20 min at 4° and the packed cells were washed five times with isotonic saline. The cells were hemolyzed with two volumes of cold, distilled water and the ghosts removed by centrifugation at 7000 rpm for 2 hr at 4°. The hemoglobin solution was dialyzed against a 0.5 M phosphate buffer at pH 6.5, recentrifuged, and concentrated by dialysis against three volumes of 30 wt % Ficoll[17] solution. The hemoglobin was then oxidized to methemoglobin by titration with 0.05 M $K_3Fe(CN)_6$, after which excess $K_3Fe(CN)_6$ was removed and the solution reconcentrated by appropriate dialysis. To prepare methemoglobin cyanide solutions, the methemoglobin at pH 6.5 was titrated with 0.5 wt % KCN, after which excess KCN was removed.

Concentration measurements were made spectrophotometrically. Pure methemoglobin solution concentrations were determined in two ways: by direct measurement at 576 mμ in a Beckman DU spectrophotometer after calibration by the pyridine hemochromagen method[18,19] or by measurement at 540 mμ in a Bausch and Lomb Spectronic 20 after treating the sample with Hycel reagent (0.15 g/l. of KCN). In the latter case, a calibration curve was obtained using Hycel cyanomethemoglobin standard. Cyanomethemoglobin sample solution concentrations were also measured at 540 mμ. Mixtures of methemoglobin and cyanomethemoglobin were examined at 540 mμ using pure methemoglobin solutions at the same total concentration as a reference.

Albumin solutions were prepared by dissolving approximately 30 g/100 ml of powdered bovine serum albumin (96–99% purity) in 0.1 M acetate buffer at pH 4.7. Solutions were stored at 4° and used within a week of preparation. To form labeled solutions, 120 ml of the concentrated albumin solution was divided into two equal volumes. To one, 2.1 ml of 1% I^{125}-radioiodinated serum albumin (obtained commercially) was added with a total activity of 115 μCi. To the second, the same amount of nonradioactive albumin in the same concentration was added. These pairs of solutions were always used together, diluted as necessary for diffusion measurements at various concentrations.

Albumin solution concentrations were determined spectrophotometrically at 280 mμ. Radioactivity was measured by liquid scintillation counting in a 1:1 toluene–ethanol solvent using 1.5 g of PPO and 0.05 g of DM–POPOP/l. of solution. Because of the relatively short half-life of I^{125} (60 days) a standard prepared from the same vial of radioisotope was always counted with the sample to allow a correction for activity decay.

Procedure. Prior to performing experiments, all solutions were equilibrated at the temperature of the experiment to avoid thermal expansion effects which could introduce errors due to convection. To run a mutual diffusion measurement, the lower reservoir of the cell was filled to excess with 5 ml of concentrated protein solution. The lower Teflon gasket was then put in place and the Millipore filter, presaturated with solvent to eliminate air bubbles from its pores, was positioned. The rest of the cell was then assembled and the excess protein solution in the upper reservoir removed with a hypodermic syringe. The upper chamber was then washed three times with the solvent (0.1 M phosphate buffer at pH 7.3 for methemoglobin; 0.1 M acetate buffer at pH 4.7 for albumin) and refilled with 2.97 ml of solvent for the experimental runs. In early experiments, the solvent was changed after 20 min and the run was repeated. However, no significant difference was observed between data obtained from the second of two runs and from a single extended run. Therefore, it was concluded that a quasisteady-state distribution was obtained during the upper reservoir rinsing operations, and in later experiments, only a single run was performed for periods ranging from 20 min to over 1 hr depending upon protein concentration. At the end of the run, the concentration in the upper reservoir was measured.

In the albumin tracer diffusion experiments, the tracer solution was placed in the lower compartment and the nonradioactive solution used for rinsing and for filling the upper reservoir. In the hemoglobin tracer diffusion experiments, cyanomethemoglobin was placed in the lower reservoir from which it diffused into methemoglobin in the upper reservoir. In contrast to the previously described procedure, in these experiments the cell was first assembled and the lower reservoir then filled by injecting the appropriate solution through the wall of the cell with a hypodermic syringe, allowing it to rise through the Millipore filter. In addition, the upper reservoir solution was changed once during the run and the concentration data from the second half of the run were used.

Applicable Equations

To convert the concentration change data obtained in these experiments to diffusion coefficients, the standard equations, discussed in some detail by Gordon[16] were used. The data yield an integral (or time–space average) diffusion coefficient, $\bar{D}$, determined as follows

$$\beta \bar{D} t = \ln \frac{(c_i' - c_i'')_0}{(c_i' - c_i'')_t} \tag{1}$$

where (′) refers to quantities in the lower reservoir, (″) to quantities in the upper reservoir, and subscripts

(17) Pharmacia Company, Uppsala, Sweden.

(18) L. Heilmeyer, "Spectrophotometry in Medicine," Hilger, London, 1945.

(19) S. I. Yum, M.S. Thesis, University of Minnesota, Minneapolis, Minn., 1967.

0 and t refer to values at the beginning and end of a run, respectively. β is the cell factor, given by

$$\beta \equiv \left(\frac{1}{V'} + \frac{1}{V''}\right)\frac{A_p}{\delta} \qquad (2)$$

where V is the reservoir volume, A_p is the cross-sectional area of the pores in the filter, and δ is the equivalent diffusional path length. A_p/δ and, therefore, β, must be determined experimentally for each type of Millipore filter since the complex geometry precludes any accurate calculation of its value.

In the binary diffusion experiments, it is necessary to convert the integral diffusion coefficient to a concentration-dependent mutual diffusion coefficient, D. Under a quasisteady-state assumption, at any instant during an experimental run

$$\overline{D}'(c_i' - c_i'') = \int_{c_i''}^{c_i'} D dc_i \qquad (3)$$

$\overline{D}'$ is the instantaneous integral diffusion coefficient and varies with time as c_i' and c_i'' change. However, if the variations in c_i' and c_i'' are kept sufficiently small, as shown by Gordon,[16] $\overline{D}$, the average integral diffusion coefficient can be expressed as

$$\overline{D}(\overline{c_i'} - \overline{c_i''}) = \int_{\overline{c_i''}}^{\overline{c_i'}} D dc_i \qquad (4)$$

where the concentrations are arithmetic means of initial and final concentrations in each reservoir.[20]

For runs of very short duration, concentration changes are negligible and since c_i'' is initially 0, under such circumstances we can define an integral diffusion coefficient $\overline{D^0}$ as

$$c_i'\overline{D^0}(c_i') = \int_0^{c_i'} D dc_i \qquad (5)$$

By combining eq 4 and 5 we obtain

$$\overline{D^0}(\overline{c_i'}) = \overline{D} - \frac{\overline{c_i''}}{\overline{c_i'}}[\overline{D} - \overline{D^0}(\overline{c_i''})] \qquad (6)$$

By an iterative technique, the experimental data for $\overline{D}$ can be used in conjunction with eq 6 to obtain a curve of $\overline{D^0}(c_i)$ vs. c_i. Equation 5 can then be differentiated to yield

$$c_i\frac{d\overline{D^0}}{dc_i} + \overline{D^0} = D \qquad (7)$$

from which D can be determined.

In the tracer diffusion studies, the overall concentration of protein is constant throughout the system. c_i refers to the concentration of tracer only and its variations do not affect the value of the diffusion coefficient. In this case the diffusion coefficient, which we identify as D^*, is equal to $\overline{D}$, the measured integral value. However, D^* is not a true mutual diffusion coefficient since

the system is, in fact, ternary during these experiments. The implications of this will be discussed later.

Finally, it should be noted that because the diaphragm diffusion cell has a fixed lower reservoir volume, fluxes across the filter must be such that the net volumetric flow is zero. Therefore all diffusion coefficients derived in this study are for fluxes relative to the volume average velocity. For the particular molecular densities involved, these coefficients will never differ by more than 2% from coefficients for fluxes relative to the mass average velocity.

Experimental Results[19,21]

The cell factor, β, was determined for the two diffusion cells used in these studies by calibration with 0.1 N KCl solutions at 25°, using the data of Stokes[22] to establish the integral diffusion coefficient of 0.1 N KCl diffusing against distilled water. For cell no. 1 (exposed filter diameter, 1.55 cm) the results of runs on five Millipore filters yielded a value of 48.69 ± 0.02 cm^{-2}. For cell no. 2 (exposed filter diameter 2.0 cm), the results of runs on 11 Millipore filters yielded a value of 77.27 ± 1.38 cm^{-2}. These values exceed the calculated ones by about 10%, a not unexpected deviation in view of the assumptions involved in fixing A_p/δ in these calculations.[19]

Hemoglobin tracer diffusion experiments were performed over a concentration range of 1 g/100 ml to 31.5 g/100 ml and at temperatures of 25 and 37° in cell no. 1. The results are summarized in Tables I and II and in Figure 2. At low concentrations, the data show an increase in diffusion coefficient with temperature at a rate of about 3.4%/°C, which is in close agreement with the usual rule of thumb of 3%/°C. Less expected is the fact that this temperature effect is relatively independent of concentration. For example, at 31.5 g/100 ml, the data indicate an increase in D with temperature of 3.2%/°C. In addition to those data shown a set of three runs was made at a concentration $(c_1')_0$ of 2.5 g/100 ml and a temperature of 15° yielding an average diffusion coefficient of 6.28 ± 0.02 cm^2/sec. From these data, the average temperature effect in the range of 15–25° appears to be 2.3%/°C.

Hemoglobin mutual diffusion experiments were performed over a similar concentration range at 25° in cell no. 2. The data are listed in Table III. Since the processing of these data requires that the slope of the integral diffusion coefficient curve be determined, to im-

(20) The $\overline{D}$ obtained in eq 1 is actually different from that defined in eq 4 because of the complex geometry of the membrane. This difference can be accounted for by an appropriate choice of β which would then be concentration dependent. Since β was determined at one concentration only, the implicit assumption in this study is that the variation in β with concentration is small.

(21) E. R. Canales, M.S. Thesis, University of Minnesota, Minneapolis, Minn., 1969.

(22) R. H. Stokes, *J. Amer. Chem. Soc.*, **72**, 763 (1950).
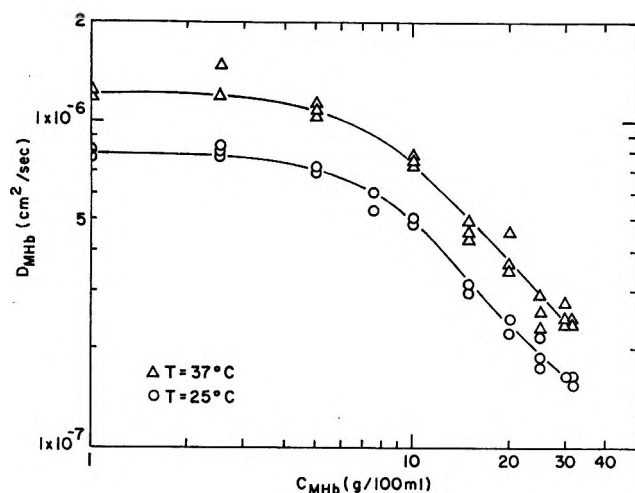
Figure 2. Hemoglobin diffusion coefficient measurements at 25° and 37° obtained by interdiffusion of methemoglobin and cyanomethemoglobin.

Table I: Tracer Diffusion Coefficients of Methemoglobin at 25°

$(c_i')_0$, g/100 ml	$(c_i'')_t$, g/100 ml	t, min	$D*_{MHb}$, (cm²/sec) $\times 10^7$
1.0	0.066	60	8.10
1.0	0.065	60	7.91
1.0	0.063	60	7.70
2.5	0.160	60	7.85
2.5	0.162	60	7.95
2.5	0.169	60	8.30
5.0	0.287	60	6.95
5.0	0.297	60	7.20
5.0	0.287	60	6.95
7.5	0.374	60	6.00
7.5	0.386	60	6.20
7.5	0.329	60	5.25
10.0	0.427	60	5.10
10.0	0.404	60	4.80
10.0	0.431	60	5.15
15.0	0.731	120	2.95
15.0	0.791	120	3.18
15.0	0.809	120	3.25
20.0	0.758	120	2.25
20.0	0.775	120	2.30
20.0	0.833	120	2.48
25.0	0.925	120	2.19
25.0	0.805	120	1.90
25.0	0.753	120	1.77
30.0	0.823	120	1.61
30.0	0.854	120	1.67
30.0	0.907	120	1.68
31.5	0.845	120	1.57
31.5	0.895	120	1.67
31.5	0.915	120	1.71

Table II: Tracer Diffusion Coefficients of Methemoglobin at 37°

$(c_i')_0$, g/100 ml	$(c_i'')_t$, g/100 ml	t, min	$D*_{MHb}$, (cm²/sec) $\times 10^7$
1.0	0.094	60	11.9
1.0	0.097	60	12.3
1.0	0.094	60	11.9
2.5	0.235	60	11.86
2.5	0.287	60	14.91
2.5	0.235	60	11.86
5.0	0.430	60	10.80
5.0	0.450	60	11.32
5.0	0.420	60	10.39
7.5	0.550	60	9.00
10.0	0.650	60	7.95
10.0	0.630	60	7.65
10.0	0.600	60	7.30
15.0	1.120	120	4.61
15.0	1.070	120	4.39
15.0	1.210	120	5.00
20.0	1.215	120	3.70
20.0	1.490	120	4.60
20.0	1.155	120	3.50
25.0	1.230	120	2.96
25.0	1.105	120	2.64
25.0	0.985	120	2.34
30.0	1.405	120	2.81
30.0	1.255	120	2.49
30.0	1.210	120	2.40
31.5	1.310	120	2.48
31.5	1.280	120	2.41
31.5	1.290	120	2.46

Table III: Data from Mutual Diffusion Experiments with Methemoglobin at 25°

$(c_i')_0$, g/100 ml	$(c_i'')_t$, g/100 ml	t, min	$\overline{D}$, (cm²/sec) $\times 10^7$	D(calcd), (cm²/sec) $\times 10^7$
1.05	0.0357	20	7.58	
1.05	0.0358	20	7.62	
1.05	0.03585	20	7.64	7.55
2.13	0.0705	20	7.38	
2.13	0.0712	20	7.46	
2.13	0.0715	20	7.50	7.24
4.88	0.170	22	7.07	
4.88	0.172	22	7.19	
4.88	0.170	22	7.10	6.43
9.45	0.393	30	6.22	
9.45	0.426	30	6.76	
9.45	0.396	30	6.31	4.96
13.88	0.894	50	5.93	
13.88	0.954	50	6.39	
13.88	0.840	50	5.57	3.46
21.38	1.350	60	4.84	
21.38	0.924	60	3.25	
21.38	1.335	60	4.78	2.48
29.25	2.22	90	3.94	
29.25	2.28	90	4.17	
29.25	2.41	90	4.43	1.74

prove the accuracy of this step the integral data of this investigation were combined with those of a previous investigation[11] before attempting to fit a curve to the experimental points. The values of the mutual diffusion coefficient thus calculated are plotted in Figure 3 along with the hemoglobin tracer diffusion data.

Albumin tracer diffusion and mutual diffusion experiments were also conducted at 25° in cell no. 2.
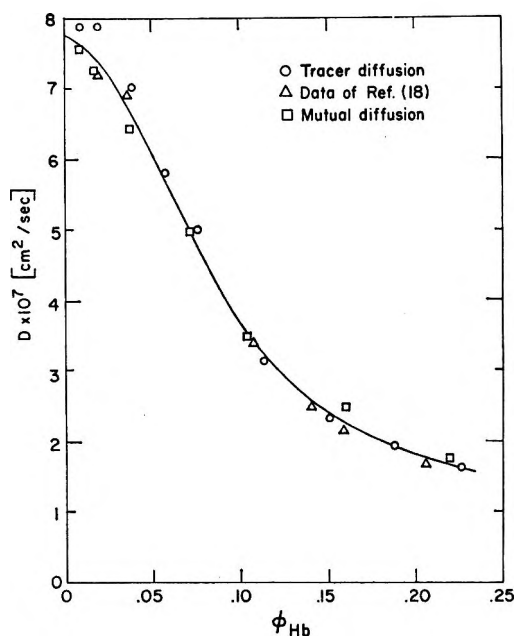
Figure 3. Mutual and tracer diffusion coefficients of hemoglobin at 25° as a function of the volume fraction of hemoglobin.
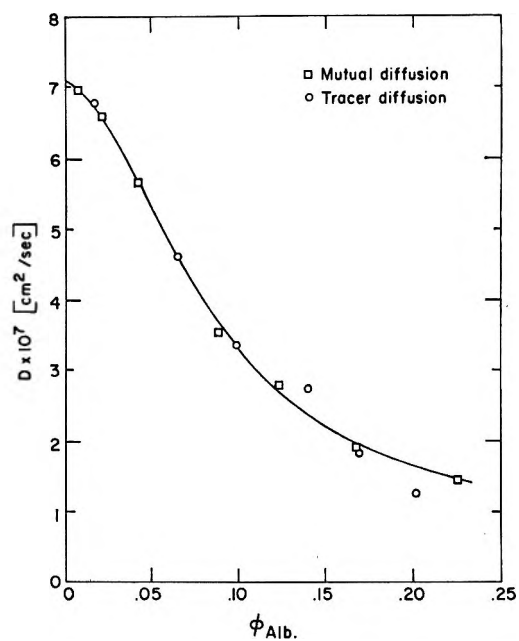
Figure 4. Mutal and tracer diffusion coefficients of serum albumin at 25° as a function of the volume fraction of serum albumin

Table IV: Tracer Diffusion Coefficients of Serum Albumin at 25°

$(c_i')_0$, g/100 ml	$(c_i'')_t$, g/100 ml	t, min	$D*_{alb}$, (cm²/sec) × 10⁷
2.19	0.160	20	6.80
2.19	0.216	20	9.46
8.54	0.434	20	4.63
8.54	0.566	20	6.12
13.11	0.477	20	3.27
13.11	0.510	20	3.49
18.56	0.624	20	3.00
18.56	0.523	20	2.50
22.52	0.452	30	1.77
22.52	0.474	30	1.86
26.87	0.360	30	1.18
26.87	0.398	30	1.30

Table V: Data from Mutual Diffusion Experiments with Serum Albumin at 25°

$(c_i')_0$, g/100 ml	$(c_i'')_t$, g/100 ml	t, min	$\bar{D}$, (cm²/sec) × 10⁷	D(calcd), (cm²/sec) × 10⁷
0.926	0.0289	20	6.97	
0.926	0.0290	20	6.99	
0.926	0.0291	20	7.01	6.98
2.79	0.0859	20	6.88	
2.79	0.0781	20	6.97	
2.79	0.0856	20	6.85	6.64
5.54	0.1628	20	6.53	
5.54	0.1621	20	6.51	
5.54	0.1653	20	6.64	5.67
11.76	0.4448	30	5.66	
11.76	0.4357	30	5.54	
11.76	0.4246	30	5.39	3.54
16.42	0.5358	30	4.86	
16.42	0.5207	30	4.72	
16.42	0.5700	30	5.18	2.79
22.32	0.7438	45	3.31	
22.32	0.8972	45	4.02	
22.32	0.9216	45	4.14	1.92
30.01	1.9175	80	3.68	
30.01	1.8567	80	3.56	
30.01	1.7848	80	3.41	1.46

These data are presented in Tables IV and V and the mutual and tracer diffusion coefficients are plotted in Figure 4.

Discussion

Two features of the data obtained require some discussion. The first is that, within the limits of experimental accuracy, there is no significant difference between D, the mutual diffusion coefficient, and $D*$, the tracer diffusion coefficient at any concentration for either methemoglobin or serum albumin. The second is that the variation of diffusion coefficient with concentration appears to have a remarkably simple form.

The theoretical difference between mutual and tracer diffusion coefficients has long been recognized and has been described in various ways. In the mutual diffu-

sion experiments only two species are involved and the measurable diffusion event is the interchange of molecules of solute and solvent. Momentum transfer between solute molecules does not affect the diffusion process directly. Such a process is describable in terms of a single diffusion coefficient. On the other hand, when a distinguishable tracer molecule of the same solute

species is introduced, a ternary system is created in which interchange of tracer and solvent, interchange of tracer and unlabeled solute, and interchange of solute and solvent are measurable diffusion events. Thus, three diffusion coefficients are required to describe the observable diffusion processes. Two of these are similar to the mutual diffusion coefficient, involving as they do the interchange of momentum between a solute molecule and the solvent. The third, however, the interaction between labeled and unlabeled solute, is precisely the event that is not of direct importance in binary system diffusion and is responsible for the theoretical difference between these processes.

Useful quantitative descriptions of these diffusion phenomena in terms of irreversible thermodynamics have been provided in several earlier papers.[23-25] We will summarize the results relevant to the present study. If subscript 1 refers to unlabeled solute and subscript 2 to labeled solute, then the fluxes of species 1 and 2 in a one-dimensional tracer system may be written as

$$J_1 = -D_{11}\frac{dc_1}{dx} - D_{12}\frac{dc_2}{dx} \qquad (8)$$

$$J_2 = -D_{21}\frac{dc_1}{dx} - D_{22}\frac{dc_2}{dx} \qquad (9)$$

Based on the Onsager reciprocal relations and assuming that labeled and unlabeled solute are indistinguishable physically, it has been shown that[23]

$$\frac{D_{12}}{c_1} = \frac{D_{21}}{c_2} \qquad (10)$$

In addition, under the conditions of the experiments in this study

$$J_1 = -J_2 \qquad (11)$$

$$\frac{dc_1}{dx} = \frac{-dc_2}{dx} \qquad (12)$$

and by substituting eq 8, 9, and 12 in eq 11, we find

$$D_{11} - D_{12} = D_{22} - D_{21} \qquad (13)^{26}$$

Based on eq 9 and 12, it is clear that the measured tracer diffusion coefficient, D^*, is equal to $(D_{22} - D_{21})$, which, by eq 13, is the same as $(D_{11} - D_{12})$. To see in a simple fashion the relation of the mutual diffusion coefficients to these quantities, consider the following heuristic argument: since eq 8 and 9 must hold for all reasonable gradients of species 1 and 2, if

$$\frac{dc_2}{dx} = 0$$

then

$$(J_1 + J_2) = -(D_{11} + D_{21})\frac{dc_1}{dx} \qquad (14)$$

Further, if species 1 and 2 are physically indistinguish-

able, no change in the above expression would result from the imaginary process of substituting unlabeled molecules (species 1) for all labeled molecules (species 2). However, with this change, the left side of eq 14 would represent the flux of solute in a mutual diffusion experiment and therefore $(D_{11} + D_{21})$ is equivalent to D the mutual diffusion coefficient. We thus see that D will be greater than D^* by $(D_{12} + D_{21})$, the sum of the coefficients describing the crosscoupling of labeled and nonlabeled species fluxes. Thus we can conclude from the results of the present study that for hemoglobin and serum albumin, $(D_{12} + D_{21}) \ll D_{11}$ for all solution concentrations examined. This contrasts with the results of Albright[27] and Albright and Mills,[28] summarized by Curran, et al.[23] In their work using the much smaller molecules, alanine and β-alanine, they found that values of D_{12} became significant at solute volume fractions above about 0.07, with deviations between D and D^* of as much as 48% at a volume fraction of 0.27.

The absence of significant differences between tracer and mutual diffusion coefficients has useful consequences. It means that experiments to obtain diffusion coefficient data can be set up in the most convenient way with assurance that the values so determined will be applicable to either the tracer-like situations which arise in carrier transport problems or the mutual diffusion situations which arise in filtration problems, diffusion-limited protein reactions (antigen–antibody reactions) etc. However, the lack of a clear mechanistic understanding of the reasons why the direct cross-coupling is negligible makes it difficult to assess the range of molecular weights and shapes for which such a situation may be expected to hold. Clearly, further work is necessary to establish these ranges.

In examining the dependence of the diffusion coefficient on the concentration of the diffusing species, it is useful to keep in mind the interpretation of the diffusion coefficient as the inverse of a hydrodynamic resistance. Using such a model it has been shown[29] that, for zero volumetric flow, the mutual diffusion coefficient, D, is given by

$$D = \frac{\kappa T}{f_{ij}}\left\{1 + \left(\frac{\partial \ln y_i}{\partial \ln c_i}\right)_{T,P}\right\}\phi_j \qquad (15)$$

In this expression, subscript i refers to solute; j refers to solvent. f_{ij} is a molar frictional coefficient which can be interpreted as the force on a molecule of species i

(23) P. F. Curran, A. E. Taylor, and A. K. Solomon, Biophys. J., 7, 879 (1967).

(24) S. R. DeGroot and P. Mazur, "Nonequilibrium Thermodynamics," North-Holland Publishing Co., Amsterdam, 1962.

(25) P. J. Dunlop, J. Phys. Chem., 69, 1693 (1965).

(26) This relationship can also be derived from the much more general relationship among these coefficients developed by Dunlop.[25]

(27) J. G. Albright, ibid., 70, 2299 (1966).

(28) J. G. Albright and R. Mills, ibid., 69, 3120 (1965).

(29) R. J. Bearman, J. Chem. Phys., 32, 1308 (1960).
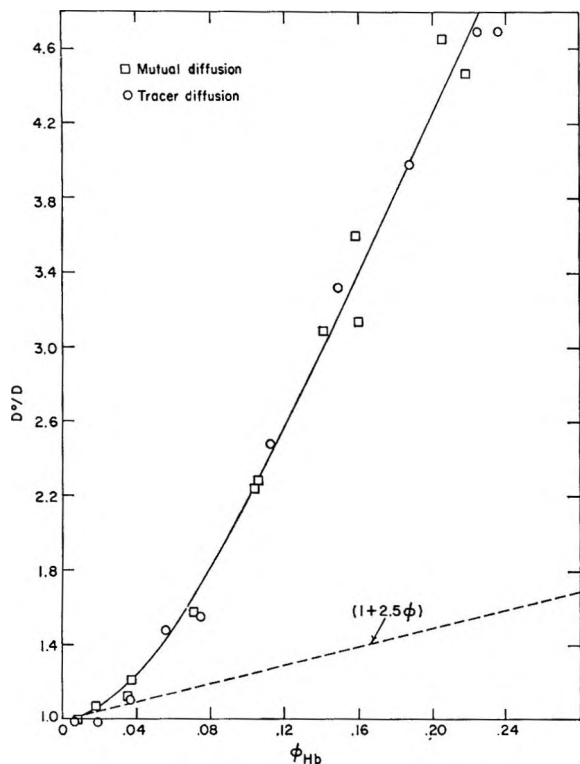
Figure 5. Ratio of the diffusion coefficient of hemoglobin at infinite dilution to that at nonzero volume fractions. Dashed line indicates the simple linear approximation to this ratio based on the Einstein equation for viscosity of a suspension of solid spheres.

Figure 6. Ratio of the diffusion coefficient of serum albumin at infinite dilution to that at nonzero volume fractions. Dashed line indicates the simple linear approximation to this ratio based on the Einstein equation for viscosity of a suspension of solid spheres.

due to all molecules of species j per unit of average velocity difference between i and j. y_i is the activity coefficient of species i and ϕ_j is the volume fraction of j in the system. Thus, as the concentration of i increases, D changes as a result of changes in the frictional coefficient, the activity coefficient, and the volume fraction.

If the quantity in brackets is identified as A and we use superscript 0 to denote values at infinite dilution, we can form the expression

$$\frac{D^0}{D} = \frac{f_{ij}}{(f_{ij})^0} A(1 + \phi_i + \phi_i^2 + \ldots) \qquad (16)$$

Equations for the ratio $(f_{ij})/(f_{ij})^0$ have been formulated using hydrodynamic models which yield power law expressions with various values of the first few coefficients.[30]

If we assume that the activity term can also be expressed as a power law, eq 16 becomes

$$\frac{D^0}{D} = 1 + k_1\phi_i + k_2\phi_i^2 + k_3\phi_i^3 + \ldots \qquad (17)$$

If the magnitude of the first coefficient is not too much less than that of the subsequent terms, a plot of D^0/D vs. ϕ_i should yield a straight line for a small, but not insignificant range of values of ϕ_i. In Figures 5 and 6

the data from the present investigation are plotted in this manner and it is clear that the curvature in the region of low concentration is quite pronounced and that the initial linear region does not cover a significant range of volume fractions. If a least-squares analysis is applied to the data, the following values of k_1 and k_2 are found. (a) For human hemoglobin at 25° ($\phi_i \leq 0.07$)

$$k_1 = 0.6$$

$$k_2 = 95.9$$

(b) For bovine serum albumin at 25° ($\phi_i \leq 0.08$)

$$k_1 = 1.51$$

$$k_2 = 109.03$$

The result that k_1 is of order unity is not unexpected nor is it surprising to find that the quadratic term quickly becomes significant. On the other hand, the behavior of the curves over a broad region of relatively high concentrations is much less expected. Within experimental error both curves can be approximated in this region by straight lines (with slopes much greater than

(30) H. L. Frisch and R. Simha in "Rheology," Vol. 1, F. R. Eirich, Ed., Academic Press, New York, N. Y., 1956, Chapter 14.

k_1) which, when extrapolated, pass through the origin. For hemoglobin the slope of the line is 21.8 and for albumin it is 21.3. A function that approximates both the low- and high-concentration behavior of both the hemoglobin and albumin data is of the form

$$\frac{D^0}{D} = \frac{\alpha\phi_i}{\tanh \alpha\phi_i} \qquad (18)$$

where α is the slope of the straight line portion of the curves. The solid lines drawn in Figures 5 and 6 are plots of this function which, although it has no obvious theoretical basis, provides a convenient single parameter fit to the data. Similar plots for low molecular weight substances such as glucose and sucrose, for which diffusion data are available over a broad range of concentration,[31-33] do not exhibit such a clearly defined high-concentration linear behavior. While it is tempting to infer that the linearity in this region is a characteristic of high molecular weight globular molecules, we have not found sufficient data for molecules of intermediate size to test this inference.

Nomenclature

A Thermodynamic correction factor, dimensionless

A_p Area of pores in filter, cm²

c_i Concentration of species i, g mol/cm³

D Mutual diffusion coefficient, cm²/sec

$\bar{D}$ Integral diffusion coefficient, cm²/sec

D^* Tracer diffusion coefficient, cm²/sec

D_{ij} Diffusion coefficient relating flux of species i to gradient in species j, cm²/sec

f_{ij} Frictional coefficient; force on a molecule of i due to all molecules of j per unit of average velocity difference between i and j

J_i Flux of species i, g mol/(cm² sec)

k_1, k_2 Coefficients of linear and quadratic volume fraction terms in a power law expression of D^0/D

T Temperature, °C

t Time, sec

V Diffusion cell reservoir volume, cm³

x Distance in direction normal to membrane, cm

y_i Chemical activity coefficient of species i, cm³/g mole

α Slope of linear portion of curves in Figures 5 and 6, dimensionless

β Diffusion cell factor defined by eq 2, cm⁻²

δ Equivalent straight path length through filter, cm

κ Boltzmann's constant

ϕ_i Volume fraction of species i, dimensionless

Subscripts

0   Value at start of experiment

t Value at time t in experiment

Superscripts

0   Value at infinite dilution

′   Value in lower reservoir

″   Value in upper reservoir

(31) J. K. Gladden and M. Dole, *J. Amer. Chem. Soc.*, **75**, 3900 (1953).

(32) R. R. Irani and A. W. Adamson, *J. Phys. Chem.*, **62**, 1517 (1958).

(33) R. R. Irani and A. W. Adamson, *ibid.*, **64**, 199 (1960).

The Solvent–Isotope Effect in the Enthalpy of Some Solutes in Methanol[1]

by C. V. Krishnan and Harold L. Friedman*

*Department of Chemistry, State University of New York at Stony Brook,
Stony Brook, New York   11790   (Received August 11, 1970)*

The enthalpies of transfer to $CH_3OD(l)$ from $CH_3OH(l)$ at 25° at infinite dilution have been measured for several solutes and compared with available data for $D_2O \leftarrow H_2O$ transfers.   The comparison serves to identify three solvation phenomena which depend on the three-dimensional branched-chain hydrogen-bonded structure present in water but not in methanol: the markedly different hydration of alkyl and aryl groups, the "icebergs" or "hydration of the second kind" associated with the hydration of alkyl groups, and the "structure-breaking" effect in the hydration of Cs^+ and I^- ions.

I. Introduction

The differences in thermodynamic properties of solutions when the solvent H_2O is replaced by D_2O have been used to test the structural ideas invoked for explaining many properties of water and aqueous solutions of electrolytes and nonelectrolytes.   The solvent–isotope effects on the free energies, enthalpies, and entropies of aqueous alkali and alkaline earth halides and numerous ionic and nonionic solutes containing nonpolar groups are the subject of an excellent review.[2]   The results are well organized by postulating that heavy water is more structured than ordinary water so those solutes that are assumed to make (or break) structure in water may make (or break) more structure in D_2O.   However, recent measurements of conductance of tetraalkylammonium halides in alcohols,[3] and osmotic and activity coefficients in N-methyl acetamide[4] have shown that many of the peculiar solution properties associated with structural effects in water are found in some other hydrogen-bonded solvents as well.   Therefore, it seemed useful to investigate the solvent–isotope effect in solutions in another hydrogen-bonded solvent.   For this reason enthalpies of transfer of a number of solutes (at practically infinite dilution) to CH_3OD from CH_3OH have been measured.

It is assumed that whatever factors may cause the $D-O-D \ldots OD_2$ hydrogen bond to be stronger than the corresponding protium hydrogen bond will have a qualitatively similar effect on the hydrogen bonds in CH_3OD-(l) relative to those in $CH_3OH(l)$.   Then such differences as may be found in the solvent isotope effect in methanol compared to water may be ascribed to the unique three-dimensional structures based on branched chains of hydrogen bonds which are possible only in water.

Some of the relevant properties of the water and alcohol systems are given in Table I.

II. Experimental Section

The instrumental aspects have been described earlier.[5]   The salts and nonelectrolytes used were all from earlier work.[6–9]   Spectrograde CH_3OH and Stohler Isotope Chemicals' 99% CH_3OD were distilled over anhydrous calcium sulfate before use.

The determinations of heats of solutions of electrolytes at infinite dilution in CH_3OH and CH_3OD were much more difficult than the determinations in H_2O and D_2O for the following reasons.

1. Since the dielectric constant of methanol is much less than that of water, the concentrations of the salts need to be smaller in order to avoid ion association.

2. Since the calorimeter is suited to solutes that dissolve quickly and since the dissolutions in methanol were much slower than in water, the experimental uncertainties are larger.

3. While in water the alkali halides show large solvent isotope effects, they mostly are difficult to dissolve in methanol and other salts must be investigated.   Apparently for this reason enthalpies of transfer of the alkali halides to methanol from water which may be obtained from Slansky's data[10] fail by about 0.5 kcal/mol to exhibit additivity in the ionic components.

4. The structural solution effects are less in methanol than in water, so the absolute solvent isotope effects are also smaller.

5. The presence of trace amounts of water in the alcohol affects the heats drastically while of course trace amounts of water in D_2O do not affect the results.

(1) The support of this research by the National Institutes of Health is gratefully acknowledged.

(2) E. M. Arnett and D. R. McKelvey, "Solute–Solvent Interactions," J. F. Coetzee and C. D. Ritchie, Ed., Marcel Dekker, New York, N. Y., 1969.

(3) D. F. Evans and P. Gardam, *J. Phys. Chem.*, **72**, 3281 (1968); **73**, 158 (1969).

(4) R. H. Wood, R. K. Wicker, and R. W. Kreis, submitted for publication in *J. Phys. Chem.*

(5) H. L. Friedman and Y. C. Wu, *Rev. Sci. Instrum.*, **36**, 1236 (1965).

(6) Y. C. Wu and H. L. Friedman, *J. Phys. Chem.*, **70**, 501 (1966).

(7) Y. C. Wu and H. L. Friedman, *ibid.*, **70**, 2020 (1966).

(8) C. V. Krishnan and H. L. Friedman, *ibid.*, **73**, 1572 (1969).

(9) C. V. Krishnan and H. L. Friedman, *ibid.*, **73**, 3934 (1969).

(10) C. M. Slansky, *J. Amer. Chem. Soc.*, **62**, 2430 (1940).

Table I: Properties of H_2O-D_2O and CH_3OH-CH_3OD at 25°

	H_2O^a	D_2O^a	CH_3OH^b	CH_3OD^b
Dielectric constant	78.40[c]	78.06[d]	32.62[e]	
$\Delta H^\circ{}_{vap}$, kcal/mol	10.52	10.85	9.01	9.14
C_p(liquid), cal/deg mol	17.99	20.16	18.11 (−3°)	19.04 (−3°)
Density, g/cm³	0.99701	1.1044	0.7915 at 20°	0.8077 at 20°
Dipole moment (in benzene solution), D	1.76	1.78	1.71	
Viscosity, cP	0.8903	1.107	0.5428[e]	0.571
Molecular polarizability, α, A^3	1.47202[b]	1.45931[b]	3.191	3.186

[a] See ref 2. [b] I. B. Rabinovich, "Influence of Isotopy on the Physico Chemical Properties of Liquids," Consultants Bureau, New York, N. Y., 1970. [c] R. L. Kay, G. A. Vidulich, and K. S. Pribadi, *J. Phys. Chem.*, **73**, 445 (1969). [d] G. A. Vidulich, D. F. Evans, and R. L. Kay, *ibid.*, **71**, 656 (1967). [e] G. P. Cunningham, G. A. Vidulich, and R. L. Kay, *J. Chem. Eng. Data*, **12**, 336 (1967).

Table II: Enthalpies of Solution of Pure Substances at 25°, kcal/mol[a]

Solute	Solvent CH₃OH	CH₃OD
C_5H_{12}	0.91	0.95
C_6H_{14}	1.12	1.20
C_7H_{16}	1.32	1.46
C_6H_6	0.37	0.43
$C_6H_5CH_3$	0.45	0.57
$C_6H_5C_2H_5$	0.57	0.69
$LiOOCF_3C$	−9.37	−9.65
$NaOOCF_3C$	−4.78	−4.94
$KOOCF_3C$	−1.07	−1.12
$RbOOCF_3C$	0.33	0.33
$CsOOCF_3C$	0.41	0.39
NaBr	−4.05, −4.00[b]	−3.97
NaI	−7.14, −7.00[b]	−6.98
KF	−5.25	−5.35
KI	−0.15, 0.175[b]	0.09
$(C_6H_5)_4AsCl$	−0.98	−0.75
$(C_6H_{11})_4NCl$	−2.37	−2.07

[a] Each datum is the average of two or more measurements agreeing within 0.05 kcal/mol. [b] See ref 10.

Table III: Enthalpies of Transfer of Solutes at 25°, kcal/mol

Solute	Solvents CH₃OD ← CH₃OH	D₂O ← H₂O
C_3H_8		−0.531[a]
		−0.222
		−0.225[b]
C_4H_{10}		−0.619[a]
		−0.142
		−0.355[b]
C_5H_{12}	0.04	
C_6H_{14}	0.08	
C_7H_{16}	0.14	
C_6H_6	0.06	
$C_6H_5CH_3$	0.12	
$C_6H_5C_2H_5$	0.12	
Li^+	−0.13[c]	0.21[c]
Na^+	0.00	0.37
K^+	0.10	0.42
Rb^+	0.15	0.44
Cs^+	0.13	0.47
$(C_5H_{11})_4N^+$	0.26	−0.62
Ph_4As^+	0.19	−0.08
F^-	−0.20	−0.37
Cl^-	(0.04)[d]	0.19
Br^-	0.09	0.33
I^-	0.13	0.47
$CF_3CO_2^-$	−0.15	−0.27

[a] Values at 4°. [b] Values at 50°. [c] All of the ionic values in this table are based on the convention that the enthalpy of transfer is the same for Cs^+ and I^-. [d] Interpolated on halide ion line in Figure 1.

The results which could be obtained in spite of these difficulties are given in Table II, together with some data for nonelectrolytes which of course are generally easier to get in methanol than in water.

III. Results and Discussion

The most direct method of studying the effect of nonpolar groups on the structural properties of water is by studying hydrocarbons as solutes. However, these are practically insoluble in water, and widely diverging values have been reported for the heats of solutions in water depending on whether they are obtained from solubilities by the Van't Hoff method or by a calorimetric method.[11] Heats of transfer to D_2O from H_2O of only two hydrocarbons, namely propane and butane, are reported[12] and even these values should be viewed with caution due to large experimental uncertainties. These values together with those obtained from the present measurements in alcohols are given in Table III. It is

clear from Table III as well as from heats of transfer to D_2O from H_2O of various types of solutes (alcohols,[12] tetraalkylammonium ions,[13] alkyl sulfonates,[14] carboxylates,[15] amino acids[12]) that the alkyl groups make a negative contribution to the observed heat of transfer,

(11) D. S. Reid, M. A. J. Quickenden, and F. Franks, *Nature*, **224**, 1293 (1969).

(12) G. C. Kresheck, H. Schneider, and H. A. Scheraga, *J. Phys. Chem.*, **69**, 3132 (1965).

(13) C. V. Krishnan and H. L. Friedman. *ibid.*, **74**, 2356 (1970).

(14) C. V. Krishnan and H. L. Friedman, unpublished work.

(15) J. Greyson and H. Snell, *J. Phys. Chem.*, **74**, 2148 (1970).

which is readily interpreted as due to more stabilization of hydrogen-bonded solvent structure in D_2O around the nonpolar groups. The new results show that, in transfers to CH_3OD from CH_3OH, the alkyl groups make a positive contribution to ΔH as expected if the dominant effect is the difference in the enthalpy required to make a cavity in the solvent, with more enthalpy required in CH_3OD due to stronger hydrogen bonds.

There do not seem to be any data for heats of transfer of aromatic hydrocarbons to D_2O from H_2O. However, the phenyl group contribution in benzyl alcohol, benzene and toluene sulfonates and tetraphenyl salts is always positive unlike the alkyl group contributions. The present measurements show that the phenyl groups also make a positive contribution to transfers to CH_3OD from CH_3OH. However, the methanol solvent isotope effect for tetraamylammonium ion is even more positive than for tetraphenylarsonium ion.

The fact that in methanol a positive solvent isotope effect in the enthalpy is found both for alkyl and aryl groups is in contrast to the behavior in water.

It may be recalled[13] that the alkali cations give large (ca. 500 cal/mol) positive heats of transfer to D_2O from H_2O. For anions the effect is smaller and ions like F^- and CF_3COO^- even have negative enthalpies of transfer to D_2O from H_2O. Good correlations of these heats with other properties such as Walden product ratios and "structural enthalpies" have been obtained.[13] These conclusions were derived from ionic enthalpies of transfer based on the convention that Ph_4As^+ and Ph_4B^- had the same enthalpy of transfer. In more recent studies[16] it transpires that these species differ markedly in solvation, both in water and in methanol. Therefore, the $Ph_4As^+ = Ph_4B^-$ convention has no particular advantage over the convention based on equal solvation[6] of Cs^+ and I^- which is used in Table III. Unfortunately, we were not able to obtain an accurate value of the enthalpy of the $CH_3OD \leftarrow CH_3OH$ transfer for $NaBPh_4$.

For the alkali metal ions the trend in the solvent isotope effect is similar in the two solvents (Figure 1) but the effect is about 0.3 kcal/mol more positive in water, presumably due to the structure-breaking effect in the outer solvation region of the alkali metal ions in water.[17] An obvious contribution to the similar trend lies in the inner solvation region of the ions; the greater strength of the $O-D\cdots O$ hydrogen bonds which must be disrupted is not compensated by greater strength of the $M^+\cdots O$ interaction which is made. This contribution, at least conceptually, does not seem to depend upon the dimensionality of the hydrogen-bonded structure in the solvent, unlike the contribution of the structure-broken region.

For the halide ions the smaller trend of the solvent isotope effect in methanol than in water may have its origin in the isotope effect of breaking $O-H\cdots O$ hy-
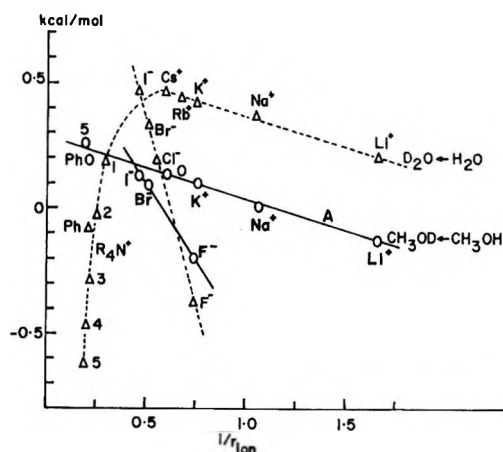
Figure 1. Ionic enthalpies of transfer: —, $CH_3OD \leftarrow CH_3OH$; —, $D_2O \leftarrow H_2O$ (data from ref 13). r_{ion} is the Pauling radius for manatomic ions and is estimated from models for the others. The tetraalkyl ammonium ions are indicated by integers: 1 for tetramethyl, 2 for tetraethyl, etc. Ph stands for Ph_4As^+. These single-ion enthalpies are based on the convention that the enthalpies of transfer of Cs^+ and I^- are equal, which is different from the convention employed in ref 13. On line A the two unlabeled data points are for Cs^+ and Rb^+.

drogen bonds being partly compensated by the inner solvation, which involves $O-H\cdots X^-$ hydrogen bonds. Evidence for the importance of the latter was found in the study of the solvent isotope effect in water.[13] For iodide, where this effect is presumed to be minimal, there is still a more negative solvent–isotope effect than in water. This fits in with the expectation that the structure-breaking effect is only important in water.

The solvent isotope effect for F^- is smaller in methanol than in water although Bernstein, et al.,[18] have found the same ^{19}F nmr shift for the solvent isotope effect of F^- in water and methanol. However, more recent measurements of the same shifts by Ramirez and Lauterbur[19] give 2.4 ppm for CH_3OD-CH_3OH as compared to 3.0 ppm for D_2O-H_2O. This is qualitatively in accord with the calorimetric data.

Having shown, by the chains of inference to which one usually has to resort in this field of study, that the comparison of the solvent isotope effect in water and methanol is generally understandable in terms of several often discussed solvation phenomena, we now emphasize those conclusions which seem to be firmly independent of the details of interpretation as well as of the convention for separating ionic contributions.

1. By comparing Ph_4As^+ with $(C_5H_{11})_4N^+$ we see that the well known[13] great difference in solvation of aryl and alkyl groups in water is reduced in methanol

(16) C. V. Krishnan and H. L. Friedman, unpublished work.

(17) H. S. Frank and M. W. Evans, *J. Chem. Phys.*, **13**, 507 (1945).

(18) C. Deverell, K. Schaumburg, and H. J. Bernstein, *ibid.*, **49**, 1276 (1968).

(19) J. Ramirez and P. C. Lauterbur, private communication.

and even appears with the opposite sign in the solvent isotope effect.

2. By comparing the solvent isotope effects of Cs^+ and $(C_5H_{11})_4N^+$ in the two solvents we see that the peculiar solvation of the latter in water, often called either the iceberg effect or hydration of the second kind, is greatly diminished if not completely removed in methanol.

3. By comparing the solvent–isotope effect for CsI in the two solvents we see that the structure breaking effect, which dominates so many of the properties of aqueous CsI, is much smaller if not completely absent in methanol.

These conclusions are offered as definite evidence that three particular solvation effects in water derive from the three-dimensional hydrogen-bonded structures based on branched chains of hydrogen bonds which one may have in water but not in methanol.

IV. Other Thermodynamic Evidence

In the classic paper by Frank and Evans[17] one of the central observations leading to the postulation of complex structures around aqueous solutes is that the entropy decrease for the hydration of two argon atoms is *greater* than that for the hydration of a potassium ion and a chloride ion

$$2Ar(g) \longrightarrow 2Ar(aq) \qquad \Delta S = -60.4 \text{ gibbs/mol} \quad (1)^{20}$$

$$K^+(g) + Cl^-(g) \longrightarrow K^+(aq) + Cl^-(aq)$$

$$\Delta S = -51.9 \text{ gibbs/mol} \quad (2)^{20}$$

Of course elementary considerations of the effect of transferring an electronic charge from one argon atom to the other to make a potassium and a chloride ion lead to a comparison with the opposite trend. The conclusions reached from a study of the solvent isotope effect imply that the complex structures around solute particles in methanol are much less important than in water so the solvation entropies might be expected to be in the normal order. In fact we find

$$2Ar(g) \longrightarrow 2Ar(MeOH)$$
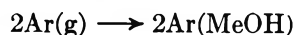
$$\Delta S = -32 \text{ gibbs/mol} \quad (3)^{20,21}$$

$$K^+(g) + Cl^-(g) \longrightarrow K^+(MeOH) + Cl^-(MeOH)$$
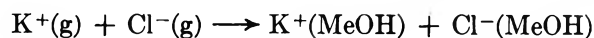
$$\Delta S = -80 \text{ gibbs/mol} \quad (4)^{20,22}$$

where now the electrostriction effect does dominate any residual hydration of the second kind about the Ar or structure breaking about the K^+ and Cl^-.

(20) Data at 25°. As in ref 17 the standard state in the gas is hypothetical 1 atm and the standard state in solution is hypothetical unit mole fraction of the solute.

(21) Calculated from the solubility data of A. Lannung, *J. Amer. Chem. Soc.*, **52**, 68 (1930).

(22) Calculated from eq 3 and the entropies in methanol and water calculated by C. M. Criss, R. P. Held, and E. Luksha, *J. Phys. Chem.*, **72**, 2970 (1968).

Thermochemistry of Some Chlorocomplex Compounds of the Rare Earths.

Third Ionization Potentials and Hydration Enthalpies

of the Trivalent Ions[1]

by Lester R. Morss[2]

Department of Chemistry and Lawrence Radiation Laboratory, University of California, Berkeley, California   94720
(Received June 30, 1970)

Publication costs assisted by Lawrence Radiation Laboratory, University of California, Berkeley

Heats of solution of the complex chlorides Cs_2NaMCl_6 (M = Y, La, Ce, Nd, Gd, Dy, Er, Lu, and Pu) were measured in a new microcalorimeter. Heats of formation of these compounds have been derived and are compared with heats of formation of the uncomplexed chlorides. Using auxiliary thermodynamic data, the third ionization potentials of the lanthanide elements and the hydration enthalpies of the trivalent rare earth ions have been calculated. The variation in the third ionization potentials of the lanthanides may be attributed to the change (upon ionization) of exchange energy of unpaired electrons. However, the variation in enthalpies of hydration and complexing cannot be interpreted in terms of ligand-field stabilization.

Introduction

Since the chemical properties of the rare earth elements and their compounds change regularly with atomic number, it is sometimes possible to interpret these changing properties simply in terms of changing nuclear charge and electronic configuration. However, the variation in most properties may be perturbed by structural changes, hydration effects, nonstoichiometry, or electronic interactions as one proceeds along the lanthanide or actinide series. It may be necessary to resort to thermochemical cycles to circumvent such effects when attempting to understand or to predict many properties of the rare earths.[3-6]

Recently prepared and characterized complex compounds Cs_2NaMCl_6, where M may be almost any trivalent cation, appeared suitable for straightforward comparisons of thermochemical properties.[7,8] The desirable characteristics of these compounds are the following. (1) They have been prepared with M being almost any trivalent rare earth ion (Y, La–Lu, Pu–Bk). The compounds are easily prepared in high purity and are less sensitive to atmospheric moisture than are the respective trichlorides. (2) They are all rapidly water soluble, making aqueous solution calorimetry feasible. (3) Extensive thermochemical data are available on the corresponding binary chlorides from which the complex chlorides are formed, and on their aqueous solutions. (4) As contrasted with binary compounds such as the trichlorides or sesquioxides, the complex chlorides are all isostructural, and of high symmetry, enabling simple calculation and interpretation of lattice energies.

The initial goals of this investigation were to determine the heats of formation of the compounds Cs_2Na-

MCl_6 and to evaluate the stability gained by the complexed salts

$$2CsCl + NaCl + MCl_3 = Cs_2NaMCl_6 \qquad (1)$$
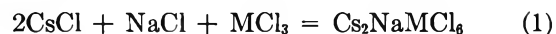
Because of the precise and accurate heats of solution, and the regularity with which the heat changed with atomic number of M, it was possible to use the thermochemical and crystallographic information obtained for these compounds to estimate third ionization potentials for the lanthanide elements and to calculate heats of hydration of the trivalent rare earth ions.

Experimental Section

The compounds Cs_2NaMCl_6 were prepared as single crystals from corresponding anhydrous binary chlorides (CsCl, NaCl, and sublimed MCl_3) by gradient solidification from a melt.[8,9] The source of anhydrous $PuCl_3$ for $Cs_2NaPuCl_6$ was a single crystal, sublimed and grown by Fuger.[10]

(1) This research was supported by the U. S. Atomic Energy Commission, Contract W-7405-eng-48.

(2) Department of Chemistry, Purdue University, Lafayette, Ind. 47907.

(3) L. A. K. Staveley, D. R. Markham, and M. R. Jones, *J. Inorg. Nucl. Chem.*, **30**, 231 (1968).

(4) A. S. Carson, P. G. Laye, and P. N. Smith, *J. Chem. Soc. A*, 1384 (1968).

(5) M. M. Faktor and R. Hanks, *J. Inorg. Nucl. Chem.*, **31**, 1649 (1969).

(6) D. A. Johnson, *J. Chem. Soc. A*, 1525 (1969).

(7) L. R. Morss and J. Fuger, *Inorg. Chem.*, **8**, 1433 (1969).

(8) L. R. Morss, M. Siegal, L. Stenger, and N. Edelstein, *ibid.*, **9**, 1771 (1970).

(9) D. M. Gruen, J. G. Conway, and R. D. McLaughlin, *J. Chem. Phys.*, **25**, 1102 (1956).

(10) J. Fuger and B. B. Cunningham, *J. Inorg. Nucl. Chem.*, **25**, 1423 (1963).

A piece of clear single crystal was broken out from the center of each cylindrical crystal of Cs_2NaMCl_6. This selected sample was crushed in a mortar to fragments ca. 0.5 mm in size; replicate samples were loaded into calorimeter bulbs. All sample-handling procedures were carried out in a drybox, even though all samples except those of Cs_2NaYCl_6 showed no evidence of deliquescence in laboratory air.

Weighings were carried out on an Ainsworth FM microbalance (not in the drybox) by enclosing each calorimeter bulb in a micro weighing bottle, with the ground-glass joint sealed with petroleum jelly. To prevent a buoyancy error when capping the weighing bottles, a small hole was drilled through the ground glass of each cap and bottle, so that pressure could be equilibrated after closing the bottle by rotating the cap. (Precision of weighings was established as ±0.02 mg by weighing and reweighing empty bulbs.)

A 30-ml gold-plated copper microcalorimeter was used for heats of solution. The microcalorimeter had an energy equivalent of 34.5 cal/°C, thermal leakage modulus of 0.001 min^{-1}, sensitivity 0.0002 cal, and precision 0.06% (standard deviation of a typical electrical energy heat calibration). A detailed description of the calorimeter has been published.[11]

Heats of solution were measured at $(25 \pm 0.1)°$ in 0.001 N HCl; this dilute acid satisfactorily suppresses hydrolysis of all of the trivalent rare earth ions. All chlorocomplex compounds dissolved within 2 min and gave clear solutions, except for one slightly clouded crystal of $Cs_2NaLuCl_6$ which required about 1 hr to complete evolution of heat. (This run was rejected.)

The calorimeter's energy equivalent was determined twice before and twice after each run by precise inputs of electrical energy which approximated the chemical heat evolution in quantity and duration. The heats of solution of Mg metal in 1 N HCl and of "tris" in 0.1 N HCl served as checks on the accuracy of the microcalorimeter (Table I). All results are reported in defined calories (1 cal = 4.184 abs J).

Table I: Heats of Solution of Standard Substances

Substance	Wt, mg	Cal	$-\Delta H$(soln), kcal/mol Found	$-\Delta H$(soln), kcal/mol Lit.
Mg metal	0.5938	2.7184	111.30	111.285[a]
"Tris"	39.41	2.3106	7.102	7.109[b]
"Tris"	29.905	1.7567	7.116	

[a] C. H. Shomate and E. Huffman, *J. Amer. Chem. Soc.*, **65**, 1625 (1943). [b] J. O. Hill, G. Öjelund, and I. Wadsö, *J. Chem Thermodyn.*, **1**, 111 (1969).

Corrections were applied for water evaporated into dry nitrogen of each bulb (and in the case of metal dissolution, for hydrogen evolved); for heat of bulb breakage (measured five times, mean −0.0002 ±

0.0002 cal); and for reducing observed data to infinite dilution. The last correction was made to the heats of solution of Cs_2NaMCl_6 by assuming only two significant heat effects to be corrected: the nonideality of M(III) salt solutions (considered equivalent to the heat of dilution of the corresponding MCl_3 solution to infinite dilution) and the complexing of M(III) with chloride ion (which proceeds significantly only as far as the monochlorocomplex ion). At molalities achieved in these experiments (final molality of Cs_2NaMCl_6 typically 0.004 m) the former correction amounts to −400 cal/mol and the latter to about −70 cal/mol (that is, both dilution effects are exothermic). Heats of dilution have been measured accurately for YCl_3 and for all lanthanide trichloride solutions;[12−15] the comparable correction for $PuCl_3$ was estimated from that of the lanthanide with comparable ionic radius, $NdCl_3$. The equilibrium constant and enthalpy of complexing of M(III) with chloride have only been estimated for a few rare earth ions; the calorimetric estimate of Montgomery[16] for the formation of $CeCl^{2+}$ $(K = 1, \Delta H = 5.4 \text{ kcal/mol})$ has been used for all the rare earths.

Results

Table II reports the experimental results of this research. The averaged heats of solution for the lanthanide chlorocomplex compounds, corrected to infinite dilution, are plotted in Figure 1. It may be seen that these heats of solution change slowly and regularly, so that it is safe to interpolate heats of solution for other lanthanide chlorocomplex compounds (most of which have been prepared and found to be isostructural).[8]

Taking the heat of solution of CsCl as 4250 ± 100 cal/mol and that of NaCl as 928 ± 5 cal/mol,[17] heats of complexing (ΔH for eq 1) may be calculated as follows

$$\Delta H_1 = \Delta H°(\text{soln, } MCl_3) + 2\Delta H°(\text{soln, CsCl}) +$$

$$\Delta H°(\text{soln, NaCl}) - \Delta H°(\text{soln, } Cs_2NaMCl_6)$$

The necessary enthalpies of solution of MCl_3, and calculated values of ΔH_1, are collected in Table III. In

(11) L. R. Morss, Ph.D. Thesis, University of California, Berkeley, Calif., 1969 (University of California Lawrence Radiation Laboratory Report UCRL-18951).

(12) F. H. Spedding and C. F. Miller, *J. Amer. Chem. Soc.*, **74**, 3158 (1952).

(13) F. H. Spedding and J. P. Flynn, *ibid.*, **76**, 1474 (1954).

(14) C. W. De Kock and F. H. Spedding, Ames Laboratory, Iowa State University, IS-1356, 1965.

(15) G. W. Pepple, Ph.D. Thesis, Iowa State University, Ames, Iowa, 1967.

(16) R. L. Montgomery, U. S. Bureau of Mines Report BMRI-6146, Washington, D. C., 1962.

(17) V. B. Parker, "Thermal Properties of Aqueous Uni-univalent Electrolytes," National Bureau of Standards NSRDS-NBS 2, U. S. Government Printing Office, Washington, D. C., 1965.
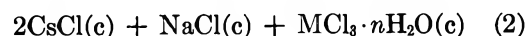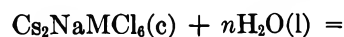
Table II: Heats of Solution of Cs₂NaMCl₆

Compd	Wt, mg	Calories evolved	—ΔH, kcal/mol—	
			Uncor	Cor
Cs₂NaYCl₆	69.44	2.1605	18.37	18.84
Cs₂NaYCl₆	59.30	1.5503	18.20	18.59
Cs₂NaLaCl₆	77.89	2.3565	19.38	19.85
Cs₂NaLaCl₆	101.25	3.0545	19.32	19.87
Cs₂NaCeCl₆	72.87	1.9552	17.22	17.65
Cs₂NaCeCl₆	81.71	2.1886	17.19	17.65
Cs₂NaNdCl₆	63.18	1.6213	16.57	16.99
Cs₂NaNdCl₆	59.28	1.5282	16.65	17.05
Cs₂NaGdCl₆	81.90	2.0237	16.28	16.78
Cs₂NaGdCl₆	78.68	1.9427	16.27	16.76
Cs₂NaDyCl₆	82.25	2.0108	16.23	16.70
Cs₂NaDyCl₆	89.47	2.1899	16.25	16.75
Cs₂NaErCl₆	67.89	1.7021	16.77	17.19
Cs₂NaErCl₆	96.91	2.4167	16.68	17.19
Cs₂NaLuCl₆	33.37	0.8370	16.97	17.26
Cs₂NaLuCl₆	36.69	0.9078	16.74	17.04[a]
Cs₂NaLuCl₆	65.83	1.6593	17.05	17.48
Cs₂NaPuCl₆	93.50	1.6443	13.02	13.50
Cs₂NaPuCl₆	93.57	1.6331	12.92	13.40

[a] Rejected because dissolution was slow and incomplete.

responding values for CsCl(c) and NaCl(c) are −98.2 and −106.9 kcal/mol.[18]

Enthalpies (ΔH₂) corresponding to the hydration of

$$Cs_2NaMCl_6(c) + nH_2O(l) =$$

$$2CsCl(c) + NaCl(c) + MCl_3 \cdot nH_2O(c) \quad (2)$$

are listed in Table III. Although they may be calculated directly from the heats of formation of the compounds in eq 2, an equivalent (and more precise) calculation from the heats of solution at infinite dilution has been utilized

$$\Delta H_2 = \Delta H°(soln, Cs_2NaMCl_6, c) -$$

$$2\Delta H°(soln, CsCl, c) - \Delta H°(soln, NaCl, c) -$$

$$\Delta H°(soln, MCl_3 \cdot nH_2O, c)$$

The heats of solution of the hydrated chlorides necessary for this calculation are those quoted by ref 11 from experimental literature data (mostly from Spedding and coworkers).[14,15]

Table III: Thermochemical Properties of MCl₃ and Cs₂NaMCl₆ at 25° (All Entries in kcal/mol)[a]

M	ΔH_f° (MCl₃, c)[b]	ΔH° (soln, MCl₃, c)	ΔH° (soln, Cs₂NaMCl₆, c)	ΔH₁[c]	ΔH_f° (Cs₂NaMCl₆, c)	ΔH₂[c,d]
Y	−239.0	−53.7	−18.7 ± 0.2	−25.6	−576.6 ± 1.1	
La	−255.9	−32.9	−19.9 ± 0.1	−3.6	−571.5 ± 0.9	−22.6
Ce	−251.5	−34.4	−17.6 ± 0.1	−7.4	−570.9 ± 1.2	−20.1
Pr	−252.0	−35.7	(−17.2)	(−9.1)	(−573.1 ± 1.1)	(−16.9)
Nd	−248.7	−37.5	−17.0 ± 0.1	−11.1	−571.8 ± 1.0	−17.3
Pm		(−38.7)	(−16.9)	(−12.4)		
Sm	−244.1	−39.9	(−16.8)	(−13.7)	(−569.8 ± 1.0)	(−17.6)
Eu	−219.5	−40.7	(−16.8)	(−14.5)	(−546.0 ± 2.2)	(−17.5)
Gd	−239.6	−43.4	−16.8 ± 0.1	−17.2	−568.8 ± 1.0	−17.1
Tb	−238.4	−46.0	(−16.7)	(−19.9)	(−570.3 ± 1.8)	(−16.6)
Dy	(−236.6)	(−50.0)	−16.7 ± 0.1	(−23.9)	(−572.5 ± 3.3)	−16.2
Ho	−237.8	−51.0	(−16.9)	(−24.7)	(−574.5 ± 2.7)	(−15.9)
Er	−238.0	−51.4	−17.2 ± 0.1	−24.8	−574.8 ± 2.0	−15.9
Tm	−236.3	−51.6	(−17.3)	(−24.9)	(−573.2 ± 1.1)	(−15.6)
Yb	−229.4	−51.6	(−17.3)	(−24.9)	(−566.3 ± 1.2)	(−15.2)
Lu	−234.5	−52.2	−17.4 ± 0.3	−25.4	−571.9 ± 1.4	−15.0
Pu	−227.0	−31.8	−13.4 ± 0.1	−9.0	−548.0 ± 1.1	−14.6

[a] Estimated values in parentheses. [b] As quoted in ref 11 ("best values" evaluated by author from experimental literature data). [c] See text (eq 1 and 2) for definition. [d] For (La, Ce)Cl₃·7H₂O; others hexahydrates.

order to calculate ΔH₁, all heats of solution have been corrected to infinite dilution.

Heats of formation of compounds Cs₂NaMCl₆ have been calculated, and the values listed in Table III, from the following relationship

$$\Delta H_f°(Cs_2NaMCl_6, c) = 2\Delta H_f°(CsCl, c) +$$

$$\Delta H_f°(NaCl, c) + \Delta H_f°(MCl_3, c) + \Delta H_1$$

For this calculation, necessary values of heats of formation of MCl₃ are tabulated in Table III; the cor-

Calculations

Lattice energies were calculated by taking advantage of the precisely determined and regularly changing unit cell dimensions of these complex chlorides, as well as the high symmetry (face-centered cubic, "ideal cryolite" structure) indicated by X-ray powder pat-

(18) The quoted heats of formation of NaCl(c), CsCl(c), Na⁺(aq), and Cs⁺(aq) are based in part on experimental data obtained since National Bureau of Standards Circular 500 (1952) was issued. See, for example, G. N. Lewis and M. Randall, "Thermodynamics," 2nd ed, revised by K. S. Pitzer and L. Brewer, McGraw-Hill, New York, N. Y., 1961, p 678.

Table IV: Born–Haber Enthalpy Cycle (and Madelung Constant, A) for Cs_2NaMCl_6 at 25° (All Entries in kcal/mol)

M	$\Delta H°_f{}^a$	$S(M)^b$	$\Sigma I(M)^c$	Misc.^{d}	$U_0{}^e$	A^f	U_0, calcd
Y	−576.6	101.5	900.0	16.6	−1594.7	54.546	−1509.6
La	−571.5	103.0	826.0	16.6	−1517.1	53.005	−1436.1
Ce	−570.9	101.0	843.1	16.6	−1531.6	53.284	−1449.8
Pr	−573.1	85.0	867.5	16.6	−1542.2	53.488	−1459.9
Nd	−571.8	78.3	882.6	16.6	−1549.3	53.622	−1466.6
Pm				16.6	−1558.0	53.787	−1474.8
Sm	−569.8	49.4	931.1	16.6	−1566.9	53.954	−1483.2
Eu	−546.0	42.4	969.7	16.6	−1574.7	54.102	−1490.6
Gd	−568.8	95.0	900.0	16.6	−1580.4	54.208	−1496.0
Tb	−570.3	92.9	908.9	16.6	−1588.7	54.363	−1503.9
Dy	−572.5	69.4	937.7	16.6	−1596.2	54.503	−1511.0
Ho	−574.5	71.9	940.3	16.6	−1603.3	54.633	−1517.7
Er	−574.8	75.8	941.5	16.6	−1608.7	54.733	−1522.8
Tm	−573.2	55.5	969.4	16.6	−1614.7	54.843	−1528.5
Yb	−566.3	36.4	1000.7	16.6	−1620.0	54.939	−1533.5
Lu	−571.9	102.2	934.3	16.6	−1625.0	55.029	−1538.2
Pu	−548.0	84.1	904.3	16.6	−1553.0	53.625	−1470.1

^{a} Transposed from Table III. ^{b} R. Hultgren, R. L. Orr, P. D. Anderson, and K. K. Kelley, "Selected Values of Thermodynamic Properties of Metals and Alloys," Wiley, New York, N. Y., 1963, plus supplements issued through July 1969. ^{c} Calculated to close cycle (except entry for La as quoted by ref 5). ^{d} $2S(Cs) + S(Na) + 3D(Cl_2) + 2I(Cs) + I(Na) + 6E(Cl) - 10RT = 2(18.67) + 25.85 + 3(58.16) + 2(89.7) + 118.4 + 6(-85.5) - 5.92 = 16.55$. References: D, D. D. Wagman, W. H. Evans, V. B. Parker, I. Harlow, S. M. Bailey, and R. H. Schumm, *Nat. Bur. Stand. (U. S.) Tech. Note*, No. 270-3, (1968); I, E, D. Cubicciotti, *J. Chem. Phys.*, **31**, 1646 (1959); **33**, 1579 (1960); **34**, 2189 (1961). ^{e} $U_0 = U_0$(calcd) × 1.0564 (see text). ^{f} Calculated in ref 11.
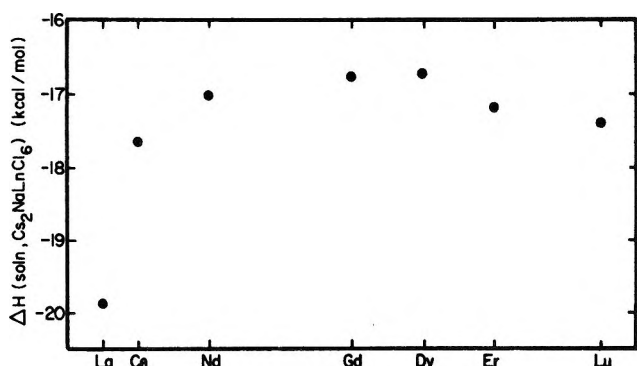

Figure 1. Averaged heats of solution, Cs_2NaMCl_6 (corrected to infinite dilution).

terns.[8] These lattice energies were necessary for Born–Haber cycle determinations of ionization potentials and hydration enthalpies. Although compressibilities and precise atomic parameters for chloride positions are required for direct calculation of *absolute* lattice energies, values which are accurate *relative* to one another may be determined from a simple Born–Landé equation and then corrected to absolute energies by completing a Born–Haber cycle for elements whose ionization potentials are known.

First, the lattice energy of $Cs_2NaLaCl_6$ was calculated from the Born–Landé equation[19]

$$U_0 = \frac{\alpha^2 e^2 NA}{ra}\left(1 - \frac{1}{n}\right) = -332.06\frac{A}{a}\left(1 - \frac{1}{n}\right) \text{ kcal/mol}$$

where A = Madelung constant, relative to unit cell length, a = unit cell length (Å), and n = power of

$(1/r)$ in repulsive potential. For the "ideal cryolite" structure of $M_2M'M''X_6$ with X atomic parameters $(0, 0, 0.25)$, A has been calculated to be 53.005.[19] Powder-pattern intensities for $Cs_2NaLaCl_6$[8] yield Cl^- parameters $(0, 0, 0.247 \pm 0.01)$, consistent with the above parameters for X. Following Pauling's rules for estimation of compressibilities,[20] $n = 9.7$, whereupon

$$U_0 = \frac{-332.06(53.005)}{10.992}\left(1 - \frac{1}{9.7}\right) \quad (3)$$

$$= -1436.1 \text{ kcal/mol}$$

Table IV presents the values for a conventional Born–Haber cycle for Cs_2NaMCl_6 at 25°

$\Delta H_f°(Cs_2NaMCl_6, c) =$

$2S(Cs) + S(Na) + S(M) + 3D(Cl_2) +$

$2I(Cs) + I(Na) + (I_1 + I_2 + I_3)(M) +$

$6E(Cl) + U_0(Cs_2NaMCl_6) - 10RT \quad (4)$

where S = heat of sublimation, D = enthalpy of dissociation, I_i = ionization potential of $M^{(i-1)+}$ to M^{i+}, and E = −(electron affinity). Since the first three ionization potentials for La have been experimentally determined to high accuracy, the Born–Haber cycle (eq 4) for $Cs_2NaLaCl_6$ may be used to estimate the lattice energy of $Cs_2NaLaCl_6$, −1517.1 kcal/mol. This

(19) J. Sherman, *Chem. Rev.*, **11**, 93 (1932). Note that processes like U and E, as used here, represent exoergic processes and are negative in sign.

(20) L. Pauling, "The Nature of the Chemical Bond," 3rd ed, Cornell University Press, Ithaca, N. Y., 1960, p 509.

Table V: Ionization Potentials and Hydration Enthalpies

M	ΣI^a	$I_1{}^b$	$I_2{}^b$	$I_3{}^a$	$I_3{}^c$	$I_3{}^d$	ΔH(hyd, M^{3+})^a
Y	39.03	6.38	12.23	20.42	(20.5)^e		−869.3
La	35.82^e	5.58	11.06	19.18^e		(19.18)	−792.9
Ce	36.56	5.60	10.85	20.11	20.0	(20.08)	−805.1
Pr	37.62	5.41	10.55	21.66	21.6	(21.57)	−815.3
Nd	38.27	5.49	10.72	22.06	22.2	22.07	−822.2
Pm		5.55	10.90				−830.8
Sm	40.38	5.62	11.07	23.68	23.7	23.68	−839.6
Eu	42.05	5.67	11.25	25.13	24.9	24.92	−847.4
Gd	39.03	6.16	12.15	20.72	20.6	20.83	−853.1
Tb	39.41	5.90	11.52	21.99	21.9	21.70	−861.3
Dy	40.66	5.88	11.67	23.11	22.9	22.94	−868.8
Ho	40.77	5.95	11.80	23.02	23.1	(22.81)	−876.1
Er	40.83	6.03	11.93	22.87	22.6	22.44	−881.8
Tm	42.04	6.10	12.05	23.89	23.8	23.56	−887.9
Yb	43.39	6.25	12.18	24.96	25.3	(25.04)	−893.2
Lu	40.51	5.32	13.9	21.29	21.2		−898.3
Pu	39.21						−822.3

^{a} This research. ^{b} As quoted in Table I of ref 6; values for Y and Lu as quoted by ref 5. ^{c} Calculated by ref 5. ^{d} Calculated by ref 6; parenthetical values are from other sources as quoted in ref 6. ^{e} As quoted in ref 5.

empirical lattice energy encompasses any errors which appear systematically in Born–Haber cycles for all these compounds, as well as non-Coulombic contributions to the lattice energies.[21] All lattice energies for other compounds calculated by eq 3 (last column in Table IV) have been corrected by $1517.1/1436.1 = 1.0564$.

For the calculation of other lattice energies in Table IV, lattice parameters, a, for eq 3 were taken from published values.[8] The change in Madelung constant has been estimated for various chloride z parameters[11] and the calculated values of A for each compound Cs_2NaMCl_6 are tabulated for information in Table IV.

The results of these thermochemical cycles yield the sum of the first three ionization potentials, $\Sigma I(M)$, for most of the rare earth elements. In Table V these values have been converted into electron volts. Johnson's literature values[6] for the first and second ionization potentials have been used to calculate the third ionization potentials, I_3, of these rare earths.

Appropriate Born–Haber cycles may also serve to calculate hydration properties of ions. The heat of hydration (not to be confused with the process of eq 2 which unfortunately bears the same name) of the ions corresponding to Cs_2NaMCl_6 may be derived from either of the following relationships

$2\Delta H$(hyd, Cs^+) $+ \Delta H$(hyd, Na^+) $+$

$\quad \Delta H$(hyd, M^{3+}) $+ 6\Delta H$(hyd, Cl^-) $=$

$\quad \Delta H_f{}^\circ(Cs_2NaMCl_6$, aq) $- 2S(Cs) -$

$\quad S(Na) - S(M) - 3D(Cl) - 2I(Cs) -$

$\quad I(Na) - (I_1 + I_2 + I_3)(M) - 6E(Cl)$ (5)

$= U_0(Cs_2NaMCl_6) -$

$\quad 10RT + \Delta H^\circ(soln, Cs_2NaMCl_6)$ (6)

These two equations must yield identical results, since eq 5 reduces to eq 6 by substitution of eq 4 and by use of the definition

$\Delta H_f{}^\circ(Cs_2NaMCl_6$, aq) $=$

$\quad \Delta H_f{}^\circ(Cs_2NMaCl_6$, c) $+ \Delta H^\circ(soln, Cs_2NaMCl_6)$

In order to consider the heats of hydration for the rare earth ions independently of the other ions in Cs_2NaMCl_6, it is necessary to separate the heats of hydration of the alkali halides into "cation" and "anion" contributions. The most useful approach is to separate the individual ionic contributions so that "absolute" values will be generated for each ion. Halliwell and Nyburg have reduced this problem to the determination of the enthalpy of hydration of the proton.[22] They recommend a "best value" of ΔH(hyd, H^+, abs) $= -260.7 \pm 2.5$ kcal/mol. Consistent with this reference value, and with experimental enthalpies as tabulated by Halliwell and Nyburg, "absolute" hydration enthalpies have been calculated for Cs^+, Na^+, and Cl^- as -66.1, -97.0 and -86.8 kcal/mol, respectively.[18] Using these values and eq 6, "absolute" hydration enthalpies have been calculated for the rare earth ions and are tabulated in Table V.

(21) Propagation of all the errors in other terms of this cycle yields an estimated standard deviation of ±6.7 kcal/mol for this lattice energy. However, if only the errors of terms not constant for all elements M, those entries in Table IV other than "Misc." are propagated, the estimated standard deviation is ±2.4 kcal/mol relative to other lattice energies.

(22) H. F. Halliwell and S. C. Nyburg, Trans. Faraday Soc., 59, 1126 (1963). For alternative values for ΔH(hyd, H⁺), see J. E. Desnoyers and C. Jolicoeur in "Modern Aspects of Electrochemistry," No. 5, J. Bockris and B. Conway, Ed., Plenum Press, New York, N. Y., 1969, chapter 1.
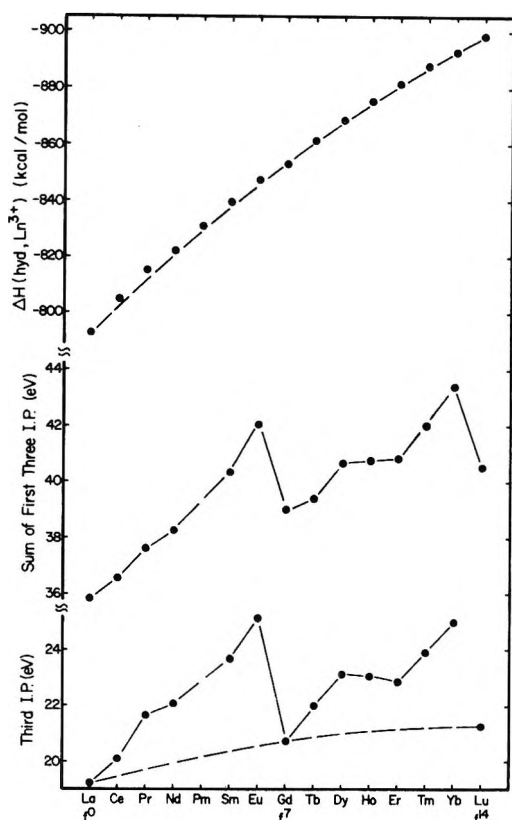
Figure 2. Lanthanide ionization potentials and hydration enthalpies.

Discussion

Both the ionization potentials and the hydration enthalpies of Table V may be compared with other recently published values. For convenience, two such sets of ionization potentials are listed in Table V. Some published values of ΔH(hyd, M^{3+}) based at least in part on experimental values are as follows: La, -806, varying smoothly to Lu, -878;[23] La, -780;[24] Pu, -821.[25] Figure 2 displays the lanthanide ionization potentials and hydration energies as calculated in this research as a function of atomic number, or, more significantly as a function of the number of f electrons in the trivalent ions. The dashed lines are second-degree polynomials fitted to the data points through La, Gd, and Lu.

Ionization Potentials. It should be noted that all three sets of ionization potentials (those calculated in this research, by Faktor and Hanks,[5] and by Johnson[6]) use Born–Haber cycles with nearly identical values for I_1 and I_2. The use of such common data facilitates comparison of the three sets of I_3 values (in fact, the author chose ionization potentials quoted by Johnson[6] wherever possible, not only because of their detailed documentation, but also for consistency). Neglect of conflicting ionization potentials from alternative sources misleadingly implies an accuracy of I_3 values as good as the mutual agreement found. For example, the value of I_2(La) tabulated by Moore[26] is 11.43 ± 0.07 eV,

differing from the value quoted by Johnson[6] in Table V by 0.37 eV. It is suggested, therefore, that tabulated I_3 values are not accurate to better than ± 0.4 eV, although relative errors may be less than ± 0.2 eV.

The ionization potentials calculated from data on the chlorocomplex compounds have some attributes which suggest their preferential use. The lattice energies used in their calculation are generated from the Born–Landé equation, based upon a single set of structurally similar, highly symmetric, predominantly ionic compounds. In addition, only a single empirical correction factor of 1.0564 is required for these lattice energies, and it is generated from the relatively trustworthy ionization potentials of lanthanum.

The deviation of I_3's from the dashed curve in Figure 2 may be interpreted as the effect of exchange energy on an $f^{n+1} \to f^n$ ionization. This interpretation, drawn from its equivalent for d electrons,[27] has been discussed in more detail by Johnson.[6] The exchange energy is proportional to the number of pairs of parallel spins, $n(n - 1)/2$. Upon ionization of $f^{n+1} \to f^n$, an exchange energy of

$$(n + 1)n/2 - n(n - 1)/2 = n$$

is lost; this loss is reflected in the increasing deviation of I_3 from the dashed line as n $\to$ 6. The transition $Gd^{2+} \to Gd^{3+}$ ($f^8 \to f^7$), however, involves no exchange energy since the lost electron had spin antiparallel to all the others; because no exchange energy is lost on this ionization, I_3 is low, like that of $La^{2+} \to La^{3+}$. Subsequent I_3 values show the effect of increasing loss of exchange energy, until the final ionization, $Lu^{2+} \to Lu^{3+}$, which also involves no loss of f electron exchange energy.

Heats of Hydration. Error limits for ΔH(hyd) of Table V can be accurately estimated. The *absolute* accuracy of ΔH(hyd, La^{3+}) is estimated as ± 11 kcal/mol by propagating estimated standard deviations of all terms in eq 5. The *relative* accuracy of each ΔH(hyd) with respect to the others, estimated by lumping all constant terms or by use of eq 6, is ± 2 kcal/mol.

The thermodynamics of hydration and similar complexing processes are unrelated to ionization potentials, of course, since these processes encompass no oxidation steps. The energetics of these transformations are functions of ionic size, ligand polarizability and electronegativity, coordination number, and ligand field. It is desirable to study these functional relationships independently of each other.

There is little agreement with respect to the "coor-

(23) S. L. Bertha and G. R. Choppin, *Inorg. Chem.*, **8**, 613 (1969).

(24) J. P. Hunt, "Metal Ions in Aqueous Solution," W. A. Benjamin, New York, N. Y., 1963.

(25) A. D. Jones and G. R. Choppin, *Actinides Rev.*, **1**, 311 (1969).

(26) C. E. Moore, *Nat. Bur. Stand.* (*U. S.*) *Circ.*, **No. 467**, 3 (1958).

(27) D. A. Johnson, "Some Thermodynamic Aspects of Inorganic Chemistry," Cambridge University Press, Cambridge, England, 1968, pp 130–132.

dination number" of rare earth ions in aqueous solution. The complicated variation of many thermodynamic complexation processes as a function of lanthanide atomic number has been used to invoke a relatively sudden change in hydration number of the lanthanide ions near the midpoint of the series.[3,23,28] However, there is fundamental thermodynamic evidence (the aqueous ionic entropies) which shows no such distinct change in coordination number.[29] The enthalpies of hydration, as calculated in this research and plotted in Figure 2, should reflect any such coordination change. The bicuspid shape of the hydration enthalpy vs. atomic number plot is much like that of the lattice energy–atomic number relationship (for which there is no coordination change, the bicuspid shape being caused by the similar variation in lattice parameter of Cs_2Na-MCl_6 with atomic number).[8] Thus, hydration enthalpies of the lanthanide ions do not show a discrete change in hydration number. (This conclusion is supported by Figure 1, since the heat of solution is the difference between hydration enthalpy and lattice enthalpy. Heats of solution of other isomorphic lanthanide compounds vary in a similarly smooth fashion.[3,23])

Effect of Ligand Field. It is tempting to ascribe the more exothermic thermodynamic properties of lanthanide ions with nonspherical f-electron subshells to a small ligand-field stabilization. Such a stabilization is suggested by the double-humped plots of lattice energy (not shown) and hydration enthalpy (Figure 2), plots similar to the well known stabilizations observed for the d-transition metal ions. With respect to the smooth curve through La^{3+}, Gd^{3+}, and Lu^{3+}, both the lattice energy and the hydration enthalpy of Cs_2NaMCl_6 become most exothermic at about Pr^{3+} (f^2) by about 4 kcal/mol and at Dy^{3+} (f^9) by about 1.4 kcal/mol. These variations are traceable to the similar variation in lattice parameter mentioned above;[8] any ion with nonspherical electron distribution favors certain spatial orientations of electron orbitals and ligands which minimize mutual repulsions and which permit the ligands to be drawn closer than they would if the same electrons were spherically distributed. A smaller ionic radius is observed for such ions, from which the thermodynamic "stabilizations" follow. It is inappropriate to consider the magnitude of such an effect as a measure of ligand-field stabilization.[30]
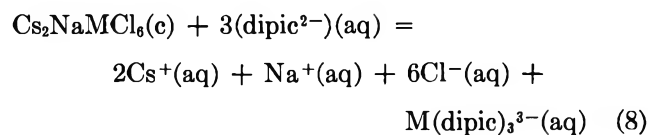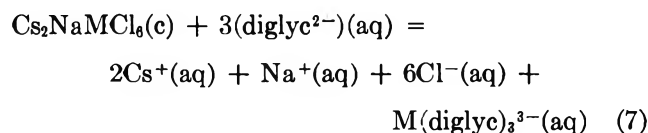
A second approach is to compare thermodynamic cycles for ions of similar size but of different electronic configurations. The ions Y^{3+} (f^0) and Ho^{3+} ($4f^{10}$) have very similar ionic radii (0.900 and 0.901 Å), as do the ions Ce^{3+} ($4f^1$) and Pu^{3+} ($5f^5$) (1.01 and 1.01 Å).[31] For both pairs of ions, the heat of hydration is more exothermic for the ion with more f electrons. Although one might surmise that this is due to the participation of f electrons in bonding, and to the greater participation of 5f than of 4f electrons, the data are neither extensive enough nor accurate enough to permit such a conclu-

sion. In particular, the heats of hydration depend for their calculation on lattice energies, which are sensitive functions of ionic radii and of n, the repulsive constant.

A final approach, by which the effect of varying hydration number may be circumvented, is to compare the heat of transformation from a series of isostructural lanthanide salts with solvated species in which the inner coordination sphere is saturated by polydentate ligands. The enthalpies of formation from the aquated ions have been measured for the $1:n$ complexes of the diglycolate and dipicolinate ions ($n = 1, 2, 3$) and for the $1:1$ complex of the diethylenetriaminepentaacetate ion (DTPA).[4,32] The former ligands are each tridentate, and since it is probable that the $1:3$ complexes of both ligands are 9-coordinate,[33] it is likely that these $1:3$ complexes have no water molecules in the inner coordination sphere. Likewise, it is possible that the DTPA ion saturates the inner coordination sphere.[4] Therefore, if the heats of solution of a series of isostructural rare earth salts are added to the heats of complexing with these ligands, the intermediate state (the aqueous ions, with varying states of hydration) can be eliminated.

Staveley, *et al.*, measured the heats of solution of the hydrated ethyl sulfates and bromates of most of the lanthanide elements.[3] When their heats of solution were added to the heats of complexing with the ligands described above, the more negative enthalpies for lanthanides *other than* La, Gd, and Lu were attributed to ligand-field stabilizations of a few hundred calories.[3,4]

The heats of solution of the chloro complex compounds Cs_2NaMCl_6 ought to be more suitable than the corresponding heats measured by Staveley, *et al.*, because the structures of Cs_2NaMCl_6 are clearly identical, they can be prepared in high purity, and the heats of solution were more reproducible and free from the corrections necessary for included mother liquor. By adding the heats of solution (Table III) to the $\Delta \mathcal{K}_3°$ values defined by Grenthe,[32] and to the ΔH_c values defined by Carson, *et al.*,[4] heats of transformation for the reactions

$$Cs_2NaMCl_6(c) + 3(diglyc^{2-})(aq) =$$
$$2Cs^+(aq) + Na^+(aq) + 6Cl^-(aq) +$$
$$M(diglyc)_3^{3-}(aq) \quad (7)$$

$$Cs_2NaMCl_6(c) + 3(dipic^{2-})(aq) =$$
$$2Cs^+(aq) + Na^+(aq) + 6Cl^-(aq) +$$
$$M(dipic)_3^{3-}(aq) \quad (8)$$

(28) I. Grenthe, *Acta Chem. Scand.*, **18**, 293 (1964).

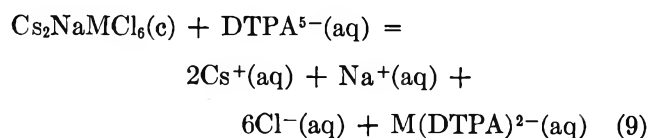(29) R. J. Hinchey and J. W. Cobble, *Inorg. Chem.*, **9**, 917 (1970).

(30) G. Beech, *Quart. Rev. (London)*, **23**, 410 (1969).

(31) R. D. Shannon and C. T. Prewitt, *Acta Crystallogr., Sect. B*, **25**, 925 (1969); **26**, 1046 (1970).

(32) I. Grenthe, *Acta Chem. Scand.*, **17**, 2487 (1963).

(33) N.-G. Vannerberg and J. Albertsson, *ibid.*, **19**, 1760 (1965).

and

$$Cs_2NaMCl_6(c) + DTPA^{5-}(aq) =$$
$$2Cs^+(aq) + Na^+(aq) +$$
$$6Cl^-(aq) + M(DTPA)^{2-}(aq) \quad (9)$$

can be calculated. Each of these composite reactions meets the conditions set by Staveley, et al., for observation of ligand-field stabilization. Plots of ΔH_7, ΔH_8, and ΔH_9 vs. lanthanide atomic number (Figure 3) may be compared with the corresponding graphs of Staveley, et al. (Figures 1 and 2, ref 3), and with Carson, et al. (Figure 2, ref 4). Not only is there no bicuspid depression to any of the graphs, but there is no trend simple enough to draw a smooth curve within estimated error limits.

The possibility remains that the nonlinear contraction of lanthanide ionic radii is responsible for the apparent ligand-field stabilizations observed by Staveley, et al.,[3] and by Carson, et al.[4] In any event, since the splitting of ground-state f electron configurations by ligand fields does not necessarily produce thermochemical stabilization,[30] and since ionic radius contractions can produce enthalpy effects much greater than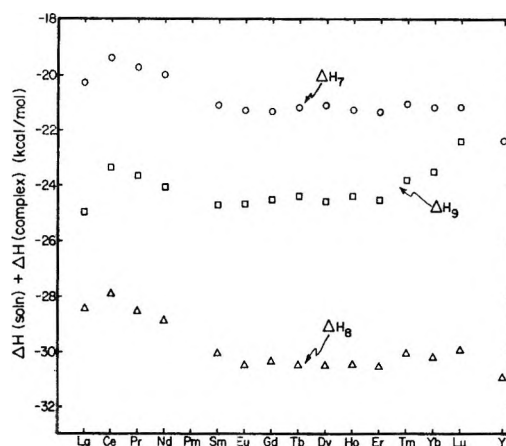 expected ligand-field stabilizations, it is perhaps inappropriate to consider that thermochemical variations which have been observed in lanthanide complexes are caused by true ligand-field effects.

Figure 3. Heats of complexing of $Cs_2NaLnCl_6$ with diglycolate, DTPA, and dipicolinate.

Coexistence of Liquid Phases in Calcium–Ammonia Solutions[1]

by Henry Teoh, P. R. Antoniewicz, and J. C. Thompson*[1]

Department of Physics, University of Texas at Austin, Austin, Texas 78712 (*Received May 11, 1970*)

Publication costs assisted by the Robert A. Welch Foundation

We report here a determination of the shape and the critical point of the coexistence curve of calcium–ammonia solutions. The conductivities of these solutions were measured as a function of temperature and the phase separation located by changes in slope of the conductivity curves. These solutions possess a parabolic curve as do alkali metal–ammonia solutions. The presence of such a curve, rather than the more common cubic curve, is believed to derive from the screening present in systems of charges. The consolute concentration was found to be 1.68 mol % of metal and the critical temperature to be 290°K. A metal–nonmetal transition is also evident in calcium–ammonia solutions and is similar to that observed in solutions of monovalent metals.

Introduction

The metals which can easily be dissolved in liquid ammonia are lithium, sodium, potassium, rubidium, cesium, calcium, strontium, barium, ytterbium, and europium.[2,3] The solutions exhibit a liquid–liquid phase transition which is correlated with a metal-nonmetal transition.[4-6] Metal–ammonia solutions of low metal concentration are inky blue in color and electrolytic in nature, whereas the concentrated solu-

tions are bronze colored and possess metallic properties. At intermediate concentrations and at temperatures below their consolute or critical temperatures, these solutions separate into two coexisting liquid phases, one phase being metallic in nature and the other nonmetallic.[5] By measuring the electrical conductivity of these solutions as a function of temperature, Kraus[7] was the first to determine accurately the boundary of the mixed phase region of sodium–ammonia solutions. Since then, the phase diagrams of sodium–, potassium–, and lithium–ammonia solutions have been investigated by Loeffler,[8] Frappe,[9] Patterson,[10] Sienko,[4] and a host of others. The critical concentrations and temperatures of sodium–, lithium–, and potassium–ammonia solutions are shown in Table I. Cesium solutions do not

Table I: Critical Points of Metal–Ammonia Solutions

Metal ion	Consolute concentration, mol % metal	Critical temp, °K	Critical exponent β
Li$^+$	4.51	209.7	1/2.1
Na$^+$	4.12	231.5	1/2.1
K$^+$	4.17	202.9	1/2.0
Cs$^+$	None	None	None
Ca^{2+}	1.68	290.0	1/2.2

show a phase separation, and the miscibility gap of rubidium–ammonia solutions, if it does exist, is so close to the freezing point of ammonia that it has not yet been detected.[10] Although the phase diagrams of alkali metal–ammonia solutions have been well established, little work has been done on alkaline earth metal–ammonia systems. The most extensively studied of the solutions of divalent metals is that of calcium, and there are indications that there may be considerable differences from the alkali metal–ammonia solutions. In particular, data from Wa She Wong,[11] Jolly,[12] Okabe,[13] and Oertel, et al.,[2b] show the critical temperature of calcium–ammonia solutions to be much higher than those of the alkali metal–ammonia solutions. Indeed, Jolly[12] reported the critical point to be above room temperature on the basis of visual observations.

The present investigation was undertaken to determine the critical temperature and the nature of the liquid–liquid coexistence curve in solutions of calcium in ammonia so that the phase separation and associated metal–nonmetal transition might be compared with similar phenomena in solutions of monovalent metals.

Experimental Section

There are many methods of detecting a phase boundary in metal–ammonia solutions. Among the most common techniques are (a) vapor pressure methods,[12–15] (b) visual observations,[10,12] (c) sound speed,[16] and (d) electrical conductivity measurements.[2b,7,8,12] In vapor

pressure methods, the accuracy may be subject to question because of the evolution of hydrogen in the reaction of metal in ammonia. Vapor pressure measurements for calcium–ammonia solutions reported by Jolly,[12] Okabe,[13] and Marshall and Hunt[15] are not in good agreement. Visual determination of the phase separation has the disadvantage that the solutions, especially calcium–ammonia solutions, tend to cling to the walls of the sample cell. Also, as the temperature of the solutions is raised, the colors of the two phases become more alike, so that the phases are increasingly difficult to distinguish. The velocity of sound changes abruptly when the solution undergoes a transition from a single phase to a mixed phase region. However, Bowen[16] reported that in some cases the change in sound speed occurred at temperatures above the accepted phase boundary.

The differing conduction mechanisms[6] in the various phases of the metal–ammonia solutions provide the basis for the most convenient means of determining the phase boundary. As shown in Figures 2 and 3, a sharp transition in the electrical conductivity occurs at the phase boundary. Kraus and Lucasse[7] obtained the first accurate phase separation curve for sodium–ammonia solutions by utilizing the transition in the electrical conductivity–temperature curve. Of the above-mentioned techniques, the electrical conductivity measurement was decidedly the most accurate for determining the phase separation and was therefore employed in the present work. Graphs similar to Figures 2 and 3, but on a linear scale, were used to locate phase boundaries. Linear plots show more detail but require more journal space.

Prior to the present experiment, most of the data for the liquid–liquid phase separation were taken below 240°K. The phase separation at higher temperatures has never been carefully investigated, primarily due to

(3) W. C. Jolly, "Inorganic Chemistry," Vol. I, Interscience, New York, N. Y., 1959.

(4) M. J. Sienko, "Metal–Ammonia Solutions," W. A. Benjamin, New York, N. Y., 1963, p 23.

(5) J. C. Thompson, Rev. Mod. Phys., **40**, 704 (1968).

(6) M. H. Cohen and J. C. Thompson, Advan. Phys., **17**, 856 (1968).

(7) C. A. Kraus and W. W. Lucasse, J. Amer. Chem. Soc., **44**, 1949 (1922).

(8) D. E. Loeffler, Ph.D. Dissertation, Stanford University, Palo Alto, Calif., 1949.

(9) G. Frappe, Ph.D. Dissertation, Universite de Lille, Lille, France, 1958.

(10) A. Patterson, Jr., and P. D. Schettler, Jr., J. Phys. Chem., **68**, 2865 (1964).

(11) W. S. Wong, Ph.D. Dissertation, University of California, Berkeley, Calif., 1966.

(12) W. C. Jolly, "Metal–Ammonia Solutions," W. A. Benjamin, New York, N. Y., 1963, p 174.

(13) T. Okabe, Kogyo Kagaku Zasshi, **60**, 1438 (1957).

(14) C. A. Kraus, J. Amer. Chem. Soc., **30**, 653 (1908).

(15) P. R. Marshall and H. Hunt, J. Chem. Eng. Data, **7**, 399 (1962).

(16) D. E. Bowen, J. C. Thompson, and W. E. Millett, Phys. Rev., **168**, 114 (1968).

experimental difficulties. The difficulties are (1) above 240°K, the vapor pressure of the solution is greater than atmospheric pressure, thereby causing difficulty in containing the sample; (2) the rate of decomposition increases at higher temperatures. In the present work, the problem of containment of these solutions at elevated temperatures was overcome by applying external pressures to the sample cell. The vapor pressure of the system was monitored by means of a Reid vapor pressure gauge, and He gas was applied manually to balance the internal pressure. The vapor pressure of these solutions follows closely that of pure ammonia. To minimize decomposition, which can become significant at elevated temperatures,[17] rigorous cleaning was employed throughout the experiment. First, the glassware was treated with 30% ammonium fluoride; it was heated and dried in an oven, followed by rinsing with a cleaning solution consisting of 5% hydrofluoric acid, 30% nitric acid, 5% Alconox, and 60% distilled water. The cell was then rinsed with distilled water several times and dried in a vacuum oven. Finally, the cell was soaked in dilute sodium–ammonia solution overnight to remove any remaining contaminants. The distillation of ammonia was conducted *in vacuo*, and the calcium metal was cleaned and weighed in an He-filled glove box. The solution was prepared directly in the sample cell and then frozen in liquid nitrogen. It was transferred to the pressure can in an He atmosphere. Data could be taken for 5 hr without appreciable decomposition.

As shown in Figure 1, the solution was contained in a thick-walled cylindrical cell 7.5 cm long and 1 cm in diameter. The electrical conductivity was measured by a standard electrode technique using a 2-kHz sine wave across the top and bottom electrodes. The voltage drop across the different pairs of electrodes 1, 2, and 3 was measured by means of a Tektronix 502A oscilloscope. The electrodes were gold-plated Kovar, so as to minimize decomposition and to avoid non-Ohmic contact[18] with the solution. The cell was calibrated for conductivity determinations by measuring the conductivity of a saturated NaCl solution at room temperature. Errors in $\sigma(T)$ amounted to a few per cent.

Temperature control was provided by Dry Ice and alcohol baths and thermistor circuits;[19] higher temperatures were achieved by means of a Variac-controlled heater tape wrapped around the pressure can. The temperature was measured by a calibrated copper–constantan thermocouple placed next to the sample cell. The relative uncertainty of the sample temperature was determined to be less than ±0.3°K.

Since the phase boundary was undefined, the sample, initially at about 210°K, was warmed to a homogeneous region above the coexistence curve. One can determine whether the solution is above the phase boundary by comparing the voltage drop across the pairs of electrodes 1–2 and 2–3 (Figure 1). The homogeneous
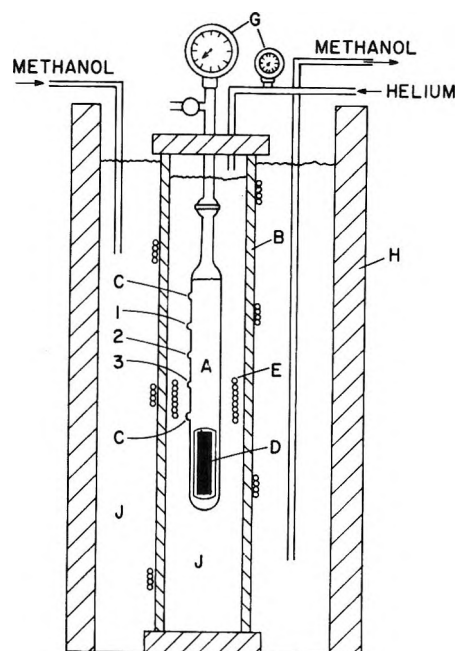

Figure 1. The conductivity measuring system for determining the phase separation of calcium–ammonia solutions: A is the conductivity cell with current electrodes C and voltage electrodes 1, 2, and 3. D is a glass-enclosed magnetic stirrer, and E is the stirrer coil. The cell is enclosed in an aluminum pressure bomb B, and the relative pressures are monitored from the pressure gauges G. Temperature control is maintained by alcohol bath indicated by J. The entire system is contained in a styrofoam Dewar H.

solution was then cooled down slowly, and the phase separation was located by changes in slope of the conductivity curves. Throughout the experiment, the solution was stirred at regular intervals by means of a glass-enclosed magnetic stirrer placed at the bottom of the sample cell.

Several experiments with lithium–ammonia solutions in the mixed phase region were performed to check the system. The phase transition and values of the electrical conductivity were in good agreement with those obtained by previous investigators.[10,20,21]

Results

Figure 2 shows typical cooling curves for the electrical conductivity of calcium–ammonia solutions near the critical temperature T_c. For solutions on the metal-rich side of the phase boundary, the conductivity *vs.* temperature curves are shown in Figure 3. Two kinds of information may be extracted from such curves: (1) the conductivity of the single phase shown on the

(17) D. C. Jackman and C. W. Keenan, *J. Inorg. Nucl. Chem.*, 30, 2047 (1968).

(18) R. D. Nasby and J. C. Thompson, *J. Chem. Phys.*, 49, 969 (1968).

(19) D. S. Kyser and J. C. Thompson, *ibid.*, 42, 3910 (1965).

(20) R. D. Nasby, Ph.D. Dissertation, University of Texas, Austin, Texas, 1968.

(21) J. A. Morgan, R. L. Schroeder, and J. C. Thompson, *J. Chem. Phys.*, 43, 4494 (1965).
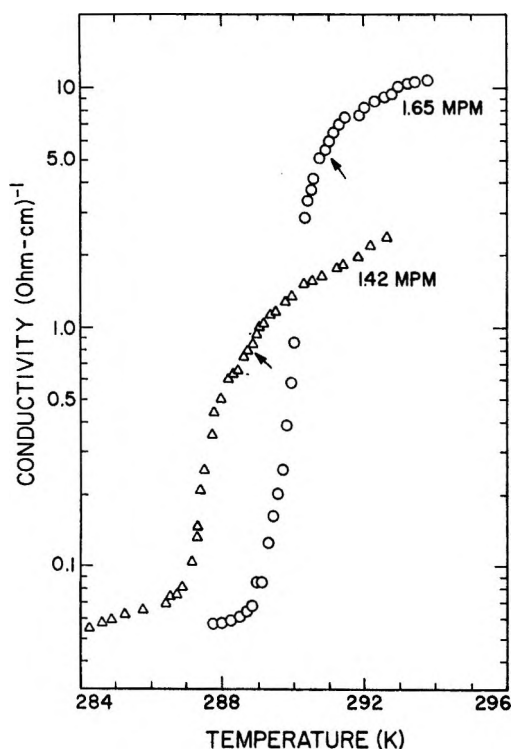
Figure 2. Typical conductivity vs. temperature curves near the critical temperature. The numbers on the right-hand edge of each curve give the metal concentrations in mpm. The arrows mark the appearance of a second phase.
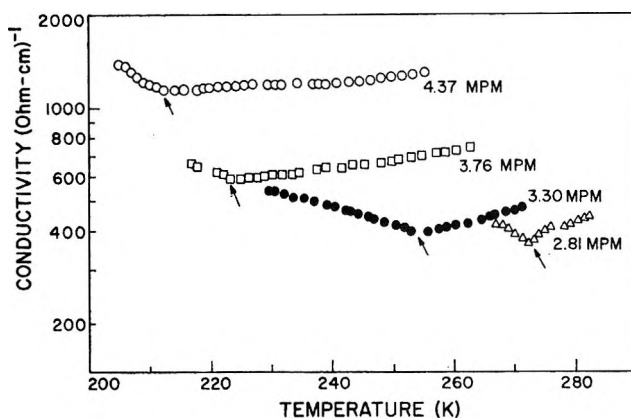

Figure 3. Conductivity of calcium–ammonia solutions vs. temperature for concentrations on the metal-rich side of the phase boundary. The concentrations, expressed in mpm, are listed on the right of each curve.
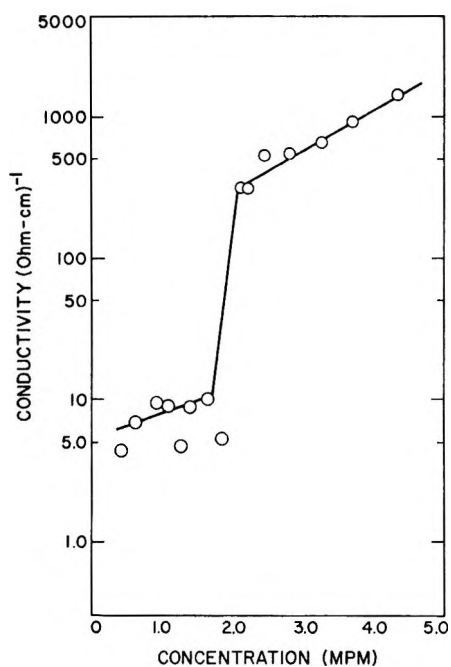

Figure 4. Conductivity of calcium–ammonia solutions as a function of concentration at 293°K. These data were all taken at temperatures above the phase separation. The rapid rise in conductivity near 2.0 mpm is the result of electron delocalization (ref 5).

right of the figure, and (2) the coexistence curve of the liquid–liquid phase separation from the locus of the transition points. We will first discuss the conductivity of the single phase as a function of temperature and concentration. Starting from the high temperature at the right side of Figures 2 and 3, the conductivity decreases with decreasing temperatures; i.e., it has a positive temperature coefficient of conductivity as do other metal–ammonia solutions.[2b,21] Recently, Ashcroft and Russakoff[22] explained the strong variation of the conductivity with increasing metal concentration by a simple model of electrons interacting with solvated metal ions and ammonia molecules. They showed the rapid increase in conductivity with increasing metal concentration to be due to both the decrease in scattering from the solvated ion and the rapid depletion of unbound ammonia molecules. There is presently no model which produces the positive temperature coefficient through it is common to many low-electron-density conductors.[23]

Evidence for a metal–nonmetal transition[5] in calcium–ammonia solutions is shown in the conductivity vs. concentration curve at 293°K (Figure 4). The abrupt change in the concentration dependence of conductivity at about 2 mpm[24] is indicative of such a transition. All the data in Figure 4 were taken above the miscibility gap. Figure 4 does not refer to a first-order phase change, but to a metal–nonmetal transition in which the valence electrons go from localized states

(solvated electron) to delocalized states (metallic, free electron). There is an enormous difference in the conductivity in the two cases, as the range of the electron wave function goes from finite to infinite. The free electrons then "short circuit" the system, whereas in the phase separation the two phases are in series. The scatter of the data is probably due to fluctuations, calibration errors, and some decomposition. The

(22) N. W. Ashcroft and G. Russakoff, Phys. Rev. A, 1, 39 (1970).

(23) R. S. Allgaier, Phys. Rev., 185, 227 (1969).

(24) Mol % of metal (mpm) = (mol of metal) × 100/(mol of metal + mol of NH₃).

metal–nonmetal (M–NM) transition in solutions of alkali metals has been discussed by several authors.[4–6] The conductivity change in the alkali–metal solutions is generally larger than observed here but appears to decrease as temperature increases. The change seen in Figure 4 is consistent with that to be expected for alkali metals at the same temperature. Thus, the only difference between monovalent and divalent solutions discernible in the present data is the lower ion concentration: 2.00 mpm in the latter compared to about 4 mpm in the former. The electronic concentrations are comparable; however, Cohen and Thompson[6] have suggested that these results are to be expected because the M–NM transition is primarily due to the overlap of wave functions of solvated electrons and the ions play only a secondary role.

Since the transition from a nonmetal to a metal is associated with the phase separation,[6] one would expect the separated phases to lie in the same concentration range. For solutions near 1.7 mpm (Figure 3), the conductivity drops abruptly on cooling and the phase separation is taken to occur at the temperature at which the change of slope first occurs. For solutions on the metal-rich side of the coexistence curve, the changes in slope as shown in Figure 4 indicate a phase separation which leaves a higher concentration phase between the electrodes. The phase diagram obtained from the transition points is shown in Figure 5 and is in good agreement with data reported by Wa She Wong[13] and by Schroeder, Oertel, and Thompson.[2b] The critical temperature obtained for calcium–ammonia solutions is 290°K and the consolute concentration is 1.68 mpm; see Table I for a comparison.

Discussion

It should be noted that although metal–ammonia solutions are not binary liquids in the conventional sense, the two different kinds of liquids may be, in a sense, regarded as a binary liquid mixture. The important difference being that, in metal–ammonia solutions, the two separate phases are dilute solutions of one component in the other.[4]

Recently there has been considerable discussion of the shape of the coexistence curve in the neighborhood of the critical point. Behavior near the critical point may be described in terms of an order parameter, which is defined by Kadanoff[25] as a numerical measure of the amount and kind of ordering in the neighborhood of the critical point. The choice of the order parameter then depends on the nature of the transition. Thus for liquid–vapor, the order parameter is density; for ferromagnetism, it is magnetization; and for a binary liquid, it is concentration. The general shape of the coexistence curve may be expressed by

$$(x_1 - x_2) = A(T_c - T)^\beta \qquad (1)$$

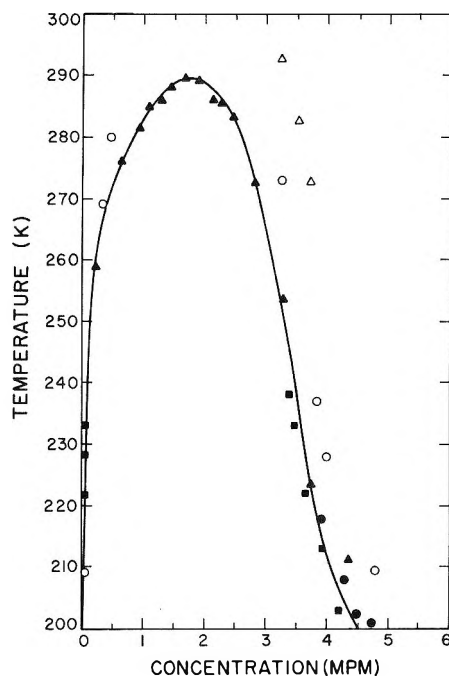where x_1, x_2 are the order parameters, T is the tempera-

Figure 5. The coexistence curve of calcium–ammonia solutions. The data reported by Jolly[12] are represented by O; by Wa She Wong,[11] ■; by Oertel,[2] ●; by Okabe,[13] △; and those obtained from this work are represented by ▲.

ture of the two phases, T_c is the critical temperature, A is a constant, and β is the critical exponent. As shown in Figure 6, a logarithmic plot of $(T_c - T)$ vs. $(x_1 - x_2)$ fixes the value of $\beta = 1/2.2$ for calcium–ammonia solutions. The values of β (Table I) for the monovalent metal–ammonia solutions indicate that the coexistence curves are parabolic[4] rather than the cubic (i.e., $\beta = 1/3$) shape obtained for most binary liquid systems[26–28] and other phase separation phenomena. Other exceptions known at present are solutions of metals in molten salts such as Bi in BiCl₃ which are also found to have parabolic coexistence curves.[4] In his study of critical phenomena of binary liquid mixtures, Prigogine[29] pointed out that the condition for stability in these systems is given by the following relations

$$\left(\frac{\partial^2 g}{\partial x^2}\right) = 0; \quad \left(\frac{\partial^3 g}{\partial x^3}\right) = 0; \quad \left(\frac{\partial^4 g}{\partial x^4}\right) > 0 \qquad (2)$$

where g is the molar free energy and x is the concentration. Rowlinson[30] showed that if the fourth derivative of the molar free energy $(\partial^4 g/\partial x^4)$ near the critical

(25) L. P. Kadanoff, W. Gotze, D. Hamblen, R. Hecht, E. A. S. Lewis, V. V. Palcianskes, M. Rayl, J. Swift, D. Aspines, and J. Kane, Rev. Mod. Phys., 39, 395 (1967).

(26) E. A. Guggenheim, J. Chem. Phys., 13, 253 (1945).

(27) B. H. Zimm, J. Phys. Colloid Chem., 54, 1306 (1950).

(28) D. Atack and O. K. Rice, J. Chem. Phys., 22, 382 (1954).

(29) I. Prigogine and R. Defay, "Chemical Thermodynamics," Longmans, Green and Co., New York, N. Y., 1965.

(30) J. S. Rowlinson, "Liquid and Liquid Mixtures," Butterworths, Washington, D. C., and London, 1959.

point is taken as the first nonvanishing term in a Taylor's series expansion of the free energy as an analytic function of the concentration, then

$$(x_1 - x_2) \propto (T_c - T)^{1/2} \qquad (3)$$

If $(\partial^{2n} g / \partial x^{2n})$ is taken as the first nonvanishing term in the Taylor's expansion, then $\beta^{-1} = 2n - 2$, where n is any integer equal to or greater than 2. These general results do not agree with numerical calculations presumably because of the absence of analyticity. An exact solution based on a two-dimensional lattice gas model gives $\beta = 1/8$, while a three-dimensional Ising model gives β near $1/3$. In contrast with these results, the molecular field theory and the simple theory of van der Waals predict coexistence curves that are parabolic.[4]

In an attempt to explain the nature and cause of the phase separation phenomena in metal–ammonia solutions, Pitzer[31] proposed that the ammonia be regarded as a dielectric medium in which the metal can undergo a liquid–vapor condensation below the critical temperature. The ammonia-rich side of the two phases was pictured to correspond to the gaseous atomic metal with no metallic properties observed, and the metal-rich side to the pure liquid metal. Krumhansl[32] has discussed the relation between a thermodynamic phase transition and the metal–nonmetal transition of dense vapors. Associated with the change of electronic configuration involved in the transition from a metallic to a nonmetallic state, there is sufficient change in the free energy to influence the thermodynamic properties of the system. There is no way to ascertain whether the phase separation is triggered by the metal–nonmetal transition or *vice versa*. Patterson, *et al.*,[33] proposed an ionic lattice model with long-range forces for alkali metal–ammonia solutions. By expressing the chemical potential of both components in both phases as a function of concentration and by determining the phase points by Maxwell equal-area construction, they were able to get a good fit for the coexistence curves of metal–ammonia solutions. However, an important term, namely the energy of the electron gas, was not included in the total energy. Mammano and Sienko[34] have shown that the electron energy is significant in the stabilization of $Li(NH_3)_4$ compound and it cannot be neglected here. In separate work, Widom[35] has pointed out that systems with parabolic coexistence curves would require each molecule to have an infinite number of neighbors or that the intermolecular forces are of infinite range.[4] The cluster formation associated with the phase separation in metal–ammonia solutions which have been discussed in detail by Cohen and Thompson[6] is consistent with Widom's argument.

We agree with Widom that a mean-field approach is required. We believe that it is the assembly of mobile electrons which provide the mean field.[36] A qualitative understanding of the differences between the various
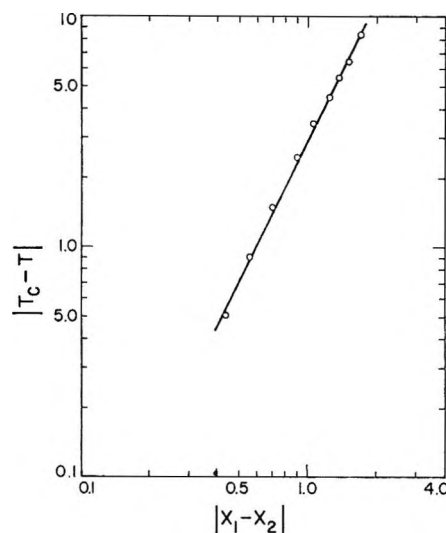

Figure 6. $(x_1 - x_2)$ *vs.* $(T_c - T)$ of the coexistence curve of calcium–ammonia solutions. The value of β obtained here is $1/2.2$.

solutions may be obtained by considering a screened Coulomb attraction between the solvated ions and electrons. The unbound ammonia molecules contribute as a background dielectric medium within which the solvated species move. These solutions cannot be regarded as electrolytes in the conventional sense because of the presence of free electrons, nor can they be considered as simple metals since we cannot disregard the existence of solvated electrons and the background ammonia. A composite of Debye–Hückel (DH) theory[37] for the ionic interaction and the Thomas–Fermi (TF) approximation[38] for the free electrons is indicated. However, the DH screening lengths are impossibly short for ions of finite size, as has been emphasized by Frank.[39] The electron gas provides adequate screening, and one may therefore use the linearized Poisson–Boltzmann equation, for example.

Several qualitative points follow immediately. One expects a dependence of T_c on ionic size and valence, because of the competition between thermal agitation and Coulomb attraction. The electron screening is

(31) K. S. Pitzer, *J. Amer. Chem. Soc.*, **80**, 5046 (1958).

(32) J. A. Krumhansl in "Physics of High Pressures," C. T. Tomizuka and R. M. Emrick, Ed., Academic Press, New York, N. Y., 1965, p 425.

(33) P. D. Schettler, Jr., P. W. Doumaux, and A. Patterson, Jr., *J. Phys. Chem.*, **71**, 3797 (1967).

(34) N. Mammano and M. J. Sienko, *J. Amer. Chem. Soc.*, **90**, 6322 (1968).

(35) B. Widom, *J. Chem. Phys.*, **37**, 2703 (1962).

(36) One of us (J. C. T.) would like to acknowledge a stimulating remark by N. W. Ashcroft.

(37) T. L Hills, "An Introduction to Statistical Thermodynamics," Addison-Wesley, Reading, Mass., 1960.

(38) S. Raimes, "The Wave Mechanics of Electrons in Metals," North-Holland Publishing Co., Amsterdam, 1967.

(39) H. S. Frank in "Chemical Physics of Ionic Solutions," B. E. Conway and R. G. Barradas, Ed., Wiley, New York, N. Y., 1966, p 53.

common to all solutes so that critical concentrations should be approximately independent of solute. Since pressure alters electron density it should affect both T_c and x_c. The very assumption of a mean field approach provides an explanation of the linear shift of T_c with the mole fraction of K substituted for Na.[40] Indeed, each of the preceding predictions is in accord with experiment (see Table I and ref 40). A quantitative working out of the problem is reserved for a later paper.

The qualitative agreement cited in the paragraph above leads one to suspect the M–NM transition to be a property of the ionic system (perhaps that discussed by Kirkwood and Poirier[41]) rather than a consequence of electron correlation.[5,6] Coulomb forces are still

dominant, but electron–electron forces are secondary to electron–ion interactions. It remains to be seen if the observed conductivity changes (Figure 4) can be derived without considering a Mott transition.[42]

In another context, one wonders if ionic fluids may not well stand next after noble gas liquids insofar as simplicity is concerned. It would be of considerable interest to determine if the other critical exponents[25] satisfy the inequalities appropriate to the classical approximation.

(40) U. Schindewolf, *Angew. Chem.*, 7, 190 (1968).

(41) J. Kirkwood and J. C. Poirier, *J. Chem. Phys.*, 58, 591 (1954); see also F. H. Stillinger and R. Lovett, *ibid.*, 48, 3858 (1968).

(42) N. F. Mott, *Phil. Mag.*, 6, 287 (1961).

Infrared Study of the NH₂ "Inversion" Vibration for Formamide

in the Vapor Phase and in an Argon Matrix

by S. T. King

Chemical Physics Research Laboratory, The Dow Chemical Company, Midland Michigan 48640
(Received July 22, 1970)

Publication costs assisted by The Dow Chemical Company

Infrared spectra of formamide in the vapor phase and in an argon matrix have been studied. The NH₂ wagging or "inversion" mode has been observed at 288 cm⁻¹ in the vapor phase spectrum and at 303 cm⁻¹ in the matrix spectrum. The vibrational assignment of monomeric formamide has been discussed.

Introduction

Formamide is the simplest member of the primary amide family. The structure of formamide has some fundamental interest and has been studied by many investigators. The C–NH₂ group in this molecule has been determined to be slightly nonplanar and the "inversion" frequency of the –NH₂ group has been calculated from the satellite intensities in the microwave spectrum by Costain and Dowling.[1] However, the direct observation of this "inversion" mode in the infrared spectrum has not been reported in the literature. The "inversion" of the NH₂ group over a very low potential barrier, such as in the case of formamide,[1] should behave quite differently than that of NH₃ which has a very high inversion barrier.[2] Therefore, it is worthwhile to study the infrared spectra of formamide both in the vapor phase and low temperature inert gas matrix, and to investigate the matrix effect on the NH₂ "inversion" transitions over a very low potential barrier.

The infrared spectrum of formamide in vapor phase has been studied by Evans from 3800 to 450 cm⁻¹.[3] Because of the spectrometer limitations the low "inversion" mode was not observed. The infrared and Raman spectra of formamide in solutions and in liquid phase have been studied by others;[3,4] the normal coordinates have been calculated based on the spectra of the condensed phases.[4] Microwave spectra[1] and nmr spectra[5] have also been studied.

Experimental Section

The formamide sample was obtained from a commer-

(1) C. C. Costain and J. M. Dowling, *J. Chem. Phys.*, 32, 158 (1960).

(2) G. Herzberg, "Molecular Spectra and Molecular Structure," 1945, pp 224, 257.

(3) (a) J. C. Evans, *J. Chem. Phys.*, 22, 1228 (1954); (b) *ibid.*, 31, 1435 (1959).

(4) I. Suzuki, *Bull. Chem. Soc. Jap.*, 33, 1359 (1960).

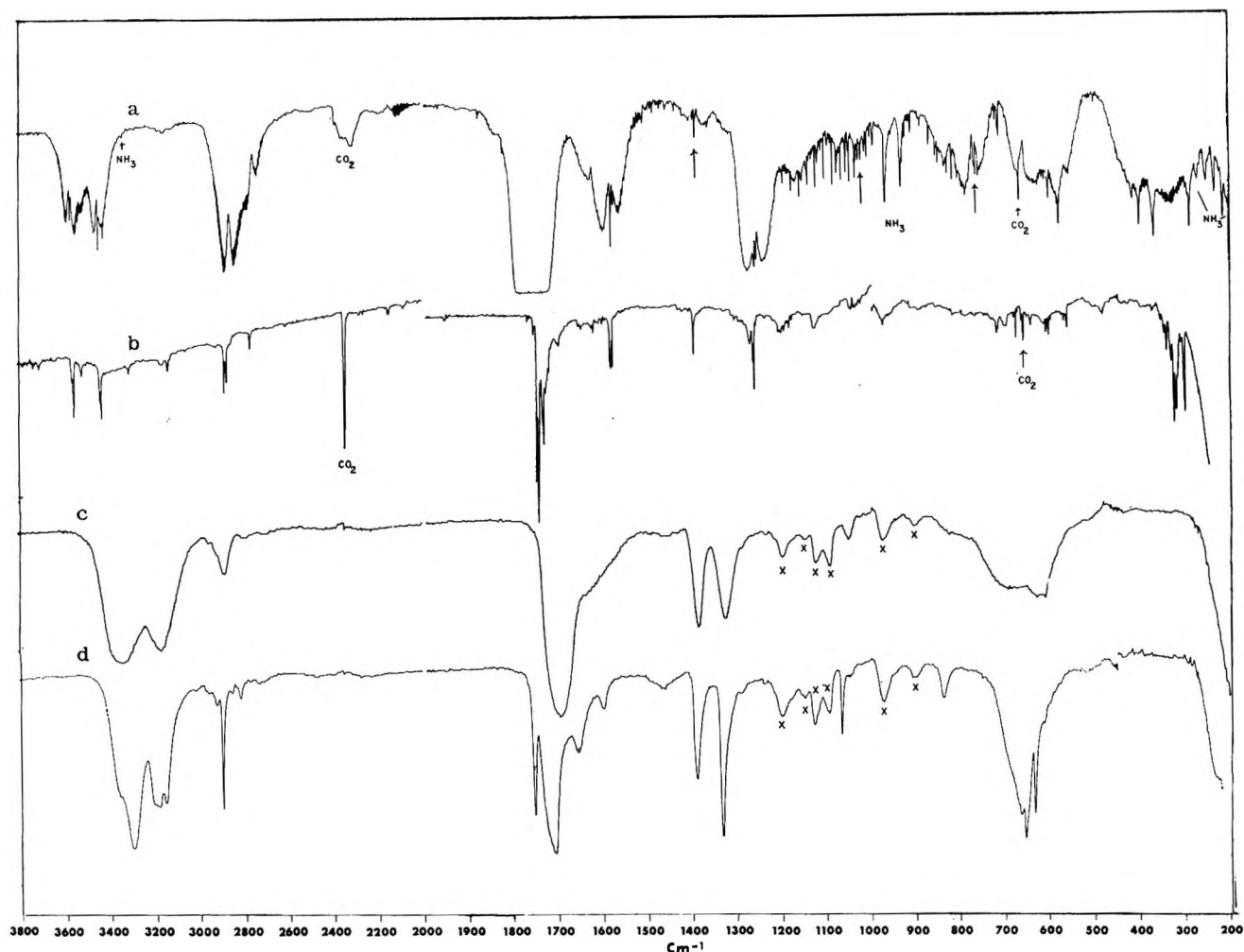(5) H. Kamei, *ibid.*, 41, 2269 (1968); T. Darkenberg and S. Forsen, *J. Phys. Chem.*, 74, 1 (1970).

Figure 1.   Infrared spectra of formamide: (a) vapor phase at 180° in 10-cm⁻¹ CsI cell;   (b) in argon matrix at 20°K;   (c) solid film at 77°K;   (d) solid film at 77°K after annealing.   The bands marked with X are due to Kel-F grease on the windows.

cial source and was stored over molecular sieve.   No water or other impurity in the sample was detected. The infrared spectrum of the vapor phase was recorded in a 10-cm CsI gas cell which was heated to 180° (Figure 1a).   Decomposition of formamide into carbon monoxide and ammonia in the hot gas cell was observed during the experiment.   (The CO_2 bands marked in Figure 1a are due to the air in the hot cell and the oxidation of CO by O_2.)   However, the spectral changes were small and did not affect the interpretation of the spectrum.

The low-temperature matrix spectrum (Figure 1b) was obtained by using a low-temperature cryostat described elsewhere.[6]   The deposition rate of the argon matrix gas was approximately 30 mmol/hr.   The sample deposition rate cannot be measured.   However, the flow rates of both matrix gas and the sample vapor were adjusted so to obtain the best matrix spectrum.   The spectrum of the solid phase (Figure 1c) was obtained in the same cryostat.   The crystalline formamide sample (Figure 1d) was obtained by annealing the frozen liquid.

All spectra were recorded on a Perkin–Elmer Model 225 spectrometer from 3800 to 200 cm⁻¹ which had CsI and CsBr windows.   The calibration of the instrument was checked against NH_3, H_2O, CO, and CO_2 absorption lines.   Reported frequencies should be accurate to ± 1 cm⁻¹.

Infrared Spectra of Formamide and Assignment 3800–1200 cm⁻¹.   Formamide has a total of 12 fundamental vibrations.   The high-frequency fundamental modes in the region 3800–1200 cm⁻¹ of the vapor phase infrared spectrum have been unambiguously assigned by Evans.[3]   Those modes are: 3 NH_2 vibrations (s–ν_{NH_2}–3570 cm⁻¹, a–ν_{NH_2} = 3448 cm⁻¹ (the value quoted in ref 3b is a misprint), δ_{NH_2} = 1580 cm⁻¹), 2 C–H vibrations (ν_{CH} = 2855 cm⁻¹, δ_{CH} = 1390 cm⁻¹), and 2 skeletal vibrations ($\nu_{C=O}$ = 1755 cm⁻¹, ν_{CN} = 1255 cm⁻¹) (Table I). The infrared spectrum of matrix isolated formamide shows only small frequency shifts compared with the vapor phase spectrum.   Large frequency shifts between the isolated phase and the solid phase spectra

(6) S. T. King, *J. Phys. Chem.*, **74**, 2133 (1970).

Table I: Infrared Assignment of Formamide in Vapor Phase and Isolated in Argon Matrix

Vapor (Figure 1a)	Argon matrix (Figure 1b)		Assignment	
3570	3555	ν_1;	$a-\nu_{NH_2}$	
3530 (?)	3518	$2\nu_4$ (or D^a)		
3448	3430	ν_2;	$s-\nu_{NH_2}$	
3337	3300		NH_3	
3135	3130	$2\nu_5$		
2855	2881⎫^{b}			
	2871⎭	ν_3;	ν_{CH}	
2758	2765	$2\nu_6$		
2350	2340		CO_2	
1755	1743⎫	ν_4;	ν_{C-O}	
	1739⎭		N.I.^{c}	
	1728		D or P^d	
1617	1617	$\nu_8 + \nu_{11}$ or $W_3 - W_0$		
	1581⎫		N.I.	
1580	1576⎭	ν_5;	δ_{NH_2}	
1390	1395	ν_6;	δ_{CH}	
	1263⎫		N.I.	
1255	1260⎭	ν_7;	ν_{CN}	
1150	1180	$\nu_{10} + \nu_{11}$ or $W_2 - W_0$		
1050	1040	ν_8;	γ_{CH}	
968⎫	970		NH_3	
932⎭				
820		$\nu_6 - \nu_{11}$		
770			$W_2 - W_1$	
660	678.5	ν_9		
667	662		CO_2	
	612⎫		N.I.	
602	605⎭	ν_{10}		
	573⎫		N.I.	
565	564⎭	ν_{11};	δ_{NCO}	
401^e				
368.6		$\nu_9 - \nu_{12}$		
	327⎫		N.I.	
	322⎬		N.I.	
288.7	303⎭	ν_{12};	$W_1 - W_0$	

^{a} D: Dimer. ^{b} Site splitting. ^{c} N.I.: Neighbor interaction. ^{d} P: Polymer. ^{e} Superposition of the subband intensities.

were observed except that of ν_{CH} and δ_{CH} modes which are expected to be little affected by hydrogen bonding in the solid phase. The splitting of the ν_{CH} band in the matrix (2881 and 2871 cm^{-1}) is presumably due to the effect of different crystal sites. The multiple band structures for all the other bands observed in the matrix spectrum are mainly due to the imperfect isolation. The identification of the monomer, aggregates, or the results of neighbor interaction, as indicated in Table I, was done by observing the intensity changes with the changing of matrix to sample ratio (M/R) in different experiments.

1200–200 cm^{-1}. The infrared spectra in this region are very complex and difficult to analyze. In the vapor phase spectrum, the impurity absorptions, *i.e.*, NH$_3$ and CO$_2$, obscured part of the spectrum. Fortunately, those impurity bands can be easily identified. The bands at 200–500, 530–700, and 730–880 cm^{-1} all have

complicated contours, but all the features in those bands, except the absorptions of NH$_3$ and CO$_2$, belong to formamide because their intensities decreased with the decreasing of the formamide concentration in the gas cell due to the decomposition. The difficulties due to overlapping and decomposition are largely reduced in the matrix spectrum.

However, most bands in this region are very sensitive to hydrogen bonding or to the neighbor interactions. A very "clean" spectrum of the completely isolated sample is very difficult to obtain. However, the absorptions due to the well isolated monomer can be distinguished from the aggregates by the intensity study as mentioned in the previous section.

There are five fundamental vibrations, *i.e.*, C–H "out-of-plane" bending (γ_{CH}), skeletal bending (δ_{NCO}), and 3 NH$_2$ vibrations, in this region. The γ_{CH} mode has been assigned to a weak band at 1030 cm^{-1} in the vapor phase spectrum.[3] In the liquid and solid phases this γ_{CH} band can be clearly observed at about 1050 cm^{-1} (Figure 1) and is very sensitive to C-deuteration.[4] Therefore, this assignment of ν_{CH} mode seems well founded.

The bands at 730–880 cm^{-1} in the vapor phase spectrum (Figure 1a) lost their intensities in the low-temperature matrix spectrum (Figure 1b). They should be assigned to the "hot bands" and will be discussed in the next section.

The complex band contour in 530–700-cm^{-1} region in Figure 1a is certainly composed of more than one band. The sharp spike at 667 cm^{-1} is the CO$_2$ band, but the broad structure under the CO$_2$ absorption is the formamide absorption and is probably a B type of band centered at 660 cm^{-1}. At the low-frequency side of this broad band two sharp maxima and one minimum can be seen at 602, 580, and 565 cm^{-1}, respectively. There are also many lines observed in the matrix spectrum in this region. However, three lines at 678.5, 605, and 564 cm^{-1} definitely increased their relative intensities with the increasing of M/R ratio, but the other lines more or less reduced their intensities. Presumably, these three lines observed in the matrix spectrum correspond to the bands centered at 660, 602, and 565 cm^{-1} in the vapor phase spectrum. The maximum at 580 cm^{-1} (Figure 1a) can be attributed to the superposition of the subband intensities of the two fundamentals on each side. In a recent study of the satellite intensities in the microwave spectrum of formamide, Crable has found three vibrational states in this region at 651, 627, and 580 cm^{-1},[7] which are in good agreement with our infrared data.

The CN bond in formamide is well known to have partial double bond character. The barrier hindering rotation of NH$_2$ group about this CN bond has been determined by nmr studies[6] and the torsional fre-

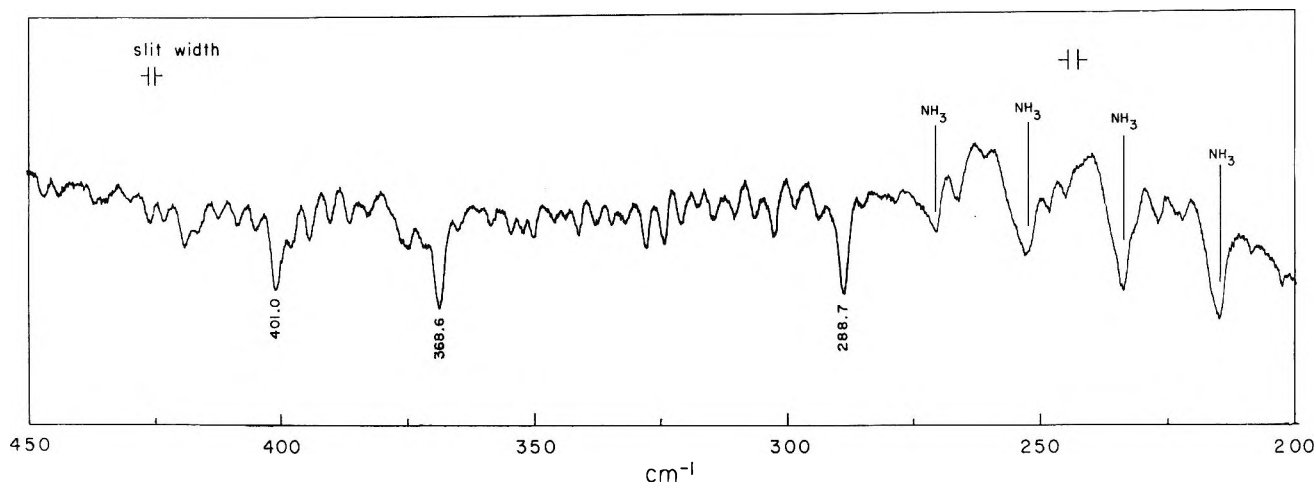(7) G. F. Crable, private discussion.

Figure 2. ν_{12} and $\nu_9-\nu_{12}$ bands of formamide in the vapor phase.

quency for NH_2 group was estimated to be about 600 cm^{-1} (see footnote 15 in ref 1). Therefore, one of the bands in this region mentioned above should be assigned to NH_2 torsion (τ_{NH_2}).

The skeletal bending, δ_{NCO}, is expected near 600 cm^{-1}. The broad band at 600 cm^{-1} in the liquid phase infrared spectrum was assigned to the overlapped bands of δ_{NCO} and NH_2 wagging (ω_{NH_2}).[4] A well defined Raman band at 612 cm^{-1} was observed by others[8] and by us for liquid formamide and was assigned to δ_{NCO} mode. Therefore, one of the observed bands in the region 500–700 cm^{-1} in the vapor phase spectrum and matrix spectrum should be assigned to δ_{NCO}.

The third band observed in the 600-cm^{-1} region should be assigned as NH_2 rocking (ρ_{NH_2}) since it can neither be assigned as NH_2 wagging (ω_{NH_2}) nor be assigned as the overtone of the anharmonic ω_{NH_2} mode at 300 cm^{-1} due to the reasons given in the next section. It should be pointed out that for the nonplanar $C-NH_2$ group, there is no NH_2 "rocking" mode. However, if the $C-NH_2$ groups is only slightly nonplanar, the "rocking" is still a better description than "twisting" because this mode will involve more NH motion parallel to the molecular plane[1] and also some CN in-plane bending motion.

The NH_2 wagging mode is the most interesting vibration of formamide and deserves more attention. A broad band with complicated fine structure was observed in the region 250–450 cm^{-1} of the vapor phase spectrum. Figure 2 is the expansion of this band recorded with a narrower slit width (1.2–2.0 cm^{-1}) than that in Figure 1a. The NH_3 rotational absorptions at 215, 234, 253, and 272 cm^{-1} are identified and marked in Figure 2. The weak lines between the NH_3 absorptions are real and belong to formamide. In the matrix spectrum a group of strong bands were observed in this region, but only the sharp line at 303 cm^{-1} increases its relative intensity with increasing M/R ratio. Obviously, the 303-cm^{-1} band is due to the well isolated

monomer and the other bands are caused by imperfect isolation. The complicated vapor spectrum from 250 to 450 cm^{-1} must be composed of one fundamental and one or more hot bands which have often been observed for molecules with low NH out of plane bending frequency.[6] The band centered at 288.7 cm^{-1} in the vapor phase spectrum is most likely the fundamental because it is in much better agreement with the microwave data[1,7] (300 cm^{-1}) than that of 368.6 or 401-cm^{-1} bands. The band at 368 cm^{-1} can be assigned to the hot band of $\nu_9 - \nu_{12}$. The maximum at 401 cm^{-1} cannot be assigned to any proper hot band and should be attributed to the superposition of the subband intensities.

The identification of this 300-cm^{-1} band as the NH_2 wagging mode is based on the following reasons. (1) This band disappeared completely in the liquid or solid phase spectra. Presumably its frequency shifts to ~ 600 cm^{-1} in the condensed phases due to hydrogen bonding. The high sensitivity to hydrogen bonding is a good indication of an NH_2 mode. (2) Very large frequency shift on N-deuteration was observed in the microwave studies.[1,7] (3) The observed infrared intensity and fine structure of this 300-cm^{-1} band are also consistent with the NH_2 wagging assignment. For the planar or nearly planar formamide molecule one expects that the ω_{NH_2} mode would have strong infrared intensity due to the large dipole moment change during the wagging vibration. The dipole moment change of ω_{NH_2} mode in formamide is mainly along the C axis.[1] For a near-prolate symmetric top molecule this vibration produced a C-type band with the Q branch spacings similar to other perpendicular bands in the vapor phase infrared spectrum.[9] In Figure 2 the subband spacings around the strong maximum at 288.7 cm^{-1} is about 4 cm^{-1}, which is the same subband spacing as the other perpendicular band for this molecule.[3]

(8) P. G. Puranik and K. Venkata Raman, J. Mol. Spectrosc., 3, 486 (1959).

(9) S. T. King and J. Overend, Spectrochem. Acta, 23A, 2875 (1967).

The subband spacings become closer as the bands progressing toward 350 ~ 355 cm^{-1} from both ends of the spectrum in Figure 2. This is most likely due to the Coriolis interaction between the fundamental and the hot band.[9]

The CH_2 wagging frequencies of $O{=}C{=}CH_2$ and $N{\equiv}N{=}CH_2$, which have well defined planar structure, were found to be unusually low (588 and 406 cm^{-1}) and have large "negative" anharmonicity by Moore and Pimentel.[10] The observed anomalous frequencies were attributed to the resonance effects between the structures

$$H_2C{=}N^{+}{=}N^{-} \longleftrightarrow H_2C^{-}{-}N^{+}{\equiv}N$$

$$H_2C{=}C{=}O \longleftrightarrow H_2C^{-}{-}C{\equiv}O^{+}$$
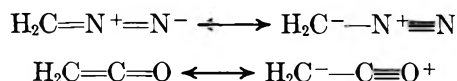
in which the ω_{CH_2} motion follows a very anharmonic potential well with probably a wide and flat bottom caused by the resonance between the sp^2 and sp^3 hybridizations. The similar resonance structures can also be drawn for formamide
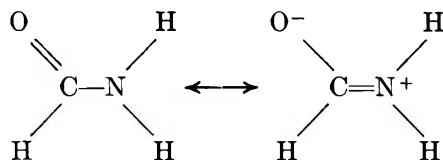
and hence it appears that the ω_{NH_2} motion in formamide should also follow a very anharmonic potential well with probably a very low barrier in the bottom. The large "negative" anharmonicity will produce the frequency of the overtone of ω_{NH_2} much higher than the value of 2 ω_{NH_2} (see discussion below). This is one reason for the assignment of τ_{NH_2} rather than the 2 ω_{NH_2} in the 600-cm^{-1} region.

The Calculation of the "Inversion" Spectrum and the Assignment of the $W_1 \rightarrow W_2$ Transition. The "inversion" frequency observed in a matrix spectrum at 303 cm^{-1} is higher than the corresponding frequency observed in the vapor phase spectrum at 288 cm^{-1}. This observation is consistent with the general frequency shift of a bending mode from the vapor phase spectrum to the matrix spectrum.[11] On the other hand, one would also expect an increasing of the height of the "inversion" barrier due to the constraint of the NH_2 motion in the matrix and consequently a decreasing of the "inversion" frequency. In order to understand the effect of changing barrier height on the "inversion" frequency, we have calculated the energy levels of the "inversion" mode of formamide by the same method as that described in ref 1, 12, and 13. Figure 3 shows the energy levels of a double minima potential by assuming the height of the C–NH$_2$ pyramid (r_0) in formamide is 0.151 Å[1] and the barrier height (V_b) changing from 10 cm^{-1} to 1600 cm^{-1}. All the calculations were performed on an IBM computer. W_i represents the energy level of the ith state. It was found that the
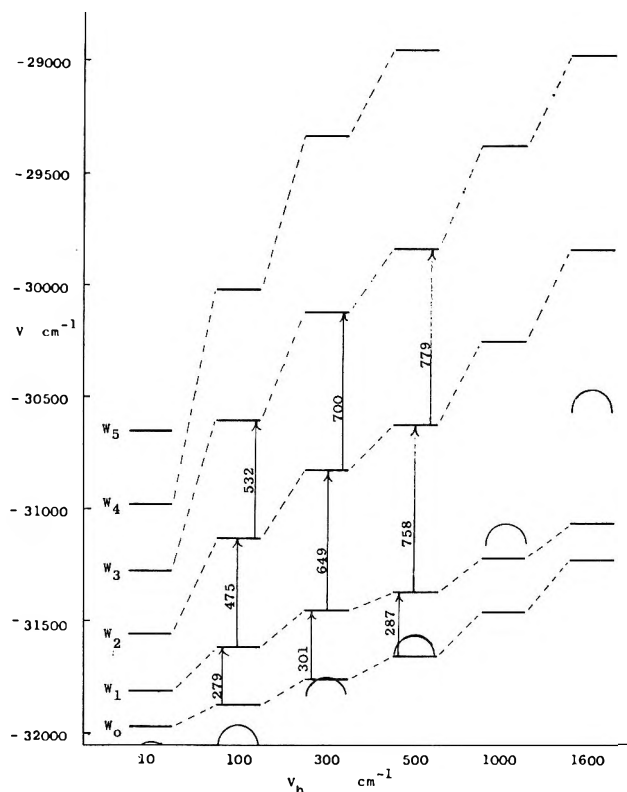

Figure 3. Calculated energy levels of the NH$_2$ "inversion" modes of formamide with fixed values of $r_0 = 0.151$ Å and $V_{r0} = 32040$ cm^{-1} (r_0 = height of the pyramidal C–NH$_2$; V_{r0} = depth of the potential well); the semicircle represents the height of the inversion barrier V_b.

spacing between W_0 and W_1 is not very sensitive to the changing of V_b over a very wide range, with the fixed value of r_0 (0.151 Å). The difference $W_1 - W_0$ has the largest value 300 cm^{-1} in the range of V_b from 250 to 450 cm^{-1} and the value of $W_1 - W_0$ decreases gradually for the V_b increasing or decreasing outside of this range. The meaning of the decreasing $W_1 - W_0$ value for $V_b < 300$ cm^{-1} is not understood. However, large uncertainty can be introduced to the calculated results for very small value of V_b due to the character of the hyperbolic potential function used.[12] With the fixed value of V_b, the increasing of the distance r_0 causes a decreasing of spacing between all the energy levels and *vice versa* as demonstrated in Figure 4. Therefore, if the matrix effect increases the barrier height slightly, say 200 ~ 400 cm^{-1}, the corresponding frequency change of $W_1 - W_0$ is small. The over compensated effects of matrix-solute interaction,[11] possibly reducing r_0 distance, and the neighbor interaction in the matrix can shift the $W_0 \rightarrow W_1$ transition to an even higher frequency as we

(10) C. B. Moore and G. C. Pimentel, *J. Chem. Phys.*, **38**, 2816 (1963); **40**, 342 (1964).

(11) G. C. Pimentel and S. W. Charles, *Pure Appl. Chem.*, **7**, 111 (1963).

(12) M. F. Manning, *J. Chem. Phys.*, **3**, 136 (1938).

(13) W. H. Fletcher and F. B. Brown, *J. Chem. Phys.*, **39**, 2478 (1963).

observed. The bands at 720–880 cm⁻¹ in the vapor phase infrared spectrum lost their intensities in the matrix spectrum (Figure 1a and 1b). Those bands should be also assigned as hot bands. They are possibly composed of two bands centered at 820 and 770 cm⁻¹.[3] The possible difference bands in this region between the fundamentals listed in Table I are $\nu_6 - \nu_{11}$ (1390 −
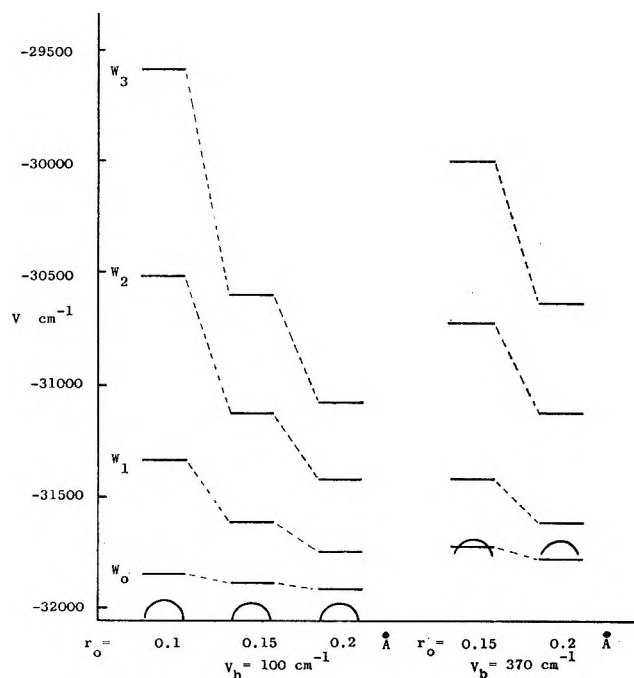

Figure 4. Calculated energy levels of the NH₂ "inversion" modes of formamide with fixed values of $V_b = 100$ cm⁻¹ and $V_{r0} = 32{,}040$ cm⁻¹.
(V_b = height of the inversion barrier).

565 = 825 cm⁻¹) and $\nu_6 - \nu_{10}$ (1390 − 602 = 788 cm⁻¹). However, the frequency of $W_1 \to W_2$ transition in the "inversion" energy diagram (Figure 3) is also very close to 770 cm⁻¹ for $V_b = 500$ cm⁻¹. It seems more reasonable to assign this 770-cm⁻¹ absorption to the hot band between the lower energy levels ($W_2 - W_1$) rather than the higher energy levels ($\nu_6 - \nu_{10}$) because this band has fairly strong intensity. Therefore, the 820-

and 770-cm⁻¹ bands in the vapor phase spectrum are assigned to $\nu_6 - \nu_{11}$ and $W_2 - W_1$, respectively.

We have explained all absorption bands in the infrared spectrum except the weak shoulders at 1150 and 1617 cm⁻¹ in the vapor phase spectrum. These two bands definitely have corresponding absorptions in the matrix spectrum. They can be either assigned respectively as the combination tones of $\nu_{10} + \nu_{11} = 1167$ cm⁻¹ and $\nu_8 + \nu_{11} = 1615$ cm⁻¹ or the higher transitions of the "inversion" mode, i.e., $W_2 - W_0$ and $W_3 - W_0$ which have the calculated frequencies close to 1100 and 1600 cm⁻¹ (Figure 3). The $W_0 \to W_2$ transition corresponds to a sym. → sym. transition according to the model of NH₃,[12] and is forbidden in the infrared spectrum. However, in the case of very low inversion barrier, such as in formamide, the W_2 energy level is located above the barrier, the perturbation to this W_2 or higher energy levels is much smaller than that in the high barrier case. Therefore, all transitions from W_0 to W_t above the barrier may be allowed in infrared spectrum.

Since the 288.7- and 368.6-cm⁻¹ bands in the vapor phase spectrum of formamide bear some resemblance to the inversion doublet of NH₃ at 932.5 and 968.3 cm⁻¹ (Figure 1a), and the possible explanation as $W_1 \to W_2$ and $W_0 \to W_3$ transitions should not be overlooked. Since no low vibrational energy level other than 300 cm⁻¹ was observed in the microwave spectrum,[1] the 288.7- and 368.6-cm⁻¹ bands cannot be interpreted as $W_1 \to W_2$ and $W_0 \to W_3$ transitions. It can also be seen in Figure 3 that for a small value of r_0, i.e., 0.151 Å, it is impossible to obtain both the values of $W_2 - W_1$ and $W_3 - W_0$ near 300 cm⁻¹.

No attempt to record the ND₂ "inversion" spectrum of formamide-d_2 was made in the present work because this frequency observed at 170 cm⁻¹ by Costain and Dowling is outside the limitation of our spectrometer.

The Electron Spin Resonance Spectra of Some

Bis(4-alkoxyphenyl) Sulfides and Ethers

by Paul D. Sullivan*

Department of Chemistry, Ohio University, Athens, Ohio 45701

and Henry J. Shine

Department of Chemistry, Texas Tech University, Lubbock, Texas 79409 (*Received August 31, 1970*)

Publication costs assisted by the Petroleum Research Foundation and the Ohio University Research Institute

The esr spectra of the cation radicals of bis(4-hydroxyphenyl) (**2**), bis(4-methoxyphenyl) (**3**) sulfides and bis(4-hydroxyphenyl) (**4**), bis(4-methoxyphenyl) (**5**) ethers have been investigated. The spectra of **2** and **3** have been obtained with much better resolution than previously obtained while the spectra of **4** and **5** have not been previously reported. The spectra were easily analyzed in terms of splittings from all the available protons. Molecular orbital calculations of the spin density distributions enable the g factors of these radicals to be correlated with the spin densities on the sulfur and oxygen atoms.

Introduction

The formation of cation radicals from aromatic sulfides and sulfoxides has been firmly established in recent years.[1,2] The same cation radical is formed by the one-electron oxidation of the sulfide and by the homolytic deoxygenation of the sulfoxide. For the most part these reactions have been carried out in concentrated sulfuric acid. This acid will remove an electron from the sulfide (and thus itself be reduced eventually to sulfur dioxide in the process) and will initiate by protonation the deoxygenation of the sulfoxide.

As far as is now known, cation radicals can be obtained from diaryl sulfides only if the aryl rings bear substituents which can stabilize the cation radical by both charge and unpaired-electron delocalization. Because of this the use of concentrated sulfuric acid as the oxidant causes severe problems. Ring sulfonation is enhanced by the same substituent properties which stabilize cation–radical formation. Thus, it has been shown that in concentrated sulfuric acid diphenyl sulfide (**1**) is disulfonated and does not form a cation radical. Bis(4-hydroxyphenyl) (**2**) and bis(4-methoxyphenyl) (**3**) sulfides form cation radicals, but in low concentration and of short life. These molecules are too susceptible to further reaction with concentrated sulfuric acid for successful cation–radical work. The use of concentrated sulfuric acid has another disadvantage. It cannot be used at low temperatures since it usually leads to esr spectra with fairly broad lines. For example, the esr spectra of **2** and **3** in concentrated sulfuric acid at room temperature have 5 and 9 broad lines, respectively, with which the correct assignment of proton-coupling interactions has been impossible.[3] The formation of cation radicals from diaryl ethers has never been reported.

In recent years solutions of aluminum chloride in nitromethane have been used very successfully for obtaining highly resolved esr spectra at low temperatures.[4-6] The technique has been adapted not only to organosulfur compounds,[6,7] but also to hydroquinones and their ethers.[4,5] We now report the use of this method for the formation of the cation radicals of compounds **2** and **3** and the corresponding ethers **4** and **5**. The method has proved adaptable only to the ethers and thio ethers carrying hydroxy and methoxy groups. Di-*p*-tolyl sulfide (**6**), which gave a cation radical in concentrated sulfuric acid, could not be oxidized with aluminum chloride in nitromethane. The esr spectra obtained with the compounds **2–5**, however, are well resolved and permit a complete analysis of the proton hyperfine splittings. Consideration of the signs and magnitudes of these splittings constants as compared to theoretical predictions together with the measured g value variations enable one to compare the relative effects of the oxygen and sulfur bridging atoms on the spin density distributions.

Experimental Section

Bis(4-hydroxyphenyl) (**2**) and bis(4-methoxyphenyl) (**3**) sulfides were obtained and purified as described earlier.[3] Bis(4-hydroxyphenyl) (**4**) and bis(4-methoxy-

(1) H. J. Shine, *Organosulfur Chem.*, 93 (1967).

(2) H. Schmidt, *Angew. Chem. Int. Ed. Engl.*, **3**, 602 (1964).

(3) H. J. Shine, M. Rahman, H. Seeger, and G.-S. Wu, *J. Org. Chem.*, **32**, 1901 (1967).

(4) W. F. Forbes and P. D. Sullivan, *J. Amer. Chem. Soc.*, **88**, 2862 (1966).

(5) W. F. Forbes, P. D. Sullivan, and H. M. Wang, *ibid.*, **89**, 2705 (1967).

(6) P. D. Sullivan, *ibid.*, **90**, 3618 (1968).

(7) H. J. Shine and P. D. Sullivan, *J. Phys. Chem.*, **72**, 1390 (1968).

phenyl) (5) ethers were obtained commercially (Eastman Kodak) and were used without further purification. The cation radicals were formed in the $AlCl_3–CH_3NO_2$ system as previously described,[4-6] and were found to be stable for several hours at $-20°$. For this series (2–5) of compounds the radical concentration was found to be a critical factor in obtaining good esr spectra. A certain amount of trial and error was therefore involved in obtaining optimum conditions of concentration[8] with respect to the esr spectra. The g values were obtained in a dual sample cavity using the perylene radical anion as a secondary standard. The errors quoted are the errors involved in reproducing the results. The absolute g values are, however, not expected to vary significantly from the values quoted since additional checks with other compounds of known g values resulted in good agreement with literature values. The computer programs for spectral simulation and molecular orbital calculations were also those previously described.[5]

Results

Bis(4-hydroxyphenyl) Sulfide (2). This compound gave an esr spectrum at $-50°$ with line widths of 70 mG which was easily interpreted in terms of two groups of four equivalent protons and a group of two equivalent protons with splitting constants of 1.61, 0.115, and 1.02 G, respectively. The 1.02-G splitting may be assigned to the hydroxyl protons but the assignment of the other groups to the ortho or meta protons will be deferred until later. The g factor for this radical was found to be 2.00687 ± 0.00003. Attempts to measure the sulfur-33 hyperfine interaction in this and the following compound were not successful due to the difficulty in preparing solutions with large radical concentrations.

Bis(4-methoxyphenyl) Sulfide (3). This compound also gave a well resolved esr spectrum with line widths of *ca.* 70 mG at $-50°$. The analysis was again straightforward in terms of a group of six equivalent proton (1.10 G) assigned to the methoxyl protons and two groups of four equivalent protons (1.55 and 0.16 G) assigned to the ring protons. The analysis was verified with a computer-simulated spectrum. The g factor of this compound was measured at 2.00686 ± 0.00002.

Bis(4-hydroxyphenyl) Ether (4) A well resolved esr spectrum was again obtained and could be readily analyzed in terms of a group of two equivalent protons (1.64 G) assigned to the hydroxyl protons and two groups of four-ring protons (1.18 and 0.94 G).

Bis(4-methoxyphenyl) Ether (5) The well resolved (line width *ca.* 60 mG) esr spectrum of this compound at $-50°$ was analyzed in terms of a 1.76 G splitting from the six equivalent methoxyl protons and splittings of 1.11 and 1.01 G from the two groups of four equivalent ring protons. The analysis was corroborated with a computer simulation. The g factor for this radical was found to be 2.00364 ± 0.00002.

Discussion

There are several points of interest about these results which warrant further consideration. It is obvious from our experiments that the unpaired electron is completely delocalized over both phenyl rings in all the compounds. In other words there is a rapid intramolecular electron transfer between the two rings. This may be contrasted with the intermediate and slow rates of intramolecular electron transfer found in the anion radicals of bis(4-nitrophenyl) sulfide and ether[9] and bis(2-nitrophenyl) ether.[10] There are also no effects observed in the spectra from the restricted rotation of the methoxyl and hydroxyl groups as observed previously in substituted benzenes[11] and biphenyls.[12] This suggests that either the potential barriers to rotation for these groups are much smaller in the compounds now being reported or that additional rotations about the central C–X–C bonds effectively average out splitting constants. An interesting correlation is observed when the splitting constants of 4 and 5 are compared with the splitting constants of the hydroquinone and p-dimethoxybenzene cation radicals. It is noted that the hydroxyl and the average ring proton splitting constants of hydroquinone (3.30 and 2.25 G, respectively) are almost twice the corresponding values of 4 (1.64 and 1.04 G, respectively). In the same way, p-dimethoxybenzene and 5 are related, *i.e.*, the methoxyl splittings are 3.40 and 1.76 G and the average ring proton splittings are 2.27 and 1.06 G, respectively. This type of behavior is similar to that observed for dimeric cation radicals[13] and one might therefore think of 4 and 5 as similar to the dimeric cation radicals of hydroquinone and p-dimethoxybenzene.

Similar correlations may also exist between 2 and 3 and the cation radicals of p-(methylthio)phenol and p-(methylthio)anisole. To date, the esr spectra of these latter radicals have not been completely analyzed;[14] however, using the data of 3 one might predict that the cation radical of p-(methylthio)anisole should have a methoxy splitting of $\sim$2.2 G and two pairs of proton splittings of 3.10 and 0.32 G. Similar predictions can also be made for the cation radical of p-(methylthio) phenol.

Molecular Orbital Calculations and Assignment of Splitting Constants. In order to compare the spin

(8) This is thought to be due to the formation of a two-electron oxidation product, *i.e.*, R $\xrightarrow{-e}$ R$^+$ $\xrightarrow{-e}$ R^{2+}. This process is being investigated further.

(9) J. E. Harriman and A. H. Maki, *J. Chem. Phys.*, 39, 778 (1963).

(10) R. K. Gupta and P. T. Narasimhan, *ibid.*, 48, 2453 (1968).

(11) A. B. Barabas, W. F. Forbes, and P. D. Sullivan, *Can. J. Chem.*, 45, 267 (1967).

(12) W. F. Forbes and P. D. Sullivan, *ibid.*, 46, 325 (1968).

(13) O. W. Howarth and G. K. Fraenkel, *J. Chem. Phys.*, 52, 6258 (1970).

(14) The spectra are very complex because of the existence of cis and trans isomers.

density distributions in **2** and **3** with **4** and **5**, molecular orbital calculations were carried out. Due to the size and complexity of the molecules the most feasible type of calculation was the McLachlan perturbation correction[15] to the Huckel molecular orbital method. These calculations involve the use of empirical coulomb (h_X) and resonance integral (k_{XY}) parameters[16] for the heteroatoms. Fortunately, calculations on simpler molecules containing similar groups enable one to suggest certain possible values for these parameters,[6,17-19] (See Table I). The calculations were restricted to the

Table I: Summary of Previous Coulomb (h_X) and Resonance Integral (k_{CX}) Parameters

Fragment	Parameters	Ref
C–S–C	$h_S = 1.20$, $k_{CS} = 0.65$, 0.55	6
C–S–R	$h_S = 1.05$, $k_{CS} = 0.97$	17
C–O–C	$h_O = 1.70$, $k_{CO} = 0.80$	6
C–O–H	$h_O = 2.00$, $k_{OC} = 1.11^a$	18
	$h_O = 1.80$, $k_{OC} = 1.14^b$	19

^{a} Calculations for hydroquinone cation radical. ^{b} Calculations for 1,4-dihydroxynaphthalene cation radical.

dihydroxy derivatives only (**2** and **4**) but the conclusions are expected to hold for the methoxy derivatives also.[20] The procedure was as follows: the spin densities at the ring carbons were calculated from McConnell's equation $a_{CH}^H = \rho_c^\pi Q_{CH}^H$ using a value of $|Q_{CH}^H| = 28$ G.[21] Recent studies on the carbon-13 and oxygen-17 interactions in the hydroquinone cation[18] have indicated that the coulomb and resonance integral parameters for the oxygen of the hydroxyl groups in this molecule should be $h_O = 2.00$, $k_{OC} = 1.11$. For 1,4-dihydroxynaphthalene the parameters are $h_O = 1.80$, $k_{OC} = 1.14$.[19] The parameters for the hydroxyl groups were then fixed at one or the other of these sets of values.[22] The h_X and k_{CX} values for the bridging atom were then allowed to vary over a wide range ($h_X = 0 - 2.0$, $k_{CX} = 0 - 2.0$). Considering **2**: it was readily apparent that over a wide range of parameters for the central sulfur atom that the spin density at the 3 position on the ring (meta to the sulfur bridge) was always less than the spin density at the 2 position. The ring proton splitting constants were thus assigned and the spin densities calculated as, $a^H(2,2,2',2') = 1.61$ G, $\rho_c^\pi(2,2,2',2') = 0.0575$; $a^H(3,3,3',3') = 0.115$ G, $\rho_c^\pi(3,3,-3',3') = 0.0041$. With regard to the signs of the splitting constants, the larger splitting from the 2 position is expected to be negative, while the smaller splitting from the 3 position could be either negative or positive. With this in mind the MO calculations were carefully carried out over a narrow range of parameter values to obtain exact agreement for the ring carbon spin densities for both possibilities. When $h_O = 2.00$, $k_{OC} = 1.11$ for the hydroxyl groups it was possible to obtain

positive spin density at both the 2 and 3 positions when values of $h_S = 1.11$ and $k_{CS} = 0.65$ were used for the bridging sulfur atom. In order to obtain positive spin density at the 2 position and negative spin density at the 3 position the appropriate values of h_S and k_{CS} were 0.995 and 0.616, respectively. When $h_O = 1.80$, $k_{OC} = 1.14$ for hydroxyl groups, the appropriate parameters for the bridging sulfur atom were $h_S = 1.02$, $k_{CS} = 0.665$ for positive spin density at both 2 and 3 positions and $h_S = 0.91$, $k_{CS} = 0.632$ for positive spin density at the 2 position and negative spin density at the 3 position.

An indication of the actual sign of the spin density at the 3 position can be obtained from empirical observations on substituted dihydroxy and dimethoxy compounds. We have observed that the sum of the ring proton splitting constants is a constant for similar dihydroxy and dimethoxy substituted benzenes or biphenyls[4,12,23] as shown in Table II. This implies that the total spin density on the ring remains constant (since splitting constants are proportional to spin density) and is merely redistributed on changing from dihydroxy to dimethoxy substituents. This type of additive relationship of splitting constants has been proposed previously in other types of systems.[24,25] For **2** and **3** as we have seen there are two possibilities—first that positions 2 and 3 both have positive spin density in which case the sum of the splitting constants would be $1.610 \pm 0.155 = 1.725$ for **2** and $1.55 + 0.16 = 1.71$ for **3**, or second, that positions 2 and 3 are of opposite sign in which case the sum of the splitting constants would be $1.61 - 0.115 = 1.495$ for **2** and $1.55 - 0.16 = 1.39$ for **3**. The first possibility leads to the most constant sum and therefore from empirical considerations we are led to believe that the spin densities at positions 2 and 3 are both positive and therefore that the ring proton splitting constants are both negative.

(15) A. D. McLachlan, *Mol. Phys.*, **3**, 233 (1960).

(16) Defined as $\alpha_x = \alpha + h_x\beta$, $\beta_{xy} = k_{xy}\beta$, where α and β are the Coulomb and resonance integrals of the carbon atom and carbon-carbon bond.

(17) W. F. Forbes and P. D. Sullivan, *Can. J. Chem.*, **46**, 317 (1968).

(18) P. D. Sullivan, J. R. Bolton, and W. E. Geiger, Jr., *J. Amer. Chem. Soc.*, **92**, 4176 (1970).

(19) P. D. Sullivan, unpublished calculations for the 1,4-dihydroxynaphthalene cation radical.

(20) Calculations involving methoxyl groups merely increase the computation time and do not lead to any great differences in the results.

(21) This value is chosen to remain consistent with our earlier calculations.

(22) Other sets tried were $h_O = 1.60$, $k_{OC} = 1.37$; $h_O = 1.60$, $k_{OC} = 1.10$; $h_O = 1.60$, $k_{OC} = 0.80$. Of these, the first and last were unable to reproduce the experimental spin densities for any values of the parameters for the central bridging atom. The second set was able to reproduce the experimental spin densities.

(23) P. D. Sullivan and J. R. Bolton, *J. Amer. Chem. Soc.*, **90**, 5366 (1968).

(24) B. Venkataraman, B. G. Segal, and G. K. Fraenkel, *J. Chem. Phys.*, **30**, 1006 (1959).

(25) B. L. Barton and G. K. Fraenkel, *ibid.*, **41**, 1455 (1964).

Table II: Comparison of Ring Proton Splittings in Some Dihydroxy and Dimethoxy-Substituted Cation Radicals

Compd	Splitting constants	Sum of splitting constants	Ref
2,3-Dimethylhydro-quinone	$a_{CH}{}^H = 2.58$ $a_{CH_3}{}^H = 1.83$	4.41	21
2,3-Dimethyl-1,4-di-methoxybenzene	$a_{CH}{}^H = 2.90$ $a_{CH_3}{}^H = 1.48$	4.38	21
4,4'-Dihydroxy-biphenyl	$a_{CH}{}^H(2,2,2',2') = 1.95$ $a_{CH}{}^H(3,3,3',3') = 0.73$	2.68	4
4,4'-Dimethoxy-biphenyl	$a_{CH}{}^H(2,2,2',2') = 1.89$ $a_{CH}{}^H(3,3,3',3') = 0.79$	2.68	12
Bis(4-hydroxyphenyl) ether (4)	$a_{CH}{}^H(4\ protons) = 0.94$ $a_{CH}{}^H(4\ protons) = 1.18$	2.12	This work
Bis(4-methoxyphenyl) ether (5)	$a_{CH}{}^H(4\ protons) = 1.01$ $a_{CH}{}^H(4\ protons) = 1.11$	2.12	This work
Bis(4-hydroxyphenyl) sulfide (2)	$a_{CH}{}^H(4\ protons) = 1.61$ $a_{CH}{}^H(4\ protons) = 0.115$	1.725 or 1.495	This work
Bis(4-methoxyphenyl) sulfide (3)	$a_{CH}{}^H(4\ protons) = 1.55$ $a_{CH}{}^H(4\ protons) = 0.16$	1.71 or 1.39	This work

The MO calculations for **4** were similar to those for **2**. However, because of the similarity of the ring proton splitting constants from the 2 and 3 positions (and hence also the spin densities which are 0.04203 and 0.03360) it was not possible to assign either $\rho_2 > \rho_3$ or $\rho_3 > \rho_2$. The calculations therefore covered both possibilities. When $h_O = 2.00$, $k_{OC} = 1.11$ for the hydroxyl groups and $\rho_2 > \rho_3$, agreement was obtained when the parameters for the bridging oxygen group were $h_O = 1.80$, and $k_{OC} = 0.75$. For the opposite assignment (*i.e.*, $\rho_3 > \rho_2$) agreement was not obtained for any reasonable values of h_O and k_{OC}.[26] When $h_O = 1.80$ and $k_{OC} = 1.14$ for the hydroxyl groups, the values for the bridging oxygen were $h_O = 1.598$, and $k_{OC} = 0.755$ when $\rho_2 > \rho_3$ and $h_O = 1.750$, and $k_{OC} = 0.736$ when $\rho_3 > \rho_2$.

The several possibilities for compounds **2** and **4** are summarized in Table III. A choice between these various possibilities is difficult to make and at best can only be done indirectly (see next section). It is obvious, however, that the parameters obtained for the bridging atoms are very similar to parameters used previously (see Table I) for the same atoms in similar bonding situations. This in itself is encouraging.

g-Factor Correlations. An obvious conclusion to be drawn from Table III is that there is considerably more spin density on the bridging sulfur atom of **2** than on the bridging oxygen atom in **3**. This result should manifest itself in the g factors of these species. The theory of g factors proposed by Stone[27] showed that the deviation (Δg) from the free spin value could be written as a summation of a number of contributions (eq 1).

$$\Delta g = \sum_{O,S} \rho_i \gamma_i + \sum_{Ci} \rho_{Ci} \gamma_{Ci} \qquad (1)$$

In this, the first term is a contribution from the oxygen and sulfur atoms and the second term is from the carbon

Table III: Summary of MO Calculations

Bis(4-hydroxyphenyl) Sulfide

Position	$h_O{}^a = 2.00$, $k_{OC}{}^a = 1.11$ $h_S{}^b = 1.11$, $k_{CS}{}^b = 0.65$ (calcd)	$h_O{}^a = 1.80$, $k_{OC}{}^a = 1.14$ $h_S{}^b = 1.02$, $k_{CS}{}^b = 0.665$ (calcd)
1	0.04646	0.03511
2	0.05734[c]	0.05702[c]
3	0.00377[c]	0.00403[c]
4	0.08822	0.07900
O^a	0.02588	0.03024
S^b	0.43442	0.46708

Bis(4-hydroxyphenyl) Ether

Position	$h_O{}^a = 2.00$, $k_{OC}{}^a = 1.11$ $h_O{}^b = 1.80$, $k_{OC}{}^b = 0.75$ (calcd)	$h_O{}^a = 1.80$, $k_{OC}{}^a = 1.14$ $h_O{}^b = 1.598$, $k_{OC}{}^b = 0.755$ (calcd)	$h_O{}^a = 1.80$, $k_{OC}{}^a = 1.14$ $h_O{}^b = 1.75$, $k_{OC}{}^b = 0.736$ (calcd)
1	0.11046	0.09611	0.10977
2	0.04174[d]	0.04196[d]	0.03358[a]
3	0.03353[d]	0.03361[d]	0.04210[d]
4	0.11459	0.10115	0.10249
O^a	0.04833	0.05737	0.06315
O^b	0.15216	0.18841	0.14641

a Hydroxyl group. *b* Bridging atom. *c* Experimental values for ρ_2 and ρ_3 are 0.0575 and 0.0041, respectively. *d* Experimental values of ρ_2 and ρ_3 are 0.04203 and 0.03360 or *vice versa*.

atoms. The ρ's are the spin densities and the γ's are terms which depend upon both the spin-orbit coupling parameters and the relative energy of the molecular orbital containing the unpaired electron. Since the spin-orbit coupling parameter of a carbon atom is small compared to those of sulfur and oxygen, the major contribution to Δg comes from the first term and the con-

(26) For agreement in this case it was necessary to use $h_O > 2.00$, a value which we did not consider physically realistic.

(27) A. J. Stone, *Mol. Phys.*, **6**, 509 (1963).

tribution from the carbon atoms can be considered as a small additional constant term (Δg_C). For molecules **2** and **4** the expressions for Δg are therefore given by eq 2 and 3.

$$\Delta g\ (2) = \rho_S \gamma_S + 2\rho_O'\gamma_O + \Delta g_C \qquad (2)$$

$$\Delta g\ (4) = \rho_O \gamma_S + 2\rho_O'\gamma_O + \Delta g_C \qquad (3)$$

In these, ρ_O' refers to the spin density on the hydroxyl oxygen atoms. Assuming that the energy level for the orbital containing the unpaired electron is the same for both compounds (the calculations suggest that this is nearly so) then we can replace the γ's by the spin-orbit coupling parameters (ζ) and obtain the ratio of $\Delta g(2)$ to $\Delta g(4)$ as

$$\frac{\Delta g(2)}{\Delta g(4)} = \frac{\rho_S \zeta_S + 2\rho_O' \zeta_O}{\rho_O \zeta_O + 2\rho_O' \zeta_O} \qquad (4)$$

The values of ζ_S and ζ_O are 382 and 151 cm^{-1}, respectively.[28] Experimentally the ratio of the g factors is found to be 45.7:13.4 = 3.42. With the six combinations of spin densities from Table III the calculated ratio is found to vary between 3.79 and 4.99. If the parameters for the hydroxyl group are assumed constant for both the sulfides and ethers then the best result is obtained when $h_O = 1.80$ and $k_{OC} = 1.14$: the ratio being calculated as 4.09. Considering the approximations made in both the molecular orbital calculations and the g factor theory the agreement between the calculated and experimental g factor ratios seems quite satisfactory.

Conclusions

In this paper the esr spectra of the cation radicals of bis(4-alkoxyphenyl) ethers and sulfides have been analyzed in detail and compared with each other. It has been shown that the bis(4-alkoxyphenyl) ethers may be considered as equivalent to the dimeric cation radicals of dialkoxybenzenes.

Molecular orbital calculations lead us to conclude that the spin density on the bridging sulfur atom in the diphenyl sulfides is much greater than the spin density on the bridging oxygen atom in the corresponding diphenyl ethers. This result is in agreement with other studies of corresponding sulfur and oxygen containing cation radicals.[6,17] The g factors of the radicals reflect these spin density differences and correlate well with the calculated spin densities.

(28) See Table 9.1 in A. Carrington and A. D. McLachlan, "Introduction to Magnetic Resonance," Harper and Row, New York, N. Y., 1967.

Electron Correlation and the Charge Distribution in Lithium Hydride

by K. E. Banyard* and M. R. Hayns

Department of Physics, University of Leicester, Leicester, England   (Received February 19, 1970)

Publication costs borne completely by The Journal of Physical Chemistry

The redistribution of charge density as a consequence of electron correlation has been examined for LiH. Two correlated wave functions of differing complexity were analyzed. A natural orbital formulation allowed a first natural configuration to be considered as a noncorrelated limit. Thus, we minimized difficulties associated with different basis sets being used for correlated and noncorrelated calculations. In this way, by means of density difference maps, our examination of the changes in electron distribution concerned the influence of correlation introduced within the confines of each model. Both correlation maps indicated an expansion of the molecular charge cloud. The electron density increased at each nucleus and a reduction of charge occurred in the internuclear region. In a relatively extensive region around each nucleus, the density difference contours exhibited characteristics of split-shell correlation similar to those possessed by two-electron ions.

I. Introduction

Wave functions derived from Hartree–Fock–Roothaan calculations[1] have given rise to energies which are a close approximation to the true Hartree–Fock limit for many atoms and molecules. The preeminence of such independent-particle models lies in their physical and procedural simplicity. However, because the Hartree–Fock treatment itself makes no allowance for electron correlation[2] other than through the Fermi hole, the calculated energy can be in error by an amount comparable with the bond dissociation energy. In addition, electron correlation is usually necessary for a correct theoretical description of adiabatic dissociation.

With the advent of sophisticated computers, correlated wave functions are now becoming available for several small systems. Clearly, it is of considerable interest to examine the influence of electron correlation on the electronic structure. In this respect, although the determination of various one- and two-particle expectation values can be quite illuminating they are, of necessity, integrated properties of the wave function. Consequently, their sensitivity to localized changes in the density may well be limited. Therefore, it seems worthwhile to study the molecular charge distribution itself. Density maps and difference maps derived from noncorrelated wave functions for molecules have already been analyzed by several other workers.[3-5] However, in this article, we examine the changes in the charge distribution which occur as a consequence of introducing some allowance for electron correlation at different levels of approximation. The need for such an investigation has been stressed by various workers.[5,6]

As an example, we have considered the ground state of LiH at its equilibrium bond length. Two different treatments have been examined. Firstly, the wave function determined by Palke and Goddard[7] and, secondly, the extensive configuration-interaction (CI) calculation of Bender and Davidson[8] based on the use of

natural orbitals.[9] Although other wave functions have been reported,[10,11] the choice of the Bender and Davidson[8] calculation was particularly pertinent since, at the time, it was energetically the best treatment of LiH. The result has only recently been improved upon by Boys and Handy,[12] who used a transcorrelated wave function. The Palke and Goddard wave function is of interest in its own right and also represents some intermediate step toward a CI function since it leads to significantly better energies than the Hartree–Fock method and yet retains an independent-particle interpretation.

II. Difference Maps, Wave Functions, and Electron Densities

The characteristics of a density difference map are

(1) C. C. J. Roothaan, *Rev. Mod. Phys.*, **23**, 69 (1951).

(2) An excellent discussion of electron correlation and correlation energy has been given by P. O. Lowdin, *Advan. Chem. Phys.*, **2**, 207 (1959).

(3) See for example, T. Berlin, *J. Chem. Phys.*, **19**, 208 (1951); R. F. W. Bader, *J. Amer. Chem. Soc.*, **86**, 5070 (1964); A. C. Wahl, *Science*, **151**, 961 (1966); P. Politzer and R. E. Brown, *J. Chem. Phys.*, **45**, 451 (1966); R. F. W. Bader, W. H. Henneker, and P. E. Cade, *ibid.*, **46**, 3341 (1967); B. J. Ransil and J. Sinai, *ibid.*, **46**, 4050 (1967); P. E. Cade, R. F. W. Bader, W. H. Henneker, and I. Keaveny, *ibid.*, **50**, 5313 (1969); I. Cohn and K. D. Carlson, *J. Phys. Chem.*, **73**, 1356 (1969); D. B. Boyd, *J. Chem. Phys.*, **52**, 4846 (1970).

(4) R. F. W. Bader, I. Keaveney, and P. E. Cade, *ibid.*, **47**, 3381 (1967).

(5) C. W. Kern and M. Karplus, *ibid.*, **40**, 1374 (1964).

(6) P. E. Cade and W. M. Huo, *ibid.*, **47**, 614 (1967).

(7) W. E. Palke and W. A. Goddard, III, *ibid.*, **50**, 4524 (1969).

(8) C. F. Bender and E. R. Davidson, *J. Phys. Chem.*, **70**, 2675 (1966).

(9) P. O. Lowdin, *Phys. Rev.*, **97**, 1474 (1955); **97**, 1490 (1955); **97**, 1509 (1955); see also, P. O. Lowdin and H. Shull, *Phys. Rev.*, **101**, 1730 (1956).

(10) For example, the separated electron-pair study of LiH by D. D. Ebbing and R. C. Henderson, *J. Chem. Phys.*, **42**, 2225 (1965). See also R. C. Sahni, B. C. Sawhney, and M. J. Hanley, *ibid.*, **51**, 539 (1969).

(11) C. F. Bender and E. R. Davidson, *ibid.*, **49**, 4222 (1968).

(12) S. F. Boys and N. C. Handy, *Proc. Roy. Soc., Ser. A*, **311**, 309 (1969).

obviously very dependent on the nature of the reference density from which the differences are measured. Since the amount of correlation energy contained within a calculation is normally measured as the improvement in energy over the Hartree–Fock result, the true Hartree–Fock density would be an ideal reference function for any study of electron correlation. Unfortunately, such densities exist for a very few systems. Although the Hartree–Fock–Roothaan (HFR) procedure can give rise to reliable energies, Kern and Karplus[5] have shown that energetically comparable results based on different basis functions can possess variations in electron density equal in magnitude to those which arise from properties of chemical interest. To avoid this difficulty, we recall that the reformulation of a correlated wave function Ψ in terms of a natural spin orbital analysis[9] helps to minimize the influence of the composition of the original basis set. Further, when the normalized Ψ is expressed as a sum of configurations built up from the natural spin orbitals, this natural expansion of the wave function is distinguished as the superposition of configurations of most rapid convergence toward the energy value E given by $\langle \Psi | H | \Psi \rangle$, where H is the Hamiltonian of the system. The first natural configuration has also been found[13] to bear a striking resemblance to the Hartree–Fock result in terms of energy and total overlap. The relationship between natural orbitals and Hartree–Fock orbitals has been discussed by several workers:[14,15] for example, Davidson and Jones[14] showed for H_2 that the difference between such orbitals is almost equal to the f function introduced by Sinanoğlu[16] in the expansion of an N-particle wave function. The f functions represent corrections to the Hartree–Fock orbitals as a consequence of correlation and, in general, their contribution to the energy is very small.[15] Thus, for each correlated treatment of LiH, we used the first natural configuration to determine a corresponding noncorrelated reference density. By means of a density difference function, derived by subtracting this reference density from the associated correlated density, we can examine charge redistributions which arise from influences of correlation effects[17] contained within each wave function.

We now discuss the wave functions considered in this analysis. For an N-particle system, Goddard[18] expressed the total wave function as

$$\Psi(1, 2, 3, \ldots, N) =$$
$$G_i{}^\mu \Phi(1, 2, 3, \ldots, N) \chi(1, 2, 3, \ldots, N)$$

where Φ is a space function and χ is a product of one-electron spin functions. $G_i{}^\mu$ is a projection operator[19] determined by the properties of a permutation group S_N such that $\Psi(1, 2, 3, \ldots, N)$ is antisymmetric and also a spin eigenfunction. For LiH, Palke and Goddard[7] used the $G1$ method and wrote

$$\Phi(1, 2, 3, 4) = \phi_1(1)\phi_2(2)\phi_3(3)\phi_4(4)$$

where each ϕ_j was a two-center molecular orbital (MO) given by

$$\phi_j = \sum_m C_{jm}\psi_m$$

The coefficients C_{jm} were determined by the variation method. The basis set $\{\psi_m\}$ was composed of Slater-type orbitals (STO's) 1s, 1s', 2s, 3s, 2pσ, 2p'σ, and 3dσ located on the Li nucleus and 1s, 2s, and 2pσ centered on H. The total wave function involved a linear combination of 24 possible products of four basis MO's and the coefficients in the linear combination were determined by the operator $G_1{}^\mu$. Such a calculation corresponds to a variational valence bond approach in which electron correlation has been introduced, essentially, by means of a different-orbitals-for-different-spins (DODS) scheme.

The CI calculation of Bender and Davidson, which involved the direct use of natural orbitals (NO's), accounted for 89.1% of the correlation energy for LiH. Briefly, Bender and Davidson describe their CI–NO technique as follows: an estimation of the

Table I: Total Energies and Correlation Energies for LiH, Li+, and H−

System	Method	−Energy, au	−E_{corr}, au	% corr
LiH	CI–NO[a]	8.0606	0.0733	89.1
	G1[b]	8.0173	0.0300	36.5
	HF[c]	7.9873		0[e]
	Expt[d]	8.0696	0.0823	100[e]
Li+[f]	CI	7.2792	0.0428	98.4
	HF	7.2364		0[e]
	Expt	7.2799	0.0435	100[e]
H−[f]	CI	0.5275	0.0395	99.2
	HF	0.4880		0[e]
	Expt	0.5278	0.0398	100[e]

[a] Reference 8. [b] Reference 7. [c] The HFR value from ref 6. [d] Corrected for relativistic effects, see ref 6. [e] By definition, see ref 2 and 21. [f] Results quoted from ref 21.

(13) G. P. Barnett, J. Linderberg, and H. Shull, *J. Chem. Phys.*, **43**, 80 (1965); B. G. Anex and H. Shull, "Molecular Orbitals in Chemistry, Physics, and Biology," P. O. Lowdin and B. Pullman, Ed., Academic Press, New York, N. Y., 1964, p 227; G. V. Nazaroff and J. O. Hirschfelder, *J. Chem. Phys.*, **39**, 715 (1963).

(14) E. R. Davidson and L. L. Jones, *ibid.*, **37**, 2966 (1962).

(15) O. Sinanoğlu, *Rev. Mod. Phys.*, **35**, 517 (1963). See also O. Sinanoğlu and D. F. Tuan, *J. Chem. Phys.*, **38**, 1740 (1963), and O. Sinanoğlu, *Advan. Chem. Phys.*, **6**, 315 (1964).

(16) O. Sinanoğlu, *J. Chem. Phys.*, **36**, 706 (1962).

(17) Within the present scheme of analysis, pair correlation terms will constitute the first, and dominant, correction for electron correlation interaction; see ref 15 and 16.

(18) W. A. Goddard III, *Phys Rev.*, **157**, 81 (1967).

(19) $G_i{}^\mu$ is such that μ is the representation of S_N required by the spin state of the system and i indicates which of the f^μ-fold degenerate spin functions in μ is to be considered. For LiH, Palke and Goddard chose $i = 1$ and, hence, $G1$ is used as a label for both the method and the wave function.

NO's in terms of some chosen basis set, the construction of a reasonable number of configurations from these NO's and the optimization of the resulting CI wave function by variational means, a determination of the subsequent natural orbitals and the iteration of the procedure until the wave function and the natural orbitals converge. For the CI–NO treatment of LiH, the wave function Ψ consisted of 45 spatial configurations built up from an original basis set of 17 elliptical functions; the foci were located on the two nuclei.

In Table I, we quote the molecular and correlation energies[20] for LiH obtained from the calculations outlined above. For comparison, Table I includes the HFR energy for LiH determined by Cade and Huo;[6] corresponding energies for Li^+ and H^- are also given. The correlation energies are defined as the energy improvement relative to the Hartree–Fock approximations.[2,6,21]

The electron density $\rho(\bar{r})$ associated with a wavefunction $\Psi(1, 2, 3, \ldots, N)$ which represents an N electron system can be defined as

$$\rho(\bar{r}) \equiv \rho(\bar{r}_1) = N \int \Psi^*(1, 2, 3, \ldots, N)$$

$$\Psi(1, 2, 3, \ldots, N) d\tau_2 d\tau_3 \ldots d\tau_N$$

where, in addition, integration is carried out over all spin coordinates. To obtain a noncorrelated reference density, the $G1$ wave function of Palke and Goddard was analyzed in terms of natural orbitals χ_k: the transformation matrix $[A_{jk}]$ and the occupation numbers n_k are presented in Table II. As mentioned above, the

Table II: Transformation Matrix $[A_{jk}]$ and Occupation Numbers n_k for the NO Analysis of the $G1$ Wave Function for LiH[a]

ϕ_j/χ_k	χ_1	χ_2	χ_3	χ_4
ϕ_{1a}	0.50632	−0.07993	−0.11185	−2.68115
ϕ_{1b}	0.51038	−0.08054	−0.03191	2.73686
ϕ_{2a}	0.00719	0.54304	1.44508	−0.39132
ϕ_{2b}	0.00694	0.53560	−1.42928	0.18407
n_k	0.99959	0.98104	0.01802	0.00137

[a] See ref 7 for details of the molecular orbitals ϕ_j.

CI–NO wave function of Bender and Davidson is already in a suitable form. Thus, the first natural configuration[9,13] arising from each calculation for LiH was used to obtain a corresponding noncorrelated density. Such quantities, indicated by a subscript "n," are denoted by $\rho(\bar{r})_{Gn}$ for the Palke and Goddard (G) treatment and $\rho(\bar{r})_{Bn}$ when evaluated from the first natural configuration for the Bender and Davidson (B) wave function. For each correlated treatment of LiH, the electron density associated with the complete wave function[7,8] is similarly designated $\rho(\bar{r})_{Gc}$ or $\rho(\bar{r})_{Bc}$.
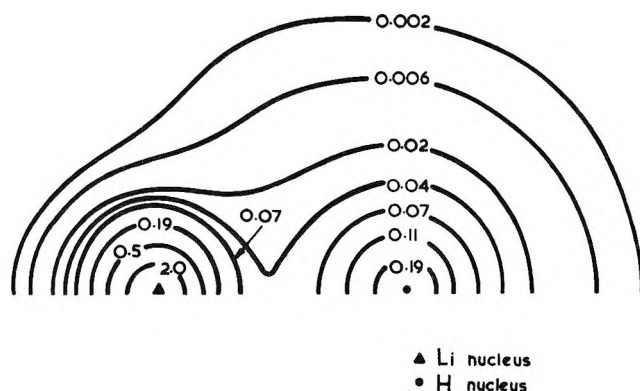
▲ Li nucleus
● H nucleus

Figure 1. Contour map of the molecular charge density $\rho(\bar{r})$ in a plane containing the bond axis for the ground state of LiH when the internuclear separation $R = 3.015$ au, calculated from the CI–NO wave function of Bender and Davidson.

Each density was normalized to four electrons. The changes in electron density due to electron correlation effects contained within the framework of each treatment of LiH are given by

$$\delta\rho(\bar{r})_G = \rho(\bar{r})_{Gc} - \rho(\bar{r})_{Gn}$$

and

$$\delta\rho(\bar{r})_B = \rho(\bar{r})_{Bc} - \rho(\bar{r})_{Bn}$$

for the G_1 and CI–NO wave functions, respectively.[22]

III. Discussion

The electron density for LiH shown in Figure 1, *i.e.*, $\rho(\bar{r})_{Bc}$, has the same general form as that obtained from an HFR wave function.[4] The contour map for $\rho(\bar{r})_{Bc}$ reveals the existence of two extensive regions of density of almost spherical symmetry, one associated with each nucleus. Thus, as before,[4] this suggests an Li^+H^- ionic interpretation of the density. This point is emphasized further by the steep gradient of the charge distribution behind the Li nucleus, a feature characteristic of an $Li^+(1s)^2$ core. A similar behavior was found for $\rho(\bar{r})_{Gc}$.

From the standpoint of our analysis, allowance for correlation effects contained within the wave functions of Palke and Goddard[7] and Bender and Davidson[8] cause density changes $\delta\rho(\bar{r})_G$ and $\delta\rho(\bar{r})_B$ shown, respectively, in Figures 2a and 2b. We see that the influence of electron correlation on the molecular charge distribution reveals several features of interest. Both difference maps indicate a reduction of charge density in the mid-bond region and an increase of charge at, and immediately around, each nucleus. Further, an increase in density also occurs in a toroidal outer

(20) Unless stated otherwise, all quantities are expressed in terms of Hartree atomic units.

(21) K. E. Banyard and C. C. Baker, *J. Chem. Phys.*, **51**, 2680 (1969); K. E. Banyard, *ibid.*, **48**, 2121 (1968).

(22) $\bar{r}$ locates a network of grid points (in a plane containing the bond axis) relative to the Li nucleus as an arbitrary origin.

Table III: Electron Densities $\rho(\bar{r})$ Evaluated Along the LiH Molecular Axis (the Internuclear Separation R is 3.015 au and Positive x Is Measured from the Midpoint in the Direction of the H Nucleus)

Density	$x = -2.25$	-2.0	-1.75	-1.50 (~Li nucleus)	-1.25	-1.00	-0.75	-0.50	-0.25
$\rho(\bar{r})_{Bc}$[a]	0.237555	0.869109	3.38835	13.15237	3.04854	0.757670	0.205183	0.070139	0.042297
$\rho(\bar{r})_{Bn}$[a]	0.237632	0.870326	3.39194	13.13822	3.05118	0.758401	0.205132	0.070145	0.042565
$\rho(\bar{r})_{Gc}$[b]	0.237550	0.868993	3.39548	13.28063	3.05272	0.759684	0.205695	0.069519	0.040850
$\rho(\bar{r})_{Gn}$[b]	0.238361	0.871189	3.39215	13.19209	3.04920	0.759786	0.205576	0.070069	0.042070
$\rho(\bar{r})_{HFR}$[c]	0.238261	0.871422	3.39076	13.18966	3.04932	0.759721	0.205656	0.070005	0.041926

Density	$x = 0.00$	$+0.25$	$+0.50$	$+0.75$	$+1.00$	$+1.25$	$+1.50$ (~H nucleus)	$+1.75$	$+2.00$
$\rho(\bar{r})_{Bc}$[a]	0.044527	0.057826	0.079247	0.111735	0.162695	0.246134	0.388315	0.231830	0.137023
$\rho(\bar{r})_{Bn}$[a]	0.045056	0.058529	0.079928	0.112051	0.162142	0.244089	0.384136	0.230011	0.136442
$\rho(\bar{r})_{Gc}$[b]	0.042218	0.054789	0.075996	0.109036	0.160938	0.243554	0.376792	0.230428	0.138459
$\rho(\bar{r})_{Gn}$[b]	0.043919	0.056488	0.077145	0.108685	0.158129	0.237925	0.367991	0.224947	0.135411
$\rho(\bar{r})_{HFR}$[c]	0.043751	0.056431	0.077089	0.108597	0.157863	0.237432	0.369988	0.222505	0.132801

[a] Derived from Bender and Davidson, ref 8.   [b] Derived from Palke and Goddard, ref 7.   [c] Derived from Cade and Huo, ref 6.

region around the bond axis at the position of the Li nucleus. Results of a similar nature have been observed from a corresponding analysis[23] for HeH$^+$. The effect of electron correlation also gives rise to closed negative contours behind the Li nucleus. This implies that, in this region of space, a slight preferential increase of charge has occurred during molecular formation. Such a feature is in general accord with the description by Bader, et al.,[4] of the charge movements associated with ionic bonding.

Some comparison of $\rho(\bar{r})_{Bc}$, $\rho(\bar{r})_{Bn}$, $\rho(\bar{r})_{Gc}$, and $\rho(\bar{r})_{Gn}$ can be obtained from inspection of Table III where values of the densities are given for various positions along the LiH molecular axis: $x = 0$ locates the midpoint of the internuclear separation $R = 3.015$ au. As a reference, values for the HFR density are also included in Table III. We see that, in the *immediate* vicinity of the nuclei, the correlated wave functions yield a charge density which is larger than the appropriate noncorrelated value: also, this trend is carried over to a comparison between the $G1$ correlated results and the HFR values. However, in contrast, the CI–NO density $\rho(\bar{r})_{Bc}$ at the Li nucleus is lower than the corresponding HFR result. From the comparisons available in Table III we also note that $\rho(\bar{r})_{Gn}$, rather than $\rho(\bar{r})_{Bn}$, has a better overall agreement with $\rho(\bar{r})_{HFR}$. At this point we recall that, although the HFR, $G1$, and CI–NO calculations each use different basis sets, the HFR and $G1$ results are derived from STO's, whereas the Bender and Davidson calculation was based on elliptical functions. Browne and Matsen[24] comment that STO's can give a better representation of the essentially spherical charge distributions near molecular nuclei than elliptical functions, but are not so well suited for a description of the valence electrons. These observations highlight difficulties associated with any direct interpretive comparisons between calculations involving the use of different basis

functions. The dependence of the present quantitative results on the nature of the basis set cannot, of course, be assessed with absolute accuracy. Certainly, this dependence has been minimized through our use of NSO analysis by the fact that the same basis set has been involved in determining the correlated and noncorrelated estimate for the electron densities within the bounds of each calculation examined here.

For each treatment of LiH, the correlated charge cloud is more diffuse throughout space than its noncorrelated counterpart. A measure of this effect was obtained from the shift of the 0.003 contour[25] for $\rho(\bar{r})$ at positions both along the LiH axis and perpendicular to it at the midpoint between the nuclei. For convenience, each result was expressed as a percentage of the "size" of the molecule given by the *noncorrelated* position of the contour. The Bender and Davidson wave function gave relative outward shifts of the 0.003 contour of 1.3% along the Li–H axis and 1.6% in the perpendicular direction: the G_1 method gave an increase, due to correlation, of 1.6% and 1.8%, respectively. These results are, of course, only a rough guide. Ideally, it would be most instructive to consider how the spatial volume, associated with a fixed large fraction of the charge, changes as a consequence of electron correlation.

A detailed comparison of the correlation maps can be obtained from the $\delta\rho(\bar{r})$ profiles given in Figure 3. The amount of charge redistribution $\delta\rho(\bar{r})_G$ is seen to be greater and spatially more extensive than $\delta\rho(\bar{r})_B$. This behavior would seem to parallel the atomic situation, where the introduction of correlation by a DODS

(23) K. E. Banyard and C. C. Baker, *Int. J. Quan. Chem.*, **4**, 431 (1970).

(24) J. C. Browne and F. A. Matsen, *Phys. Rev.*, **135**, 1227 (1964).

(25) This contour generally contains well over 90% of the total electronic charge and hence provides some assessment of molecular size.
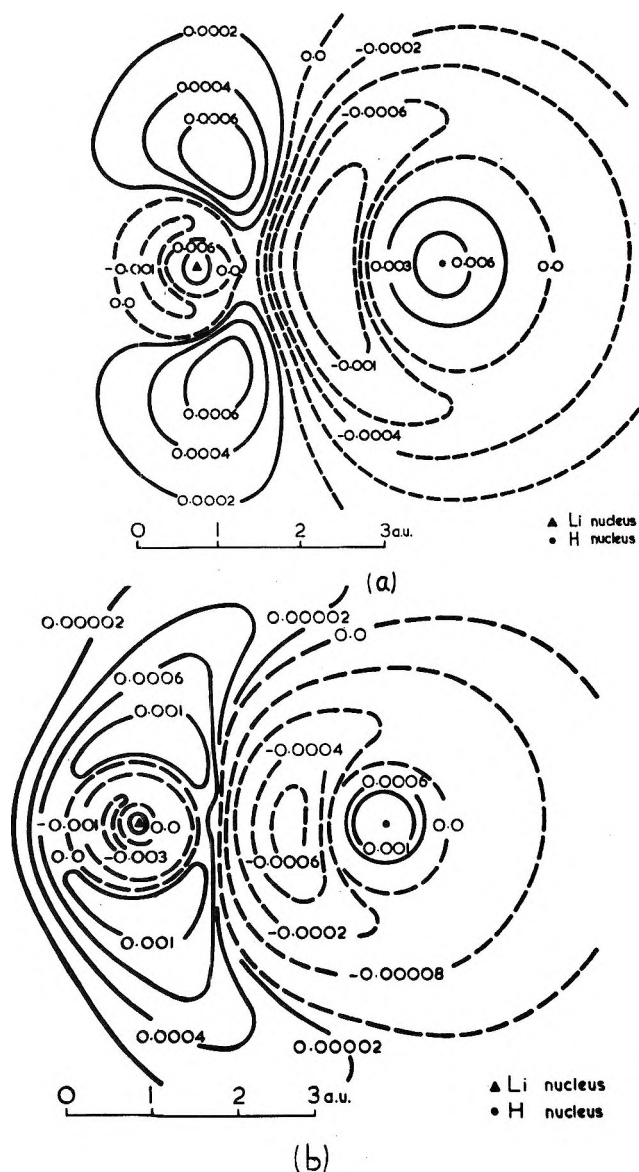
Figure 2. Correlation density difference maps for LiH.
(a) $\delta\rho(\bar{r})_G$ arises from correlation effects contained in the
$G1$ wave function of Palke and Goddard.   (b) $\delta\rho(\bar{r})_B$
is due to correlation effects contained in the CI–NO
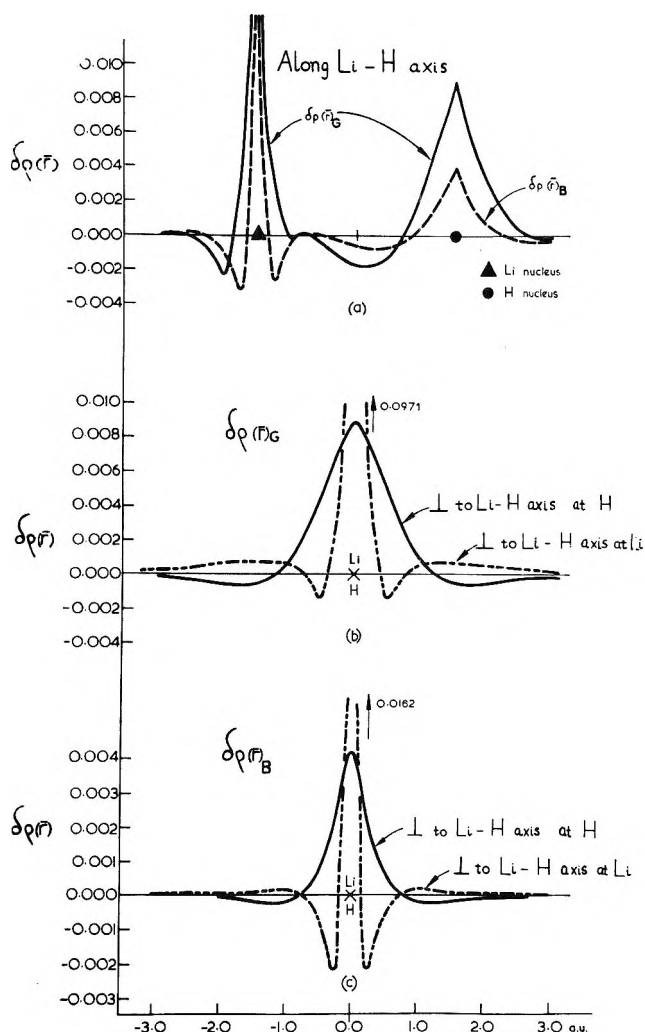wave function of Bender and Davidson.

Figure 3.   Profiles of $\delta\rho(\bar{r})_G$ and $\delta\rho(\bar{r})_B$.   (a) Along the bond
axis: solid line represents $\delta\rho(\bar{r})_G$, and the broken line
is $\delta\rho(\bar{r})_B$.   (b) Values of $\delta\rho(\bar{r})_G$ in a direction
perpendicular to the bond axis at the Li nucleus
(dashed line) and the H nucleus (solid line), and
(c) shows corresponding results for $\delta\rho(\bar{r})_B$.

scheme overemphasizes the density change by com-
parison with the results obtained from the analysis of a
CI treatment.[21]   Figures 3b and 3c indicate that,
around the Li nucleus, each calculation produces a
correlated "split-shell" effect. A similar behavior,
but more diffuse, occurs around the H nucleus.   These
features are also shown in Figure 3a; however, the
decrease in charge density due to correlation effects
in the internuclear region makes such an interpretation
less obvious.   An interesting extension of the present
analysis would be to examine the behavior of $\delta\rho(\bar{r})$ for
the ground state, and perhaps excited states, of LiH
as we move from the separated atoms to the united-
atom limit.[26]   Such an examination, based on a dif-

ferent model, has already been reported[23] for the ground
state of HeH$^+$.

Finally, a brief comment on the correlation energies[2]
is appropriate.   For LiH, E_{cor} is estimated to be 0.0823
au[20] where, in the absence of a Hartree–Fock energy,
we have used the HFR value as our reference.   The $G1$
method recovered only 36.5% of E_{cor} compared with
89.1% for the CI–NO treatment.   The difference
arises, essentially, from the representation of instan-
taneous correlation contained in the CI–NO scheme.
The limitation of the $G1$ method was reflected, as seen,
as an overdiffuseness in the correlation map.   In con-
clusion, we note that the value of 0.0823 au for E_{cor}

(26) Energies for LiH as a function of R have been reported recently
by Bender and Davidson (ref 11) and Sahni, Sawhney, and Hanley
(see ref 10).   See also the separated pair calculations for LiH by
E. L. Mehler, K. Ruedenberg, and D. M. Silver, $J.$ $Chem.$ $Phys.$,
52, 1181 (1970).   However, at R = 3.015 au, none of these calcula-
tions is energetically as accurate as the CI–NO wave function
analyzed here.

(LiH) is quite close to the total E_{cor} of 0.0833 au associated with the Li$^+$ and H$^-$ ions.

IV. Summary

The influence on the electron density of correlation effects inherent within each of two correlated wave functions has been investigated for LiH. A natural orbital analysis provided a first natural configuration which was used as a noncorrelated limit. Charge movements were illustrated by means of density difference maps and profile diagrams. The wave functions examined were those of Palke and Goddard and of Bender and Davidson which recovered, respectively, about 36% and 89% of the correlation energy for LiH.

Briefly, although the introduction of correlation effects caused the charge cloud to expand in both calculations, the Palke and Goddard calculation overemphasized the effect by comparison with the CI treatment. This conclusion parallels a similar situation found for atoms. Within the framework of our analysis, electron correlation increased the density at each nucleus and also reduced the charge in the internuclear region. Further, in the vicinity of the nuclei, the charge redistributions exhibited characteristics of split-shell correlation similar to those associated with two-electron ions. Although not part of this investigation, the study suggests some general support for an Li$^+$H$^-$ interpretation of the bonding in LiH.

Nuclear Magnetic Resonance Spectra and Substituent Effects for

Symmetrically Substituted Dihalobiphenyls

by A. R. Tarpley, Jr.,[1] and J. H. Goldstein*

Department of Chemistry, Emory University, Atlanta, Georgia 30322 (Received August 10, 1970)

Publication costs assisted by Emory University

Nmr spectra have been analyzed for the twelve symmetrically substituted dihalobiphenyls. Additivity of substituent effects has been observed for coupling constants and chemical shifts. The effects of substituents on the coupling parameters have been shown to correlate quite well with substituent electronegativity, in agreement with previous work on disubstituted benzenes. Substituent effects on the chemical shifts have been discussed in terms of ring current modification in the second ring and in terms of other well-known mechanisms. Downfield shifts at certain positions have been attributed to steric interactions. An inter-ring seven-bond H–F coupling has been observed in the case of 4,4'-difluorobiphenyl but no such inter-ring coupling was found for 3,3'- or 2,2'-difluorobiphenyl.

Introduction

Considerable interest has been directed toward obtaining and interpreting the nmr parameters of substituted benzenes.[2-24] Many of these studies have been concerned with additivity of substituent effects on coupling constants and chemical shifts, demonstrating the great utility of additivity values in the analysis and assignments of aromatic nmr spectra. Improvements in spectrometer performance and the availability of high-speed, iterative computer programs for nmr spectral analysis have greatly facilitated the study of these spectra and the resulting very precise values from these analyses have made the study of substituent effects much more reliable. Following the example of previous work,[22,23,25-35] statistical correlations between substituent electronegativity and nmr coupling param-

eters were established in monohalo- and dihalobenzenes[36] where the changes in coupling values with sub-

(1) NDEA Fellow, 1967–1970; Tennessee Eastman Fellow, 1970–1971.

(2) (a) P. L. Corio and B. P. Dailey, J. Amer. Chem. Soc., 78, 3043 (1956); (b) J. B. Leane and R. E. Richards, Trans. Faraday Soc., 55, 707 (1959).

(3) I. Yamaguchi and N. Hayakawa, Bull. Chem. Soc. Jap., 33, 1128 (1960).

(4) P. Diehl, Helv. Chim. Acta, 44, 829 (1961).

(5) H. Spiesecke and W. G. Schneider, J. Chem. Phys., 35, 731 (1961).

(6) J. C. Schug and J. C. Deck, ibid., 37, 2618 (1962).

(7) J. Martin and B. P. Dailey, ibid., 37, 2594 (1962).

(8) J. S. Martin and B. P. Dailey, ibid., 39, 1722 (1963).

(9) S. Castellano and C. Sun, J. Amer. Chem. Soc., 85, 380 (1963).

(10) T. K. Wu and B. P. Dailey, J. Chem. Phys., 41, 2796 (1964).

(11) S. Castellano and J. Lorenc, J. Phys. Chem., 69, 3552 (1965).

stituent are relatively small. Substituent effects on chemical shifts have been treated in general by Dewar, et al.,[37-39] while other workers have been concerned with substituted benzenes.[8,10,18,24] Extensive correlations have been obtained relating ortho effects of the substituent with the parameter Q.[14,19,24,40-44] Recently, substituent effects on chemical shifts have been discussed for various substituted biphenyls.[45,46]

In this article the results of nmr spectral analyses for the twelve symmetrically substituted dihalobiphenyls are given, all carried out under uniform experimental conditions. The analyses were greatly simplified by the availability of nmr analyses for biphenyl[15] and the monohalobenzenes.[16,17] It was found that the assumption of additivity of substituent effects between biphenyl and the monohalobenzenes provided very useful initial parameters for these analyses. Coupling parameters for this series of compounds are shown to correlate quite well with substituent electronegativity values. Substituent effects on the chemical shifts are discussed in terms of well known mechanisms, particularly steric interactions at crowded positions. An inter-ring seven-bond coupling has been found for 4,4'-difluorobiphenyl in several solvents.

Experimental Section

All compounds used in this study were the commercially available materials except 3,3'-dichlorobiphenyl, 3,3'-dibromobiphenyl, 3,3'-diiodobiphenyl, and 2,2'-diiodobiphenyl which were not obtainable commercially and were synthesized in this laboratory. The commercial materials required no further purification, as indicated by their nmr spectra, except for 2,2'-difluorobiphenyl which was zone refined. A preliminary investigation of the physical properties of these compounds indicated that perhaps deuterated benzene would be the only uniformly suitable solvent for the series because of the lack of solubility of some members of this series in other solvents. Normally an inert solvent such as cyclohexane is to be preferred here for studies of aromatic proton chemical shifts.[43,44] However, as shown in Table VI, the substituent effects for adding the second ring to benzene, as in biphenyl, are roughly the same for the common solvents which have been used for work with biphenyls. In addition, the results in any one solvent should be internally self-consistent under uniform conditions and low concentrations. Therefore, substituent effects have been determined in the chosen solvent by obtaining the spectra of all relevant compounds under very uniform conditions.

The samples were prepared as approximately 5 mol % solutions in C_6D_6 and were degassed with a stream of nitrogen. Approximately 1% TMS was added as an internal reference. 4,4'-Dibromobiphenyl, 4,4'-dichlorobiphenyl, and 4,4'-diiodobiphenyl were found to be relatively insoluble and were run as saturated solutions of 1–2 mol %. All spectra were recorded on a Varian

A-60-A nmr spectrometer except fluorine spectra, which were recorded on a Bruker Scientific HFX-90 spectrometer. Calibrations were performed by the usual sideband technique using an audio oscillator constantly monitored by a frequency counter. The reported line frequencies are averages of at least three forward and three reverse traces and the mean deviation for a typical resonance line is approximately 0.05 Hz. All frequencies are referenced to the 1% internal TMS.

2,2'-Diiodobiphenyl was prepared from commercially available 2,2'-dinitrobiphenyl via 2,2'-diaminobiphenyl

(12) W. B. Smith and G. M. Cole, J. Phys. Chem., 69, 4413 (1965).

(13) B. Dischler, Z. Naturforsch., 20, 888 (1965).

(14) F. Hruska, H. M. Hutton, and T. Schaefer, Can. J. Chem., 43, 2392 (1965).

(15) R. E. Mayo and J. H. Goldstein, Mol. Phys., 10, 301 (1966).

(16) J. M. Read, Jr., and J. H. Goldstein, J. Mol. Spectrosc., 23, 179 (1967).

(17) J. E. Loemker, J. M. Read, Jr., and J. H. Goldstein, Mol. Phys., 13, 433 (1967).

(18) W. B. Smith and J. L. Roark, J. Amer. Chem. Soc., 89, 5018 (1967).

(19) T. Schaefer, F. Hruska, and H. M. Hutton, Can. J. Chem., 45, 3143 (1967).

(20) S. Castellano and R. Kostelnik, Tetrahedron Lett., 51, 5211 (1967).

(21) R. W. Crecely, J. M. Read, Jr., R. S. Butler, and J. H. Goldstein, Spectrochim. Acta, Part A, 24, 685 (1968).

(22) J. E. Loemker, J. M. Read, Jr., and J. H. Goldstein, J. Phys. Chem., 72, 991 (1968).

(23) H. B. Evans, Jr., A. R. Tarpley, and J. H. Goldstein, ibid., 72, 2552 (1968).

(24) W. B. Smith, A. M. Ihrig, and J. L. Roark, ibid., 74, 812 (1970).

(25) D. N. Grant, R. C. Hirst, and H. S. Gutowsky, J. Chem. Phys., 38, 470 (1963).

(26) R. J. Abraham and K. G. R. Pachler, Mol. Phys., 7, 165 (1964).

(27) P. F. Cox, J. Amer. Chem. Soc., 85, 380 (1963).

(28) A. D. Cohen and T. Schaefer, Mol. Phys., 10, 209 (1966).

(29) S. Castellano and C. Sun, J. Amer. Chem. Soc., 88, 4741 (1966).

(30) R. R. Fraser, Can. J. Chem., 44, 2737 (1966).

(31) D. G. de Kowalewski and E. C. Ferra, Mol. Phys., 13, 547 (1967).

(32) T. Schaefer and H. M. Hutton, Can. J. Chem., 45, 3154 (1967).

(33) S. Castellano and R. Kostelnik, J. Amer. Chem. Soc., 90, 141 (1968).

(34) S. Castellano, R. Kostelnik, and C. Sun, Tetrahedron Lett., 46, 4635 (1967).

(35) K. Hayamizu and O. Yamamoto, J. Mol. Spectrosc., 25, 422 (1968).

(36) A. R. Tarpley, H. B. Evans, and J. H. Goldstein, Anal. Chem., 41, 402 (1969).

(37) M. J. S. Dewar and P. J. Grisdale, J. Amer. Chem. Soc., 84, 3539 (1962).

(38) M. J. S. Dewar and P. J. Grisdale, ibid., 84, 3548 (1962).

(39) M. J. S. Dewar and A. P. Marchand, ibid., 88, 354 (1966).

(40) J. L. Roark and W. B. Smith, J. Phys. Chem., 73, 1043 (1969).

(41) J. L. Roard and W. B. Smith, ibid., 73, 1046 (1969).

(42) W. B. Smith and J. L. Roark, ibid., 73, 1049 (1969).

(43) B. Richardson and T. Schaefer, Can. J. Chem., 46, 2195 (1968).

(44) T. Schaefer, B. Richardson, and R. Schwenk, ibid., 46, 2775 (1968).

(45) Y. Nomura and Y. Takeuchi, Tetrahedron Lett., 53, 5585 (1968).

(46) Y. Nomura and Y. Takeuchi, ibid., 54, 5665 (1968).

Table I: Substituent Contributions to Chemical Shifts and Proton–Proton Coupling Constants with Deuterated Benzene as Solvent

Compd	Chemical shift			Substituent parameters[a,b,c] Proton–proton couplings					
	S_o	S_m	S_p	S_{23}	S_{24}	S_{25}	S_{26}	S_{34}	S_{35}
Biphenyl	−16.80	−3.17	1.72	0.28	−0.12	−0.10	0.68	−0.10	0.06
Fluorobenzene	20.99	14.00	22.82	0.82	−0.31	−0.27	1.35	−0.06	0.48
Chlorobenzene	2.91	18.53	19.71	0.57	−0.25	−0.24	0.91	−0.02	0.37
Bromobenzene	−6.09	23.40	18.25	0.53	−0.27	−0.24	0.76	−0.05	0.23
Iodobenzene	−18.22	30.72	15.71	0.43	−0.20	−0.25	0.53	−0.05	0.39

[a] All values in Hz at 60 MHz. [b] Benzene, 5 mol % in C_6D_6, has a chemical shift of −429.00 Hz relative to 1% internal TMS. [c] S_o, S_m, S_p, and S_{ij} are as defined in ref 23.

(prepared by the catalytic method of Ross, Kahan, and Leach[47]) according to the method described by Lothrop.[48,49] The resulting material was recrystallized from ethanol to an mp of 108°.

The 3,3′-dichlorobiphenyl, 3,3′-dibromobiphenyl, and 3,3′-diiodobiphenyl were prepared according to the method described by Snyder, Weaver, and Marshall.[50] 3,3′-Dichlorobiphenyl was recrystallized from ethanol and melted at 23–25°. 3,3′-Dibromobiphenyl was also recrystallized from ethanol and melted at 51–52°. It was necessary to purify the 3,3′-diiodobiphenyl by column chromatography with the purified product melting at 58–59°.

Analysis and Calculations

All spectra were analyzed using an iterative computer program patterned after the Laocoon-II program of Bothner-By and Castellano.[51] Trial parameters for the analysis of the monosubstituted halobenzenes and biphenyl in deuterated benzene were taken from previous work.[15–17] In the disubstituted biphenyls, trial chemical shifts and coupling constants were calculated assuming additivity of substituent effects in biphenyl and the corresponding monosubstituted halobenzenes. As is customary for benzene derivatives[52,53] all the proton couplings were assumed to be positive. In the case of AA′BB′ spectra, as in the 4,4′-dihalobiphenyls, the analyses do not distinguish between $\nu_{A'}$ and $\nu_{B'}$ or between $J_{AA'}$ and $J_{BB'}$. In these cases the assignment followed the choice which best agreed with the additivity prediction.

The quality of the spectral fitting is indicated by the low root-mean-square deviations obtained, on the average ~0.03 Hz, between calculated and observed frequencies. Visual comparisons of observed spectra and theoretical Lorentz-shape patterns indicated that the computed intensities were satisfactory in each case.

Results

Table I lists the substituent contributions to the chemical shifts and proton–proton coupling constants for biphenyl and the monohalobenzenes as determined in deuterated benzene. These substituent contributions are simply the appropriate parameter value

Table II: H–H Coupling Constants for Dihalobiphenyls[a,b,c]

Compd X =	J_{12}	J_{13}	J_{14}	J_{23}	J_{24}	J_{34}

F	8.58	0.37	2.75	2.56	0.37	8.58
	(8.64)	(0.32)	(2.81)	(2.53)	(0.32)	(8.64)
Cl	8.40	0.42	2.36	2.37	0.42	8.40
	(8.39)	(0.35)	(2.42)	(2.34)	(0.35)	(8.39)
Br	8.38	0.42	2.43	2.19	0.42	8.38
	(8.35)	(0.35)	(2.45)	(2.19)	(0.35)	(8.35)
I	8.25	0.38	2.44	1.98	0.38	8.25
	(8.25)	(0.34)	(2.44)	(1.96)	(0.34)	(8.25)

F	8.29	0.95	2.58	7.79	0.40	1.74
	(8.26)	(0.94)	(2.63)	(7.76)	(0.32)	(1.74)
Cl	7.98	1.03	2.10	7.89	0.47	1.79
	(8.01)	(1.00)	(2.16)	(7.80)	(0.35)	(1.80)
Br	7.94	1.01	2.02	7.75	0.45	1.72
	(7.97)	(0.98)	(2.01)	(7.77)	(0.35)	(1.78)
I	7.85	1.04	1.73	7.81	0.38	1.85
	(7.87)	(1.05)	(1.78)	(7.77)	(0.34)	(1.85)

F	8.34	1.23	0.43	7.50	1.75	7.67
	(8.26)	(1.12)	(0.32)	(7.38)	(1.73)	(7.76)
Cl	8.06	1.27	0.40	7.52	1.66	7.67
	(8.01)	(1.18)	(0.35)	(7.42)	(1.62)	(7.78)
Br	8.11	1.21	0.40	7.48	1.69	7.62
	(7.97)	(1.16)	(0.35)	(7.39)	(1.65)	(7.77)
I	7.99	1.22	0.40	7.46	1.64	7.66
	(7.87)	(1.23)	(0.34)	(7.39)	(1.64)	(7.77)

[a] All values in Hz. [b] Additivity values are given in parenthesis. [c] Numbering as shown.

(47) S. D. Ross, G. J. Kahan, and W. A. Leach, J. Amer. Chem. Soc., 74, 4122 (1952).

(48) W. C. Lothrop, ibid., 63, 1187 (1941).

Table III: Chemical Shifts for Dihalobiphenyls[a,b,c]

Compd X =	Shifts calculated by additivity				Experimental shifts			
	(1)	(2)	(3)	(4)	(1)	(2)	(3)	(4)
F	−432.81	−411.18	−411.18	−432.81	−422.36	−409.04	−409.04	−422.36
					(+10.45)	(+2.14)	(+2.14)	(+10.45)
Cl	−428.28	−429.26	−429.26	−428.28	−417.88	−426.43	−426.43	−417.88
					(+10.40)	(+2.83)	(+2.83)	(+10.40)
Br	−423.41	−438.26	−438.26	−423.41	−412.42	−435.89	−435.89	−412.42
					(+10.99)	(+2.37)	(+2.37)	(+10.99)
I	−416.09	−450.39	−450.39	−416.09	−405.07	−448.16	−448.16	−405.07
					(+11.02)	(+2.23)	(+2.23)	(+11.02)

	(1)	(2)	(3)	(4)	(1)	(2)	(3)	(4)
F	−406.43	−418.17	−423.99	−425.82	−405.80	−414.56	−416.05	−420.33
					(+0.63)	(+3.61)	(+7.94)	(+5.49)
Cl	−424.51	−413.64	−427.10	−443.90	−423.86	−410.73	−415.34	−436.20
					(+0.65)	(+2.91)	(+11.76)	(+7.70)
Br	−433.51	−408.77	−428.56	−452.90	−432.67	−405.25	−415.19	−445.59
					(+0.84)	(+3.52)	(+13.37)	(+7.31)
I	−445.64	−401.45	−431.10	−465.03	−445.21	−398.30	−417.47	−458.28
					(+0.43)	(+3.15)	(+13.63)	(+6.75)

	(1)	(2)	(3)	(4)	(1)	(2)	(3)	(4)
F	−411.18	−413.42	−409.35	−432.81	−413.02	−415.46	−410.54	−428.96
					(−1.84)	(−2.04)	(−1.19)	(+3.85)
Cl	−429.28	−408.89	−412.46	−428.28	−435.13	−412.15	−414.43	−420.33
					(−5.85)	(−3.26)	(−1.97)	(+7.95)
Br	−438.26	−404.02	−413.92	−423.41	−446.77	−407.18	−416.81	−418.57
					(−8.51)	(−3.16)	(−2.89)	(+4.84)
I	−450.39	−396.70	−416.46	−416.09	−463.66	−397.12	−419.02	−415.06
					(−13.27)	(−0.42)	(−2.56)	(+1.03)

[a] All values in Hz at 60 MHz, relative to 1% internal TMS. [b] The values given in parentheses are the experimental shifts minus those shifts calculated by additivity. [c] Numbering as shown.

minus the corresponding value in benzene.[23] Table II gives the experimental proton–proton coupling constants for the dihalobiphenyls with the numbering schemes as shown. The values given in parentheses were calculated assuming additivity of substituent effects between biphenyl and the monohalobenzenes and as discussed later are only approximate for dihalobiphenyls. Table III shows the experimental shifts and those calculated by additivity as above for dihalobiphenyls. The values in parentheses are the experimental values minus the additivity values. In Table IV are summarized the substituent effects for adding a second ring to the monohalobenzenes. The ring positions are numbered as shown for the various dihalobiphenyls. H–F coupling parameters are given in Table V for difluorobiphenyls analyzed in various solvents. Table VI gives the solvent dependence of biphenyl substituent effects for adding a second ring to benzene.

Discussion

Previous nmr spectral analyses have been reported
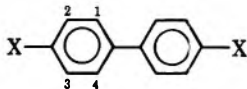
(49) J. W. Smith, Bedford College (University of London), private communication.

(50) H. R. Snyder, C. Weaver, and C. D. Marshall, *J. Amer. Chem. Soc.*, **71**, 289 (1949).

(51) S. Castellano and A. A. Bothner-By, *J. Chem. Phys.*, **41**, 3863 (1964).
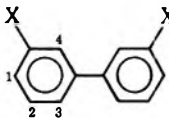
(52) R. W. Fessenden and J. S. Waugh, *ibid.*, **31**, 966 (1959).

(53) C. N. Banwell, *Mol. Phys.*, **4**, 265 (1961).

Table IV: Effects on Chemical Shifts of Adding Second Ring for Halobiphenyls[a,b]
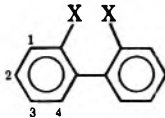
X =	Ring position (1)	(2)	(3)	(4)
H	−16.80	−3.17	−3.17	−16.80
F	−7.36	−1.03	−1.03	−7.36
Cl	−7.41	−0.34	−0.34	−7.41
Br	−6.82	−0.80	−0.80	−6.82
I	−6.79	−0.94	−0.94	−6.79

3,3′-Dihalobiphenyls
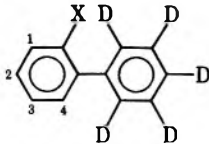
H	+1.72	−3.17	−16.80	−16.80
F	+2.21	+0.44	−9.87	−12.32
Cl	+2.23	+0.26	−6.05	−10.11
Br	+2.42	+0.35	−4.44	−10.59
I	+2.01	−0.02	−4.18	−11.06

2,2′-Dihalobiphenyls

H	−3.17	+1.72	−3.17	−16.80
F	−5.01	−0.46	−4.36	−13.96
Cl	−9.04	−1.68	−5.14	−9.86
Br	−11.68	−1.58	−6.06	−12.97
I	−16.44	+1.16	−5.73	−16.78
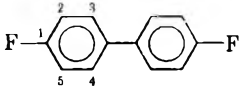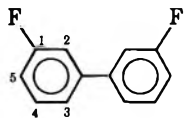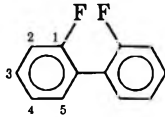
1-Perdeuteriophenyl-2-X-benzenes[c]

H	−3.99	+1.70	−3.99	−13.62
F	−4.04	+4.26	−2.13	−5.34
Cl	−6.95	+2.17	−2.96	−2.63
Br	−9.03	+4.47	−1.69	−4.53
I	−13.97	+6.55	−1.47	−10.85

[a] All values in Hz. [b] Numbering is as shown. [c] The chemical shift values are taken from ref 24. Since the data in ref 24 were obtained from 10 mol % CCl₄ samples, the substituent effects were derived from 10 mol % CCl₄ data for the monohalobenzenes taken from ref 34.

for 4,4′-dichlorobiphenyl and 4,4′-difluorobiphenyl. The coupling constants reported in this study agree to within 0.1 Hz with those reported previously for 4,4′-dichlorobiphenyl.[25] However, no attempt was made in the previous study to assign chemical shifts to the ortho or meta hydrogens. In this series the ortho and

Table V: H–F Couplings for Difluorobiphenyls[a,b]

Solvent	J_{12}	J_{13}	J_{14}	J_{15}	Inter-ring H–F

4,4′-Difluorobiphenyl

C₆D₆	8.56	5.21	5.21	8.56	0.16
CH₂Cl₂	8.66	5.36	5.36	8.66	0.21
CCl₄	8.39	5.21	5.21	8.39	0.21

3,3′-Difluorobiphenyl

C₆D₆	10.14	0.08	6.04	8.48	
CH₂Cl₂	10.19	0.10	6.10	8.61	
CCl₄	9.92	0.02	5.87	8.35	

2,2′-Difluorobiphenyl

C₆D₆	10.02	4.96	−0.16	8.34	
CH₂Cl₂	10.07	5.13	−0.15	8.36	

[a] All values in Hz. [b] Numbering is as shown.

Table VI: Solvent Dependence of Chemical Shift Substituent Effects on Biphenyl

Solvent	Chemical shift of benzene[a]	Biphenyl S_o[b]	S_m	S_p
TMS	−432.98	−13.98	−3.38	+2.11
C₆D₆	−429.00	−16.80	−3.17	+1.72
CDCl₃	−440.33	−12.89	−2.57	+2.96
CCl₄	−435.44	−13.62	−3.99	+1.70

[a] All values are in Hz relative to 1% internal TMS at 60 MHz. [b] Substituent effect ortho, meta, and para to the second ring as defined in ref 24. All spectra were obtained from 5 mol % solutions and the substituent effects in biphenyl were derived relative to the chemical shift value for benzene in the corresponding solvent.

meta proton shifts are assigned on the basis of agreement with additivity calculations and, as shown in Figure 1, on the basis of correlations with substituent electronegativity.[54] The chemical shifts of the protons ortho to the substituent increase with decreasing electronegativity of the substituent while the meta proton

(54) The E_x for −C₆H₅ and −X where X is halogen are those reported by Dailey and Shoolery [B. P. Dailey and J. N. Shoolery, J. Amer. Chem. Soc., 77, 3977 (1955)].
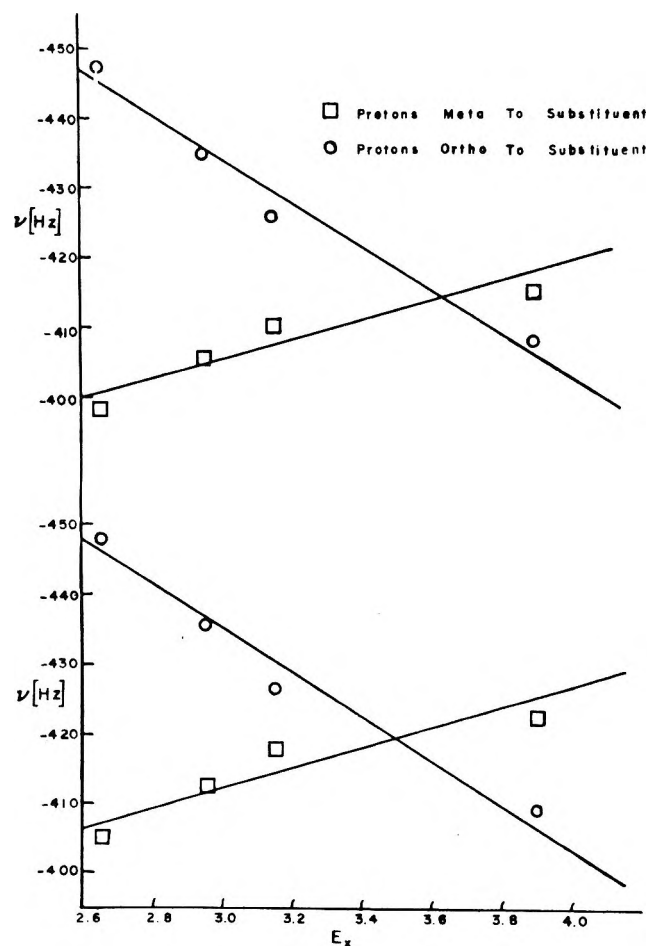
Figure 1. Plot of chemical shifts vs. substituent electronegativity (E_x) in monohalobenzenes (upper) and in 4,4'-dihalobiphenyls (lower).

Figure 2. Experimental (upper) and calculated (lower) proton nmr spectra for 3,3'-difluorobiphenyl.

chemical shifts decrease with increasing substituent electronegativity. This same alternating effect has been noted in the monohalobenzenes.[16,17]

The proton–proton couplings reported here for 4,4'-difluorobiphenyl agree to within 0.1 Hz of the values reported by Gestblom and Rodmar.[55] However, the H–F couplings do not agree quite as well, possibly reflecting the solvent dependence of these couplings. Also, Gestblom and Rodmar report that the low-field multiplet of the A_2B_2 system is slightly broadened probably due to unresolved coupling to the other ring. In the present study this broadening is resolved and is assigned to an inter-ring H–F coupling. In deuterated benzene as solvent we measure this coupling to be 0.16 Hz while in both methylene chloride and carbon tetrachloride the coupling is found to be 0.21 Hz. This inter-ring coupling also is used to assign the chemical shifts to the ortho and meta hydrogens since the hydrogens which are meta to the substituent and ortho to the second ring will certainly be involved in the coupling with the fluorine on the second ring.

As pointed out above, an inter-ring seven-bond H–F coupling has been observed here for 4,4'-difluorobi-

phenyl. 3,3'-Difluorobiphenyl, however, exhibited no such inter-ring coupling within experimental error, as shown in Figure 2, and was analyzed in three different solvents as summarized in Table V. The fluorine spectrum was fit with these same parameters requiring no inter-ring F–F or H–F coupling. 2,2'-Difluorobiphenyl was analyzed as a five-spin system disregarding the inter-ring F–F coupling which is known to exist.[56] It was possible to fit all the lines in the spectrum except that some of these lines were superimposed on a broad hump in the base line. However, the proton analysis is considered essentially correct and both the H–H and H–F coupling values are in very good agreement with those reported for 1-perdeuteriophenyl-2-F-benzene.[24]

The fluorine spectrum for 2,2'-difluorobiphenyl was a broad resonance having no observable fine structure and could not be analyzed. However, from the quality of the fit and the sharpness of the proton resonance lines it is believed that there is no inter-ring H–F coupling within experimental error. The presence of inter-ring H–F coupling in 4,4'-difluorobiphenyl and the apparent absence of this coupling in the 3,3'- and 2,2'-difluorobiphenyls perhaps points up the relative loss of conjugation between the two rings as has been shown in the ultraviolet spectra of these two compounds[57] and the importance of this conjugation in determining long range H–F couplings. Since the H–F couplings for these compounds have been obtained in several solvents, it is

(55) B. Gestblom and S. Rodmar, Acta Chem. Scand., 18, 1767 (1964).

(56) K. L. Servis and K. Fang, J. Amer. Chem. Soc., 90, 6712 (1968).

(57) G. H. Beaven and D. M. Hall, J. Chem. Soc., Part 4, 4637 (1956).

interesting to note that solvent effects on aromatic H-F couplings cannot be disregarded.[58]

Additivity of substituent effects on couplings[13,21-23] and chemical shifts[8,18,21-23,43] have been well established. The additivity values calculated here (shown in parentheses in Table II and also given in Table III) are really for monohalobiphenyls rather than dihalobiphenyls since the calculation assumes additivity between biphenyl and the corresponding monohalobenzene. However, these additivity values should approximate very closely the true additivity values and were very useful as trial parameters in the analyses. For example, as shown in Table II, for the 4,4'-dihalobiphenyls the average deviation between experimental and additivity values is only 0.03 Hz with all couplings predicted well within 0.10 Hz. For 3,3'-dihalobiphenyls the average deviation is 0.04 Hz while for 2,2'-dihalobiphenyls the average deviation is 0.08 Hz with single deviations as high as 0.15 Hz, very likely indicating the influence of the substituent in the second ring and the breakdown of the approximate additivity calculation. These same approximate additivity calculations are given in Table III for the chemical shifts. These values were profitably used as initial trial parameters for the analyses but have questionable significance otherwise, since the substituent on the second ring may have a marked effect on the proton shifts in the first ring. However, in most cases these additivity values predicted the final observed values within 0.05 ppm, although exceptions as high as 0.2 ppm are noted particularly at positions ortho to the substituent in 2, 2'-dihalobiphenyls.

Previous empirical efforts to interpret substituent effects on H-H couplings in aromatic systems have, as a rule, involved correlations with substituent electronegativity, E_x.[17,23,27,29,33,35]

Recently, a statistical approach to the determination of nmr coupling for monohalo- and dihalobenzenes has provided equations for determining the H-H couplings in ortho, meta, and para dihalobenzenes.[36] These equations have been applied to the present work on dihalobiphenyls, using the E_x values of Daily and Shoolery[54] for the substituent and adopting E_x of an unsubstituted phenyl ring for the substituted second ring. By this procedure, the values of all but a few couplings in the dihalobiphenyls can be calculated to better than 0.10 Hz. In the few cases where agreement to within 0.10 Hz cannot be obtained, the equation shows that the coupling value depends very heavily on the electronegativity of the second substituted ring which, as pointed out above, is only approximate. Figure 3 shows plots of one-half the sum of two coupling constants vs. the sum of the electronegativities of the substituents, in this case the halogen and $-C_6H_5$. The plots are linear as predicted, with slopes of 0.37, 0.31, and 0.15. These values are to be compared with cor-
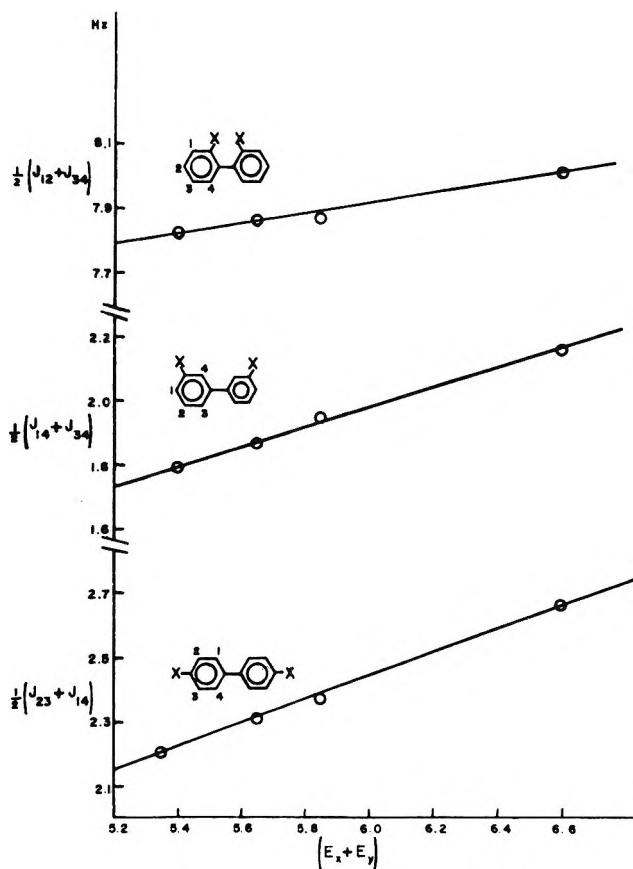
Figure 3. Plot of one-half the sum of coupling constants vs. the sum of substituent electronegativities in dihalobiphenyls.

responding values of 0.40, 0.32, and 0.12, obtained for the dihalobenzenes.[36]

Considerable attention has been given to substituent effects on chemical shifts in aromatic molecules in general[1,5,10,11,59-61] and also to various halobiphenyls.[24,45,46,62,63] For biphenyl the substituent effect of the second ring can be attributed primarily to the ring current effect of the second ring upon the protons of the first ring and is in agreement with the calculations of Mayo[15] and Johnson and Bovey.[64] However, for 4-4'-dihalobiphenyls, the addition of halogen to the second ring in the para position, as shown in Table IV, causes an average of 10.7 Hz and 2.4 Hz upfield shift in substituent effect compared with X = H for positions

(58) J. E. Loemker and J. H. Goldstein, Spectrosc. Lett., 1, 153 (1968).

(59) A. A. Bothner-By and R. E. Glick, J. Chem. Phys., 26, 1647 (1957).

(60) J. L. Garnett, L. J. Henderson, W. A. Sollich, and G. V. D. Tiers, Tetrahedron Lett., 516 (1961).

(61) F. Longenbucher, E. D. Schmid, and R. Mecke, J. Chem. Phys., 39, 1901 (1963).

(62) M. J. S. Dewar and A. P. Marchand, J. Amer. Chem. Soc., 88, 3318 (1966).

(63) S. Brownstein, ibid., 80, 2300 (1958).

(64) G. E. Johnson and F. A. Bovey, J. Chem. Phys., 29, 1012 (1958).

1 and 2, respectively.[65] It can be seen in Table IV that this effect is approximately the same irrespective of the halogen atom substituted, which is in general agreement with the work of Nomura and Takeuchi.[45]

As pointed out by Mayo and Goldstein,[15] biphenyl should undergo essentially free rotation at the temperature employed in this study (38°) and the same should be the case for the 4,4'-dihalobiphenyls. Thus, mesomeric effects are not expected to be important, which is in agreement with the lack of variation with substituent. Both diamagnetic anisotropy and field effects are proportional to R^{-3}, where R is the distance from the substituent to the proton in question. Therefore, such long-range effects can probably be neglected in this case.[38,43] As pointed out, inductive effects of the halogen substituent are probably not important here due to lack of variation of substituent effect with the electronegativity of the substituent though the inductive effect of the halogen is difficult to separate from that of the phenyl ring. An explanation which seems reasonable was proposed by Figey and Flammang[66] and allows for reduction in ring current with substitution. In the present work it is proposed that the halogen substituent on the second ring lessens the effect of the ring current of the second ring and perhaps accounts for the approximately 60 and 75% reductions in the effects at positions 1 and 2, respectively. In the work of Figey and Flammang as much as 25% reductions were noted at a position para to the substituent but they propose that ring current effects may be one of the major contributors at the meta position. Suggestions have been made that some important contribution other than ring current effect is applicable but as yet this contribution has not been well defined.[24,67]

For 3,3'-dihalobiphenyls the effects are more difficult to disentangle. As shown in Table IV at position 1 which is para to the second ring the effects are small, do not vary significantly with the nature of the substituent on the second ring, and show only a small variation from the value where X = H. Also, at position 2 the effects do not vary significantly with the nature of the substituent on the second ring and it is also evident that the effect compared with X = H is about the same as that observed at positions 2 and 3 in 4,4'-dihalobiphenyls. Certainly here the barriers to free rotation are greater than with the 4,4'-dihalobiphenyls and thus one would perhaps not expect free rotation at 38°. Hence, the ring current effect from the second ring would be smaller due to the increased angle between the planes of the two rings,[15] displacing the shifts upfield in accord with observation. At position 3 in the 3,3'-dihalobiphenyls, the effect of the halogen substituents is to move the shift upfield compared to the case where X = H in accord with either the lowering of the ring current by the substituents, or the increased angle of orientation between the two rings.[15] The substituent effects of the second ring at this position 3 are in
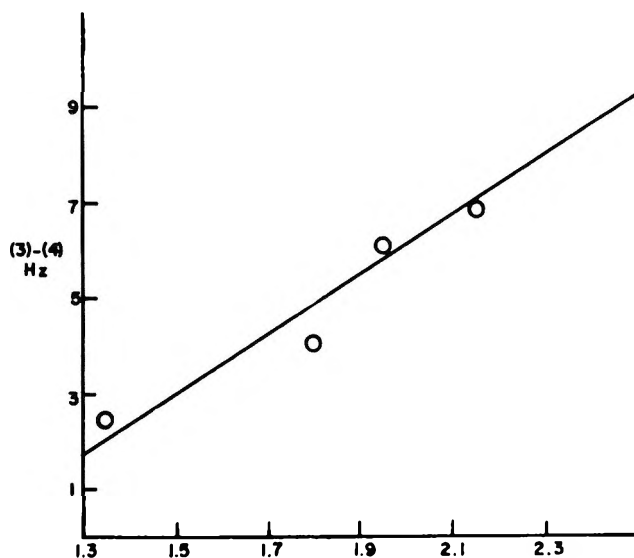
Figure 4. Plot of the difference in substituent effects between positions 3 and 4 in 3,3'-dihalobiphenyls vs. van der Waals radii for the halogens.

general agreement with those observed at the 1 or 4 position in the 4,4'-dihalobiphenyls, except that there is significant variation in the values with the nature of the substituent. For example, when X = F a downfield shift of ~2 Hz relative to X = F at positions 1 or 4 in 4,4'-difluorobiphenyl is observed while for X = Cl, Br, or I there is an upfield shift of ~2 Hz compared with the corresponding values in the 4,4'-dihalobiphenyls. For X = F this downfield shift perhaps is related to field effects[37] or to π-inductive effects of the substituent on the second ring. Comparison of position 4 with position 3 in 3,3'-dihalobiphenyls reveals downfield shifts for 4 compared to 3 of approximately 2.5 Hz, 4.0 Hz, 6.0 Hz and 7.0 Hz for X = F, Cl, Br, or I, respectively. These values give a monotonic and apparently linear relationship when plotted against van der Waals radii for the halogens[68] as shown in Figure 4. These downfield shifts at position 4 relative to 3 may thus be attributed to steric interactions and subsequent deformation of the C–H bond. Low-field shifts of 0.1–0.6 ppm have been reported in other studies irrespective of the nature of the atom which is in juxtaposition to the proton being examined.[69]

In the 2,2'-dihalobiphenyls the barriers to free rotation are much larger, particularly for X = I and X = Br[70] than found for 4,4'-dihalobiphenyls. One would expect that free rotation does not occur and that the

(65) For numbering scheme see Table IV.

(66) H. P. Figey and R. Flammang, Mol. Phys., 12, 581 (1967).

(67) F. A. Bovey, "Nuclear Magnetic Resonance Spectroscopy," Academic Press, New York, N. Y., 1969, p 69.

(68) L. Pauling, "Nature of the Chemical Bond," Cornell University Press, Ithaca, N. Y., 2nd ed, 1942, p 189.

(69) S. Weinstein, P. Carter, F. A. L. Anet, and A. J. R. Bourn, J. Amer. Chem. Soc., 87, 5247 (1965).

(70) K. E. Howlett, J. Chem. Soc., Part 1, 1055 (1960).

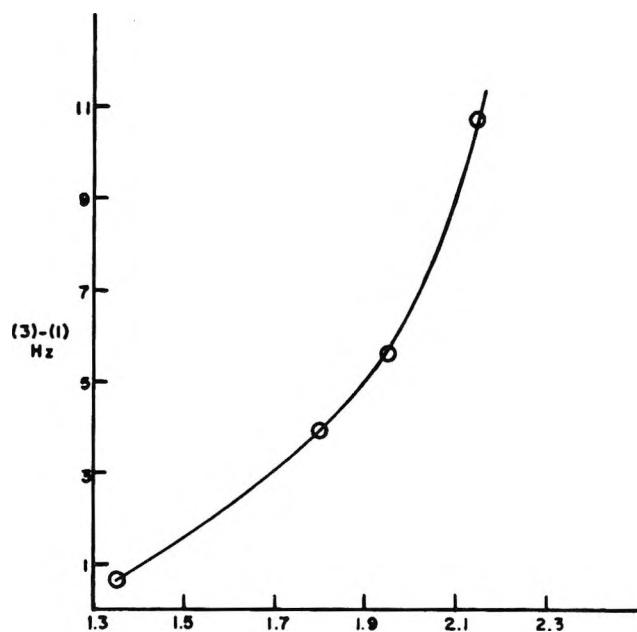Figure 5. Plot of the difference in substituent effects between positions 3 and 1 in 2,2'-dihalobiphenyls vs. van der Waals radii for the halogens.

angles of twist between the planes of the benzene rings are between 45 and 90°.[63,71-73] Thus, the mutual conjugation between the rings would be lowered if not eliminated, and it would be expected that the ring current effect of the second ring would be lowered at the ortho and meta positions relative to the second ring.[15] At position 2 in 2,2'-dihalobiphenyls, para to the second ring, the substituent effects of the second ring are small, not significantly different from the case where X = H, and do not vary significantly with the halogen on the second ring in general agreement with the observation for position 1 in 3,3'-dihalobiphenyls. However, the substituent values for position 2 in 2,2'-dihalobiphenyls are somewhat different from the comparable values given in Table IV for 1-perdeuteriophenyl-2-X-benzenes, indicating that the halogen on the second ring in 2,2'-dihalobiphenyls produces some effect relative to the deuterated ring even at this relatively far-removed position. As Table IV shows, at positions 2 or 3 in the 4,4-dihalobiphenyls and at the comparable position 2 in the 3,3'-dihalobiphenyls, there is a very small substituent effect from adding the second ring, which is in agreement with the work reported by Nomura and Takeuchi.[45] However, at the comparable 3 position in the 2,2'-dihalobiphenyls there is a significant downfield substituent effect noted in disagreement with the work of Nomura and Takeuchi[46] and in contrast to the much smaller downfield substituent effects noted for 1-perdeuteriophenyl-2-X-benzenes. Perhaps the field effect of the halogen substituent or possibly the halogen diamagnetic anisotropy effect, which was discounted by Nomura and Takeuchi, is important here.[46] Again, as in the case of the 3,3'-dihalobiphenyls, position 1 rela-
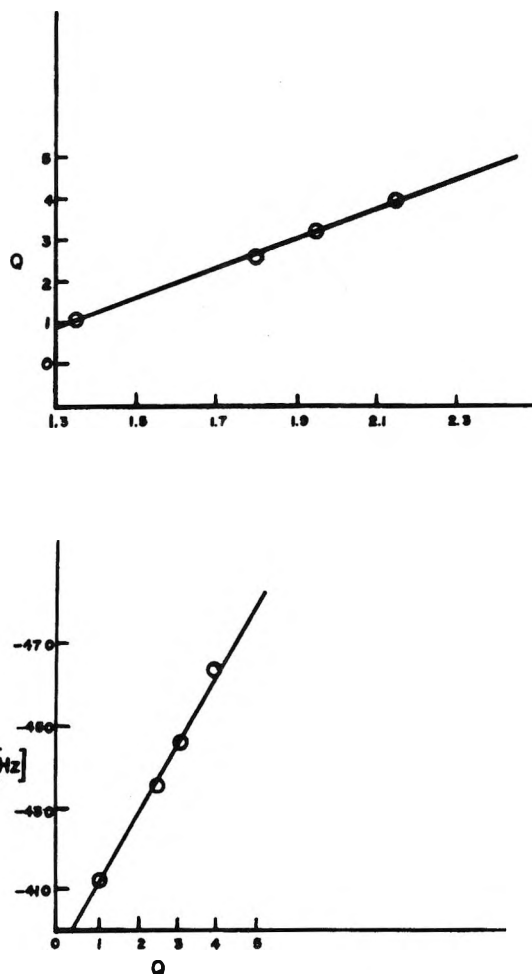
Figure 6. Plot of Q for the halogens vs. the corresponding van der Waals radius for each halogen (top). Plot of the chemical shift at position 1 in 2,2'-dihalobiphenyls vs. Q values for the halogens (bottom).

tive to position 3 in 2,2'-dihalobiphenyls exhibits downfield shifts which have been correlated with van der Waals radii for the halogens as shown in Figure 5. At position 4 in the 2,2'-dihalobiphenyls downfield shifts are noted relative to position 3 in 3,3'-dihalobiphenyls and positions 1 or 4 in the 4,4'-dihalobiphenyls although upfield shifts would be expected on the basis of increased angle of twist between the benzene rings and the corresponding lowered ring current effect.[15] Downfield shifts are also noted for this position in disubstituted halobenzenes.[21] There are significant downfield shifts noted at position 4 for the 2,2'-dihalobiphenyls relative to the same position in 1-perdeuteriophenyl-2-X-benzenes amounting to ~8 Hz regardless of the halogen involved. The origin of these downfield shifts

(71) O. Bastiansen and L. Smedvik, Acta Chem. Scand., 8, 1593 (1954).

(72) G. H. Beaven and D. M. Hall, J. Chem. Soc., Part 4, 4637 (1956).

(73) A. C. Littlejohn and J. W. Smith, ibid., Part 3, 2552 (1954).

is difficult to assign because many effects may be operative at this position ortho to the second ring.

It should be noted that positions 1 and 4 are ortho to the two ortho substituents in the 2,2'-dihalobiphenyls. Smith, et al.,[24] have made extensive correlations between the shifts at such ortho positions to the substituent and the parameter Q. $Q = P/Ir^3$ where P is the polarizability of the C–X bond, r is the C–X bond length, and I is the first ionization potential of X.[14] Smith obtains a correlation with Q for the halogens at the 1 position in 1-perdeuteriophenyl-2-X-benzenes and indicates that position 4 correlates with Q for phenyl but he does not list the Q value for phenyl. The chemical shift values obtained here for the 2,2'-dihalobiphenyls correlate well at position 1 with the Q

values given by Smith, et al.,[24] for the halogens as shown in Figure 6. Though Q values do not account for steric interactions, it has been noted that Q increases with the size of the substituent[24] and in fact correlates very well with van der Waals radii for the halogens (Figure 6). Thus, it appears unclear whether ortho substituent effects are to be accounted for by factors represented by Q or whether steric interactions arising from the size of the substituent are important.

NOTES

Simultaneous Determination of Equilibrium and Rate Constants for First-Order Reactions

by Johnson C. H. Chen and William D. Huntsman*[1]

Department of Chemistry, Clippinger Laboratories,
Ohio University, Athens, Ohio 45701
(Received September 14, 1970)

Although the sum of the rate constants for the forward and reverse reactions of a first-order process may be obtained from rate data, evaluation of the individual rate constants requires a knowledge of the equilibrium constant in cases where the reaction is significantly reversible.[2]

We wish to report a method by which the equilibrium constant can be obtained from rate data. For the reaction

$$A \underset{k_{-1}}{\overset{k_1}{\rightleftharpoons}} B$$
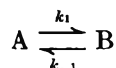
the integrated rate expression in the case in which pure A is used as reactant is given by[2]

$$\ln \frac{k_1[A_0]}{(k_1 + k_{-1})[A] - k_{-1}[A_0]} = (k_1 + k_{-1})t \quad (1)$$

where $[A_0]$ represents the initial concentration of A and $[A]$ represents the concentration at time t. The analogous expression 2 applies to the case in which pure B is used as reactant. If separate experiments

$$\ln \frac{k_{-1}[B_0]}{(k_1 + k_{-1})[B] - k_1[B_0]} = (k_1 + k_{-1})t \quad (2)$$

are conducted in which A and B are allowed to react for the *same period of time*, the left-hand sides of (1) and (2) can be equated. The resulting expression (3)

$$\frac{k_1[A_0]}{(k_1 + k_{-1})[A] - k_{-1}[A_0]} = \frac{k_{-1}[B_0]}{(k_1 + k_{-1})[B] - k_1[B_0]} \quad (3)$$

is simplified if concentrations are expressed as mole fractions, and the resulting expression is cleared of fractions giving (4). Dividing both sides of (4) by

$$(k_1 + k_{-1})\{k_1[B] - k_{-1}[A]\} = k_1^2 - k_{-1}^2 \quad (4)$$

$(k_1 + k_{-1})$ and rearranging gives (5). The value of K can be checked by running a series of experiments in

$$K = \frac{k_1}{k_{-1}} = \frac{1 - [A]}{1 - [B]} \quad (5)$$

which the reaction time is varied, and the rate constants can also be computed from the data in the customary way.

The numerator in (5) represents the mole fraction of B formed in the first experiment and the denominator represents the mole fraction of A formed in the second. Hence eq 5 simply signifies that the ratio of products

(1) Author to whom inquiries should be addressed.

(2) A. A. Frost and R. G. Pearson, "Kinetics and Mechanism," 2nd ed, Wiley, New York, N. Y., 1961, p 186.

formed in equal periods of time is the same as the equilibrium ratio.

We have used this method for determining the equilibrium constant for the geometric isomerization of *cis*- and *trans*-1,3-pentadiene at 430° in a flow system which has been described previously.[3] Prepurified nitrogen
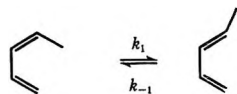
was used as carrier gas, and the contact time was varied by varying the gas flow rate, which was measured by means of a soap-film flowmeter at the exit of the product trap. After the gas flow had been adjusted, a small sample of hydrocarbon (30 μl) was injected as a slug into the vaporizer and swept into the reactor[4] by the carrier gas. Immediately after the product had been collected, a 30-μl sample of the other isomer was passed through the reactor. This procedure ensured equal contact times and temperatures for the two reactions. Analyses were performed by vpc, and the results are summarized in Table I. The average value of K, 2.01, agrees well with the value of 1.99 computed from the equation given by Egger and Benson.[5] The sum of the rate constants, $k_1 + k_{-1}$, was determined for each isomer; the least-squares value for experiments starting with the trans isomer was 3.38×10^{-3} sec^{-1} and for experiments starting with the cis isomer the value was 3.35×10^{-3} sec^{-1}. Of course, because of uncertainties in the actual contact time, these rate constants are

Table I: Isomerization of *cis*- and *trans*-1,3-Pentadiene at 430°

Contact time, sec	% isomerization of *cis*-1,3-pentadiene	% isomerization of *trans*-1,3-pentadiene	K
62.6	15.0	7.6	1.97
96.1	21.0	10.3	2.04
112.6	24.2	11.9	2.03
133.4	27.9	13.8	2.02
186.9	32.1	15.7	2.04
196.2	34.5	17.5	1.97
223.4	38.1	18.9	2.02
283.5	42.1	20.9	2.02
		Av	2.01

subject to the same uncertainties that are present in rate constants determined in flow systems in general. However, these uncertainties should not be present in the equilibrium constant because experiments with the two isomers were carried out under identical conditions.

(3) W. D. Huntsman and H. J. Wristers, *J. Amer. Chem. Soc.*, **89**, 342 (1967).

(4) It was found necessary to coat the walls of the reactor with potassium chloride to obtain reproducible results.

(5) K. W. Egger and S. W. Benson, *J. Amer. Chem. Soc.*, **87**, 3311 (1965).

Methyl Radical Formation during Photolysis of N,N,N',N'-Tetramethylparaphenylenediamine in 3-Methylpentane at 77°K[1]

by P. J. Bekowies* and A. C. Albrecht

*Baker Chemistry Laboratory, Cornell University,
Ithaca, New York 14850* (*Received July 16, 1970*)

Publication costs assisted by Cornell University

The photochemistry of N,N,N',N'-tetramethylparaphenylenediamine (TMPD) is of interest because of its widespread use as an electron donor in trapped electron studies. Several workers have reported the appearance of methyl radicals or other hydrocarbon fragments during photolysis of aromatic molecules in organic glasses such as 3-methylpentane (3MP) at 77°K and have offered evidence that the radicals originate in the glass itself by energy transfer from the aromatic molecule, followed by homolytic cleavage of a solvent C–C bond.[2a,b] An alternative route to radical production is the β scission of the aromatic molecule. Arimitsu, Kimura, and Tsubomura, for example, have reported the spectrum of the N-methylanilino radical by uv photolysis of N,N-dimethylaniline.[3] It is the purpose of this communication to report that after uv photolysis of a dilute solution of TMPD in a glass of perdeuterated 3MP at 77°K, the only methyl radical esr signal observed is that of $\cdot CH_3$.

Experimental Section

Perdeuterated 3MP supplied by Merck Sharp and Dohme of Canada, Limited was purified by refluxing for several hours over molecular sieves (Linde 5A, 10X, and 13X grades in equal parts). This treatment was sufficient to move the ultraviolet transmission cutoff of a 1-cm path of the solvent from 3500 Å to below 2000 Å. No CH_3^+ fragment could be detected in the mass spectrum of the solvent. The parent peaks of the cracking pattern agree well with an isotopic purity of 99.45%, at which level one expects only about $1.7 \times 10^{-4}\%$ of the molecules to contain a CH_3 group. The solvent was degassed by the freeze–pump–thaw method, then vacuum distilled onto a mirror of triply distilled potassium for storage until needed. Metal to metal seals were employed throughout the vacuum system, including all valve closures. In this way all possibility of contamination from grease or elastomer seals was avoided.

(1) This work has been supported primarily by Public Health Service Research Grant GM-10865. Additional support by the Materials Science Center of Cornell University is also acknowledged.

(2) (a) T. Tanei and H. Hatano, *Bull. Chem. Soc. Jap.*, **42**, 3369 (1969); (b) P. M. Johnson, Ph D. Thesis, Cornell University, 1966, p 18.

(3) S. Arimitsu, K. Kimura, and H. Tsubomura, *Bull. Chem. Soc. Jap.*, **42**, 1858 (1969).

TMPD was crystallized from the hydrochloride (Eastman White Label grade), then vacuum sublimed and further purified by thirty passes through a zone refiner. The center cut was stored under vacuum in an ordinary weighing bottle when not actually being used. CH_3I (Aldrich Chemical Company) and CD_3I (Stohler Isotope Company, 99.5 atom % D) were used as received.

Sample tubes of Spectrosil (3-mm i.d., 4-mm o.d.) containing weighed crystals of TMPD were evacuated to pressures between 10^{-6} and 10^{-8} Torr, the lower end of the sample tube in each case being chilled in a Dry Ice–acetone bath to retard evaporation of the TMPD crystal. After briefly warming the sample tubes to room temperature in order to remove any residual water or CO_2, sufficient 3MP was distilled over to make 10^{-3} molar solutions. The tubes were isolated from the vacuum system under all-metal valves and removed.

The esr spectrometer is described elsewhere.[4] Experiments were carried out by irradiating the sample under liquid nitrogen in a quartz Dewar (Varian Associates Model V-4502) with 313-nm radiation from a General Electric Model A-H6 lamp. Some irradiations also were performed using a Hanovia 2.5-kW Xe–Hg lamp. A Corning 7-54 filter was used with a 0.25-m Aminco monochromator to isolate the 313 nm line in all cases. Intensity dependence of the methyl radical formation was checked by use of a neutral density filter. The irradiated sample was then placed in the esr cavity. The spectrometer was operated with 100-kHz modulation at 0.5-mW incident power. Modulation amplitude was 1.0 g.

Results

1. Identification of $\cdot CH_3$ in Perdeuterated 3MP.
Figure 1 shows the first derivative spectrum obtained from a typical sample. The four outside lines are split 22.5 G and have relative intensities of 2.4 : 6.8 : 6.9 : 2.4 or, to the nearest integer values, 1 : 3 : 3 : 1, as expected for the methyl radical. The remainder of the spectrum consists of a broad underlying signal due to TMPD cation and a central signal due probably to a radical fragment from the photolyzed TMPD.

2. Intensity Dependence of $\cdot CH_3$ Formation. As a check on the irradiation intensity dependence of the signal, a sample was irradiated using a neutral density
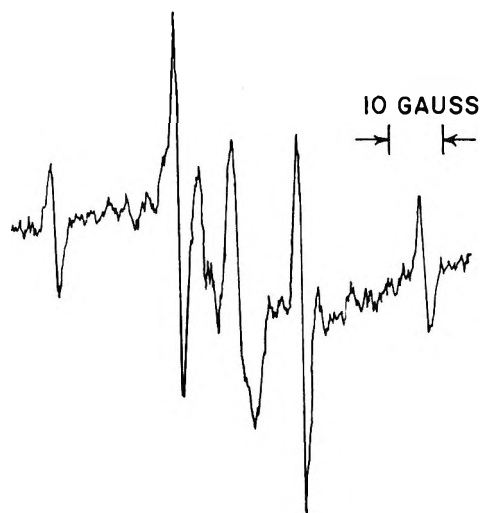
Figure 1. Esr spectrum of TMPD in 3-MP(dl4) at 77°K. Receiver gain is 1000, modulation amplitude is 1.0 G at 100 kHz and incident power is 0.5 mW.
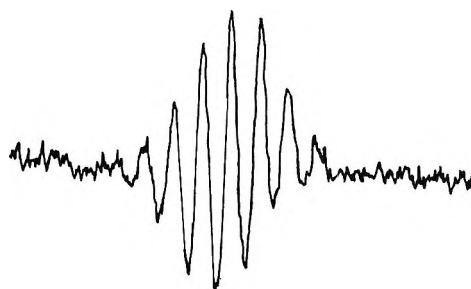
Figure 2. Esr spectrum of TMPD + 1.0 mol % CD_3I in 3-MP(d14) at 77°K. Receiver gain is 2000, modulation amplitude is 1.0 G at 100 kHz, and incident power is 0.5 mW.

filter. Table I shows that the ratios of signal intensities for the $\cdot CH_3$ hyperfine lines seem consistent with a two-photon process within the limits of experimental error. Time dependence of those ratios was not measured.

3. CD_3 Radical Formation in Perdeuterated 3MP. In order to verify that CD_3 radical does not contribute to the central portion of the spectrum, a degassed 1.0 mol % solution of CD_3I in perdeuterated 3MP was photolyzed at 77°K and was examined. The resulting spectrum consisted of a seven-line signal with a splitting constant of 3.64 ± 0.06 G and had an apparent line width of 1.8 G. No correction was made for overlap, since the lines were probably somewhat broadened by the large modulation amplitude (1.0 G). Figure

Table I: Production of $\cdot CH_3$ by Photolysis of TMPD in 3MP(dl4) Intensity of Hyperfine Lines

Spectral index no.	Signal height (arbitrary units) Intensity = 1	Intensity = $^1/_2$	Ratio
−2	24 ± 5	6 ± 5	4.0
−1	68 ± 5	20 ± 5	3.4
+1	69 ± 5	21 ± 5	3.3
±2	24 ± 5	7 ± 5	3.4

(4) R. Kooser, Ph.D. Thesis, Cornell University, 1969, p 18.

2 shows the spectrum, which is attributed to the CD_3 radical on the basis of the line intensities and splitting constant. Comparison of Figures 1 and 2 shows that $\cdot CD_3$ formation by solvent cleavage cannot account for any significant portion of the central line of Figure 1.

4. Summary and Discussion. The esr spectrum of protonated methyl radical in a glass of TMPD and perdeuterated 3MP at 77°K is shown to arise from the β scission of TMPD, with a biphotonic mechanism indicated. It is of interest to note that the $\cdot CH_3$ signal appears only after prolonged irradiation, but the trapped electron (seen at a much lower microwave power) appears after only a few minutes. Since β scission does occur in this perdeuterated glass, this pathway should also be viable in the protonated systems. Whether or not it is the dominant mechanism for producing the methyl radical fragment in the protonated systems remains to be established. A similar study of perdeuterated TMPD in protonated 3-MP could greatly clarify this question.

Keto–Enol Equilibria in 2,4-Pentanedione and 3,3-Dideuterio-2,4-pentanedione

by David W. Thompson and A. L. Allred*

*Department of Chemistry and Materials Research Center,
Northwestern University, Evanston, Illinois 60201*
(Received April 3, 1969)

The goal of this research was to investigate hydrogen isotope effects on intramolecular hydrogen bonds. The per cent of each enol tautomer, apparently containing intramolecular hydrogen bonds, in D_2O solutions of 3-deuterio-3-methyl-2,4-pentanedione[1,2] and 1-deuterio-2-acetylcyclohexanone[3] is less than the per cent enol tautomer present in the corresponding completely protonated compound in H_2O. Values of acid ionization constants show that there is less intramolecular hydrogen bonding for the deuterio maleate ion in D_2O than for the hydrogen maleate ion in H_2O.[4] Interpretation of the above results is difficult owing to the possibility of different solvent effects from H_2O and D_2O. Deuterium, in several systems,[5–7] forms stronger *intermolecular* hydrogen bonds than protium. In this research, keto–enol equilibria were measured by nmr for pure β-diketones and 0.5 mole fraction solutions in cyclohexane and by uv spectroscopy for dilute solutions in cyclohexane.

Experimental Section

Preparation of 3,3-Dideuterio-2,4-pentanedione. 3,3-Dideuterio-2,4-pentanedione was prepared by stirring 2,4-pentanedione (Eastman Organic Chemicals) with excess deuterium oxide (99.7 mol % D_2O), extracting with methylene chloride, and finally fractionally distilling the deuterated product. This exchange process was repeated three times.

Anal. Calcd for $C_5H_6D_2O_2$: C, 58.80; total hydrogen, 9.87. Found: C, 58.60, 58.64; total hydrogen assuming H:D = 3:1, 9.75, 10.1. Analysis was by Micro-Tech Laboratories, Inc., Skokie, Ill.

The purity of the product was confirmed by nmr, uv, ir,[8] and mass spectra.[9] Substitution of deuterium at the 3 position of 2,4-pentanedione was ~93% as shown by peak height measurements of the nmr signals from the methylene protons of 2,4-pentanedione and 3,3-dideuterio-2,4-pentanedione, under similar instrument settings. The hydroxyl group and the vinyl carbon have the same per cent of protium within the experimental error of nmr measurements.

No attempt was made to increase the methylene deuterium content to the theoretical limit since approximately 2% deuterium substitution into the terminal methyl groups was observed by nmr after the last exchange reported above.

Spectra. The keto–enol equilibrium constants were determined by electronically integrating, with a Varian Associates, Inc., A-60 spectrometer, the nmr signals of the terminal methyl groups of the two tautomers. Integrations were optimized according to the guidelines of Jungnickel and Forbes.[10] Uv data were obtained with a Cary Model 14 spectrophotometer.

Results

The equilibrium and thermodynamic constants derived from nmr data for 2,4-pentanedione and 3,3-dideuterio-2,4-pentanedione are summarized in Table I.

The ultraviolet spectrum of 2,4-pentanedione exhibits a maximum at 271 mμ due to the enol tautomer. Substitution of deuterium into the 3 position does not alter noticeably either the position or the shape of the enol

(1) F. C. Nachod, *Z. Phys. Chem., Abt. A,* **182,** 193 (1938).

(2) F. A. Long and D. Watson, *J. Chem. Soc.,* 2019 (1958).

(3) T. Riley and F. A. Long, *J. Amer. Chem. Soc.,* **84,** 522 (1962).

(4) G. Dahlgren, Jr., and F. A. Long, *ibid.,* **82,** 1303 (1960).

(5) C. J. Creswell and A. L. Allred, *ibid.,* **84,** 3966 (1962), and references therein.

(6) (a) G. R. Plourde, *Diss. Abstr.,* **22,** 1400 (1961); (b) R. West, personal communication.

(7) D. W. Thompson, Ph.D. Thesis, Northwestern University, 1968.

(8) H. Ogoshi and K. Nakamoto, *J. Chem. Phys.,* **45,** 3113 (1966).

(9) "Catalog of Mass Spectral Data," American Petroleum Institute, Project No. 44, Carnegie Institute of Technology, Pittsburgh, Pa.

(10) J. L. Jungnickel and J. W. Forbes, *Anal. Chem.,* **35,** 938 (1963).

Table I: Equilibrium and Thermodynamic Constants for Enolization of 2,4-Pentanedione and 3,3-Dideuterio-2,4-pentanedione from Nmr Measurements

	% keto	K	T, °C	ΔH, kcal mol^{-1}	ΔS, cal mol^{-1} deg^{-1}
O O ‖ ‖ CH$_3$CCH$_2$CCH$_3$ (pure)	21.8 ± 0.3[a]	3.59	37.3	−2.4 ± 0.2[b]	−5.2 ± 0.6[b]
	13.6 ± 0.5	6.35	2.5		
	10.5 ± 0.3	8.52	−19.0		
O O ‖ ‖ CH$_3$CCD$_2$CCH$_3$ (pure)	19.1 ± 0.4	4.24	37.3	−0.10 ± 0.04	2.6 ± 0.2
	18.5 ± 0.3	4.41	2.5		
	18.6 ± 0.3	4.38	−19.0		
O O ‖ ‖ CH$_3$CCH$_2$CCH$_3$ (0.5 mole fraction in C$_6$H$_{12}$)	10.4 ± 0.2	8.62	37.3	−1.8 ± 0.1	−1.4 ± 0.2
	7.4 ± 0.3	12.51	0.0		
	5.8 ± ∼1	16.2	−18.5		
O O ‖ ‖ CH$_3$CCD$_2$CCH$_3$ (0.5 mole fraction in C$_6$H$_{12}$)	11.0 ± 0.2	8.09	37.3	0.09 ± 0.12	4.5 ± 0.4
	10.7 ± 0.3	8.34	0.0		
	11.4 ± 0.3	7.77	−18.5		

[a] Standard deviation. [b] Probable error.

absorption band. With the assumption that the molar absorptivity for 2,4-pentanedione does not change upon substitution of deuterium into the 3 position, uv data at 25° for dilute (ca. 10^{-5} M) cyclohexane solutions of 2,4-pentanedione and 3,3-dideuterio-2,4-pentanedione unambiguously show that K_H is significantly larger than K_D.

Discussion

The magnitudes, Table I, of $\Delta H_{enolization}$ for both pure 2,4-pentanedione and a 50:50 2,4-pentanedione–cyclohexane solution are much more negative than those of the deuterated analog. As reported earlier,[11] the intensity of the 1712 cm^{-1} peak, due to carbonyl stretching, in the infrared spectrum of 2,4-pentanedione in cyclohexane is considerably smaller than for the deuterium analog. Also, uv studies of dilute solutions, ca. 10^{-5} M, of 2,4-pentanedione in cyclohexane at 25° show that the enol content is significantly larger than in a comparable solution of 3,3-dideuterio-2,4-pentanedione. If stabilization of the enol tautomer by intramolecular hydrogen bonding is an important factor in determining the overall enthalpy of enolization, protium apparently forms a stronger hydrogen bond *in this system* than does deuterium.

For the normal protium-containing compound, both pure and in cyclohexane solutions, the ΔH and ΔS values in Table I are comparable to other recently reported values.[12-14]

The entropy of enolization is much more positive for 3,3-dideuterio-2,4-pentanedione than for 2,4-pentanedione. This difference can be attributed to the deuter-

ated enol tautomer being less ordered as a consequence of less intramolecular hydrogen bonding. Both intermolecular hydrogen bonding and the existence of some nonhydrogen-bonded enol tautomer would make ΔS more positive. Free hydroxyl groups in the gas phase and in carbon tetrachloride solutions have been observed by ir.[11] Evidence for molecular association comes from both nmr spectra and cryoscopic measurements. Rogers and Burdett[15] concluded from the chemical shifts of 2,4-pentanedione in various concentrations of cyclohexane and from temperature studies that intermolecular association is important. Our chemical shift measurements confirm the work of Rogers and Burdett and furthermore show sigmoid variations at concentrations below 0.2 mole fractions, thus probably explaining why others[12,13] reported no chemical shifts for this system. Freezing point depressions of 2,4-pentanedione–cyclohexane solutions are consistent with intermolecular association. For example, the apparent molecular weight of 2,4-pentanedione is 105 in 0.10 m solution and 113 in 0.18 m solution, whereas the true molecular weight is 100.

The large differences in enol–keto ratios and thermodynamic constants for 2,4-pentanedione and 3,3-dideuterio-2,4-pentanedione are difficult to explain. Isotope

(11) S. Bratož, D. Hadži, and G. Rossmy, *Trans. Faraday Soc.*, **52**, 464 (1956).

(12) L. W. Reeves, *Can. J. Chem.*, **35**, 1351 (1957).

(13) G. Allen and R. A. Dwek, *J. Chem. Soc. B*, 161 (1966).

(14) J. Kuo, *Diss. Abstr. B*, **27**, 3064 (1967).

(15) M. T. Rogers and J. L. Burdett, *Can. J. Chem.*, **43**, 1516 (1965).

effects of the keto form are doubtless small and mainly confined by zero point energy differences of vibrations involving the methylene group. The maximum difference in bond dissociation energies for $[E_0(O\text{-}H) - E_0(C\text{-}H)] - [E_0(O\text{-}D) - E_0(C\text{-}D)]$[16] is too small to account for the differences in enthalpy values in Table I. Conceivably, enolization of 3,3-dideuterio-2,4-pentanedione is less favored as a consequence of the mean O–D bond length being less than that of OH, and therefore the hydrogen bond, –D–O, being longer and weaker. Normal bonds, for example –O–D, involving deuterium always are shorter than analogous protium bonds due to anharmonic vibrations.[17] Williams reported[18] the following bond distances and angles from an investigation by X-ray crystallography
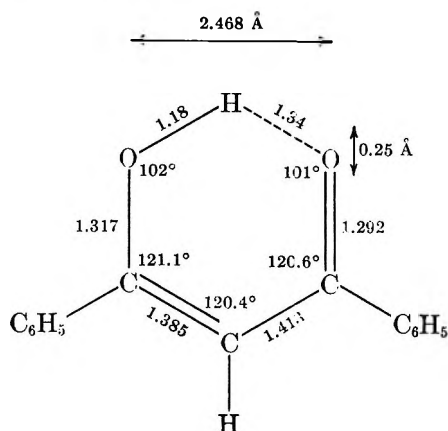
If this planar, chelated enol structure had involved average[17] bond lengths ($r_{C-C} = 1.537$ Å, $r_{C=C} = 1.335$, $r_{C-O} = 1.426$, $r_{C=O} = 1.215$) and bond angles of either 120° or 105°, the O–O separation would be 2.50 Å and the hydrogen atom would be >0.30 Å from the O–O line. The actual O–H distance above is ~0.22 Å greater than the average O–H distance[17] in nonhydrogen bonded compounds. Thus, formation of the enol ring apparently is accompanied by bond strains, and the small difference in O–H and O–D bond lengths may be unusually important.

The data presented here indicate that acidity constant data[4] and keto–enol equilibrium data[1-3] for β-diketones in light and heavy water are indeed best explained in terms of protium forming a stronger intramolecular hydrogen bond than deuterium *in these systems* and that solvent differences between light and heavy water are not dominant.

Comparative Ligand Field Studies of Manganese(II) Spectra

by A. Mehra

College of Environmental Sciences, University of Wisconsin—Green Bay, Green Bay, Wisconsin 54305 *(Received May 18, 1970)*

Publication costs assisted by the University of Wisconsin—Green Bay

A comparative study of Mn^{2+} spectra in different ligand coordinations is undertaken in this work. The large number of bands in the spectrum of Mn^{2+} allows a free variation of various parameters and provides a good check on ligand field calculations. Spectra in hydrated, fluoride, chloride, and bromide complexes are investigated and regularities have been observed.

The energy levels from d^5 configuration of Mn^{2+} and the general features of observed spectra have been reviewed earlier.[1-3] The observed band positions in several cases are given in Tables I and II. Several schemes for fitting the band energies have been suggested.[4-8] One of the best is that of Heidt, Koster, and Johnson[4] using free variation of the three crystal field parameters B, C, and Dq. However, it is found that these three parameters are not enough to give good agreement with all the band energies. A similar case is encountered for the free ion where the use of only two electrostatic parameters B and C does not give good agreement for all the terms.[9-11] Consequently, several correction terms for fitting the free ion term values have been suggested. Among these, Trees' correction term is found to be most important.[10,11] Following its success for the free ion, we have included this term in our ligand field calculations. The significance of this correction[11] and the matrix elements in

(16) K. B. Wiberg, *Chem. Rev.,* **55,** 713 (1955).

(17) L. E. Sutton, "Tables of Interatomic Distances and Configuration in Molecules and Ions" (Special Publication No. 18), The Chemical Society, London, 1965.

(18) D. E. Williams, *Acta Crystallogr.,* **21,** 340 (1966).

(1) N. S. Hush and R. J. H. Hobbs, *Progr. Inorg. Chem.,* **10,** 259 (1968).

(2) D. S. McClure, *Solid State Phys.,* **9,** 399 (1959).

(3) C. H. Ballhausen, "Introduction to Ligand Field Theory," McGraw-Hill, New York, N. Y., 1962.

(4) L. J. Heidt, G. F. Koster, and A. M. Johnson, *J. Amer. Chem. Soc.,* **80,** 6471 (1958).

(5) L. E. Orgel, *J. Chem. Phys.,* **23,** 1004 (1955).

(6) J. W. Stout, *ibid.,* **31,** 709 (1959).

(7) W. Low and G. Rosengarten, *J. Mol. Spectrosc.,* **12,** 319 (1964).

(8) A. Mehra and P. Venkateswarlu, *J. Chem. Phys.,* **45,** 3381 (1966).

(9) J. C. Slater, "Quantum Theory of Atomic Structure," McGraw-Hill, New York, N. Y., 1960.

(10) R. E. Trees, *Phys. Rev.,* **83,** 756 (1951); **84,** 1089 (1951); and **85,** 382 (1952).

(11) G. Racah, *ibid.,* **85,** 381 (1952).

Table I: Calculated and Observed Band Energies (cm⁻¹) for the Absorption Spectrum of $Mn(ClO_4)_2 \cdot Aq$ and MnF_2 at Room Temperature

Transitions ⁶A₁(S) →	Mn(ClO₄)₂·Aq			MnF₂		
	Observed[a] energy	Calculated[b] energy (I)	Calculated[c] energy (II)	Observed[d] energy	Calculated[e] energy (I)	Calculated[f] energy (II)
⁴T₁(G)	18,870	19,400	18,880	19,440	19,464	19,431
⁴T₂(G)	23,120	22,800	23,013	23,500	22,861	23,505
⁴A₁(G)	24,960 ⎫	25,200	25,120	25,190 ⎫	25,400	25,395
⁴E(G)	25,275 ⎭			25,500 ⎭		
⁴T₂(D)	27,980	28,200	28,141	28,370	28,409	28,601
⁴E(D)	29,750	29,900	29,796	30,230	30,230	30,211
⁴T₁(P)	32,960	35,000	32,747	33,060	35,416	32,817
⁴A₂(F)	40,810	40,700	40,512	41,400	41,080	41,057

[a] Reference 4. [b] Calculated energies of Heidt, Koster, and Johnson (ref 4) for $B = 670$, $C = 3710$, and $Dq = 848$ cm⁻¹. [c] Calculated energies in the present case for $B = 820$, $C = 3080$, $Dq = 780$, and $\alpha = 76$ cm⁻¹. [d] Reference 6. [e] Calculated energies before including α, for $B = 690$, $C = 3700$, and $Dq = 860$ cm⁻¹. [f] Calculated energies after including α, for $B = 840$, $C = 3095$, $Dq = 3095$, and $\alpha = 76$ cm⁻¹.

Table II: Calculated and Observed Band Energies (cm⁻¹) for the Absorption Spectra of $MnCl_2$ and MnO (the Values Are Taken from the Reported Liquid Nitrogen Temperature Spectra)

Transitions ⁶A₁(S) →	MnCl₂			MnO		
	Observed[a] energy	Calculated[b] energy (I)	Calculated[c] energy (II)	Observed[d] energy	Calculated[e] energy (I)	Calculated[f] energy (II)
⁴T₁(G)	18,500	18,588	18,424	15,890	15,947	15,905
⁴T₂(G)	22,000	21,558	22,085	20,210	19,454	20,296
⁴A₁(G)	23,590 ⎫	23,700	23,720	23,078	23,078	23,720
⁴E(G)	23,825 ⎭					
⁴T₂(D)	26,750	26,474	26,631	25,910	25,910	26,093
⁴E(D)	28,065	28,075	28,046	27,912	27,912	27,906
⁴T₁(P)	30,500	32,875	30,415			
⁴A₂(F)	38,400	38,180	38,152			

[a] References 17–19. [b] $B = 625$, $C = 3490$, and $Dq = 760$ cm⁻¹. [c] $B = 770$, $C = 2900$, $Dq = 670$, and $\alpha = 76$ cm⁻¹. [d] Reference 22. [e] Calculated energy in ref 22 for $B = 601$, $C = 3540$, and $Dq = 1010$ cm⁻¹. [f] Calculated energy in the present case for $B = 750$, $C = 2940$, $Dq = 940$, and $\alpha = 76$ cm⁻¹.

Table III: Crystal Field Parameters and Positions (cm⁻¹) of [⁴A₁(G), ⁴E(G)] and ⁴E(D) Levels of Mn⁺ in Various Coordinations (the Values of Parameters Have Been Obtained in the Present Work as Described in the Text)

Systems	B	C	Dq	⁴A₁(G), ⁴E(G) level	⁴E(D) level	Ref
Free ion	915	3235		26,850	32,340	13
RbMnF₃	835	3080	760	25,278	30,067	14
MnF₂	840	3095	750	25,270	30,230	6
Mn²⁺:NaF	835	3070	745	25,230	30,060	a
Mn(ClO₄)₂·Aq	820	3080	780	24,960	29,750	4
Mn(CH₃COO)₂·4H₂O	820	3000	760	24,740	29,454	15
MnCl₂·4H₂O	810	2980	710	24,590	29,100	16
MnCl₂	770	2900	670	23,560	28,065	17–19
Mn²⁺:NaCl	780	2910	620	23,714	28,329	20
Mn²⁺:KCl	760	2955	590	23,882	28,137	8
MnBr₂	750	2860	630	23,084	27,505	17,18
MnO	750	2940	940	23,708	27,912	21,22

[a] A. Mehra, unpublished work.

ligand field case[12] have been discussed earlier. The inclusion of this term (called α term) is also found to improve the accuracy of ligand field calculations.

Thus, in our fitting we consider four parameters,

B, C, Dq, and α. Due to the lesser percentage contribution of α term we fix the parameter α at the free ion

(12) A. Mehra, *J. Chem. Phys.*, **48**, 4384 (1968).

value of 76 cm^{-1}, although from a theoretical point of view its value may be slightly lower in complexes, like other parameters. After this, preliminary values of B and C are determined from the two Dq independent transitions to [$^4A_1(G)$, $^4E(G)$] and $^4E(D)$ states and that for Dq is determined from the position of $^4T_1(G)$ band which is most sensitive to the value of Dq. After obtaining this trial set, the parameters are varied over a small range to give a good fit for all bands, particularly the low-energy ones. In most of the cases, the trial set itself is found to be quite good, which supports our procedure.

In Tables I and II results are compared with and without the inclusion of α term for different cases. The calculated energies without the α term for Mn-$(ClO_4)_2 \cdot Aq$ and MnO are taken from references mentioned in the tables.[13-22] For MnF_2 and $MnCl_2$, calculations were also performed without the α term and reasonable set of parameters, by inspection, were chosen for the calculated energies given in the tables. The agreement is seen to be improved for most of the bands on including α and in particular for the $^4T_1(P)$ band where the deviation is reduced from about 2000 cm^{-1} to about 250 cm^{-1}. Regarding the relative improvement among different complexes, it is found that the energy levels in complexes with lesser amount of covalency are better described by this theory in comparison to those with higher covalency.

The values of parameters were obtained in this way for all the complexes. These are given in Table III along with the positions of the Dq-independent [$^4A_1(G)$, $^4E(G)$] and $^4E(D)$ levels. A comparison of these and values of parameters B and C shows the validity of nephelauxetic series.[3] Similarly, a comparison of Dq values shows the validity of spectrochemical series. It is found for all the Mn^{2+} spectra that the deviations between calculated and experimental energies are larger for the higher energy bands. The theory used in the present work neglects the interactions with higher configurations and since the higher lying energy states are closer to excited configurations, the departures from the theory are more pronounced for the bands involving these states. A least-squares fitting is not tried in the present work since, in view of the theory being less accurate at higher energies, such a fitting makes the

set of parameters equally bad for all the levels and is not very useful for interpretation. In our fitting, which gives preference to the lower levels, the errors from configurational mixing are minimized and the parameters may be evaluated for physical meaning in terms of the environment of the ion.

A Gas-Phase Density-Dependent Directly Bonded Coupling Constant

by A. Keith Jameson* and John P. Reger

Department of Chemistry, Loyola University of Chicago, Chicago, Illinois 60626 (*Received September 14, 1970*)

Solvent shifts of nuclear spin–spin coupling constants have previously been noted.[1] Of particular interest are the relatively large shifts of $^1J(^{28}Si-^{19}F)$ in SiF_4 in various solvents.[2] The shifts are all to larger magnitudes of J relative to the gas and are as large as 5%.

One might be tempted to explain solvent shifts in J on the basis of some property of the solution ("reaction field" for instance). If this is so, then there should be no significant dependence of the coupling constant in the gas phase. If such a dependence on density could be found, it would most likely be in cases where large solvent shifts have been observed if the gas-phase shifts are caused by the same mechanism(s) as the liquid-phase shifts. Also J itself should be relatively large in order that changes in J be large enough to be experimentally measurable. On the basis of these considerations, we decided to search for density dependence of coupling constants in SiF_4 gas, although Coyle, et al., found no measurable difference between the coupling constants in SiF_4 at 30 and 110 atm.

The samples were sealed in borosilicate tubing having an inside diameter of 1.2 mm and an outside diameter of 3.9 mm. The volume was usually about 0.1 ml. When the tubes were carefully prepared and properly annealed we could safely obtain pressures as high as 200 atm. A Varian A-56/60 high resolution spectrometer was used. For SiF_4, calibrated audio side bands of the $^{28}Si^{19}F$ fluorine singlet were impressed on both the upfield and downfield sides of each member of the $^{29}Si^{19}F$ doublet and a linear interpolation was made. Several spectra of each sample were taken. In all cases the standard deviation in the measured J was about ±0.15 Hz. This corresponds to measurement of the position

(13) C. Moore, *Nat. Bur. Stand. (U.S.), Circ.*, No. 467, 2 (1952).

(14) A. Mehra and P. Venkateswarlu, *J. Chem. Phys.*, 47, 2334 (1967).

(15) A. Mehra and P. Venkateswarlu, *ibid.*, 48, 4381 (1968).

(16) R. Pappalardo, *Phil. Mag.*, 2, 1397 (1957).

(17) R. Pappalardo, *J. Chem. Phys.*, 31, 1050 (1959).

(18) R. Pappalardo, *ibid.*, 33, 613 (1960).

(19) A. Mehra, *ibid.*, 48, 1871 (1968).

(20) A. Mehra, *Physica Status Solidi*, 29, 847 (1968).

(21) G. W. Pratt and R. Coelho, *Phys. Rev.*, 116, 281 (1959).

(22) D. R. Huffman, R. L. Wild, and M. Shinmei, *J. Chem. Phys.*, 50, 4092 (1969).

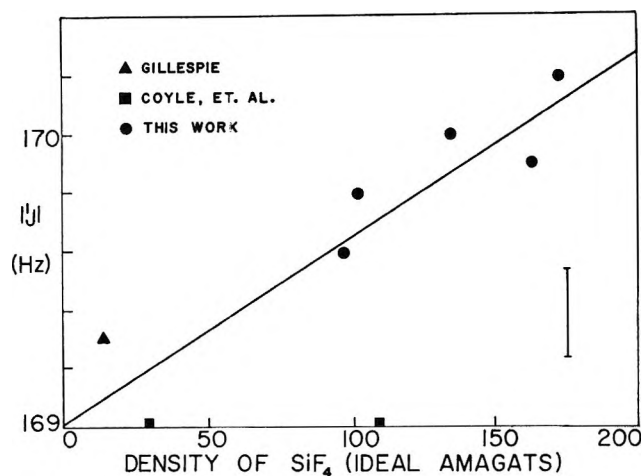(1) For an extensive review see P. Laszlo in "Progress in Nuclear Magnetic Resonance Spectroscopy," Vol. 3, J. W. Emsley, J Feeney, and L H. Sutcliffe, Ed., Pergamon Press, Oxford, 1967.

(2) T. D. Coyle, R. B. Johannesen, F. E. Brinckman, and T. C. Farrar, *J. Phys. Chem.*, 70, 1682 (1966).

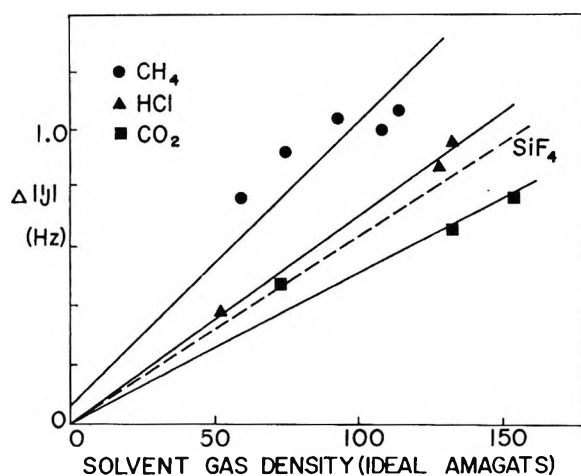Figure 1. The gas-phase density dependence of pure SiF$_4$.

Figure 2. Density dependence of ^1J (SiF$_4$) in various solvent gases.

of each member of the doublet to ± 0.1 Hz. All line widths were about 0.3–0.5 Hz at half-height, except in the CO$_2$ mixtures in which they were about 1.5 Hz. A combination of experimental factors (low filling factor, 5% natural abundance of ^{29}Si) prevented our proceeding to SiF$_4$ densities lower than about 100 ideal amagats. At this density we could obtain a signal to noise ratio of about 5 with very careful tuning. In Figure 1 we see that the values obtained extrapolate nicely to a value consistent with the low density values obtained by Gillespie and Quail[3] and by Coyle, et al.[2]

The results are shown in Figures 1 and 2. Clearly there is a gas-phase density-dependent coupling constant (even in the case of SiF$_4$ itself, contrary to the findings of Coyle, et al.). If we assume that binary collisions cause this effect, then we can write for a binary gas mixture

$$J_A = J_A(0) + \left(\frac{\partial J}{\partial \zeta_A}\right)_{A-A} \zeta_A + \left(\frac{\partial J}{\partial \zeta_B}\right)_{A-B} \zeta_B$$

where $J_A(0)$ = coupling constant for the isolated mole-

cule, $(\partial J/\partial \zeta_A)_{A-A}$ = density dependence of the coupling constant because of binary collisions between A molecules, $(\partial J/\partial \zeta_B)_{A-B}$ = density dependence of the coupling constant because of A–B collisions, ζ_A and ζ_B being the densities of molecules A and B in the gas mixture. The results can be interpreted reasonably well in these terms as shown in Figures 1 and 2. The value obtained for $(\partial J/\partial \zeta)_{\text{SiF}_4-\text{SiF}_4}$ is used in determining $(\partial J/\partial \zeta_B)_{\text{SiF}_4-B}$.

The effect of the second gas is independent of the effect of SiF$_4$ as was demonstrated by data on CH$_4$ at two different densities of SiF$_4$ (ca. 100 and 150 amagats of SiF$_4$). We see in Figure 2 that the nature of the second molecule clearly affects $(\partial J/\partial \zeta_B)_{\text{SiF}_4-B}$. It is interesting to note that when the density of the solvent gas is extrapolated to the densities of the liquids, we obtain $J_{\text{SiF}} \cong 172, 174,$ and 175 Hz for SiF$_4$ in CO$_2$, HCl, and CH$_4$ at densities of 560, 730, and 590 ideal amagats, respectively. Although these gaseous molecules are different from the liquids used by Coyle, et al.,[2] the extrapolated hypothetical liquid phase values fall nicely into the range of values (170.5–178.5 Hz) they found. Therefore, it appears likely that it will not be necessary to invoke an effect peculiar to the liquid phase to explain solvent shifts in directly bonded coupling constants.

We are beginning to search for other molecules in which there may be density dependent directly bonded coupling constants. We have found no density dependence in CH$_4$, SiH$_4$, or PF$_3$. We are in agreement with other workers on the magnitudes of ^1J however.[4] We looked at CH$_4$ alone at densities from 20 to 200 ideal amagats and in the presence of SiF$_4$ at 100 and 150 ideal amagats. We covered a density range from 20 to 200 ideal amagats in SiH$_4$ and from 100 to 190 ideal amagats in PF$_3$. In all cases except PF$_3$ our line widths were 0.3–0.5 Hz at half-height. In PF$_3$ they were about 3.5 Hz at half-height. As a consequence, in PF$_3$ our precision was not so good. Nevertheless, within our experimental error we can see no definite density dependence in the coupling constant for CH$_4$, SiH$_4$, or PF$_3$. These results are summarized in Table I.

At the present time we are not in a position to do much more than speculate as to the cause for most directly bonded coupling constants having no density dependence. It may be that the Fermi contact, orbital, and spin-dipolar terms are affected differently by binary collisions. If this is so, then gas-phase work might give us an experimental measure of the terms affected most highly. We are extending our observations to more binary fluorides in an attempt to find more than a single case of density dependent ^1J.

(3) R. J. Gillespie and J. W. Quail, J. Chem. Phys., 39, 2555 (1963).

(4) (a) CH$_4$: N. Muller and D. E. Pritchard, ibid., 31, 768 (1959); (b) SiH$_4$: E. A. V. Ebsworth and J. J. Turner, ibid., 36, 2628 (1962); (c) PF$_3$: H. S. Gutowsky and C. J. Hoffman, ibid., 19, 1259 (1951).

Table I: $(\partial J/\partial \zeta_B)_{A-B}$ for Various Gas Mixtures

Solute molecule	Solvent molecule	$(\partial J/\partial \zeta_B)_{A-B}$, Hz/ideal amagat	$\frac{10^4}{J_0} \cdot (\partial J/\partial \zeta_B)_{A-B}$, (amagat)$^{-1}$ [a]
SiF$_4$	SiF$_4$	0.0064 ± 0.0009	3.8 ± 0.6
	CH$_4$	0.0097 ± 0.0010	5.7 ± 0.6
	HCl	0.0070 ± (0.0002)	4.1 ± (0.1)
	CO$_2$	0.0050 ± (0.0004)	3.0 ± (0.2)
CH$_4$	CH$_4$	0.0008 ± (0.0006)	0.6 ± 0.5
	SiF$_4$	Nil	...
PF$_3$	PF$_3$	0.00 ± 0.01	0.00 ± 0.07
SiH$_4$	SiH$_4$	−0.0008 ± 0.0008	−0.4 ± 0.4

[a] We take J_0 to be 169.0 ± 0.1 Hz for $J_{Si^{29}F^{19}}$ in SiF$_4$. We measured J_0 as 125.3 ± 0.07 Hz for $J_{C^{13}H^1}$ in CH$_4$, 1402 ± 1 Hz for $J_{P^{31}F^{19}}$ in PF$_3$, and 201.9 ± 0.1 Hz for $J_{Si^{29}H^1}$ in SiH$_4$.

In any case we have demonstrated that all the solvent dependence in coupling constants does not have to be due to reaction field effects. Valence and/or van der Waals interactions may very well be important, as has been suggested by Laszlo and Speert.[5]

Acknowledgment. It is a pleasure to acknowledge assistance in this work from Research Corporation.

(5) P. Laszlo and A. Speert, *J. Mag. Res.*, 1, 291 (1969).

The Effect of Mercury on the Photolysis of 1,1,1-Trifluoroacetone

by C. Pearce and D. A. Whytock*

Department of Chemistry, University of Essex, Colchester, Essex, England (*Received June 10, 1970*)

It is well established that mercury vapor can deactivate the n,π^* triplet state of hexafluoroacetone.[1] Thus the lifetime and Φ decomposition of that state at room temperature are smaller by a factor of 11 than the values under mercury-free conditions.

A much smaller effect on the phosphorescence lifetime of 1,1,1-trifluoroacetone (1,1,1-TFA) has also been reported,[1] the ratio being $\tau_p/(\tau_p)_{Hg} = 1.80$. Thus, by analogy with the primary photolysis process of hexafluoroacetone, it is predicted that for 1,1,1-TFA $\Phi_\infty/(\Phi_\infty)_{Hg} = 1.80$, where Φ_∞ is the quantum yield of decomposition at infinite pressure, *i.e.*, the quantum yield of decomposition from the triplet excited state.

The photodecomposition of 1,1,1-TFA leads to a complex mixture of products[2,3] and a chain reaction is operative at high temperatures.[2] The available evidence suggests that two primary photochemical splits are important. Both reactions 1 and 2 may eventually

$$CF_3COCH_3^* \longrightarrow CF_3CO + CH_3 \quad (1)$$

$$CF_3COCH_3^* \longrightarrow CH_3CO + CF_3 \quad (2)$$

lead to formation of CO. A measurement of ΦCO should then be proportional to the total Φ decomposition. Furthermore, if ΦCO is measured using the same incident intensity under mercury-free conditions as under mercury-saturated conditions, then

$$\frac{(\Phi CO)_\infty}{(\Phi CO)_{\infty \cdot Hg}} = \frac{\Phi_\infty}{(\Phi_\infty)_{Hg}} \quad (3)$$

Measurements of ΦCO from the photolysis of 1,1,1-TFA at 3130 Å in a mercury-free system are shown in Figure 1. It can be seen that ΦCO approaches a limiting value at high pressure, yielding the values $(\Phi CO)_\infty = 0.008_6$ at 25° and $(\Phi CO)_\infty = 0.75_0$ at 117°.

As predicted by measurements of τ_p,[1] the ΦCO mea-
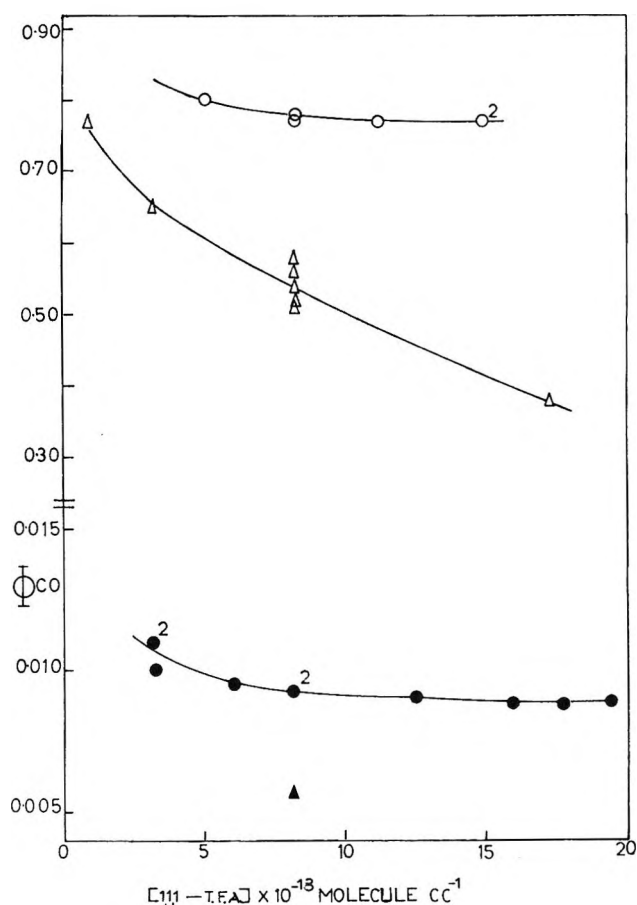
Figure 1. ΦCO values at 3130 Å. Filled symbols refer to 25°, open symbols to 117°. Triangles refer to the values from ref 2 and 4, obtained in the presence of mercury, while circles represent the reported results in the absence of mercury.

(1) A. Gandini, D. A. Whytock, and K. O. Kutschke, *Ber. Bunsenges. Phys. Chem.*, 72, 296 (1968).

(2) R. A. Sieger and J. G. Calvert, *J. Amer. Chem. Soc.*, 76, 5197 (1954).

(3) E. A. Dawidowicz and C. R. Patrick, *J. Chem. Soc.*, 4250 (1964).

surements reported here are higher than those obtained using the same incident intensity in a system containing mercury vapor.[2,4] While $(\Phi CO)_\infty$ in the presence of mercury vapor at 25° has not been measured, the shape of the ΦCO plot at 25° in Figure 1 indicates that the value of $\Phi CO = 0.005_7$ at a concentration of 8.20×10^{18} molecules cc^{-1}[4] may be directly compared to the mercury-free value obtained here, at the same concentration, of $\Phi CO = 0.009_2$, and that

$$\frac{\Phi CO}{(\Phi CO)_{Hg}} = \frac{0.009_2}{0.005_7} = 1.62 = \frac{(\Phi CO)_\infty}{(\Phi CO)_{\infty \cdot Hg}} \quad (4)$$

This value compares favorably with the value of 1.80 predicted on the basis of τ_p measurements[1] and indicates that the quenching reaction

$$CF_3COCH_3{}^* + Hg \longrightarrow CF_3COCH_3 + Hg \quad (5)$$

provides an efficient path for the degradation of the triplet electronic energy of 1,1,1-TFA.

Experimental Section

Apparatus and procedures were almost identical with those used previously.[1] The cylindrical quartz reaction vessel, 20 cm in length, was filled with a parallel beam of light from a dc operated Osram HBO 100-W mercury arc. Light was restricted to wavelengths in the region of 3130 Å by means of a Bausch and Lomb high-intensity monochromator with a band pass of 100 Å. The transmitted light was measured using an RCA 935 photocell and an electrometer. The incident intensity was maintained at 10^{15} quanta sec^{-1}.

Acetone was used as an actinometer, ΦCO at 150° being taken as unity. Quantum yield values were obtained using first-order reflection corrections from the cell and furnace windows.[5]

The CO was collected at −210° and was analyzed by means of a gas buret and a copper oxide furnace in the normal manner.[5] Two U-traps in series were maintained indefinitely at −78° so that no contamination of the mercury-free part of the apparatus occurred when analyses were being performed.

1,1,1-TFA was purified by bulb-to-bulb distillation in vacuo. Different samples from Koch-Light and Fluorochem, Ltd., gave identical results. The decadic molar extinction coefficient at 25° was $\epsilon = 3.95$.

(4) R. A. Sieger, M.Sc. Thesis, The Ohio State University, 1954.

(5) G. B. Carter, R. K. Boyd, and K. O. Kutschke, *Can. J. Chem.*, 46, 175 (1968).

COMMUNICATIONS TO THE EDITOR

Secondary Unimolecular Reactions Subsequent to Substitution Reactions by High-Energy Chlorine-38 and Chlorine-39 Atoms

Sir: The gas-phase substitution reactions of energetic Cl atoms from nuclear recoil have recently been of renewed interest[1-4] and offer interesting comparisons with similar reactions of recoil ^{3}H and ^{18}F.[5] Secondary unimolecular decompositions following high energy substitution reactions have been shown to be quite significant for both recoil ^{3}H[5-13] and ^{18}F[13-18] and accurate measurements of the original primary yields of substitution products can only be relied upon after systematic evaluation of the secondary reactions in each particular system.[12] The percentage depletion of primary yields ranges as high as 100% for CH$_2$TNC from T/H in CH$_3$NC,[10] 98% for methylcyclobutane-t from T/CH$_3$ in dimethylcyclobutane,[11] 100% for c-

C$_3$F$_5$^{18}F from ^{18}F/F in c-C$_3$F$_6$,[17] and 89% for CF$_2$=CF^{18}F from ^{18}F/F in C$_2$F$_4$.[16] While previous detailed studies

(1) L. Spicer and R. Wolfgang, *J. Amer. Chem. Soc.*, 90, 2426 (1968).

(2) C. M. Wai and F. S. Rowland, *ibid.*, 90, 3638 (1968).

(3) L. Spicer and R. Wolfgang, *J. Chem. Phys.*, 50, 3466 (1969).

(4) C. M. Wai and F. S. Rowland, *J. Phys. Chem.*, 74, 434 (1970).

(5) R. Wolfgang, *Progr. React. Kinet.*, 3, 97 (1965).

(6) E. K. C. Lee and F. S. Rowland, *J. Amer. Chem. Soc.*, 85, 897 (1963).

(7) Y.-N. Tang, E. K. C. Lee, and F. S. Rowland, *ibid.*, 86, 1280 (1964).

(8) Y.-N. Tang and F. S. Rowland, *ibid.*, 90, 574 (1968).

(9) Y.-N. Tang and F. S. Rowland, *ibid.*, 90, 570 (1968).

(10) C. T. Ting and F. S. Rowland, *J. Phys. Chem.*, 72, 763 (1968).

(11) C. T. Ting and F. S. Rowland, *ibid.*, 74, 445 (1970).

(12) Y.-N. Tang, E. K. C. Lee, E. Tachikawa, and F. S. Rowland, submitted for publication in *J. Phys. Chem.*

(13) C. McKnight, N. J. Parks, and J. Root, *ibid.*, 74, 217 (1970).

(14) Y.-N. Tang and F. S. Rowland, *ibid.*, 71, 4576 (1967).

(15) Y.-N. Tang, T. Smail, and F. S. Rowland, *J. Amer. Chem. Soc.*, 91, 2130 (1969).

(16) T. Smail, G. Miller, and F. S. Rowland, *J. Phys. Chem.*, 74, 3464 (1970).

Table I: Secondary Unimolecular Reactions from High-Energy Chlorine Atom Substitution Reactions

Parent molecules[a]	CH₂Cl₂	CH₃CH₂Cl	CH₃CH₂Cl	c-C₄H₈	
Type of hot substitution	³⁸Cl-for-Cl	³⁸Cl-for-H	³⁸Cl-for-Cl	³⁸Cl-for-H	³⁹Cl-for-H
Observed stabilization products	CH₂Cl³⁸Cl	CH₃CHCl³⁸Cl CH₂ClCH₂³⁸Cl	CH₃CHCl³⁸Cl	c-C₄H₇³⁸Cl	c-C₄H₇³⁹Cl
Observed unimolecular reaction products	c-C₃H₅³⁸Cl	CH₂=CH³⁸Cl	CH₂=CH³⁸Cl	CH₂=CH³⁸Cl	CH₂=CH³⁹Cl
Product ratio at 1 atm[b] secondary/primary	2.1[c]	≥8.4[d]	4.5	≥1.5	≥1.8
% of Secondary unimolecular reaction at ~1/3 to 1 atm	67%	≥89%	82%	≥60%	≥65%

[a] Typical sample composition in Torr: (i) CH_2Cl_2 (350), C_2H_4 (350), O_2 (50); (ii) C_2H_5Cl (700), O_2 (50); (iii) CH_3CHCl_2 (200), O_2 (50); (iv) (³⁸Cl): c-C₄H₈ (350), CF_3Cl (350), O_2 (50); (v) (³⁹Cl): c-C₄H₈ (350), Ar (350), O_2 (50). [b] Total amount of observed unimolecular reaction products corrected for isotopic loss of H³⁸Cl as appropriate and divided by the total amount of stabilization products. [c] Corrected for c-C₃H₅Cl from C_2H_4 reactions, see text. [d] The secondary/primary ratio has been measured over a factor of 8 in pressure and increases at lower pressure, as expected for such decomposition processes. The actual measured ratios were: 4.18 at 800 Torr, 4.47 at 200 Torr and 4.55 at 100 Torr. Correction for an equal amount of unmeasured decomposition to CH₂=CHCl + H³⁸Cl leads to estimates of 89–90% decomposition.

of the energetic reactions of ³⁸Cl or ³⁹Cl with CH₃Cl[2] or ³⁹Cl with CH₄[3] have failed to give positive evidence of a pressure dependence for excited CH₃³⁸Cl* or CH₃³⁹Cl*, the expected C–Cl bond break for methyl chloride leaves no radioactive label on a readily isolable molecular fragment.[7] We have therefore made a systematic search for the complementary products of such secondary decompositions with systems in which the substitution products sometimes react by a pathway involving survival of the C–Cl bond. Such products include dichloro compounds for which loss of the nonradioactive Cl can occur in 50% of such reactions, and chlorocyclanes which do not react by C–Cl bond break. With each of four molecular targets and utilizing either ³⁸Cl or ³⁹Cl as the energetic recoil species, we have observed secondary unimolecular processes following both the ³⁸Cl-for-Cl, ³⁹Cl-for-H, and ³⁹Cl-for-H substitution reactions.[19] The pertinent data are summarized in Table I.

The simplest system analytically is the substitution of ³⁸Cl-for-Cl in CH₃CHCl₂, for which the excited product CH₃CHCl³⁸Cl* is either stabilized by collision or decomposes by elimination of HCl to form CH₂=CH³⁸Cl.[20] At 200 Torr of CH₃CHCl₂, the observed yield of CH₂=CH³⁸Cl is 2.25 times as great as that of stabilized CH₃CHCl³⁸Cl. After allowance for an assumed equal amount of decomposition to CH₂=CHCl plus H³⁸Cl, the measured decomposition/stabilization ratio is 4.5, corresponding to 82% decomposition of the primary product.[21]

The substitution of energetic ³⁸Cl-for-H with cyclobutane gives c-C₄H₇³⁸Cl*, whose decomposition can lead to CH₂=CH³⁸Cl plus C_2H_4 with an activation energy of about 60 kcal/mol.[22] This system has been investigated with both ³⁸Cl and ³⁹Cl with essentially equivalent results; decomposition is >60% at about 1 atm. In each case, the percentage decomposition is

only a lower limit, for excited molecules of c-C₄H₇Cl* presumably also decompose through the 55 kcal/mol thermal pathway of elimination of HCl,[22] without any radioactive trace measured in this system.

The substitution of ³⁸Cl-for-Cl in CH_2Cl_2 creates excited CH₂Cl³⁸Cl, which decomposes chiefly by elimination of HCl.[8] The other decomposition product, CH³⁸Cl, was efficiently trapped with ethylene and measured as c-C₃H₅³⁸Cl. The quantitative accuracy of this experiment is limited by the necessity for a substantial correction, measured in CF₃Cl-C₂H₄ mixtures, for formation of CH³⁸Cl by energetic ³⁸Cl reaction with C_2H_4.

The substitution of ³⁸Cl-for-H in CH₃CH₂Cl produces both CH₃CHCl³⁸Cl* and CH₂ClCH₂Cl*. Quantitative measurements in this system are complicated by the probable decomposition of the latter by C–Cl bond break,[23] since neither ³⁸Cl nor CH₂CH₂³⁸Cl would eventually be detected in the particular gas chromatographic analysis employed. On the assumption that both parent molecules decomposed *only* by HCl loss (and H³⁸Cl in equal yield), the lower limit to per cent decomposition for these ³⁸Cl-for-H products is

(17) C. McKnight and J. Root, *J. Phys. Chem.*, **73**, 4430 (1969).

(18) A. Richardson and R. Wolfgang, *J. Amer. Chem. Soc.*, **92**, 3480 (1970).

(19) S. Krutzig and A. P. Wolf have observed fragmentation yields several times higher than the stabilized substitution yields for hot ³⁸Cl reactions with all three of the 1-chloro-2,3-dimethylcyclopropanes; Fifth Informal Hot Atom Conference, Cambridge, England, July 1969.

(20) D. H. R. Barton and K. E. Howlett, *J. Chem. Soc.*, 165 (1949).

(21) If CH₃CHCl³⁸Cl* also decomposes by C–Cl bond break (see ref 23), then some decomposition products would not be detected and 82% decomposition would be only a lower limit.

(22) A. T. Cocks and H. M. Frey, *J. Amer. Chem. Soc.*, **91**, 7583 (1969).

(23) K. E. Howlett, *J. Chem. Soc.*, 1409 (1951). With the higher energies available in our system, HCl elimination is also possible.

calculated as > 89% at 1 atm, and still larger at lower pressures.

The pressure dependence of the secondary/primary ratio indicated in footnote d of Table I is consistent with the general picture that CH_2=$CH^{38}Cl$ is formed by secondary elimination of HCl from $CH_2ClCH_2{}^{38}Cl^*$ and/or $CH_3CHCl^{38}Cl^*$. With percentage decompositions in the 90% range, little change in the yield of CH_2=$CH^{38}Cl$ is expected with pressure. In these systems, it has also been difficult to find a monitor reaction that is pressure independent and can serve as a standard for comparison; the most effective procedure has been the measurement of variations in secondary/primary ratios, as in footnote d, even though potentially misleading if both products happen to vary with pressure in the same manner.

In addition to the data given in Table I, other preliminary experiments have shown the chloropropene isomerization products[24] from both ^{38}Cl-for-H and ^{39}Cl-for-H reactions with c-C_3H_6 and the formation of $CH^{38}Cl$ following ^{38}Cl-for-H reactions with CH_3Cl. Thus, six separate systems have already given evidence for appreciable secondary decomposition or isomerization after hot chlorine atom reactions in the $^1/_3$ to 1 atm range. With the 3 ± 0.5 eV activation energies of the reactions involved here, the typical excitation energies of the primary product molecules must include substantial fractions with >5 eV to account for the extensive secondary reactions noted. These excitation energies appear to be crudely comparable to those previously found with both ^3H and ^{18}F and indicate that such substitution processes commonly follow mechanistic pathways requiring the deposition of substantial excitation energies in the product molecules.

As has been previously noted for both ^3H and ^{18}F substitution reactions,[6-17] the primary yields measured at about 1 atm can be seriously in error by large factors (>4.5 for ^{38}Cl-for-H with C_2H_5Cl), which probably vary with the particular mechanisms for secondary reaction and with individual molecular properties. Consequently, theoretical conclusions based solely on stabilized parent molecule yields in the 1-atm range are placed in serious doubt, pending evaluation of the significance of secondary decomposition in such systems.[1,3]

Gas samples were prepared by standard techniques, and were irradiated either with high energy bremsstrahlung for the $^{40}Ar(\gamma,p)^{39}Cl$ nuclear reaction or with thermal neutrons for the $^{37}Cl(n,\gamma)^{38}Cl$ reaction.[2,4,5] Free radical reactions induced by the background radiation were successfully eliminated by inclusion of 50 Torr of O_2 in each sample. Product analysis was performed by the usual radio gas chromatographic techniques with a variety of columns to ensure product separation and identification.[25]

(25) J. K. Lee, E. K. C. Lee, B. Musgrave, Y.-N. Tang, J. W. Root, and F. S. Rowland, Anal. Chem., 34, 741 (1962).

(26) This research was supported by A.E.C. Contracts No. AT-(40-1)-3898 and AT-(11-1)-34, Agreement No. 126. A small part of this work was presented at the 156th National Meeting of the American Chemical Society, Atlantic City, N. J., Sept 1968.

Department of Chemistry[26]   Yi-Noo Tang
Texas A. and M. University   W. S. Smith
College Station, Texas   77843   J. L. Williams
                                                                 K. Lowery

Department of Chemistry[26]   F. S. Rowland*
University of California
Irvine, California   92664

On the Intrinsic Viscosity of Polyelectrolytes

Publication costs borne completely by The Journal of Physical Chemistry

Sir: The intrinsic viscosity of polyelectrolyte–salt solutions has been recently studied in great detail by Takahashi, Nagasawa, and coworkers,[1-3] both with respect to its dependence on the polymer molecular weight, M, and on the salt concentration, m_s. The ratio of this intrinsic viscosity in a non-θ and θ solvent is related to the chain expansion coefficient, α (or α_η), as

$$[\eta]/[\eta]_\theta = \alpha^3 \qquad (1)$$

Now, theories dealing with the (linear) chain expansion due to excluded volume derive expressions describing α as function of the parameter z, where

$$z \sim M^{1/2}\beta \qquad (2)$$

β being the excluded volume of a free jointed chain link. With nonionic polymers, no theoretical treatment of β has been attempted and the functional dependence $\alpha(z)$ is therefore actually studied as $\alpha(M^{1/2})$ at constant β. With polyelectrolytes, however, β is related to the comparatively well known polyelectrolyte potential and as such becomes more amenable to a theoretical treatment. Specifically polyelectrolyte theories let one derive an expression for $\beta(m_s)$, so that the dependence of α on two controllable variables can be given as follows

$$\alpha(z) = \alpha[M^{1/2} \times \beta(m_s)] \qquad (3)$$

This type of relationship had been derived some time ago by the present author.[4] Starting from his theory

(1) A. Takahashi and M. Nagasawa, J. Amer. Chem. Soc., 86, 543 (1964).

(2) A. Takahashi, T. Kato, and M. Nagasawa, J. Phys. Chem., 71, 2001 (1967).

(3) I. Noda, T. Tsuge, and M. Nagasawa, ibid., 74, 710 (1970).

(4) Z. Alexandrowicz, J. Chem. Phys., 47, 4377 (1967).

(24) 3-Chloropropene was the only isomerization product observed from thermally excited c-C₂H₅Cl, see R. C. S. Grant and E. S. Swinburne, Chem. Commun., 620 (1966). With the extra excitation energy available in our system, the 1-chloropropenes are also observed as products.

on excluded volume, which for practical purposes could be approximated by the line

$$\alpha^2 \simeq 1.7 \, z^{1/2}; \text{ for } 2 < \alpha^2 < 25 \qquad (4)$$

and identifying the excluded volume with the coaxial shell surrounding the polyelectrolyte filament, it was found that

$$\alpha^2(M, m_s) = K M^{1/4} \chi \gamma \qquad (5)$$

Here K is specified in terms of molecular parameters but, except for a guess of its magnitude, is treated as an adjustable parameter. The product function $\chi \gamma$ depending on m_s represents the polyelectrolyte excluded volume per chain link. Thus $\chi(m_s)$ is related to the high potential shell radius b, with subtraction of the θ solvent negative contribution to excluded volume as follows

$$\chi^2 = b^2 - b_\theta^2 \qquad (6)$$

so that $\chi = 0$ at θ. The other function, $\gamma(m_s)$, is defined as

$$\gamma \begin{cases} = 1; \text{ for } \chi < L \\ = (L/\chi)^{1/4}; \text{ for } \chi > L \end{cases} \qquad (7)$$

It is used to express the loss of chain flexibility with increasing thickness of the excluded shell, which becomes effective when $b(\simeq \chi)$ becomes greater than the length, L, of the chain's equivalent free-jointed links.

The functional dependence of $\chi \gamma$ on m_s has been computed by the author[4] for the polyacrylate chains studied by Takahashi and Nagasawa[1] and subsequently[5] for the polystyrene sulfonate chains studied by Takahashi, Kato, and Nagasawa;[2] indeed, except at high m_s, the dependence is much the same for the two polyelectrolytes and for other chains of similar charge density. Consequently, a twofold check on the fit of eq 5 with experimental data could be presented: First, α_η^2 computed from viscosity was plotted vs. $M^{1/4}$ at constant m_s and was found to obey very well the required straight line relationship. Second, the slopes of the lines, reduced by an arbitrary constant (K), could be satisfactorily fitted into the theoretical curve describing $\chi \gamma$ vs. $m_s^{-1/2}$. Admittedly, the evidence of the second plot is regarded as less conclusive since the calculation of $\chi \gamma(m_s)$ depends to some extent on the value of L, which could only be estimated. Still the data certainly did not disagree with the theory's prediction.

Hence I would like to dispute the view taken subsequently by Noda, Tsuge, and Nagasawa (NTN).[3] Rephrasing in brief their argument (in the introductory and concluding paragraphs, as well as in the synopsis) we might say: (a) The intrinsic viscosity according to NTN and to many other results depends linearly on $m_s^{-1/2}$. (b) With respect to all theories one can take that z depends linearly on m_s^{-1}, so that $z^{1/2} \sim m_s^{-1/2}$.
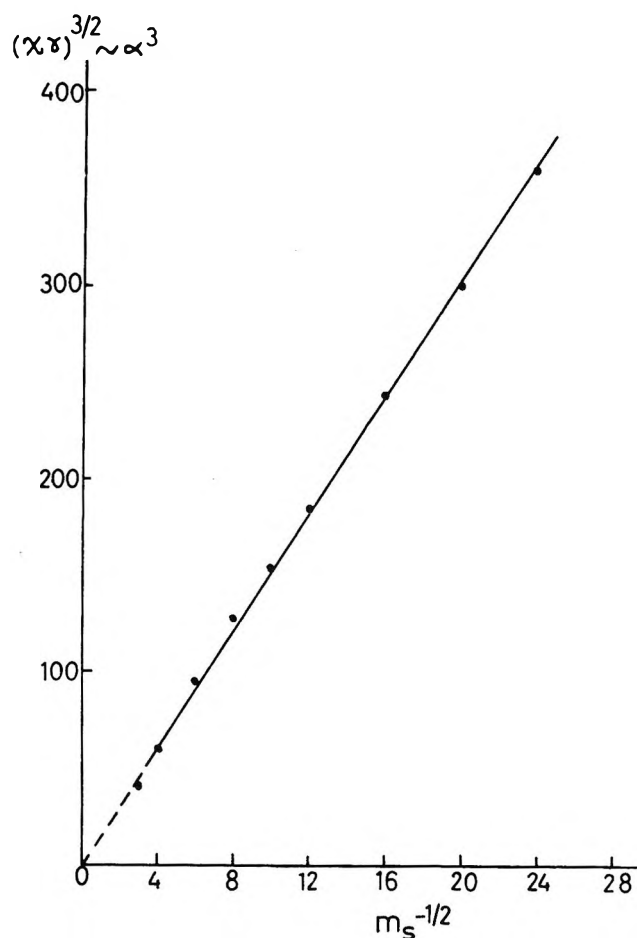
Figure 1. The dependence of the polyelectrolyte theory[4] product function $(\chi \gamma)^{3/2} \sim \alpha^3$, on the reciprocal square root of the salt concentration, $m_s^{-1/2}$ (●). Solid line describes $\alpha^3 \sim m_s^{-1/2}$.

(Though a detailed argument is presented only for the case of low polyelectrolyte potential, this limitation is not stressed throughout the NTN article.) (c) The present author's theoretical line $\alpha^2 \sim z^{1/2}$ (eq 4) implies therefore

$$\alpha^3 = [\eta]/[\eta]_\theta \sim z^{3/4} \sim m_s^{-3/4} \qquad (8)$$

which contradicts point a.

Now the fault with this argument resides at point b, for the author's product function $\chi \gamma$ ($\sim z^{1/2}$, eq 4 and 5) is by no means linearly dependent on $m_s^{-1/2}$, as shown in the relevant figures.[4,5] To make matters clearer, the theoretical line of these figures has been replotted here, (Figure 1), giving $(\chi \gamma)^{1/2} \sim \alpha^3$ (see eq 5) vs. $m_s^{-1/2}$; the figure shows that above $m_s^{-1/2} = 3$, the theoretical α^3 is proportional to $m_s^{-1/2}$, in full accord with point a.

Admittedly this linear dependence extends, neither to high values of m_s, nor for chains of low charge density (for which the concept of excluded high potential shell ceases to be valid), but then these regions are comparatively less important in the context of the wide

(5) Z. Alexandrowicz, J. Polymer Sci. A2, 6, 1227 (1968).

sweep study of $\alpha(z)$—a field pioneered to a large extent by the measurements of Takahashi and Nagasawa. The same goes for the molecular weight dependence argued by NTN. True, low to medium values of α satisfactorily obey Fixman's equation[6]

$$\alpha^3 - 1 \sim M^{1/2} \qquad (9)$$

but as Takahashi, Nagasawa, and coworkers point out themselves[1-3] their high α's increase with $M^{1/2}$ less rapidly than required by the above equation. (Unfortunately the relevant points are not reproduced in the figures given by the authors; still they may be easily extracted from the tabulated data.) On the other hand, as stated before, the wide sweep variation of α with $M^{1/4}$, for all $\alpha^2 > 2$, is quite adequately described by the author's ec 5.

(6) M. Fixman, *J. Chem. Phys.*, **41**, 3772 (1964); **23**, 1656 (1955); **36**, 3123 (1962).

POLYMER DEPARTMENT   Z. ALEXANDROWICZ
WEIZMANN INSTITUTE OF SCIENCE
REHOVOT, ISRAEL

RECEIVED SEPTEMBER 8, 1970

Ion Lifetimes in Gaseous Ammonia

Sir: We have recently reported values in the range 1.0 to 2.0 $\times$ 10^{-6} ion pairs^{-1} cm^3 sec^{-1} for combination coefficients of ions formed in the radiolysis of several electron-attaching gases at pressures of $\sim$600 Torr and room temperature.[1] Using the same pulsed X-ray and ion collection technique we have observed a much larger ion combination coefficient in ammonia, in which electrons should remain free. The magnitude of this coefficient is also much greater than those reported for electron–ion combinations in plasmas.[2]

Matheson research grade ammonia was purified by careful degassing and by preirradiation to a dose of $\sim$1.5 $\times$ 10^{19} eV g^{-1} to clean up electron attaching impurities. Typical results are shown in the form of the second-order decay plots A and B in Figure 1. The X-ray intensity for line B was adjusted to give about twice the ion concentration at the end of the pulse as that used for line A. Within experimental error the plots are parallel and linear over at least one half-life. This shows that the recombination reaction is second order–first order in both the negative and the positive ion concentration. The mean value of several pulsed X-ray determinations of the ion combination coefficient α_1 in the ammonia pressure range 550–650 Torr was 2.5 $\pm$ 0.5 $\times$ 10^{-6} ion pairs^{-1} cm^3 sec^{-1}. An identical result was calculated from the steady-state ion concentrations existing in a continuous radiolysis using the expression α_1 = (rate of ion formation) $\times$ (steady-state
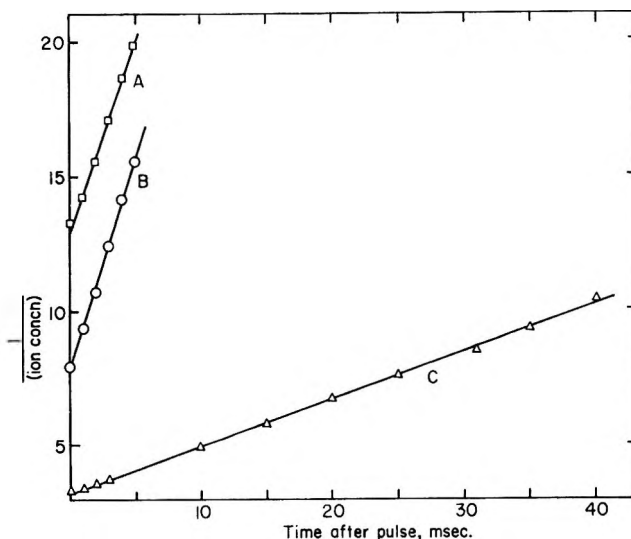
Figure 1. Second-order plots for the decay of ions in pulse-irradiated NH$_3$: lines A and B, ammonia purified as described in text; line C, same ammonia sample with $\sim$2 $\times$ 10^{-3} Torr of oxygen added. Ion concentrations are in arbitrary units.

ion concentration)$^{-2}$. The steady-state ion concentrations were measured by the method of McGowan.[3]

At the pressures used in this study ion neutralization reactions are normally three-step processes

$$A^+ + B^- \rightleftharpoons (A^+ \ldots B^-)^* \qquad (1a,b)$$

$$(A^+ \ldots B^-)^* + M \rightleftharpoons (A^+ \ldots B^-) + M \qquad (1c,d)$$

$$(A^+ \ldots B^-) \longrightarrow \text{neutrals} \qquad (1e)$$
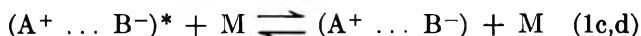
with reaction 1c corresponding to collisional stabilization[2,4] of the ions to form an orbiting ion pair $(A^+ \ldots B^-)$. The maximum value of the ion combination coefficient occurs when reaction 1d is negligible and $(M) \times k_{1c} \gg k_{1b}$. It is equal to k_{1a} and hence from kinetic theory $\alpha = k_{1a} = \Pi b_c^2 \times (8kT/\Pi\mu)^{1/2}$. The impact parameter b_c should be $\simeq 2e^2/3kT$ to a first approximation,[2] and for normal molecular weight ions $(\mu \sim 30$ atomic mass units or larger if clustering is significant) it follows that the recombination coefficient at room temperature should be $<3 \times 10^{-6}$ ion pairs^{-1} cm^3 sec^{-1} as has been observed.[1,4] The much larger value of α_1 in ammonia can be explained if B$^-$ is a free electron, since μ is then $\sim$10^4 times less and $(8kT/\Pi\mu)^{1/2} \sim 10^2$ times larger than when both A$^+$ and B$^-$ have normal molecular weights.

The main positive ion in irradiated ammonia at our pressure is clustered NH$_4^+$.[5] The effective cross section

(1) D. E. Wilson and D. A. Armstrong, *Can. J. Chem.*, **48**, 598 (1970).

(2) E. W. McDaniel, "Collision Phenomena in Ionised Gases," Wiley, New York, N. Y., 1964.

(3) S. McGowan, *Phys. Med. Biol.*, **10**, 25 (1965).

(4) B. H. Mahan and J. C. Person, *J. Chem. Phys.*, **40**, 392 (1964).

(5) A. M. Hogg and P. Kebarle, *ibid.*, **43**, 449 (1965).

calculated from α_1 on the assumption that reaction 1a with $A^+ = NH_4^+$ and $B^- = e^-$ is the rate-controlling process actually turns out to be some twenty times smaller than the capture cross section observed for typical *ion–ion* neutralization reactions (Πb_c^2 is typically 4×10^{-11} cm^2 [4]). Hence either reaction 1d is not negligible or 1c is much less efficient for electrons than for ions, or both. In reaction 1c the electron, which has gained kinetic energy in entering the coulombic potential field of NH_4^+, loses kinetic energy in a collision with an ammonia molecule. The average fraction of kinetic energy lost by a 0.03 to 3 eV electron in such a collision is only ~ 0.02,[6] which is much less than the fractional energy loss per collision between an ion and a molecule of similar mass. Hence the second situation noted above is highly probable. However, the electron–NH_4^+ reaction may be more complex than this simple picture implies. Studies of the temperature and pressure dependence of α_1 are being conducted in an attempt to obtain further information about the reaction.

From the foregoing it can be seen that addition of an electron scavenger to the ammonia system should decrease the recombination coefficient to a more normal value. The data of line C in Figure 1 were obtained from the same ammonia sample as lines A and B after the addition[7] of sufficient oxygen to remove electrons in reaction 2

$$e + O_2 + M \longrightarrow O_2^- + M \qquad (2)$$
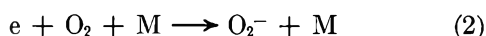
before they could react with NH_4^+. The much reduced ion-combination coefficient calculated from the slope of line C, 1.8×10^{-6} ion pairs^{-1} cm^3 sec^{-1}, lies in the range for normal molecular weight ions. Hence capture of the electrons has the anticipated effect.

(6) L. G. Christophorou and J. G. Carter, *Chem. Phys. Lett.*, **2**, 607 (1968).

(7) A few microns pressure of dry air was admitted to the irradiation cell while the ammonia was momentarily condensed in a liquid nitrogen trap. From the rate constant of reaction 2 [see J. A. Stockdale, L. G. Christophorou, and G. S. Hurst, *J. Chem. Phys.*, **47**, 3267 (1967)] it can be shown that 2×10^{-2} Torr of O_2 is sufficient to capture all electrons under our conditions.

Department of Chemistry   D. E. Wilson
The University   D. A. Armstrong*
Calgary 44, Alberta, Canada

States of Atomic Carbon Produced in

Decomposition of Organic Compounds

in a Microwave Plasma

Sir: Carbon atoms have been studied in a number of systems using a great variety of techniques. The sources of atomic carbon have included nuclear trans-

formations,[1,2] the carbon arc,[3] pulse radiolysis,[4] photolysis,[5] explosion of graphite filaments,[6] evaporation of graphite rods,[7] and shock heating.[8] These studies have enriched our knowledge of qualitative aspects of carbon chemistry, but the techniques are of limited utility in kinetic studies of carbon atom reactions. Even double flash photolysis[5b] and pulse radiolysis[4] experiments which permit direct and quantitative monitoring of carbon atom concentrations are limited to reaction substrates less labile than the precursors of the carbon atoms.

Recently, Martinotti, Welch, and Wolf[9] generated carbon atoms in a flow system such that reaction substrates could be introduced downstream from the microwave-sustained helium plasma which converted carbon suboxide into free carbon atoms. This arrangement allows *any* gaseous reactant to be introduced into a helium stream containing an initial carbon atom concentration of *ca.* 10^{-10} mol/l. within 1 msec after generation.

When a similar flow system is combined with apparatus for atomic emission and absorption spectroscopy, three low lying excited states of atomic carbon ^1P, ^1S, and ^1D can be observed directly.

A helium stream containing a trace amount of organic substance was passed through an electrodeless microwave discharge which was maintained by a 2450-MHz diathermy unit coupled to the flow system through a foreshortened $^1/_4$ wave coaxial cavity.[10] Power input to the cavity was measured with a bidirectional power meter.

The emission spectrum of the plasma was recorded on film using a 3.4-m Ebert spectrograph. In the region 2200 to 4200 Å a single sharp line was observed at 2478.6 Å when carbon suboxide, carbon monoxide, and benzene were passed through the plasma. Operating conditions are summarized in Table I. In addition to the sharp atomic line, several broad molecular emission bands were observed. The observation of the $^1S \leftarrow ^1P$ transition of carbon confirms the production of carbon atoms which had been deduced by Martinotti,

(1) A. P. Wolf, *Advan. Phys. Org. Chem.*, **2**, 201 (1964).

(2) R. Wolfgang, *Progr. React. Kinet.*, **3**, 97 (1965).

(3) P. S. Skell and R. F. Harris, *J. Amer. Chem. Soc.*, **91**, 4440 (1969).

(4) G. M. Meaburn and D. Perner, *Nature*, **212**, 1042 (1966).

(5) (a) E. Tschuikow-Roux and S. Kodama, *J. Chem. Phys.*, **50**, 5297 (1969); (b) W. Braun, A. M. Bass. D. D. Davis, and J. D. Simmons, *Proc. Roy. Soc., Ser. A.*, **312**, 417 (1969); (c) R. T. Mullen and A. P. Wolf, *J. Amer. Chem. Soc.*, **84**, 3214 (1962).

(6) C. W. Spangler, S. K. Lott, and M. J. Joncich, *Chem. Commun.* 842 (1966).

(7) J. L. Sprung, S. Winstein, and W. F. Libby, *J. Amer. Chem. Soc.*, **87**, 1812 (1965).

(8) A. R. Fairbairn, *J. Quant. Spectrosc. Radiat. Transfer*, **9**, 943 (1969).

(9) F. F. Martinotti, M. J. Welch. and A. P. Wolf, *Chem. Commun.*, 115 (1968).

(10) F. C. Fehsenfeld, K. M. Evenson, and H. P. Broida, *Rev. Sci. Instrum.*, **36**, 294 (1965).

Table I: Conditions under Which Emission of 2478-Å Carbon Line Was Observed

Substrate	Power input, W	Main flow, cc/min at STP	Substrate feed in rate cc/min at STP	Press. in line, Torr
C_3O_2	32	16	0.05	0.4
C_3O_2	42	21	0.17	0.7
C_3O_2	56	2730	0.94	27.5
C_3O_2	41	14	0.002	0.3
C_3O_2	41	16	0.012	0.4
C_3O_2	88	2620	0.027	46
C_3O_2	85	2620	0.11	46
CO	48	2335	1.8	40
CO	48	2450	52	42
CO	36	14	0.37	0.2
CO	41	18	10.6	0.5
Benzene	65	2480	~0.28/min	40

et al., from chemical evidence.[9] Emission at 1930.9 Å due to the atomic transition of carbon $^1D \leftarrow {}^1P$ was detected when the plasma radiation was examined with a 0.5-m Ebert monochromator in a Jarrell-Ash atomic emission and absorption scanning spectrometer equipped with a type R106 photomultiplier tube. The $^3P \leftarrow {}^3P_0$ transition to the ground state of atomic carbon could not be detected because it falls in the vacuum ultraviolet region (1656-1658 Å) inaccessible to the available equipment.

Having established by emission studies the production of ^1P, ^1S, and ^1D carbon atoms from various carbon compounds in the helium plasma, an experiment was undertaken to detect carbon atoms in the flow system *downstream* from the discharge region. This was accomplished by atomic absorption spectroscopy, using the optical transitions of ^1D and ^1S carbon atoms at 1930.9 and 2478.6 Å, respectively.

An optical cell 8 cm in length with parallel quartz windows was incorporated in the flow system within 4 cm of the discharge region. Thus the gas stream enters the optical cell *ca.* 1 msec after it leaves the plasma. A microwave-excited electrodeless discharge lamp containing 10 Torr of helium and a trace of carbon suboxide served as the light source for the carbon resonance lines at 2478.6 and 1930.9 Å. The discharge lamp was focused through the optical cell of the flow system onto the entrance slit of the monochromator of the atomic absorption spectrometer. The light source was modulated by a mechanical chopper to whose frequency the photomultiplier amplifier was tuned.

In an absorption experiment the monochromator was set to focus one of the carbon resonance lines on the exit slit. The optical cell was evacuated without gas flow, and the photomultiplier amplification was adjusted to give a full scale reading I_0 on an auxiliary recorder. Helium flow was adjustable over a wide range, 10 to 4000 cc/min STP at pressures in the flow system of 0.2-80 Torr. I_0 was not affected by the pressure in

the flow system nor by ignition of the plasma. When a mixture of an organic substrate and helium was introduced into the plasma, a sharp decrease in I_0 was observed at both 2478 and 1930 Å, indicating the formation of a species capable of absorption ΔI of the carbon resonance lines. The light intensity impinging on the photomultiplier could be restored to I_0 by either extinguishing the plasma with the substrate still flowing through the system, or by discontinuing the feeding of substrate into the plasma.

Although a number of simple carbon compounds were utilized as substrates, carbon suboxide and allene were found to give the highest absorption of the two carbon lines. The extent of absorption of the carbon resonance lines varied with several operational parameters. ΔI increased with total pressure and flow rate in the flow system. ΔI also increased with increased feed rate of the substrate and increased power input into the cavity. When the distance between the plasma discharge and the optical cell was increased, ΔI decreased. This indicates that the absorbing species is a short-lived transient.

In order to ascertain that carbon atoms were responsible for absorption at 2478 and 1930 Å, absorption at other wavelengths was investigated. Under identical conditions in the flow system, absorption of various atomic lines produced by hollow cathode discharge lamps was compared with the absorption of the carbon resonance lines. The results are given in Table II and indicate that absorption at 1930.9 and 2478.6 Å is always greater than that at other wavelengths. It is

Table II: ΔI at Different Wavelengths

Substrate	Main flow, cc/min at STP	Substrate feed in rate cc/min STP	Press. in line Torr	Wavelength, Å	ΔI, %
C_3O_2	1880	0.9	20	2478	3.2
C_3O_2	1880	0.9	20	1930	3.3
C_3O_2	1880	0.9	20	2320	2.1
C_3O_2	1880	0.9	20	2483	1.8
C_3O_2	1880	0.9	20	3579	0.5
C_3O_2	1880	0.9	20	2795	1.0
C_3O_2	3930	0.013	78	2478	16
C_3O_2	3930	0.013	78	2483	10
C_3O_2	3930	0.013	78	2795	6
C_3O_2	3200	0.9	100	2478	35
C_3O_2	3200	0.9	100	2463	5
C_3O_2	3200	0.9	100	2465	4
Allene	2150	1.2	38.5	2478	5
Allene	2150	1.2	38.5	2483	0
Allene	2800	0.4	76	2478	32
Allene	2800	0.4	76	1930	29
Allene	2800	0.4	76	2483	12
Allene	2800	0.4	76	2320	12
Allene	2800	0.4	76	3525	7
Allene	2800	0.4	76	2795	12
Allene	2800	0.4	76	2428	20

significant that there is a substantial decrease in absorption on going from 2478.6 to 2483 Å, a change of only 4 Å. This strongly suggests that the absorption at 2478.6 Å is due to a sharp atomic line. Nevertheless, since absorption at other wavelengths is not negligible compared to that at 1930.9 and 2478.6 Å, it is clear that at the concentration of excited carbon atoms available there is some interference from molecular bands. An alternate explanation suggesting that the observed absorption is due to molecular absorptions is quite unlikely since as noted the lines are quite sharp and both lines appear in the spectra of the systems studied. The coincidence of finding these two lines at the wavelengths corresponding to the two carbon transitions listed, in the spectra of two chemically different substrates, C_3O_2 and C_3H_4, is strong evidence that the absorbing species is indeed atomic carbon.

The present results indicate that carbon atoms are formed in the plasmolysis of carbon suboxide and allene and that sufficient carbon atoms in excited ^1S and ^1D states survive collision at ca. 10^1 Torr for 10^{-3} sec to be observed by absorption spectroscopy. By combining a discharge-flow system with atomic absorption spectroscopy, a method has been developed which will allow direct kinetic studies on the reactions of carbon atoms with a variety of substrates. The use of a vacuum spectrograph will allow detection of the more abundant ^3P ground state of atomic carbon and facilitate the study of its reactions.

CHEMISTRY DEPARTMENT   ERNEST Y. Y. LAM
BROOKHAVEN NATIONAL LABORATORY   PETER GASPAR
UPTON, NEW YORK 11973   ALFRED P. WOLF*

RECEIVED AUGUST 17, 1970

Effects of Deuterium Substitution on

the Electron-Transfer Reactions

Sir: Since the pioneering work of Ward and Weissman in 1957,[1] the electron spin resonance (esr) technique has been shown to be uniquely suitable in the study of fast organic electron transfer reactions.[2] We report here what we believe to be the first study of the deuterium isotope effect on the rate of electron transfer of the following reactions

$$C_{10}H_8{}^- + C_{10}H_8 \underset{}{\overset{k_{HH}}{\rightleftarrows}} C_{10}H_8 + C_{10}H_8{}^- \quad (1)$$

$$C_{10}D_8{}^- + C_{10}D_8 \underset{}{\overset{k_{DD}}{\rightleftarrows}} C_{10}D_8 + C_{10}D_8{}^- \quad (2)$$

$$C_{10}H_8{}^- + C_{10}D_8 \underset{k_{DH}}{\overset{k_{HD}}{\rightleftarrows}} C_{10}H_8 + C_{10}D_8{}^- \quad (3)$$
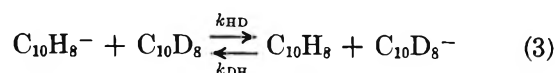
where $C_{10}H_8$ and $C_{10}D_8$ represent naphthalene and perdeuterionaphthalene, $C_{10}H_8{}^-$ and $C_{10}D_8{}^-$ the corresponding anion radicals, and k_{HH}, k_{DD}, k_{HD}, and k_{DH} the second-order rate constants. The rates were measured in both the slow and intermediate limit,[3] using the computer simulation technique described by Norris.[4] The results are summarized in Table I.

Table I: Rate Constants for Electron Transfer between Potassium Naphthalenide and Naphthalene in Tetrahydrofuran at 25°

	$k_{DD}{}^a \times 10^{-7}$, M^{-1} sec^{-1}	$k_{HH} \times 10^{-7}$, M^{-1} sec^{-1}	$k_{HD} \times 10^{-7}$, M^{-1} sec^{-1}	$k_{DH}{}^b \times 10^{-7}$, M^{-1} sec^{-1}
Slow limit		3.3 ± 0.1	2.8 ± 0.2	7.0 ± 2.2
Intermediate limit	3.0 ± 0.3	3.3 ± 0.1	2.8 ± 0.3	7.0 ± 2.5

^{a} Because of the large number of overlapping lines, the values obtained in the slow limit are unreliable. ^{b} Calculated from the equation $K_{HD} = k_{HD}/k_{DH}$, where K_{HD} is the equilibrium constant for reaction 3.

From the nearly equal values of k_{HH} and k_{DD}, it can be concluded that the deuterium effect on the transfer rate, if any, is small. The results obtained for reaction 3, however, are of considerable interest. The equilibrium constant K_{HD} for the forward reaction is found to be 0.4 ± 0.1 at room temperature. Figure 1 shows the esr spectrum of a mixture of $C_{10}H_8{}^-$ and $C_{10}D_8{}^-$.[5] At $-60°$, K_{HD} is equal to 0.6 ± 0.05.[6] Applying Marcus's equation to our system, we write[7]

$$k_{HD} = \sqrt{k_{HH}k_{DD}K_{HD}}$$

and using the upper limit values for k_{HH}, k_{DD}, and K_{HD}, we obtain a value of 2.4×10^7 M^{-1} sec^{-1} for k_{HD} which agrees to about 10% of the lower limit experimentally measured value. Similarly, a value of 4.7×10^7 M^{-1} sec^{-1} is calculated for k_{DH}. However, this

(1) R. L. Ward and S. I. Weissman, *J. Amer. Chem. Soc.*, **70**, 2068 (1957).

(2) For a complete list of such reactions studied by esr to date, see G. L. Malinoski, W. H. Bruning, and R. G. Griffin, *ibid.*, **92**, 2665 (1970).

(3) L. H. Piette and W. A. Anderson, *J. Chem. Phys.*, **30**, 899 (1959).

(4) J. R. Norris, *Chem. Phys. Lett.*, **1**, 333 (1967).

(5) The ratio $[C_{10}D_8{}^-/[C_{10}H_8{}^-]$ is measured by comparing the intensity of the esr lines due to the two radicals and correcting for degeneracies. The lines chosen are fairly well separated from the adjacent lines so that only small errors are involved in the measurements.

(6) This gives the following thermodynamic quantities: $\Delta H° = 600$ cal and $\Delta S° \sim 0$.

(7) R. A. Marcus, *Ann. Rev. Phys. Chem.*, **15**, 155 (1964). Marcus's original equation for our system should be written as $k_{HD} = \sqrt{k_{HH}k_{DD}K_{HD}f}$ where $\ln f = (\ln K_{HD})^2/4 \ln (k_{HH}k_{DD}/Z^2)$. If one chooses values between 10^{11} and 10^{12} for the collision frequency Z, then $\ln f$ becomes close to zero, or $f \sim 1$. We thank Professor Marcus for his helpful comments.
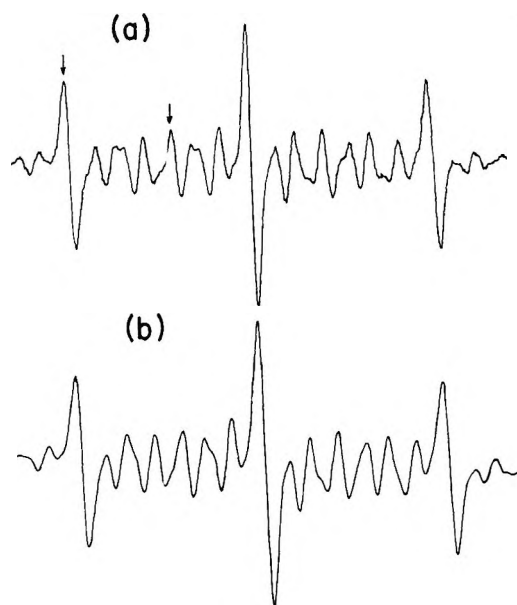
Figure 1. (a) The center portion of the esr spectrum of a
mixture of naphthalene and perdeuterionaphthalene anion
radicals, prepared by the reduction with potassium in
tetrahydrofuran at 25°. The scale is indicated by the distance
from the center to the tallest line on either side, which is 1.85 G.
The concentrations of the neutral molecules are: $[C_{10}H_8]$ =
0.002 and $[C_{10}D_8]$ = 0.007. The arrows indicate the lines
chosen for measuring the ratio of the radical concentrations.
(b) Computer-simulated spectrum assuming
$[C_{10}D_8{}^-]/[C_{10}H_8{}^-]$ = 1.40.

equation may not be strictly applicable here since the
inclusion of isotope effects, which are relatively small
effects, was approximate.[8]

Qualitatively, the difference in k_{HD} and k_{DH} is in
accord with the electron-donating effect of deuterium,
although it is a surprisingly large secondary isotope

effect.[9] The small equilibrium constant value suggests
that the reduction potentials for naphthalene and per-
deuterionaphthalene should differ by about 25 mV,[10]
and this has indeed been confirmed by polarographic
measurements.[11] No difference could be detected when
k_{HH} was measured in perdeuteriotetrahydrofuran.
This suggests that the reorganization of the solvation
sphere during the transfer process is a relatively un-
important step.

We are presently investigating the kinetics of electron
transfer and half-wave potentials of a number of deu-
terated systems.

(8) R. A. Marcus, private communication.

(9) The more reliable value of k_{DH} here is that calculated using the
slow limit value of k_{HD}. In this limit the concentration of the neutral
species used is of the order of $5 \times 10^{-2} M$. Since this is still a dilute
solution, we can assume that the same type of potassium naph-
thalenide ion pair is studied in the rate and equilibrium constant
measurements. The concentration of the neutral species varied be-
tween 0.1 and 0.6 M in the intermediate limit. The concentration of
the radicals, which was monitored optically, varied between 10^{-5} and
$5 \times 10^{-4} M$ for all the measurements.

(10) A. Streitwieser, "Molecular Orbital Theory," Wiley, New York,
N. Y., 1961, p 175.

(11) These measurements were made in dimethylformamide using
tetrabutylammonium iodide as supporting electrolyte. We thank
Dr. Raymond Petersen for carrying out these measurements.

DEPARTMENT OF CHEMISTRY   RAYMOND CHANG
WILLIAMS COLLEGE   ROBERT COOMBE
WILLIAMSTOWN, MASSACHUSETTS   01267

Journal of Chemical and Engineering Data
JANUARY 1971, Vol. 16, No. 1

TABLE OF CONTENTS

What you don't know about ESCA may be costing you time and knowledge!
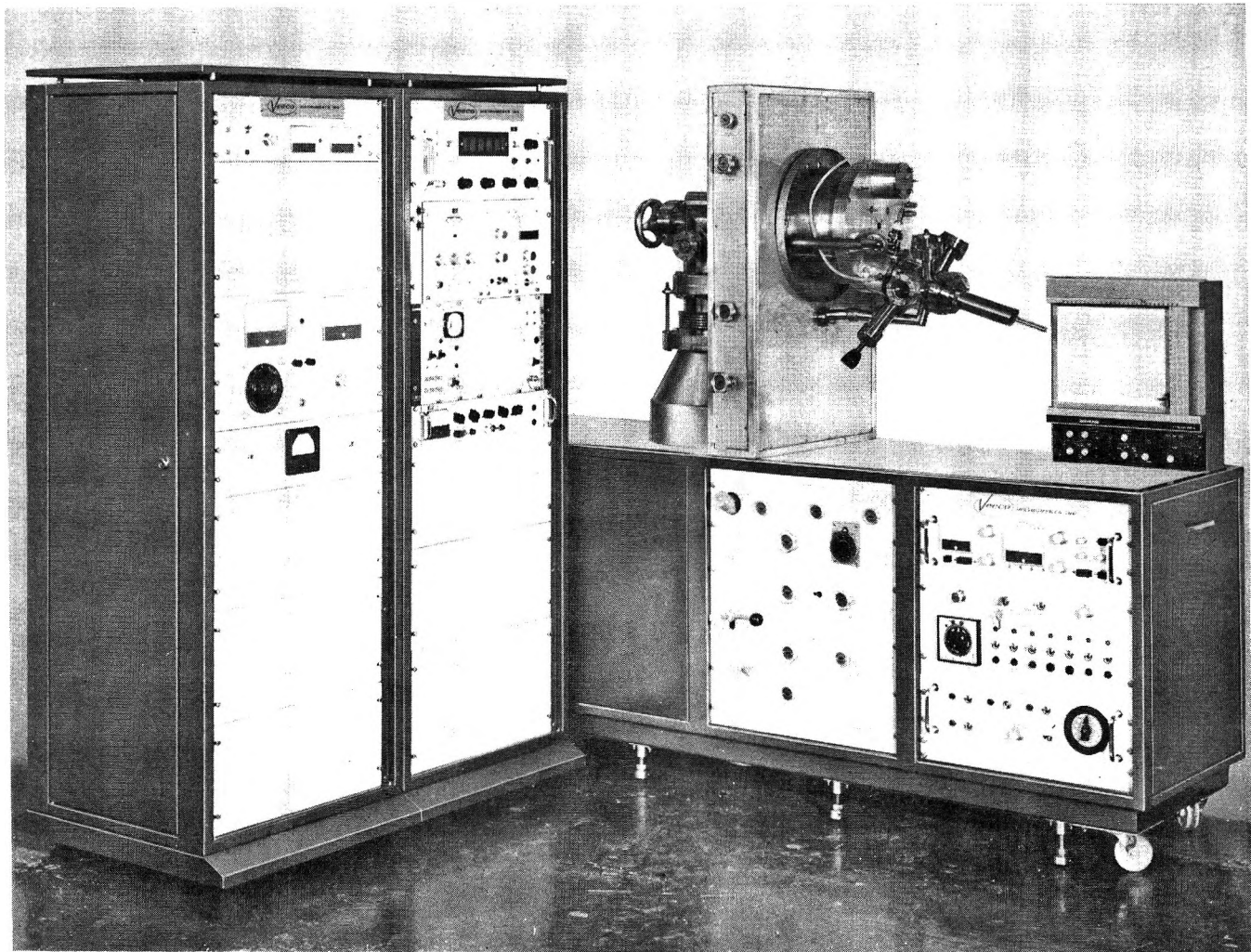
What is ESCA?

ESCA is an electron spectrometer for chemical analysis. A photoelectron spectrometer reads out the binding energies of electrons in atoms and molecules with resolution previously unattainable with existing techniques.

What can ESCA do for you?

Resolving power of Veeco's ESCA 1 and 2 is so high that it can be used to study chemical shift effects about an order of magnitude smaller than shifts detectable by X-Ray emission spectroscopy.

What's more, sensitivity is extremely high. Even very small concentrations of a constituent in a chemical compound can be detected and measured. Samples can be analyzed in solid, powder, liquid or gaseous form. Sensitivity and resolution remain high independent of the molecular weight of the sample.

Who can use ESCA?

ESCA 1 and 2 is ideal for physicists and chemists who need reliable information about chemical structures and binding energies in all forms of matter. Scientists now using other spectroscopic techniques—such as I-R Raman, UV, ORD, NMR, NQR, ESR, X-Ray Emission and Absorption, and Mass Spectrometry—will find that ESCA 1 and 2 has unique advantages not available in these other techniques.

Want to know more?

Get the whole story. Write for our new Analytical Instruments brochure today.